
ANALYTICA CHIMICA ACTA

An international journal devoted to all branches of analytical chemistry

Editors: Harry L. Pardue (West Lafayette, IN, USA)
Alan Townshend (Hull, Great Britain)
J.T. Clerc (Berne, Switzerland)
Willem E. van der Linden (Enschede, Netherlands)
Paul J. Worsfold (Plymouth, Great Britain)

Associate Editor: Sarah C. Rutan (Richmond, VA, USA)

Editorial Advisers:

F.C. Adams, Antwerp
M. Alzawa, Yokohama
W.R.G. Baeyens, Ghent
C.M.G. van den Berg, Liverpool
A.M. Bond, Bundoora, Vic.
M. Bos, Enschede
J. Buffle, Geneva
R.G. Cooks, West Lafayette, IN
P.R. Coulet, Lyon
S.R. Crouch, East Lansing, MI
R. Dams, Ghent
P.K. Dasgupta, Lubbock, TX
Z. Fang, Shenyang
P.J. Gemperline, Greenville, NC
W. Heineman, Cincinnati, OH
G.M. Hieftje, Bloomington, IN
G. Horvai, Budapest
T. Imasaka, Fukuoka
D. Jagner, Gothenburg
G. Johansson, Lund
D.C. Johnson, Ames, IA
A.M.G. Macdonald, Birmingham

D.L. Massart, Brussels
P.C. Meier, Schaffhausen
M. Meloun, Pardubice
M.E. Meyerhoff, Ann Arbor, MI
H.A. Mottola, Stillwater, OK
M. Otto, Freiberg
D. Pérez-Bendito, Córdoba
A. Sanz-Medel, Oviedo
T. Sawada, Tokyo
K. Schügerl, Hannover
M.R. Smyth, Dublin
R.D. Snook, Manchester
J.V. Sweedler, Urbana, IL
M. Thompson, Toronto
G. Tölg, Dortmund
Y. Umezawa, Tokyo
J. Wang, Las Cruces, NM
H.W. Werner, Eindhoven
O.S. Wolfbeis, Graz
Yu.A. Zolotov, Moscow
J. Zupan, Ljubljana

ANALYTICA CHIMICA ACTA

Scope. *Analytica Chimica Acta* publishes original papers, rapid publication letters and reviews dealing with every aspect of modern analytical chemistry. Reviews are normally written by invitation of the editors, who welcome suggestions for subjects. Letters can be published within **four months** of submission. For information on the Letters section, see inside back cover.

Submission of Papers

Americas

Prof. Harry L. Pardue Department of Chemistry 1393 BRWN Bldg, Purdue University West Lafayette, IN 47907-1393 USA Tel: (+1-317) 494 5320 Fax: (+1-317) 496 1200

Computer Techniques

Prof. J.T. Clerc Universität Bern Pharmazeutisches Institut Baltzerstrasse 5, CH-3012 Bern Switzerland Tel: (+41-31) 6314191 Fax: (+41-31) 6314198
--

Prof. Sarah C. Rutan Department of Chemistry Virginia Commonwealth University P.O. Box 2006 Richmond, VA 23284-2006 USA Tel: (+1-804) 367 7517 Fax: (+1-804) 367 8599
--

Other Papers

Prof. Alan Townshend Department of Chemistry The University Hull HU6 7RX Great Britain Tel: (+44-482) 465027 Fax: (+44-482) 466410
--

Prof. Willem E. van der Linden Laboratory for Chemical Analysis Department of Chemical Technology Twente University of Technology P.O. Box 217, 7500 AE Enschede The Netherlands Tel: (+31-53) 892629 Fax: (+31-53) 356024

Prof. Paul Worsfold Dept. of Environmental Sciences University of Plymouth Plymouth PL4 8AA Great Britain Tel: (+44-752) 233006 Fax: (+44-752) 233009

Submission of an article is understood to imply that the article is original and unpublished and is not being considered for publication elsewhere. *Anal. Chim. Acta* accepts papers in English only. There are no page charges. Manuscripts should conform in layout and style to the papers published in this issue. See inside back cover for "Information for Authors".

Publication. *Analytica Chimica Acta* appears in 16 volumes in 1994 (Vols. 281-296). *Vibrational Spectroscopy* appears in 2 volumes in 1994 (Vols. 6 and 7). Subscriptions are accepted on a prepaid basis only, unless different terms have been previously agreed upon. It is possible to order a combined subscription (*Anal. Chim. Acta* and *Vib. Spectrosc.*).

Our p.p.h. (postage, packing and handling) charge includes surface delivery of all issues, except to subscribers in the U.S.A., Canada, Australia, New Zealand, China, India, Israel, South Africa, Malaysia, Thailand, Singapore, South Korea, Taiwan, Pakistan, Hong Kong, Brazil, Argentina and Mexico, who receive all issues by air delivery (S.A.L.—Surface Air Lifted) at no extra cost. For Japan, air delivery requires 25% additional charge of the normal postage and handling charge; for all other countries airmail and S.A.L. charges are available upon request.

Subscription orders. Subscription prices are available upon request from the publisher. Subscription orders can be entered only by calendar year and should be sent to: Elsevier Science B.V., Journals Department, P.O. Box 211, 1000 AE Amsterdam, The Netherlands. Tel: (+31-20) 5803 642, Telex: 18582, Telefax: (+31-20) 5803 598, to which requests for sample copies can also be sent. Claims for issues not received should be made within six months of publication of the issues. If not they cannot be honoured free of charge. Readers in the U.S.A. and Canada can contact the following address: Elsevier Science Inc., Journal Information Center, 655 Avenue of the Americas, New York, NY 10010, U.S.A. Tel: (+1-212) 633 3750, Telefax: (+1-212) 633 3990, for further information, or a free sample copy of this or any other Elsevier Science journal.

Advertisements. Advertisement rates are available from the publisher on request.

US mailing notice – *Analytica Chimica Acta* (ISSN 0003-2670) is published 3 times a month (total 48 issues) by Elsevier Science B.V. (Molenwerf 1, Postbus 211, 1000 AE Amsterdam). Annual subscription price in the USA US\$ 3035.75 (valid in North, Central and South America), including air speed delivery. Second class postage paid at Jamaica, NY 11431. *USA Postmasters:* Send address changes to *Anal. Chim. Acta*, Publications Expediting, Inc., 200 Meacham Av., Elmont, NY 11003. Airfreight and mailing in the USA by Publication Expediting.

ANALYTICA CHIMICA ACTA

An international journal devoted to all branches of analytical chemistry

(Full texts are incorporated in CJELSEVIER, a file in the Chemical Journals Online database available on STN International; Abstracted, indexed in: Aluminum Abstracts; Anal. Abstr.; Biol. Abstr.; BIOSIS; Chem. Abstr.; Curr. Contents Phys. Chem. Earth Sci.; Engineered Materials Abstracts; Excerpta Medica; Index Med.; Life Sci.; Mass Spectrom. Bull.; Material Business Alerts; Metals Abstracts; Sci. Citation Index)

VOL. 292 NO. 1-2

CONTENTS

JUNE 30, 1994

Letter

- Electrothermal vaporization of trace beryllium via in situ alkylation for inductively coupled plasma atomic emission spectrometry
S. Tao and T. Kumamaru (Higashi-Hiroshima, Japan) 1

Chromatography

- Diagnosis and resolution of multiwavelength chromatograms by rank map, orthogonal projections and sequential rank analysis
Y.-z. Liang and O.M. Kvalheim (Bergen, Norway) 5
- Relationship between the physicochemical parameters of 3,5-dinitrobenzoic acid esters and their retention behaviour on β -cyclodextrin polymer support
T. Cserhádi (Budapest, Hungary) 17
- Immobilization of glucosidase onto silica-based, amino functionalized beads for enzymatic hydrolysis of urinary phenol prior to liquid chromatographic analysis
J.-F. Jen, J.-H. Zen, F.-C. Cheng and G.-Y. Yang (Taichung, Taiwan) 23
- Experimental studies on the enrichment of carboxylic acids with tri-*n*-octylphosphine oxide as extractant in a supported liquid membrane
Y. Shen, L. Grönberg and J.Å. Jönsson (Lund, Sweden) 31

Electroanalytical Chemistry and Sensors

- Optical sensors for a wide pH range based on azo dyes immobilized on a novel support
G.J. Mohr and O.S. Wolfbeis (Graz, Austria) 41
- Immobilisation of photosynthetic cells based on film-forming emulsion polymers
N. Martens and E.A.H. Hall (Cambridge, UK) 49
- Total urinary protein sensor based on a piezoelectric quartz crystal
S. Imai, H. Mizuno (Aichi, Japan), M. Suzuki, T. Takeuchi, E. Tamiya, F. Mashige, A. Ohkubo and I. Karube (Tokyo, Japan) 65
- New anaerobic thin-layer spectroelectrochemical cell
T.B. Jarbawi and M.T. Stankovich (West Bank, Israel) 71
- Chromium(VI) determination at a rotating disc electrode
N.G. Smart, M.L. Hitchman, R.O. Ansell and J.D. Fortune (Glasgow, UK) 77
- Differential pulse polarographic study of the degradation of H^+/K^+ ATPase inhibitors SK&F 95601 and omeprazole in acidic media and the subsequent reactions with thiols
S. McClean, E. O'Kane, V.N. Ramachandran and W.F. Smyth (Coleraine, UK) 81
- Adsorptive stripping voltammetry of trace uranium: critical comparison of various chelating agents
J. Wang, J. Wang, J. Lu (Las Cruces, NM, USA) and K. Olsen (Richland, WA, USA) 91
- Static and flow-injection voltammetric determination of periodate by reduction at a rotating platinum wire electrode
H.İ. Gökçel and G. Nişli (Izmir, Turkey) 99

(Continued overleaf)

ห้องสมุดรวมวิทยาศาสตร์บริการ

11 ส.ค. 2537

Contents (continued)

Catalytic oxidation and flow detection of acetaminophen at a dicyanobis(1,10-phenanthroline)iron(II)-modified electrode H. Li (Changchun, China), R. Ge (Beijing, China) and E. Wang (Changchun, China)	107
<i>Thermal Lens Spectrometry</i>	
Disproportionation and thermal lens effects produced by Ar ⁺ laser radiation on silver halide suspensions M.A. Rius Revert, M.C. García Alvarez-Coque and G. Ramis Ramos (València, Spain)	113
<i>Fluorimetry</i>	
Multi-wavelength analysis of synchronous fluorescence spectra of the complexes between a soil fulvic acid and Cu(II) A.A.S.C. Machado, J.C.G. Esteves da Silva and J.A.C. Maia (Porto, Portugal)	121
Study of the Eu(III)–tetracycline–thenoyltrifluoroacetone system by using the stopped-flow mixing technique: Determination of tetracycline in serum P. Izquierdo, A. Gómez-Hens and D. Pérez-Bendito (Córdoba, Spain)	133
Towards a quantitative determination of retinoids complexed to cyclodextrin: the diphenyl polyene model J.-C. Guilleux, K.N. Barnouin and D.A. Lerner (Montpellier, France)	141
<i>Chemiluminescence</i>	
Catalytic effect of rhodium(III) on the chemiluminescence of luminol in reverse micelles and its analytical application Imdadullah, T. Fujiwara and T. Kumamaru (Higashi-Hiroshima, Japan)	151
Study of the chemiluminescent characteristics of some xanthone dyes G.N. Chen, J.P. Duan and Q.F. Hu (Fujian, China)	159
Flow-injection chemiluminescence determination of the hydrazones of aromatic ketones T.E.A. Ahmed and A. Townshend (Hull, UK)	169
<i>Atomic Absorption Spectrometry</i>	
Determination of mercury(II), monomethylmercury cation, dimethylmercury and diethylmercury by hydride generation, cryogenic trapping and atomic absorption spectrometric detection R. Puk and J.H. Weber (Durham, NH, USA)	175
<i>Flow Injection</i>	
A screening method for trace mercury analysis using flow injection with urease inhibition and fluorescence detection D. Narinesingh, R. Mungal (St. Augustine, Trinidad and Tobago) and T.T. Ngo (Irvine, CA, USA)	185
Dispersion behaviour of chromogenic reagents in a microwave field in a flow system. Application to the spectrophotometric flow-injection determination of palladium and rhodium Y. Xu, X. Chen and Z. Hu (Lanzhou, China)	191
Flow-injection determination of kanamycin by inhibition of the lucigenin–H ₂ O ₂ –Co ²⁺ system A.A. Alwarthan, S.A. Al-Tamrah and A.A. Akel (Riyadh, Saudi Arabia)	201
<i>Other Topics</i>	
Recovery of polonium from microwave bomb digestions P.H. Towler and J.D. Smith (Parkville, Australia)	209
<i>Book Reviews</i>	213

ANALYTICA CHIMICA ACTA
VOL. 292 (1994)

ANALYTICA CHIMICA ACTA

*An international journal devoted to all branches of analytical chemistry
Revue internationale consacrée à tous les domaines de la chimie analytique
Internationale Zeitschrift für alle Gebiete der analytischen Chemie*

Editors: Harry L. Pardue (West Lafayette, IN, USA)

Alan Townshend (Hull, Great Britain)

J.T. Clerc (Berne, Switzerland)

Willem E. van der Linden (Enschede, Netherlands)

Paul J. Worsfold (Plymouth, Great Britain)

Associate Editor: Sarah C. Rutan (Richmond, VA, USA)

Editorial Advisers:

F.C. Adams, Antwerp

M. Aizawa, Yokohama

W.R.G. Baeyens, Ghent

C.M.G. van den Berg, Liverpool

A.M. Bond, Bundoora, Vic.

M. Bos, Enschede

J. Buffle, Geneva

R.G. Cooks, West Lafayette, IN

P.R. Coulet, Lyon

S.R. Crouch, East Lansing, MI

R. Dams, Ghent

P.K. Dasgupta, Lubbock, TX

Z. Fang, Shenyang

P.J. Gemperline, Greenville, NC

W. Heineman, Cincinnati, OH

G.M. Hieftje, Bloomington, IN

G. Horvai, Budapest

T. Imasaka, Fukuoka

D. Jagner, Gothenburg

G. Johansson, Lund

D.C. Johnson, Ames, IA

A.M.G. Macdonald, Birmingham

D.L. Massart, Brussels

P.C. Meier, Schaffhausen

M. Meloun, Pardubice

M.E. Meyerhoff, Ann Arbor, MI

H.A. Mottola, Stillwater, OK

M. Otto, Freiberg

D. Pérez-Bendito, Córdoba

A. Sanz-Medel, Oviedo

T. Sawada, Tokyo

K. Schügerl, Hannover

M.R. Smyth, Dublin

R.D. Snook, Manchester

J.V. Sweedler, Urbana, IL

M. Thompson, Toronto

G. Tölg, Dortmund

Y. Umezawa, Tokyo

J. Wang, Las Cruces, NM

H.W. Werner, Eindhoven

O.S. Wolfbeis, Graz

Yu.A. Zolotov, Moscow

J. Zupan, Ljubljana



Anal. Chim. Acta, Vol. 292 (1994)

ELSEVIER, Amsterdam–Lausanne–New York–Oxford–Shannon–Tokyo

© 1994 ELSEVIER SCIENCE B.V. ALL RIGHTS RESERVED

0003-2670/94/\$07.00

No part of this publication may be reproduced, stored in a retrieval system or transmitted in any form or by any means, electronic, mechanical, photocopying, recording or otherwise, without the prior written permission of the publisher, Elsevier Science B.V., Copyright and Permissions Dept., P.O. Box 521, 1000 AM Amsterdam, The Netherlands.

Upon acceptance of an article by the journal, the author(s) will be asked to transfer copyright of the article to the publisher. The transfer will ensure the widest possible dissemination of information.

Special regulations for readers in the U.S.A. – This journal has been registered with the Copyright Clearance Center, Inc. Consent is given for copying of articles for personal or internal use, or for the personal use of specific clients. This consent is given on the condition that the copier pays through the Center the per-copy fee for copying beyond that permitted by Sections 107 or 108 of the U.S. Copyright Law. The per-copy fee is stated in the code-line at the bottom of the first page of each article. The appropriate fee, together with a copy of the first page of the article, should be forwarded to the Copyright Clearance Center, Inc., 27 Congress Street, Salem, MA 01970, U.S.A. If no code-line appears, broad consent to copy has not been given and permission to copy must be obtained directly from the author. The fee indicated on the first page of an article in the issue will apply retroactively to all articles in the journal, regardless of the year of publication. This consent does not extend to other kinds of copying, such as for general distribution, resale, advertising and promotion purposes, or for creating new collective works. Special written permission must be obtained from the publisher for such copying.

No responsibility is assumed by the publisher for any injury and/or damage to persons or property as a matter of products liability, negligence or otherwise, or from any use or operation of any methods, products, instructions or ideas contained in the material herein.

Although all advertising material is expected to conform to ethical (medical) standards, inclusion in this publication does not constitute a guarantee or endorsement of the quality or value of such product or of the claims made of it by its manufacturer.

∞ The paper used in this publication meets the requirements of ANSI/NISO 239.48-1992 (Permanence of Paper).

PRINTED IN THE NETHERLANDS

Letter

Electrothermal vaporization of trace beryllium via in situ alkylation for inductively coupled plasma atomic emission spectrometry

Shiquan Tao, Takahiro Kumamaru *

Department of Chemistry, Faculty of Science, Hiroshima University, Higashi-Hiroshima, 724 Japan

(Received 22nd March 1994)

Abstract

A novel sample introduction method based on in situ alkylation for inductively coupled plasma atomic emission spectrometry was proposed for determination of beryllium. A very low detection limit (1.1 pg of beryllium) was obtained.

Key words: Inductively coupled plasma; Atomic emission spectrometry; In situ alkylation; Diethylberyllium; Beryllium

1. Introduction

In inductively coupled plasma atomic emission spectrometry (ICP-AES), the hydride generation procedure has been adopted as an efficient sample introduction process for the enhancement of sensitivity together with separation of analyte from matrix [1-3]. However, only a limited number of elements has been introduced into the ICP as volatile hydrides. For introducing analytes into ICP as gaseous species, there are other groups of compounds such as alkoxyboron [4] and some halides [5], neither of which volatilize at room temperature, but can be vaporized by mild heating. Such sample introduction procedures obviously share the merits of hydride generation. Alkylmetals are also among these groups of compounds and their boiling points are usually below

300°C. However, most alkylmetal compounds are highly reactive and some are unstable on exposure to moisture and even to air. These properties make it inconvenient to transport metals into the ICP as alkylmetals.

In this letter, an in situ alkylation system is reported for introducing beryllium as diethylberyllium into the ICP. With on-line vaporization, beryllium was efficiently carried into the ICP and a sensitive atomic emission signal was obtained.

2. Experimental

2.1. Apparatus

A Kyoto Koken (Kyoto, Japan) Model UOP-1S high-resolution inductively coupled plasma atomic emission spectrometer was used, by which the second derivative emission signals from the ICP were measured on a strip chart recorder. For

* Corresponding author.

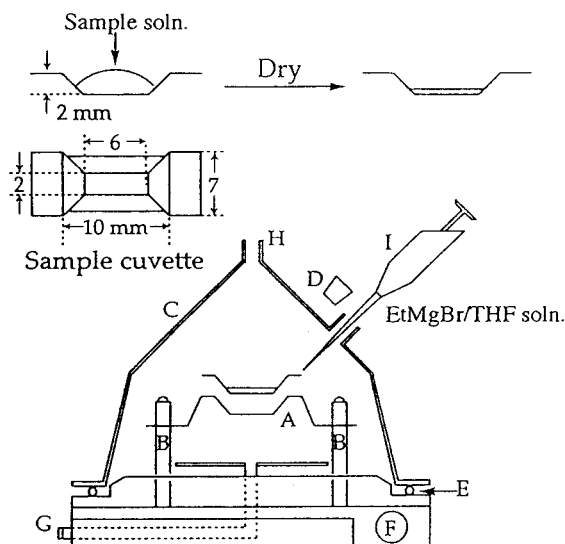


Fig. 1. Experimental procedure and schematic diagram of the apparatus for in situ alkylation. A, Tungsten boat furnace; B, furnace electrodes; C, glass dome; D, silicone rubber stopper; E, O-ring; F, electrode terminal; G, argon carrier gas inlet; H, outlet to ICP; I, micropipette.

vaporization of diethylberyllium into the plasma, a Seiko Instrument (Tokyo) Model SAS-705V metal furnace atomizer for atomic absorption spectrometry equipped with a tungsten boat furnace was used after modification. Sample cuvettes were also made by cutting both edges of the tungsten boats. A schematic diagram of the apparatus used for the alkylation and vaporization of beryllium is shown in Fig. 1.

2.2. Reagents

Beryllium(II) standard solutions were prepared by diluting a stock standard solution ($1000 \text{ mg Be l}^{-1}$; Kanto, Tokyo) with water. For alkylation, an ethylmagnesium bromide solution in tetrahydrofuran (0.9 mol l^{-1} ; Kanto) was used as received.

2.3. Recommended procedure

A $10\text{-}\mu\text{l}$ aliquot of aqueous sample solution was pipetted into the cuvette. After the sample was dried in an oven at 110°C , the cuvette was

loaded into the boat furnace and $15 \mu\text{l}$ of the ethylmagnesium bromide solution was added. The program for heating the atomizer was set at 70°C (40 s) for desolvation, and then at 600°C (15 s) for vaporization of diethylberyllium. An argon carrier gas flowed through the dome at a flow-rate of 0.45 l min^{-1} to carry diethylberyllium vapour into the ICP; the beryllium emission signal from the plasma was recorded.

The ICP was operated at 1.5 kW with an argon plasma gas flow-rate of 16 l min^{-1} and auxiliary argon gas flow-rate of 1.5 l min^{-1} . The beryllium emission signal at 313.042 nm (Be II) was monitored 6 mm above the load coil.

3. Results and discussion

Beryllium can form various alkyl compounds by a Grignard reaction, but none of these com-

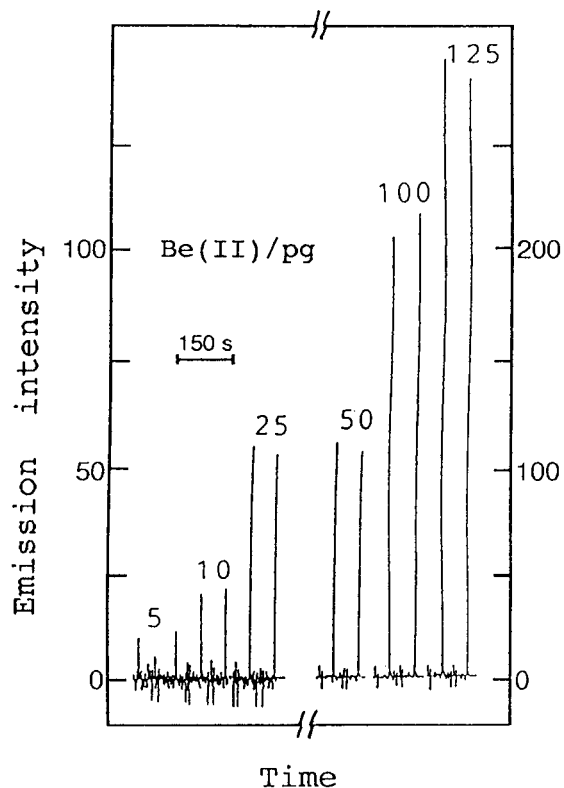


Fig. 2. Atomic emission signals vs. the amount of beryllium(II).

pounds is stable in the presence of water. Thus, for introducing beryllium into the ICP as diethylberyllium, it is necessary to ethylate beryllium in an anhydrous atmosphere. In this work, after the aqueous sample in the cuvette was heated completely to dryness, the ethylmagnesium bromide solution was added in the argon stream (Fig. 1).

As for the amount of ethylmagnesium bromide, 15 μ l of the reagent solution was sufficient to give quantitative results. Diethylberyllium was formed immediately after the addition of the Grignard reagent. For the vaporization of diethylberyllium, a heating temperature of 600°C was optimal though the appearance temperature of the beryllium emission signal was at around 230°C (the boiling point of diethylberyllium is 194°C). The optimum temperature is much lower than the boiling points of most inorganic matrices.

A calibration graph was prepared according to the recommended procedure. An example of the signals obtained is shown in Fig. 2. The emission peak height signal increased linearly with increas-

ing amounts of beryllium(II) up to at least 125 pg. The relative standard deviation ($n = 8$) was 5.2% for 10 pg of beryllium. The detection limit (3σ) was 1.1 pg of beryllium, which is nearly half of that obtained by conventional electrothermal vaporization ICP-AES [1–3].

The application of this method to the determination of beryllium in aluminium-based alloys and geochemical samples is now being studied.

References

- [1] K.C. Ng and J.A. Carso, in J. Sneddon (Ed.), *Sample Introduction In Atomic Spectroscopy*, Analytical Spectroscopy Library Vol. 4, Elsevier, Amsterdam, 1990.
- [2] T. Nakahara, *Spectrochim. Acta Rev.*, 14 (1991) 95.
- [3] F. Nakata, H. Sunahara, H. Fujimoto, M. Yamamoto and T. Kumamaru, *J. Anal. Atom. Spectrom.*, 3 (1988) 579.
- [4] T. Kumamaru, H. Matsuo, Y. Okamoto, M. Yamamoto and Y. Yamamoto, *Anal. Chim. Acta*, 186 (1986) 267.
- [5] S. Tesfalidet and K. Irgum, *Fresenius' J. Anal. Chem.*, 338 (1990) 741.

Diagnosis and resolution of multiwavelength chromatograms by rank map, orthogonal projections and sequential rank analysis

Yi-zeng Liang¹, Olav M. Kvalheim^{*}

Department of Chemistry, University of Bergen, N-5007 Bergen, Norway.

(Received 12th October 1993; revised manuscript received 19th January 1994)

Abstract

Cases with unresolved chromatographic peaks, where the diagnosis and subsequent resolution using common procedures from evolutionary factor analysis fails, are investigated and discussed in some detail. A new procedure is then developed. Local principal component analysis is first performed using a window procedure called eigenstructure tracking analysis. This evolving and dynamic procedure provides the best possible sensitivity for assessment of the number of coeluting analytes at a particular retention time as the method adapts the window size to the number of coeluting analytes. The result is a rank map in retention time direction, showing, in any retention time interval, the number of eluting analytes. The information in the rank map is subsequently used to define a set of n orthogonal projection matrices (n is the total number of detected analytes in the chromatogram). Each projection matrix is constructed from $n - 1$ loading vectors obtained, e.g., from principal component analysis of the zero-concentration window for a particular analyte. This procedure enables unambiguous identification of the peak pattern in an unresolved region. Resolution of the chromatographic peaks can then be accomplished by the combined use of orthogonal projections and a procedure called sequential rank analysis to solve the problem of embedded peaks. Sequential rank analysis assumes local symmetry around peak maxima and uses first-order differentiation for unique resolution of embedded peaks. The approach is demonstrated on some simulated chromatographic systems.

Key words: Principal component analysis; Chromatography; Multiwavelength chromatograms; Rank map; Orthogonal projections; Sequential rank analysis

1. Introduction

Evolving factor analysis (EFA) is an established method for resolving multiwavelength chromatographic data. Maeder and co-workers [1–3] pioneered multicomponent analysis by their

realization of the treasury provided by the evolving nature of many analytical profiles, e.g., the continuous character of chromatographic elution profiles with sequential appearance and disappearance of each analyte. The implementation of this insight as the resolution method EFA, however, has certain limitations and deficiencies. For instance, the peak detection procedure of EFA with stepwise increasing matrix size in forward and backward directions is rather vulnerable to, e.g., correlated and heteroscedastic noise and

^{*} Corresponding author.

¹ On leave from the Department of Chemistry and Chemical Engineering, Hunan University, Changsha, China.

strong spectral correlation between analytes [4–6]. In order to extract and use the evolving information more efficiently, several new methods have therefore recently been developed, among others, the fixed-size moving window evolving factor analysis (FSMWEFA) [7,8], evolutionary factor analysis (EVOLU) [9,10] and heuristic evolving latent projections (HELP) [4–6]. With these developments most of the practical and theoretical problems encountered with the original EFA method have been solved and the usability of evolutionary factor analysis improved.

A key assumption for correct utilisation of the evolving nature of analytical profiles which has so far escaped evaluation in the literature, is that the so-called zero-concentration window for each eluting analyte can be unambiguously identified. In order to obtain this crucial information, evolving factor analysis focuses its attention to retention times at which the analytes appear and disappear. A basic assumption for the procedure is that the order of appearance and disappearance is the same, i.e., that the first analyte to appear is also the first one to disappear [1,2]. This assumption is necessary in order to define uniquely the zero-concentration window for each eluting analyte. Unfortunately, this assumption does not always hold. A common example is represented by cases where tailing of major peaks corrupt the assumption of the same order of appearance and disappearance of peaks with fatal results for the subsequent resolution. Such cases are commonly encountered in the separation of complex natural products, peak purity analysis and other real world problems [11–13].

Fig. 1 highlights the kind of interpretation problem that may be encountered using the assumption in evolving factor analysis for the location of the zero-concentration window for the eluting analytes. The two elution situations A and B result in almost identical patterns for the evolving eigenvalues (lower part of Fig. 1). The assumption of the same order of appearance and disappearance of the overlapping peaks thus results in the interpretation shown in B also for system A. It is obvious that if the elution pattern denoted by A in Fig. 1 is misinterpreted as the one denoted by B in Fig. 1, the resolution proce-

dures fails completely. Correct diagnosis of the elution pattern is mandatory for successful resolution.

The aim of this work is two-fold: (i) to present a new diagnostic procedure for evolutionary factor analysis that enables correct identification of the elution pattern, and (ii) the development of a resolution procedure that can adapt to the different elution patterns. The new approach can be outlined as follows: (i) obtain the rank map in the retention time direction by eigenstructure tracking analysis [6], (ii) identify the elution pattern by use of orthogonal projections defined through the information contained in the rank map, and finally, (iii) resolve the chromatogram into pure peaks by means of orthogonal projections alone or for the case of embedded peaks in combination with so-called sequential rank analysis [14] upon the first-order differentiated two-way chromatogram. The novel approach is illustrated on multiwavelength chromatograms simulating different elution patterns.

2. Theory

2.1. Rank map by eigenstructure tracking analysis

Instead of extracting only the retention times of appearance and disappearance in the chromatographic direction as done in EFA, eigen-

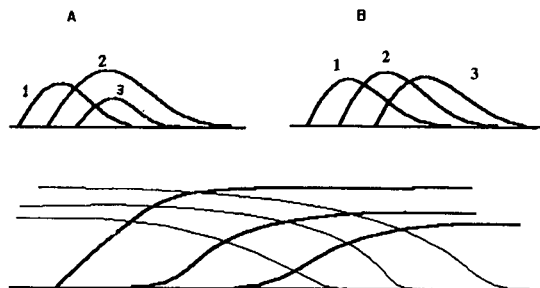


Fig. 1. Limitation of EFA for diagnosis of different elution patterns. Top part: two different elution patterns. Lower part: evolving eigenvalues for both elution patterns obtained by EFA.

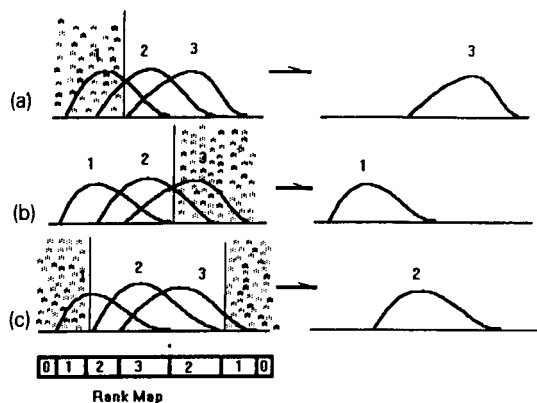


Fig. 2. Orthogonal projection procedures (denoted by a, b and c) for all the possible $(n-1)$ component submatrices for the elution pattern with same order of appearance and disappearance of three analytes. Left part: the (presently unknown) concentration profiles for three analytes with the shaded part defining subregions embracing $(n-1)$ analytes. Right part: the evolving information from orthogonal projections.

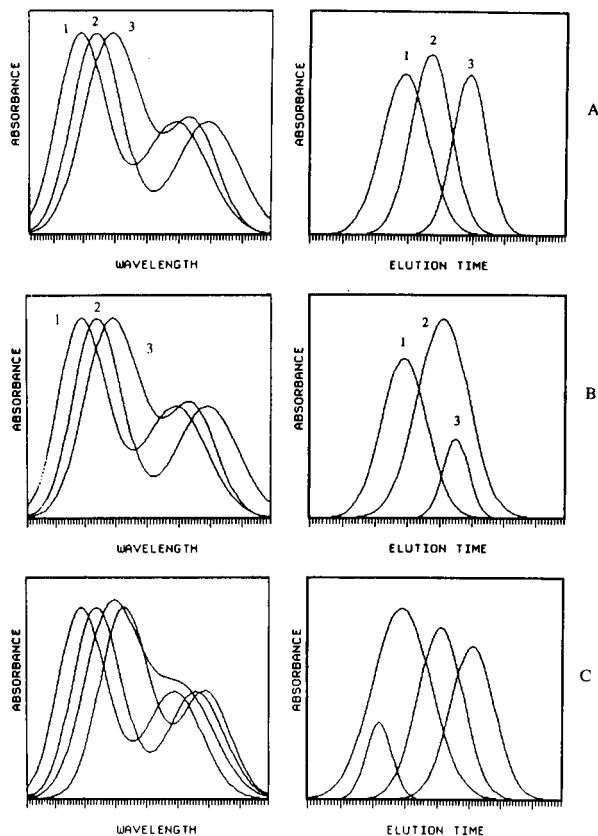


Fig. 3. Pure spectra and concentration profiles for three different simulated systems.

structure tracking analysis (ETA) [6] focuses upon the construction of a rank map which shows the number of analytes at every retention time (and/or wavelength). The ETA procedure analyses the whole chromatogram several times by use of a moving and expanding window. It starts with a window size of two, then increases the window size in steps by one and repeats the analysis until the window size just exceeds the largest number of coeluting analytes by one. Ref. 6 contains the detailed procedure for determining the rank map in retention time direction (consult Fig. 1 and the accompanying text in Ref. 6). The rank map is the key to unambiguous identification of elution pattern and thus correct resolution (see later in the text). Three kinds of regions have previously been shown to be of particular interest: (i) the zero-component regions, which can be utilised to take care of background and to establish noise level and detection limit in a chromatogram, and (ii) the selective regions, i.e., regions with only

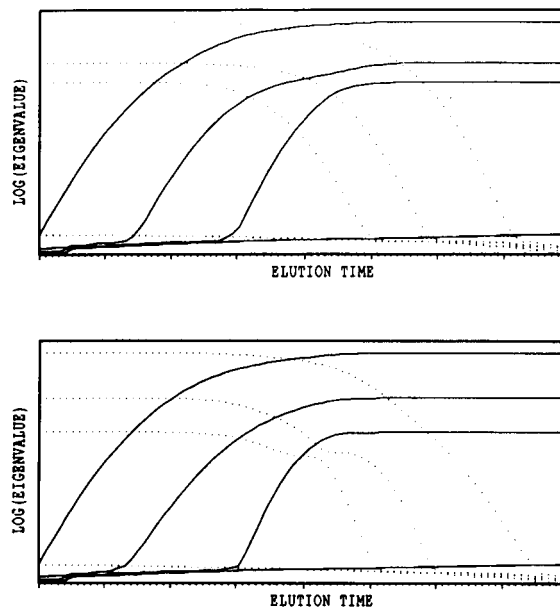


Fig. 4. Results from EFA for the two systems A and B in Fig. 3. Similar results are obtained although the elution patterns corresponding to systems A and B are completely different (see Fig. 3).

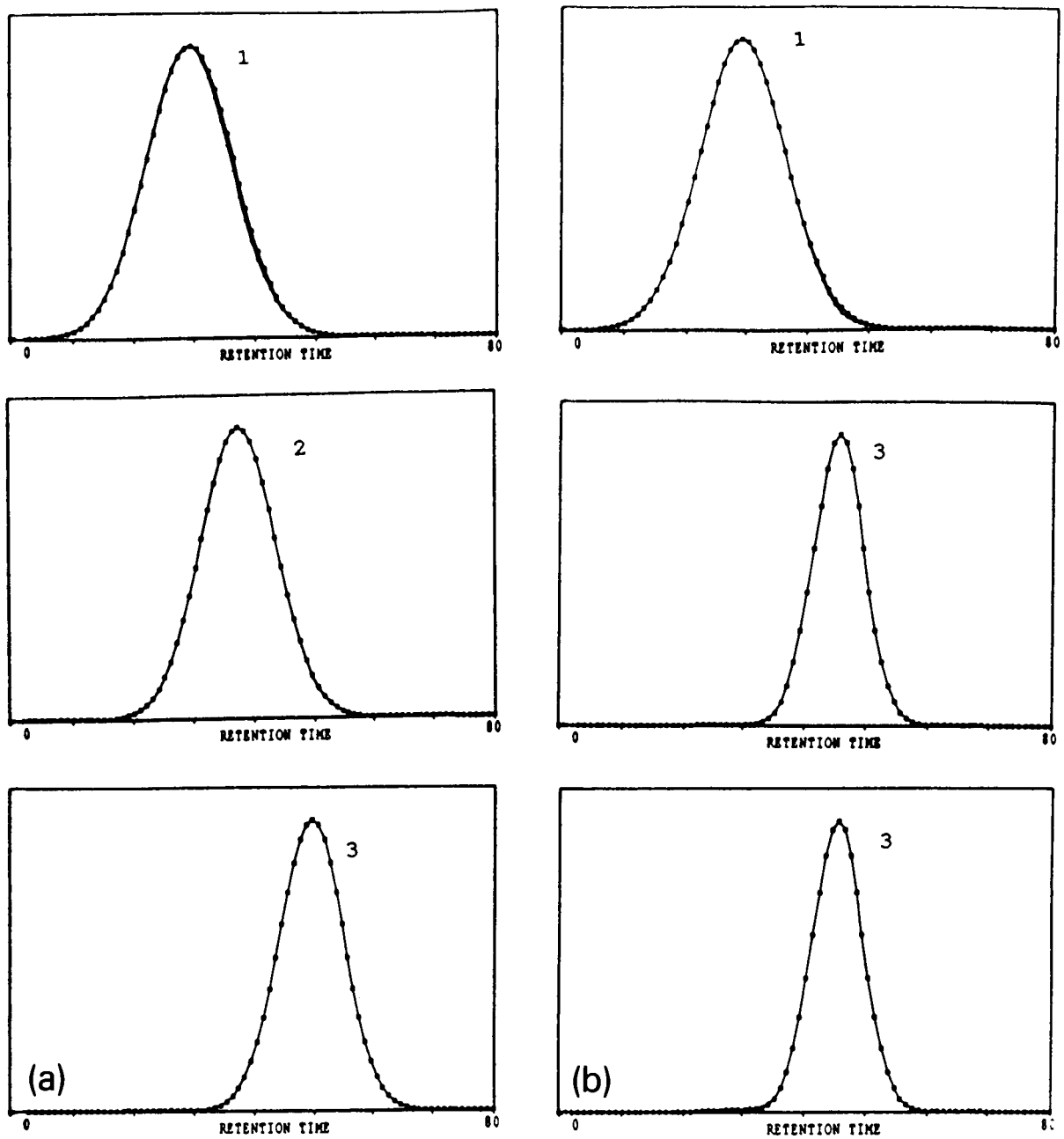


Fig. 5. The normalised concentration profiles obtained by orthogonal projections of all three $(n-1)$ submatrices for system A (Fig. 5a) and system B (Fig. 5b). Crosses imply the estimated concentration profiles and squares the real ones. The numbering in the plots denotes the results from the different projections. The numbering is the same as used in Fig. 2.

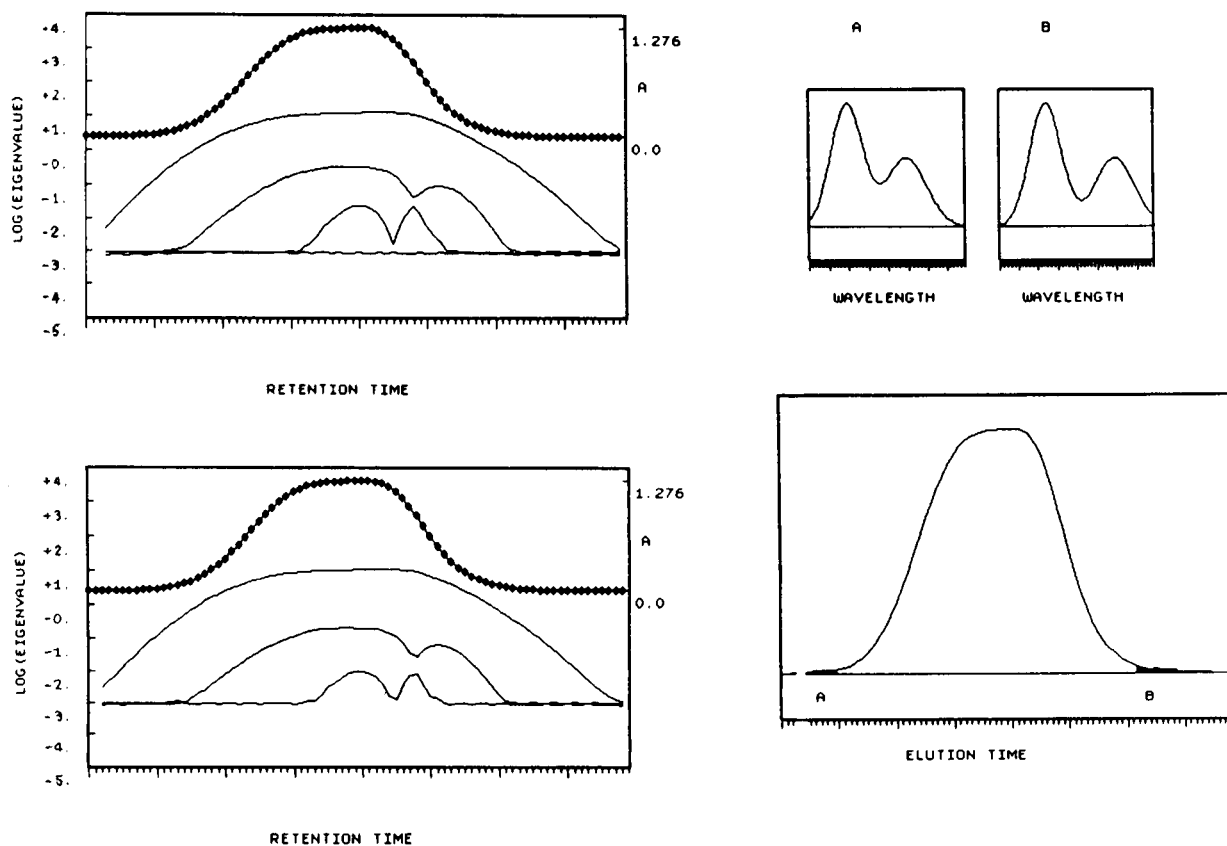


Fig. 6. Some results for system B (see Fig. 3) from heuristic evolving latent projections (HELP). Left part shows the results of the eigenstructure tracking analysis. Right part shows pure spectra (upper) and the resolved chromatogram with the selective regions for analyte A and B marked.

one eluting analyte, and (iii) the zero-concentration regions for each analyte. In this work, we focus our attention to the latter region.

2.2. Concentration profiles of the pure analytes by orthogonal projections

With the rank map available from ETA, a procedure of orthogonal projections can be performed to determine the concentration profile of each analyte. Lorber used projection matrices for defining the net analytical signal of an analyte in a mixture [15]. In this work, we use projection methodology for acquiring the concentration profiles of the analytes.

Projection matrices are constructed through the following steps: (i) use the rank map to determine the probable number n of eluting analytes

in the studied peak cluster, (ii) select/combine local regions to obtain submatrices $\{A_k; k = 1, 2, \dots, n\}$ each embracing $(n-1)$ analytes, (iii) factor-analyse every submatrix A_k thus obtained to calculate $(n-1)$ orthonormal loading vectors $\{p_{i(k)}; i = 1, \dots, n-1; k = 1, 2, \dots, n\}$, and finally, (iv) construct the projection matrix M_k for each submatrix as

$$M_k = (I - P_k^{(n-1)} G_k^{(n-1)} P_k^{(n-1)t}) \quad (k = 1, 2, \dots, n) \quad (1)$$

Here $P_k^{(n-1)}$ is the matrix of loading vectors, i.e., $P_k^{(n-1)} = (p_{1(k)}, p_{2(k)}, \dots, p_{n-1(k)})$, $G_k^{(n-1)}$ is the diagonal matrix of eigenvalues of $A_k^t A_k$, and I is the $(n-1)$ times $(n-1)$ identity matrix. Superscript t is used for transposition.

At every retention time j , a composite spectrum \mathbf{a}_j^t is acquired which can be expressed as a linear combination of the (presently unknown) spectra of the pure analytes:

$$\mathbf{a}_j^t = (c_1 \mathbf{s}_1 + c_2 \mathbf{s}_2 + \dots + c_n \mathbf{s}_n)_j^t \quad (2)$$

The spectra of the pure analytes are denoted $\{\mathbf{s}_i; i = 1, 2, \dots, n\}$, while $\{c_i; i = 1, 2, \dots, n\}$ are the corresponding concentrations of the analytes at retention time j . By projecting the matrix \mathbf{M}_k onto the mixture spectra $\{\mathbf{a}_j^t; j = 1, 2, \dots, m\}$, we obtain

$$\mathbf{a}_j^{t*} = \mathbf{a}_j^t \mathbf{M}_k = (c_n \mathbf{s}_n^*)_j \quad j = 1, 2, \dots, m \quad (3)$$

In Eq. 3, $\mathbf{s}_n^* = \mathbf{s}_n^t \mathbf{M}_k$. Proof of Eq. 3 is found in the Appendix.

Eq. 3 shows that the mixture spectra $\{\mathbf{a}_j^{t*}; j = 1, 2, \dots, m\}$ resulting from the use of an orthogonal projection spanning $(n - 1)$ analytes are a function of information exclusively related to analyte n with no contribution from the other coexisting $(n - 1)$ analytes. This is a very useful feature of the orthogonal projection technique. Thus, Eq. 3 shows that when the orthogonal projection is repeated for all the mixture spectra $\{\mathbf{a}_j^t; j = 1, 2, \dots, m\}$, a chromatographic profile re-

sults which is proportional to the concentration profile of analyte n . The concentration profile can be extracted simply by calculating the norm of the row vectors $\{\mathbf{a}_j^{t*}; j = 1, 2, \dots, m\}$:

$$(c_n)_j = \|\mathbf{a}_j^{t*}\| / \|(\mathbf{s}_n^*)_j\| \quad (j = 1, 2, \dots, m) \quad (4)$$

Note that the \mathbf{s}_n^* is independent of the subscript j (retention time point) and therefore constant throughout elution. However, $\|\mathbf{a}_j^{t*}\|$ changes at every retention time j and so it maps the relative concentration profile. Thus, we can rewrite Eq. 4 in vectorial form:

$$\mathbf{c}_n = \left\{ \|\mathbf{a}_j^{t*}\| \right\} / \|(\mathbf{s}_n^*)\| = \beta^{-1} \mathbf{d} \quad (5)$$

Here $\beta = \|(\mathbf{s}_n^*)\|$ and $\mathbf{d} = (\|\mathbf{a}_1^{t*}\|, \|\mathbf{a}_2^{t*}\|, \dots, \|\mathbf{a}_m^{t*}\|)$.

2.3. Resolution of the ordinary case by orthogonal projections

The projection procedure described above is performed for all n analytes. All we have to ensure is correct selection/combination of local regions containing the coexisting $(n - 1)$ analytes. A common situation for a three-component peak cluster is illustrated in Fig. 2. From this figure, we observe that the normalised concentration profiles for all three analytes can be obtained by use of orthogonal projections. With this information at hand, the pure spectra of the three analytes is obtained by a simple least-squares calculation. Thus, the measurement matrix \mathbf{A} can be expressed as a product of the two matrices \mathbf{C} and \mathbf{S} containing concentration profiles and spectral profiles, respectively:

$$\mathbf{A} = \mathbf{C} \mathbf{S}^t \quad (6)$$

Least-squares calculation provides the spectra of the pure analytes as

$$\mathbf{S}^t = (\mathbf{C}^t \mathbf{C})^{-1} \mathbf{C}^t \mathbf{A} \quad (7)$$

It should be pointed out that the procedure of orthogonal projections can be readily extended to deal with multicomponent systems with more than three components (see example below).

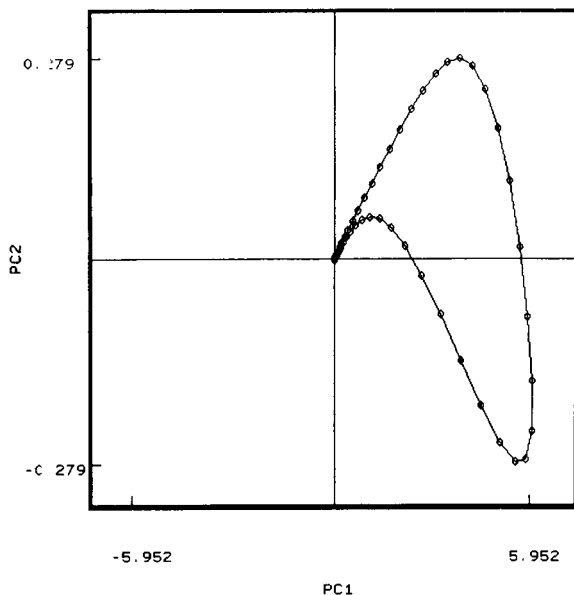


Fig. 7. The latent-projective graph for system B after stripping off the contribution from analyte 1.

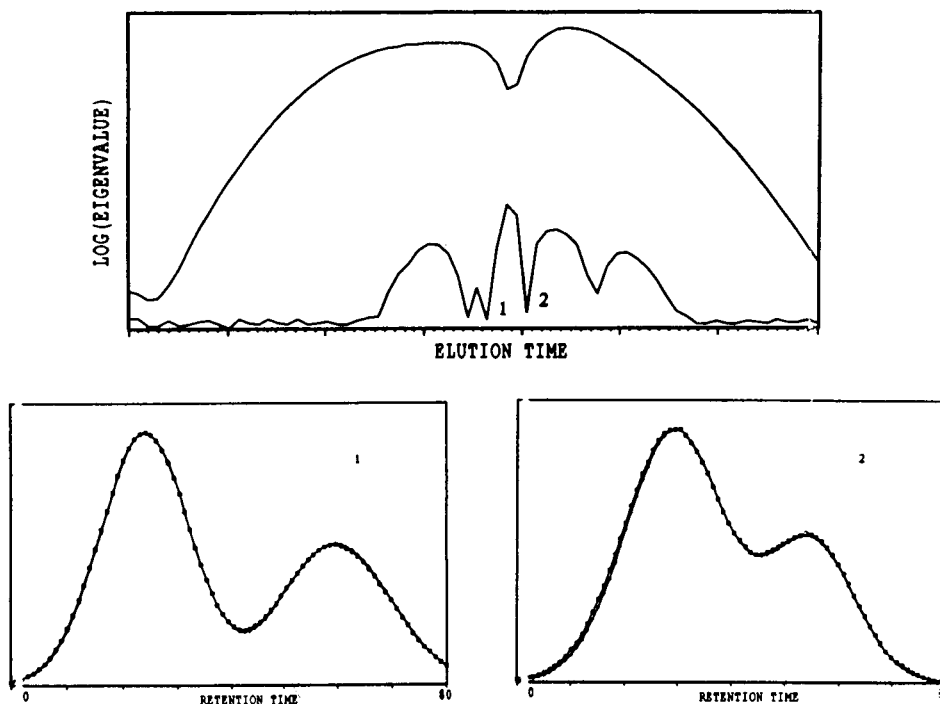


Fig. 8. The results of sequential rank analysis upon the first-order derivative matrix obtained by differentiation in chromatographic direction of system B, Fig. 3, after stripping of analyte 1. Upper part shows the plot from sequential rank analysis, points denoted by 1 and 2 signify the maxima for both the large and embedded peaks. The corresponding spectra for these two maximum points are shown in the lower part. Crosses indicate the spectra selected at these two points, while the squares signify the real pure spectra for the two analytes.

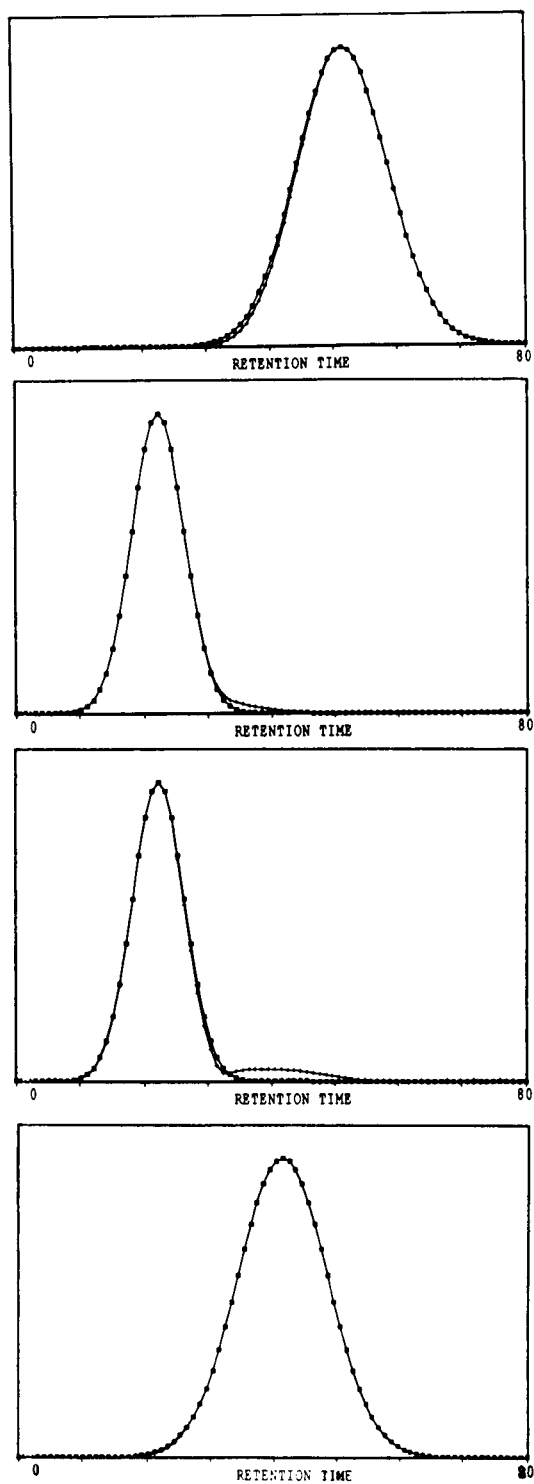
2.4. Unambiguous identification of elution patterns by orthogonal projections

Using the two different systems shown in Fig. 1 as examples, we shall now illustrate how the orthogonal projections can be utilised for identification of the elution pattern.

For the identification of the elution pattern in the two three-component systems, we first carry out principal components analysis of all possible submatrices embracing $(n - 1)$ analytes in order to obtain the corresponding orthogonal projection matrices. The selection of regions is governed by the rank map. Fig. 2 illustrates the selection procedure and the result of applying the three possible projection matrices with rank 2 to the measurement matrix **A** acquired for system B in Fig. 1, i.e. the ordinary case in which the

common EFA interpretation also accomplish the task. Three different (normalised) concentration profiles are obtained as shown in Fig. 2 (left side) and the spectra can subsequently be obtained by least-squares using Eq. 7

For systems of type A in Fig. 1, two of the three concentration profiles obtained by use of orthogonal projections are identical: the concentration profile of analyte 3 is obtained twice, while the profile of analyte 2 is not obtained at all. This fact makes it possible to distinguish the two elution patterns exemplified by A and B in Fig. 1. Inspection of the rank map and the extracted concentration profiles for analytes 1 and 3, makes it possible to unambiguously define the elution window also for analyte 2. The orthogonal projection procedure therefore provides unambiguous identification of the elution pattern in



the two cases, a necessary but not sufficient condition for resolution in both cases.

2.5. Resolution of embedded peaks by orthogonal projections and sequential rank analysis

As discussed above, one of the three concentration profiles for systems of type A in Fig. 1 cannot be obtained by means of orthogonal projections. The pure concentration profiles for analytes 1 and 3 can be estimated by orthogonal projections due to the presence of well-defined regions for the $(n - 1)$ coeluting analytes. The concentration profile for analyte 2 cannot be obtained by orthogonal projections, since a local region for the other two analytes does not exist. On the other hand, pure spectra for the analytes labelled 1 and 2 in Fig. 1 can be estimated by local factor analysis upon the selective regions as prescribed by the HELP method [4]. However, without any knowledge of the spectrum for analyte 3, the concentration profile for analyte 2 is still out of reach.

It is obvious that we need some additional technique for complete resolution of the studied overlapping peaks. Since both the concentration profile and the pure spectrum of the first analyte are available, the component stripping technique developed in the heuristic evolving latent projections (HELP) method [14] can be used for subtracting the contribution from the first eluting analyte. After application of that procedure, the three-component peak cluster becomes a two-component one with an embedded peak. Such a system can be resolved by means of sequential rank analysis using first-order differentiation as described in detail in a previous paper [14]. Through the determination of the retention time of the chromatographic peak maximum for the major analyte, the resolution of the overlapping peaks becomes possible if the peaks are symmetric just around peak maximum [14].

Fig. 9. The normalised concentration profiles obtained by the orthogonal projections of all four $(n - 1)$ submatrices for system C. Crosses show the estimated concentration profiles, while squares signify the real ones.

3. Experimental

The procedures described in the Theory section has been implemented in VAX FORTRAN as a part of the heuristic evolving latent projections (HELP) program [4–6]. The implementation is running on a VAX station 2000. Three different multiwavelength chromatograms were created to simulate mixtures with three and four coeluting analytes. Spectra and chromatograms of the pure analytes are shown in Fig. 3. Random noise with a relative standard deviation of 0.0001 was added. This is comparable to what is commonly observed in real LC-DAD data [5].

4. Results and discussion

4.1. Diagnosis and resolution of three-component systems

The results of EFA on systems A and B in Fig. 3 are shown in Fig. 4. Although the two systems have quite different elution patterns, the evolving information from the EFA is for all practical purposes the same. The subsequent resolution for these two analytical systems produces results that are either uncertain (case A) or wrong (case B).

The orthogonal projection technique described in the Theory section can provide useful information for the identification of the elution patterns in the two analytical systems. If we carry out the projection procedure illustrated in Fig. 2 for both analytical systems, concentration profiles are obtained as shown at the left side of Fig. 5a for system A and at the right side of Fig. 5b for system B. These two clearly different sets of concentration profiles suggest two systems with different elution patterns. For system A, we further observe three different concentration profiles (Fig. 5a), while for system B, we only obtain two different concentration profiles. In the case of system B, two of the three calculated concentration profiles are the same (Fig. 5b). These observations confirm that the two studied analytical systems are different.

For system A, the pure spectra of the three analytes can now be obtained by simply using the

simple least-squares technique (Eq. 7 in the Theory section). However, we need to use a more sophisticated technique for the resolution of the system B, since the orthogonal projections only provided concentration profiles for two of the analytes. By means of the heuristic evolving latent projections (HELP) method, one can also reveal selective regions for two analytes. The results from the eigenstructure tracking analysis (Fig. 6a, left side) and the corresponding rank map are shown together with the spectra of the pure analytes and their selective regions in the retention time direction (Fig. 6b, right side). The two pure concentration profiles (obtained by orthogonal projections) correspond to the two analytes numbered 1 and 3 in Fig. 3a, while the two pure spectra (obtained by HELP method) represent the two analytes numbered 1 and 2 in Fig. 3b. Complete information, both spectral and concentration profile, is only available for analyte 1. Stripping off the contribution from analyte 1 changes system B into a two-component system with one embedded peak (see Fig. 7). The resolution for such systems has been discussed in detail in a previous paper [14]. The results from so-called sequential rank analysis upon the first-order derivative matrix differentiated in chromatographic direction are shown in Fig. 8a. Assuming local symmetry of the pure analytes around chromatographic peak maxima, the estimate of the pure spectrum for the embedded chromatographic peak is obtained (Fig. 8b). With all the pure spectra at hand, the pure concentration profiles can then be obtained by applying the least squares technique to Eq. 6, completely analogous to the way that Eq. 7 was obtained.

4.2. Diagnosis and resolution of a four-component system

The methodology described above can be directly extended to handle multicomponent systems with more than three coeluting analytes. The results from the orthogonal projections on the four-component system C in Fig. 3 are shown in Fig. 9. Since we only obtain three different concentration profiles for four different orthogonal projection procedures, the studied system

must include one embedded peak in a peak cluster of four analytes. After stripping off the contributions from the two analytes with concentration profiles and spectral profiles estimated by orthogonal projections and the HELP method, respectively, the system reduces to a two-component system with one embedded peak. The resolution of this subsystem can be conducted by the same procedure as described in the last paragraph above.

5. Conclusion

As discussed in previous papers, limitations of evolving factor analysis [1–3], such as low ability for detection of minor analytes coeluting with major ones [5], can be cured by heuristic evolving latent projections (HELP) and fixed size moving window evolving factor analysis (FSMWEFA) in conjunction with proper correction for the presence of heteroscedastic noise [5,8]. In this paper, we have presented a new procedure in order to overcome another limitation of evolving factor analysis: the diagnosis and resolution of peak clusters with elution patterns disobeying the assumption of same order of appearance and disappearance of analytes. By means of the eigenstructure tracking analysis, rank map in retention time direction, construction and use of orthogonal projections and sequential rank analysis [14] using first order differentiation, the identification and resolution of systems with rather complex elution patterns has been accomplished.

Acknowledgement

The Norwegian Research Council for Science and Humanities (NAVF) is thanked for a visitor grant to Y.-z Liang.

Appendix

Proof of Eq. 3

Assuming that $\mathbf{A}^{(n-1)}$ is a matrix involving $(n-1)$ analytes in some local region and $(\mathbf{A}^{(n-1)})^+$ its

generalised inverse (Moore-Penrose inverse), an orthogonal projection matrix \mathbf{M} can be constructed as

$$\mathbf{M} = (\mathbf{I} - (\mathbf{A}^{(n-1)} + \mathbf{A}^{(n-1)})^+) \quad (\text{A1})$$

The matrix $\mathbf{A}^{(n-1)}$ can be decomposed by principal component analysis to obtain

$$\mathbf{A}^{(n-1)} = \mathbf{T}^{(n-1)} \mathbf{P}^{(n-1)t} \quad (\text{A2})$$

The score and loading matrices, $\mathbf{T}^{(n-1)}$ and $\mathbf{P}^{(n-1)t}$, respectively, contain the $(n-1)$ score and loading vectors with largest eigenvalues. The generalised inverse $(\mathbf{A}^{(n-1)})^+$ can then be obtained in the following way:

$$(\mathbf{A}^{(n-1)})^+ = (\mathbf{T}^{(n-1)} \mathbf{P}^{(n-1)t})^{-1} = \mathbf{P}^{(n-1)} \mathbf{T}^{(n-1)t} \quad (\text{A3})$$

Eq. A3 follows because $\mathbf{T}^{(n-1)}$ and $\mathbf{P}^{(n-1)t}$ are orthogonal matrices. The orthogonal projection matrix for the studied case is obtained simply as

$$\begin{aligned} \mathbf{M} &= (\mathbf{I} - \mathbf{A}^{(n-1)} + \mathbf{A}^{(n-1)})^+ \\ &= (\mathbf{I} - \mathbf{P}^{(n-1)} \mathbf{G}^{(n-1)} \mathbf{P}^{(n-1)t}) \end{aligned} \quad (\text{A4})$$

$\mathbf{G}^{(n-1)}$ is the diagonal matrix of eigenvalues of $\mathbf{A}^{(n-1)t} \mathbf{A}^{(n-1)}$. The generalised inverse matrix has the following important property:

$$\mathbf{A}^{(n-1)} \mathbf{A}^{(n-1)} + \mathbf{A}^{(n-1)} = \mathbf{A}^{(n-1)} \quad (\text{A5})$$

Eq. A5 shows that for one row in $\mathbf{A}^{(n-1)}$

$$\mathbf{a}_i^{(n-1)t} \mathbf{A}^{(n-1)} + \mathbf{A}^{(n-1)} = \mathbf{a}_i^{(n-1)t} \quad (\text{A6})$$

The vector $\mathbf{a}_i^{(n-1)t}$ is the i th row in the matrix $\mathbf{A}^{(n-1)}$. Any mixture spectrum in the matrix $\mathbf{A}^{(n-1)}$ can involve $(n-1)$ analytes, so the mixture spectra $\mathbf{a}_i^{(n-1)t}$ can be expressed as

$$\mathbf{a}_i^{(n-1)t} = (c_1 \mathbf{s}_1 + c_2 \mathbf{s}_2 + \dots + c_{n-1} \mathbf{s}_{n-1})_i^t \quad (\text{A7})$$

Here $\{\mathbf{s}_j; j = 1, 2, \dots, n-1\}$ and $\{c_j; j = 1, 2, \dots, n-1\}$ denote the pure spectrum of the species j and the concentration of the corresponding analytes at retention time i . For a mixture spectrum \mathbf{a}_j^t with contributions from all n analytes, we have

$$\begin{aligned} \mathbf{a}_j^t &= (c_1 \mathbf{s}_1 + c_2 \mathbf{s}_2 + \dots + c_{n-1} \mathbf{s}_{n-1} + c_n \mathbf{s}_n)_j^t \\ &= (\mathbf{a}^{(n-1)} + c_n \mathbf{s}_n)_j^t \end{aligned} \quad (\text{A8})$$

By utilising the property defined by Eq. A6, the orthogonal projection onto the mixture spectrum \mathbf{a}_j^t proceeds as follows:

$$\begin{aligned} \mathbf{a}_j^t \mathbf{M} &= (\mathbf{a}^{(n-1)} + c_n \mathbf{s}_n)_j^t (\mathbf{I} - \mathbf{A}^{(n-1)+} \mathbf{A}^{(n-1)}) \\ &= (\mathbf{a}_j^{(n-1)t} - \mathbf{a}_j^{(n-1)t} \mathbf{A}^{(n-1)+} \mathbf{A}^{(n-1)}) \\ &\quad + (c_n \mathbf{s}_n)_j^t (\mathbf{I} - \mathbf{A}^{(n-1)+} \mathbf{A}^{(n-1)}) \\ &= (c_n \mathbf{s}_n^t \mathbf{M})_j = (c_n \mathbf{s}_n^*)_j \end{aligned} \quad (\text{A9})$$

This is Eq. 2 in the text above. The vector \mathbf{s}_n^* spans an orthogonal complement subspace of $\mathbf{A}^{(n-1)}$.

References

- [1] M. Maeder and A.D. Zuberbuhler, *Anal. Chim. Acta*, 181 (1986) 287.
- [2] M. Maeder, *Anal. Chem.*, 59 (1987) 527.
- [3] M. Maeder and A. Zilian, *Chemom. Intell. Lab. Syst.*, 3 (1988) 205.
- [4] O.M. Kvalheim and Y.-z. Liang, *Anal. Chem.*, 64 (1992) 936.
- [5] Y.-z. Liang, O.M. Kvalheim, H.R. Keller, D.L. Massart, P. Kiechle and F. Erni, *Anal. Chem.*, 64 (1992) 946.
- [6] Y.-z. Liang, O.M. Kvalheim, A. Rahmani and R.G. Brereton, *J. Chemom.*, 7 (1993) 15.
- [7] H.R. Keller and D.L. Massart, *Anal. Chim. Acta*, 246 (1991) 279.
- [8] H.R. Keller and D.L. Massart, Y.-z. Liang and O.M. Kvalheim, *Anal. Chim. Acta*, 263 (1992) 125.
- [9] K.J. Schostack and E.R. Malinowsky, *Chemom. Intell. Lab. Syst.*, 8 (1990) 121.
- [10] K.J. Schostack and E.R. Malinowsky, *Chemom. Intell. Lab. Syst.*, 10 (1991) 303.
- [11] B.G.M. Vandeginste, R. Esser, T. Bosman, J. Reijnen and G. Kateman, *Anal. Chem.*, 57 (1985) 971.
- [12] H.R. Keller, D.L. Massart and J.O. De Beer, *Anal. Chem.*, 65 (1993) 471.
- [13] M.D. Hämäläinen, Y.-z. Liang, O.M. Kvalheim and R. Andersson, *Anal. Chim. Acta*, 271 (1993) 101.
- [14] Y.-z. Liang, R. Manne and O.M. Kvalheim, *Chemom. Intell. Lab. Syst.*, 22 (1994) 229.
- [15] A. Lorber, *Anal. Chem.*, 58 (1986) 1167.
- [16] Y.-z. Liang and O.M. Kvalheim, *Chemom. Intell. Lab. Syst.*, 20 (1993) 115.

Relationship between the physicochemical parameters of 3,5-dinitrobenzoic acid esters and their retention behaviour on β -cyclodextrin polymer support

Tibor Cserhádi

Central Research Institute for Chemistry, Hungarian Academy of Sciences, P.O. Box 17, 1525 Budapest, Hungary

(Received 26th October 1993; revised manuscript received 20th January 1994)

Abstract

The retention of fourteen 3,5-dinitrobenzoic acid esters on thin layers prepared from a water-insoluble β -cyclodextrin polymer was determined using water–methanol mixtures as eluents. Linear correlations were calculated between the R_M value of the solutes and the methanol concentration in the eluent, and the relationship between the chromatographic characteristics (slope and intercept values of the above correlation) and the physicochemical parameters was elucidated by stepwise regression analysis. The R_M value of solutes decreased or increased with increasing methanol concentration in the eluent. This anomalous retention behaviour was tentatively explained by possible ternary complex formation: cyclodextrin–solute–methanol. Stepwise regression analysis proved that the steric parameters of solutes have the highest impact on their retention on the polymer layers.

Key words: Thin-layer chromatography; Water-insoluble β -cyclodextrin polymer; 3,5-Dinitrobenzoic acid esters

1. Introduction

A wide variety of organic and inorganic compounds form inclusion complexes with cyclodextrins (CDs) [1,2]. Due to their modification of the physicochemical parameters of the guest molecule (hydrophobicity, adsorption capacity, etc.) CDs have found growing acceptance and application in many fields of chromatography such as capillary gas–liquid chromatography [3,4], capillary zone electrophoresis [5,6], supercritical fluid chromatography [7,8], isotachopheresis [9] and

liquid chromatography (LC). In LC CDs can be used either as eluent additives [10,11] or covalently bonded to the surface of silica supports. LC supports with covalently bonded CDs on the surface can be used either in the reversed phase [12,13] or direct separation mode [14,15]. It has recently been reported that phenylethyl and naphthylethyl carbamate substituted CD bonded phases can be successfully used in both separation modes [16]. CD polymer coated LC columns have recently been introduced [17] and their retention characteristics have been determined [18].

As a rapid and easy to carry out analytical technique thin-layer chromatography (TLC) has frequently been used. Polar inorganic and organic

* Corresponding author.

supports such as silica, alumina, cellulose and diatomaceous earth (Kieselguhr) are generally used in TLC, but apolar sorbents as octadecyl modified silica have also gained some limited application. In this instance the support is more apolar and the mobile phase (water and organic modifiers miscible with water) is relatively polar. The retention of solutes in reversed-phase TLC (RP-TLC) is determined by their hydrophobic (lipophilic) character; the more lipophilic solute shows higher retention. New TLC sorbents such as aminopropyl-, cyanopropyl- [19] and diol-bonded silicas [20] make possible the separation of compounds which cannot be easily separated on traditional adsorptive and reversed-phase layers. These new supports can be used both in adsorptive and reversed-phase separation modes [21,22].

The objectives of our investigation were to study the possible application of water-insoluble β -cyclodextrin polymer (BCDP) beads as TLC sorbents, to find the physicochemical parameters of solutes influencing the retention, and to gain a more profound insight in the binding properties of β -cyclodextrin polymer supports. As it has been proved that TLC can be successfully used to predict the retention of solutes in LC [23,24], the data can help to predict the retention behaviour of solutes on BCDP coated LC columns.

2. Experimental

Water insoluble β -CD polymer was a pilot product of CYCLOLAB Research and Development Laboratory (Budapest). It was prepared by crosslinking β -CD monomers with epichlorohydrin and ethyleneglycolbis(epoxypropyl ether). It was ground and the 10–50 μm fraction was used in the experiments. TLC plates were prepared on 20 \times 20 cm glass plates: 5 g BCDP and 25 mg poly(vinylalcohol) were suspended in the potential eluent, spread on the glass surface and dried at room temperature. Owing to the considerable swelling of the β -cyclodextrin polymer, the preparation of the TLC plates has to be carried out in the eluent. The use of poly(vinyl alcohol) was motivated by the low mechanical stability of

the BCDP layer. The methyl (compound I), ethyl (II), *n*-propyl (III), isopropyl (IV), *n*-butyl (V), isobutyl (VI), *tert.*-butyl (VII), *n*-amyl (VIII), isoamyl (IX), *tert.*-amyl (X), cyclopentyl (XI), cyclohexyl (XII), *n*-octyl (XIII) and *n*-dodecyl esters (XIV) of 3,5-dinitrobenzoic acid were applied as test compounds. Solutions containing 5 mg of compound in 1 ml isopropanol were prepared, and 5 μl of these solutions were spotted on the plates. Water–methanol mixtures were used as the eluent; the methanol concentration varied from 0 to 90 vol.% at 10 vol.% intervals. The use of the wide range of methanol concentration was motivated by the very different binding of solutes to the BCDP surface. All experiments were run in four independent parallel determinations. The developments were carried out in sandwich chambers of 22 \times 22 \times 3 cm at room temperature, the distance of development was about 16 cm. After development and drying the plates the spots were detected by their UV–visible spectra.

The R_M value characterizing the molecular lipophilicity in RP-TLC was separately calculated for each solute in each eluent system: $R_M = \log(1/R_F - 1)$. When the coefficient of variation of the parallel determinations was higher than 8% the R_M value was omitted from the following calculations. To increase the reliability of hydrophobicity determination the R_M values were extrapolated to zero organic phase (methanol) concentration: $R_M = R_{M0} + bC$, where R_M is the value for a solute determined at a given methanol concentration; R_{M0} is the R_M value extrapolated to zero methanol concentration (best estimate of the retention capacity of solutes); b represents the decrease in the R_M value caused by 1 vol.% concentration change of methanol in the eluent (related to the specific surface area of solute in contact with the stationary phase) [25]; and C is the methanol concentration in the eluent (vol.%).

To check the validity of the hypothesis that in the case of homologous series of solutes the retention capacity and specific contact surface (R_{M0} and b values above) are strongly intercorrelated [26,27] and linear correlation was calculated between the two chromatographic parameters.

To find the physicochemical parameters of solutes significantly influencing their retention on

BCDP layers stepwise regression analysis was applied [28]. In the common multivariate regression analysis the presence of independent variables which exert no significant influence on the dependent variable lessens the significance level of those independent variables which have significant influence on the dependent variable. To overcome this difficulty stepwise regression analysis automatically eliminates from the selected equation the insignificant independent variables. This procedure increases the information content of the calculation. The retention capacity of solutes (R_{M0} value) is the dependent variable, and the various calculated physicochemical parameters are the independent variables. The physicochemical parameters included in the calculation are:

π = Hansch-Fujita's substituent constant characterizing hydrophobicity [29,30];

H-Ac and H-Do = indicator variables for proton acceptor and proton donor properties, respectively [31];

M-RE = molar refractivity [32];

F and R = electronic parameters characterizing the inductive and resonance effect, respectively [33];

σ = Hammett's constant, characterizing the electron-withdrawing power of the substituent [34];

Es = Taft's constant, characterizing steric effects of the substituent [35];

B1 and B4 = Sterimol width parameters determined by distance of substituents at their maximum point perpendicular to attachment [36,37].

As the character of the correlation (linear or quadratic) had not previously been established the quadratic forms of the above parameters were also included in the calculation.

Table 1

Parameters of linear correlations between the R_M value of 3,5-dinitrobenzoic acid esters and the methanol concentration in the eluent (C, vol.%)

Parameter	$R_M = R_{M0} + bC$ Compound No.					
	I	II	III	IV	V	
n	16	16	14	14	9	
R_{M0}	0.67	0.88	-0.03	-0.09	-0.37	
b	-1.12×10^{-2}	-1.42×10^{-2}	8.24×10^{-3}	9.01×10^{-3}	9.95×10^{-3}	
s_b	9.69×10^{-4}	1.27×10^{-3}	5.90×10^{-4}	8.40×10^{-4}	1.97×10^{-3}	
$F_{\text{calc.}}$	133.57	124.78	195.53	115.13	25.53	
r^2	0.9051	0.8991	0.9422	0.9056	0.7848	
Parameter	Compound No.					
	VI	VII	VIII	IX	X	
n	9	9	12	12	11	
R_{M0}	-0.38	-0.36	-0.34	-0.44	-0.50	
b	1.13×10^{-2}	9.31×10^{-3}	1.21×10^{-2}	1.20×10^{-2}	1.14×10^{-2}	
s_b	1.44×10^{-3}	7.31×10^{-4}	1.66×10^{-3}	1.24×10^{-3}	1.28×10^{-3}	
$F_{\text{calc.}}$	61.57	162.32	53.26	92.52	78.50	
r^2	0.8979	0.9587	0.8419	0.9025	0.8971	
Parameter	Compound No.					
	XI	XII	XIII	XIV		
n	10	10	10	10		
R_{M0}	-0.45	-0.50	-0.80	-1.04		
b	9.21×10^{-3}	9.68×10^{-3}	1.62×10^{-2}	1.79×10^{-2}		
s_b	1.01×10^{-3}	7.14×10^{-4}	1.91×10^{-3}	9.80×10^{-4}		
$F_{\text{calc.}}$	81.98	183.88	72.51	335.21		
r^2	0.9111	0.9583	0.9006	0.9767		

3. Results and discussion

The parameters of linear correlations describing the dependence of the R_M value of the solutes on the methanol concentration in the eluent are compiled in Table 1. In each instance a significant linear correlation was found between the dependent and independent variables. Except for compound V, the significance level was always over 99.9% (see $F_{\text{calc.}}$ values). The change in methanol concentration accounted for 78–98% of the change in R_M value (r^2 values). The fact that the retention of solutes strongly depended on the length of the alkyl chain makes it improbable that inclusion complex formation between the cyclodextrin cavity and the bulky dinitrobenzene group determines the retention behaviour. The role of alkyl substitution can tentatively be explained by the supposition that the longer alkyl chain and not the dinitrobenzene part of the solutes enters the cavities on the surface of the BCDP support. The longer alkyl chain can bind more strongly to the apolar inner surface of the cavity by hydrophobic forces. However, it cannot be excluded that the alkyl chains interact only with the relatively hydrophobic substructures of the BCDP surface formed by the crosslinking agents.

Only the esters with short alkyl chains (methyl and ethyl derivatives) follow the general rule of RP-TLC that their retention decreases with increasing concentration of methanol in the eluent. Esters with longer alkyl chains exhibit markedly anomalous retention behaviour, their retention increasing with increasing methanol concentration. It is assumed that methanol, although forming very weak complexes with cyclodextrins [38], can also enter the cyclodextrin cavity and promote the formation of cyclodextrin–solute–methanol ternary complexes. The stability of the ternary complex increases with increasing concentration of methanol, which results in enhanced retention. Unfortunately, there is no experimental proof to support this hypothesis.

A highly significant linear correlation was found between the adsorption capacity (R_{M0}) and specific contact surface (b) of the solutes: $R_{M0} = 0.15 - 53.34 \cdot b$, $n = 14$, $r_{\text{calc.}} = 0.9613$, $r_{99.9\%} =$

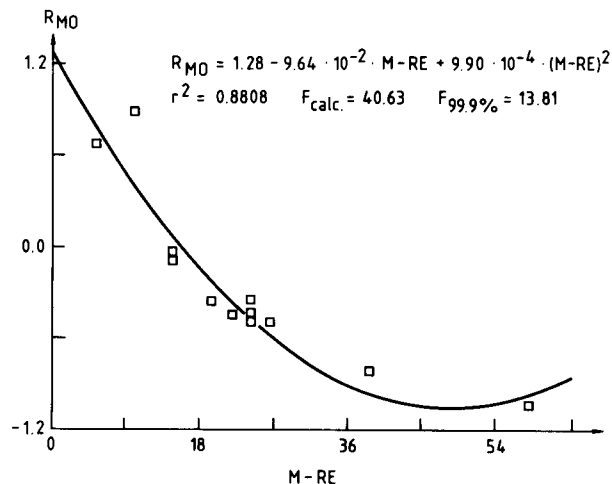


Fig. 1. Relationship between the retention capacity of 3,5-dinitrobenzoic acid esters (R_{M0}) and the molar refractivity (M-RE).

0.7800. This indicates that the strong relationship between the two chromatographic parameters also exists for the BCDP support and the solutes behave from a chromatographic point of view as a homologous series of compounds.

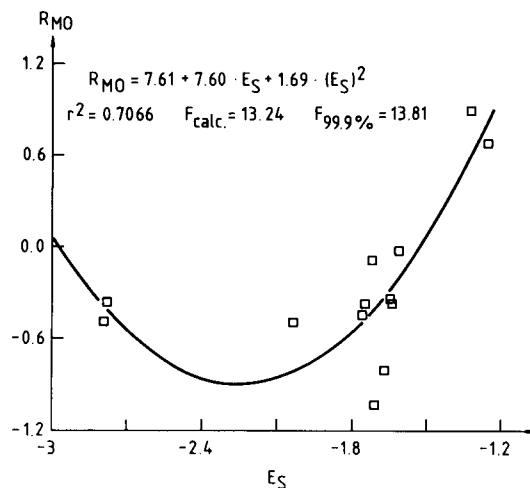


Fig. 2. Relationship between the retention capacity of 3,5-dinitrobenzoic acid esters (R_{M0}) and the steric effect of substituents (E_S).

Marked non-linear correlations were found between the steric characteristics of 3,5-dinitrobenzoic acid esters and their adsorption capacity on the BCDP support (Figs. 1 and 2). The correlations are highly significant, the significance level being over 99 or 99.9% (compare $F_{\text{calc.}}$ values with the tabulated F values). The steric parameters explained 70–88% of the retention capacity of the solutes (see r^2 values). The non-linear dependence of the retention capacity on the steric parameters can easily be explained by the relatively rigid structure of the β -cyclodextrin cavity. Only solutes with certain dimensions can fit well into the cavity. When the molecule is too big or too small, the stability of the complex decreases resulting in increased chromatographic mobility. The considerable impact of steric parameters on the retention indicates also that accessible CD cavities remained on the surface of the BCDP support even after polymerization and they influence the retention behaviour of the support.

It can be concluded that the β -cyclodextrin polymer support exhibits retention characteristics different from those of well-known TLC sorbents. Inclusion complex formation between the solutes and the accessible cyclodextrin cavities on the surface of the BCDP support is involved in the separation mechanism. The steric parameters of solutes have the highest impact on the retention.

Acknowledgements

This work was supported by the OTKA grant 2670.

References

- [1] J. Szejtli, in J.L. Atwood, J.E. Davis and D.D. McNicol (Eds.), *Inclusion Compounds*, Vol. III, Academic Press, London, 1984, p. 331.
- [2] J. Szejtli, *Cyclodextrins and Their Inclusion Complexes*, Akademiai Kiadó, Budapest, 1982.
- [3] B. Feibush, C.L. Wolley and V. Mani, *Anal. Chem.*, 65 (1993) 1130.
- [4] I.D. Smith and C.F. Simpson, *J. High Resolut. Chromatogr.*, 15 (1992) 800.
- [5] M.W.F. Nielen, *Anal. Chem.*, 65 (1993) 885.
- [6] M.J. Stepaniak, R.O. Roderic and B.K. Clark, *J. Liquid Chromatogr.*, 15 (1992) 1023.
- [7] D.W. Armstrong, Y. Tang, T. Ward and M. Nichols, *Anal. Chem.*, 65 (1993) 1114.
- [8] J.S. Bradshaw, G. Yi, B.E. Ossitter, S.L. Reese, P. Petersson, K.E. Markides and M.L. Lee, *Tetrahedron Lett.*, 34 (1993) 79.
- [9] E. Dubrovčakova, B. Gas, J. Vacik and E. Smolkova-Keulemansova, *J. Chromatogr.*, 623 (1992) 337.
- [10] D. Sybilska, A. Bielejewska, R. Nowakowski, K. Duszczyk and J. Jurczak, *J. Chromatogr.*, 625 (1992) 349.
- [11] M.L. Vazquez, C.M. Franco, A. Cepeda, P. Prognon and G. Mahuzier, *Anal. Chim. Acta*, 269 (1992) 239.
- [12] S.C. Chang, L.R. Wang and D.W. Armstrong, *J. Liquid Chromatogr.*, 15 (1992) 1411.
- [13] T. Hargitai and Y. Okamoto, *J. Liquid Chromatogr.*, 16 (1993) 843.
- [14] T. Hargitai, Y. Kaida and Y. Okamoto, *J. Chromatogr.*, 628 (1993) 11.
- [15] C.N. Nakatsu and A.M. Stalcup, *J. Liquid Chromatogr.*, 16 (1993) 209.
- [16] M.L. Hilton, S.C. Chang, M.P. Gasper, M. Pawlowska and A.M. Stalcup, *J. Liquid Chromatogr.*, 16 (1993) 127.
- [17] N. Thuaud, B. Sebillé, A. Deratini, B. Popping and C. Pellet, *Chromatographia*, 36 (1993) 373.
- [18] T. Cserhádi, E. Forgács and A. Ujházy, *Anal. Chim. Acta*, 279 (1993) 107.
- [19] W. Fischer, H.E. Hauck and W. Jost, in F.A.A. Dallas (Ed.), *Recent Adv. Thin-Layer Chromatogr.*, Proc. Chromatogr. Soc. Int. Symp. 1987, Plenum Press, New York, 1988, p. 139.
- [20] L. Witherow, R.J. Thorp, I.D. Wilson and A. Warrander, *J. Planar Chromatogr.*, 3 (1990) 169.
- [21] T. Cserhádi and H.E. Hauck, *J. Chromatogr.*, 514 (1990) 45.
- [22] T. Cserhádi, *J. Chromatogr. Sci.*, 29 (1991) 210.
- [23] J.K. Rozylo and M. Janicka, *J. Planar Chromatogr.*, 3 (1990) 413.
- [24] J.K. Rozylo and M. Janicka, *J. Liquid Chromatogr.*, 14 (1991) 3197.
- [25] C. Horvath, W. Melander and I. Molnar, *J. Chromatogr.*, 125 (1976) 129.
- [26] T. Cserhádi, *Chromatographia*, 18 (1984) 318.
- [27] K. Valkó, *J. Liquid Chromatogr.*, 7 (1984) 1405.
- [28] H. Mager, *Moderne Regressionsanalyse*, Salle, Sauerlander, Frankfurt am Main, 1982, p. 135.
- [29] T. Fujita, J. Iwasa and C. Hansch, *J. Am. Chem. Soc.*, 86 (1964) 5175.
- [30] A. Leo, C. Hansch and M. Ames, *J. Pharm. Sci.*, 64 (1975) 559.
- [31] C. Hansch and A. Leo, *Substituent Constants for Correlation Analysis in Chemistry and Biology*, Wiley, New York, 1979, p. 1.
- [32] L. Pauling and D. Pressman, *J. Am. Chem. Soc.*, 67 (1945) 1003.

- [33] R.W. Taft and I.C. Lewis, *J. Am. Chem. Soc.*, 80 (1958) 2436.
- [34] L.P. Hammett, *Chem. Rev.*, 17 (1935) 125.
- [35] R.W. Taft, *J. Am. Chem. Soc.*, 74 (1952) 3120.
- [36] A. Verloop and J. Tipker, *Pestic. Sci.*, 7 (1976) 379.
- [37] A. Verloop, W. Hoogenstraaten and J. Tipker, in J. Ariens (Ed.), *Drug Design*, Vol. VII, Academic Press, New York, 1976, p. 165.
- [38] A. Buvári, J. Szejtli and L. Barcza, *J. Incl. Phenom.*, 1 (1983/84) 151.

Immobilization of glucosidase onto silica-based, amino functionalized beads for enzymatic hydrolysis of urinary phenol prior to liquid chromatographic analysis

Jen-Fon Jen ^{a,*}, Jen-Haw Zen ^a, Fu-Chou Cheng ^b, Goang-Yean Yang ^b

^a Department of Chemistry, National Chung-Hsing University, Taichung, 402 Taiwan,

^b Department of Medical Research, Taichung Veterans General Hospital, Taichung, 407 Taiwan

(Received 7th September 1993; revised manuscript received 16th December 1993)

Abstract

An amino-functionalized silica commercial liquid chromatography packing material was used instead of controlled-pore glass as the support to react with glutaraldehyde and then to directly immobilize the β -glucosidase. After enzymatic hydrolysis, the urinary phenol was separated by reversed-phase liquid chromatography and monitored by an electrochemical detector at 0.85 V (vs. Ag/AgCl). Factors that affect the immobilization and hydrolysis were investigated. The proposed method provides a simpler procedure with a less expensive material for glucosidase immobilization, and the electrochemical detection avoids the interference from other urinary species and hence simplifies the chromatogram obtained. The detection limit was 0.2 ng with a 20 μ l injection. The relative standard deviations for 1.2 ng and 2.0 ng levels of phenols were 1.16% and 3.38%, respectively.

Key words: Enzymatic methods; Liquid chromatography; Packing materials; Glucosidase immobilization; Phenol; Urinary phenol

1. Introduction

Conjugation of phenols with D-glucuronic acid or sulfate ions is a common metabolic pathway of benzene in human [1–4]. These compounds are regarded as metabolic products for excretion in urine [5,6]. Since in vivo about 30% of all retained benzene finally turns out to be phenol, the urinary excreted phenol is therefore applied in

the evaluation of the biological exposure index (BEI) for benzene.

The conjugates are usually analyzed via chemical or enzymatic hydrolysis procedures, followed by measurement of the liberated phenol [7–10]. The enzymatic hydrolysis using β -glucuronidase or sulfatase is preferred over the acid hydrolysis because of the mild reaction conditions. However, there are some disadvantages for the use of soluble enzymes in hydrolysis, such as high cost, long incubation time, introduction of contamination and potential interference in a chromatogram. Immobilization of enzyme onto a solid

* Corresponding author.

support is an alternative approach to decrease these limitations associated with the soluble enzymatic hydrolysis [11–15]. Controlled-pore glass (CPG) is the most popular support for enzymes determined via a silanization and a glutaraldehyde immobilization scheme [11–19]. Due to occasional difficulties of silanization and the high costs of CPG, a conventional LC-NH₂ liquid chromatographic, silica-based packing material is proposed to substitute for CPG. The LC-NH₂ beads were first reacted with glutaraldehyde, and then with the enzyme.

The purpose of this study is to investigate the optimal conditions for immobilizing glucosidase by using the LC-NH₂ support and for enzymatic hydrolysis to release urinary phenols. A conventional electrochemical detector was used to monitor the phenol species.

2. Experimental

2.1. Apparatus

An ICI LC 1100 pump module equipped with a Rheodyne 7125 injection valve (20- μ l sample loop) and a Spherisorb 5 ODS column (250 \times 4.6 mm i.d., Supelco, Bellefonte, PA) was used as the chromatographic system. An ICI LC 1260 electrochemical detector working at 0.85 V vs. Ag/AgCl, with a DP 800 Analysis System was used to detect and collect the chromatographic data. A Beckman Module 168 diode array detector (PDAD) was also used to detect and identify the separated species.

An UV U-3210 spectrophotometer (Hitachi, Kyoto) was used to detect the enzymatic hydrolysis product (*p*-nitrophenol) at 397 nm.

2.2. Reagents

Distilled-deionized water was used to prepare all solutions. The liquid chromatographic (LC) eluent was prepared from HPLC-grade methanol (Mallinckrodt, St. Louis, MO) and water (30%, v/v, CH₃OH in pH 6.8 phosphate buffer–0.01% H₃PO₄ adjusted with NaOH). The eluent was filtered through a 0.45- μ m PVDF membrane filter and degassed ultrasonically.

β -Glucuronidase, sulfatase (type H-2 from Helix), glutaraldehyde, phenyl β -D-glucuronide, *p*-nitrophenylglucuronide, (3-aminopropyl)diethoxysilane, Tris buffer, *p*-cresol, and Controlled Pore Glass (Stock No. PG-75-400 with 200–400 mesh, 77 Å mean pore diameter, \pm 7.1% pore distribution, 0.47 ml/g pore volume, and 182 m²/g surface area), were all from Sigma (St. Louis, MO). LC-NH₂ supports were obtained from Supelco (Bellefonte, PA, Supelclean LC-NH₂, Cat No. 5-7205) which are silica-based monomerically bonded packings with 40- μ m particles and 60-Å pores. All other chemicals were of analytical grade and obtained from commercial suppliers.

Phosphate buffers (pH 5.0, 5.8, 8.5, 9.5): NaH₂PO₄ (2.3996 g) and Na₂HPO₄ · 2H₂O (7.1196 g) were dissolved in 480 ml water, the pH was adjusted with NaOH (3.0 M) and HCl (1.0 M) and diluted to 500 ml.

Acetate buffer (pH 4.82): acetic acid (0.6005 g) and sodium acetate (4.102 g) were dissolved in 500 ml water.

Tris–HCl buffers (pH 5.00, 6.82, 7.82, 8.50, 9.00, 9.50): tris(hydroxymethyl)aminomethane (24.23 g) was dissolved in 970 ml water, the pH was adjusted with NaOH (1.0 M) and HCl (1.0 M), and the solution was diluted to 1000 ml.

Enzymes in buffer: β -glucuronidase (H-5, contains sulfatase, 5.7 mg) was dissolved in 25 ml acetate buffer solution. Each ml of solution contained 400 IU β -glucuronidase and 200 IU sulfatase. The solution was stored in a refrigerator.

2.3. Immobilization of enzymes

Immobilization onto CPG

The immobilization method used was based on the procedure developed by Bowers and Johnson [20]. The CPG (3.0 g) was first washed with nitric acid (5%) at 90°C for 2 h and then silanized with 10% 3-aminopropyltriethoxysilane (3-APTES) (50 ml in toluene) at 120°C for 24 h. A solution of 25 ml glutaraldehyde (0.5%) in acetate buffer (pH 4.82) was reacted with the activated CPG for 1 h at room temperature to generate aldehyde functional groups on CPG for the reaction with the enzymes. Excess glutaraldehyde was removed by

washing with 100 ml each of water and then acetate buffer (pH 4.82). β -Glucuronidase (5.7 mg in 25 ml acetate buffer, pH 4.82) was attached onto the modified CPG by reaction with gentle stirring for 1 h and standing overnight at 4°C. The immobilized CPG was then washed with 200 ml each of water and Tris buffer (pH 7.82) to remove any absorbed or entrapped enzymes. The immobilized β -glucuronidase was stored in a refrigerator (4°C) by wetting with Tris buffer (pH 7.82).

Immobilization onto the LC-NH₂ solid support

The LC-NH₂ beads (3.0 g) were reacted directly with 25 ml of glutaraldehyde (0.5% in water) in a 50-ml flask for 1 h at room temperature to generate aldehyde functional groups there. At this time, the LC-NH₂ beads turned from white to yellowish. After filtration, excess glutaraldehyde was removed by washing with 100 ml each of water and acetate buffer (pH 4.82). β -Glucuronidase (5.7 mg in 25 ml acetate buffer, pH 4.82) was attached to the modified LC-NH₂ beads by reaction with gentle stirring at room temperature for 1 h and standing overnight at 4°C. After pipetting the solution, the immobilized LC-NH₂ beads were washed with 200 ml each of water and Tris buffer (pH 7.82) to remove any absorbed or entrapped enzymes. The immobilized β -glucuronidase was stored in a refrigerator after wetting with Tris buffer (pH 7.82) at 4°C.

2.4. Determination of the immobilized enzyme activity

After the immobilization of enzyme, it was necessary to determine the quantity of glucuronide which could be hydrolyzed. A 10 ppm ($\mu\text{g/ml}$) *p*-nitrophenylglucuronide solution (10 ml) was mixed with the immobilized enzyme product (0.5 g) in a rotary evaporator at 150 rpm at 30°C for 2 min. The resulting *p*-nitrophenol was separated and determined by LC with electrochemical detection (ECD). The activity of the immobilized enzyme was evaluated. (1 U = the amount of enzyme required to hydrolyze *p*-nitrophenylglucuronide and to produce one μmol of *p*-nitrophenol per min)

2.5. Collection and pretreatment of urine samples

The urine samples were collected in 100-ml pyrex glass flasks and frozen immediately. They were stored in a freezer (–20°C) until analyzed. When the sample was analyzed, it was first defrozen at room temperature, and the suspended matter removed by centrifugation (1000 rpm) for 10 min. Finally the sample was filtered through a 0.45- μm PVDF membrane filter, and was ready for pre-column enzymatic hydrolysis.

2.6. Pre-column enzymatic hydrolysis of urine samples

After 1 + 6 dilution with Tris buffer (0.1 M, pH 7.82) the diluted urine sample solution (3 ml) was mixed with 0.5 g of the immobilized enzyme product in a rotary evaporator (150 rpm) at 30°C for 20 min. After filtration, the hydrolyzed solution was ready for chromatographic analysis.

3. Results and discussion

The reactions related to the immobilization of enzyme onto various supports have been discussed elsewhere [15,21,22], and will not be described here. However, the optimal conditions of immobilization on various supports are different. Thus, factors that affect the immobilization of β -glucuronidase and sulfatase onto the LC-NH₂ support, such as concentration of glutaraldehyde and coupling reaction time, were studied to find the optimum immobilized conditions. In addition, factors that influence the hydrolysis activity of immobilized enzyme, such as amounts of enzyme, reaction time, buffer pH, temperature and urine concentration, were also investigated.

3.1. Immobilization of enzyme onto LC-NH₂

Because glutaraldehyde acted as the coupling bridge between the LC-NH₂ support and the enzyme, the bonded glutaraldehyde had great influence on the coupling of β -glucuronidase and sulfatase and thus on the hydrolysis efficiency.

The influence of glutaraldehyde in the coupling reaction on hydrolysis efficiency is demonstrated in Fig. 1. It indicates that the activity of immobilized enzymatic hydrolysis decreases as the glutaraldehyde concentration increases. This is due to the coupling of two NH_2 groups between the LC- NH_2 supports with glutaraldehyde. More seriously, polymerization of LC- NH_2 supports will arise through the glutaraldehyde bridge if much excess of glutaraldehyde is added. Hence, the bonding sites for enzyme on the modified supports decreased as the concentration of glutaraldehyde increased, and thus caused the decrease of hydrolysis efficiency. Fig. 2 is the influence of reaction time for enzyme bonding on the hydrolysis efficiency. Initially, the efficiency increased as the time increased and reached a maximum in about 1 h, then decreased smoothly. Therefore, 1-h reaction in the enzyme immobilization is chosen to obtain the optimum activity of the immobilized enzymatic hydrolysis.

3.2. Comparison of the enzyme activity immobilized on LC- NH_2 to that on CPG

The enzyme activities immobilized onto LC- NH_2 and onto CPG were compared by determin-

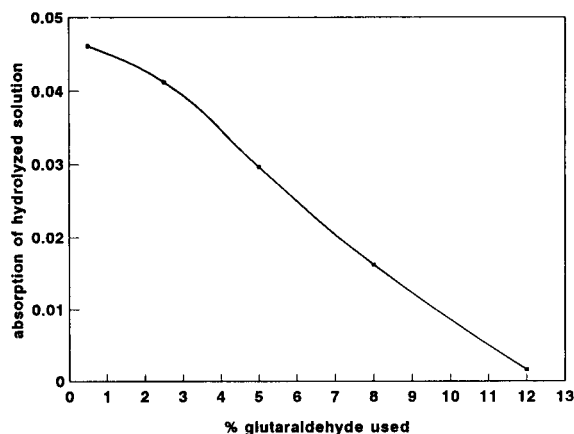


Fig. 1. Influence of glutaraldehyde usage on the immobilized enzymatic hydrolysis. Enzymatic hydrolysis of *p*-nitrophenylglucuronide (10 ppm, 10 ml) at pH 7.82 and 30°C for 10 min by immobilized enzyme with different amounts of glutaraldehyde for bridging glucosidase onto LC- NH_2 . The hydrolysis product was detected by UV at 397 nm.

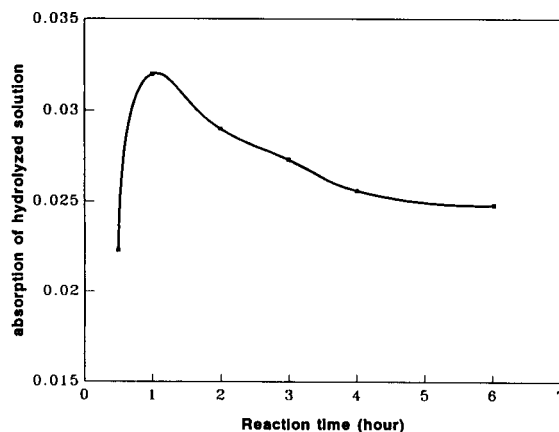


Fig. 2. Influence of the time for the enzyme-bonding reaction on enzymatic activity. Enzymatic hydrolysis of *p*-nitrophenylglucuronide (10 ppm, 10 ml) at pH 7.82 and 30°C for 10 min by immobilized enzyme produced with different enzyme-bonding reaction. The hydrolysis product was detected by UV at 397 nm.

ing their hydrolysis efficiencies with 10 ppm *p*-nitrophenylglucuronide (10 ml). The hydrolysis products were analyzed by LC. According to the definition of activity unit, the LC- NH_2 support carried 19.2 units of enzyme activity, whereas the CPG support carrier only 10.4 units. This difference might derive from less NH_2 sites placed on CPG support which could relate to the surface area of the supports or unskillful silanization of CPG to provide NH_2 groups. Immobilization of enzyme onto the LC- NH_2 support therefore has the advantages of higher enzymatic activity, a simpler process and lower price. It is also easy to handle.

3.3. Enzymatic hydrolysis of *p*-nitrophenylglucuronide

In order to investigate factors such as amounts of immobilized enzyme, reaction time, temperature, pH, and urine matrix, that affect the hydrolysis efficiency, *p*-nitrophenylglucuronide was used as the reference sample for enzymatic hydrolysis. Fig. 3 shows the hydrolysis of *p*-nitrophenylglucuronide with various amounts of immobilized enzyme at different reaction times. As expected, the extent of hydrolysis increased initially with

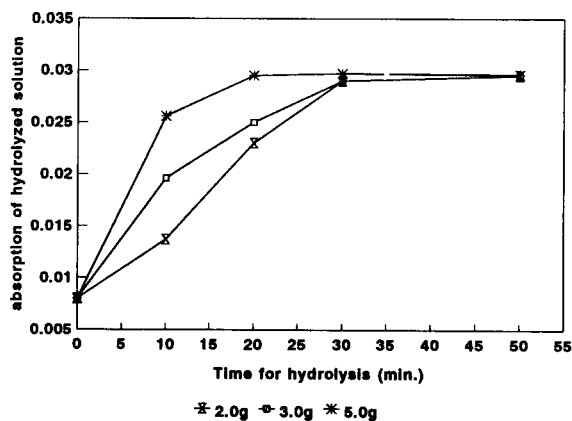


Fig. 3. Hydrolysis of *p*-nitrophenylglucuronide under varied amounts of immobilized enzyme and reaction time. Enzymatic hydrolysis of *p*-nitrophenylglucuronide (10 ppm, 10 ml) at pH 7.82 and 30°C. The hydrolysis product was detected by UV at 397 nm.

time initially, then reached a constant value after several minutes of reaction. Meanwhile, the hydrolysis efficiency also increased with the increase in amount of immobilized enzyme used. Fig. 4 shows the variation of UV spectra during the enzymatic hydrolysis. Spectrum A is for *p*-nitrophenylglucuronide before hydrolysis, B and C are those for 30 min and 50 min of reaction, respectively. The characteristic absorbance of *p*-nitrophenylglucuronide at 301.8 nm decreased from 0.358 and 0.156 to 0.097, and the 397 nm absorbance for the hydrolysis product (*p*-nitrophenol) increased from 0.03 and 0.089, to 0.148 as the reaction proceeded. These results confirmed the occurrence of enzymatic hydrolysis.

Enzyme activity increased as the temperature increased. However, a higher temperature (over 40°C) might destroy the enzyme activity. Thus, the enzymatic hydrolysis was chosen at 30°C for the study. Usually, the enzyme activity is also affected by the pH. Fig. 5 shows the effect of pH on enzyme activity. As can be seen, the immobilized enzyme has optimal activity at pH 7.8 which is somewhat higher than those while using the soluble enzymes. Bowers [21] explained this phenomenon as being an interaction of the support

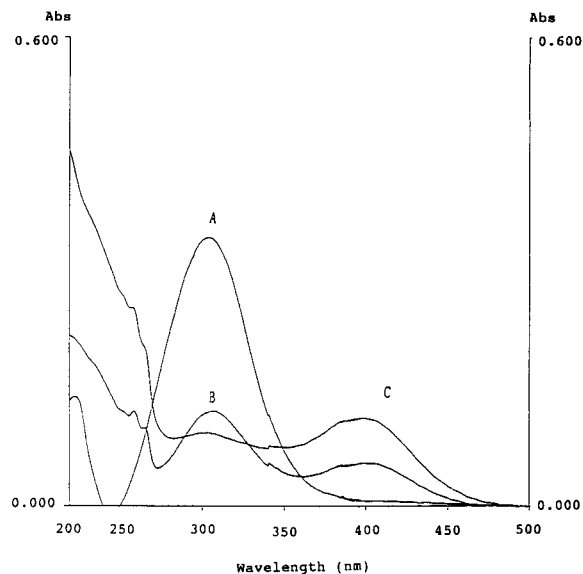


Fig. 4. Variation of UV spectra in the immobilized enzymatic hydrolysis of *p*-nitrophenylglucuronide. Enzymatic hydrolysis of *p*-nitrophenylglucuronide (10 ppm, 10 ml) at pH 7.82 and 30°C. The hydrolysis product was detected by UV scanning from 200 to 500 nm. Scan speed, 120.0 nm/min, and 2.00 nm band pass.

with the active site of the enzyme or being the result of a difference between the bulk properties of solution and the microenvironment near the

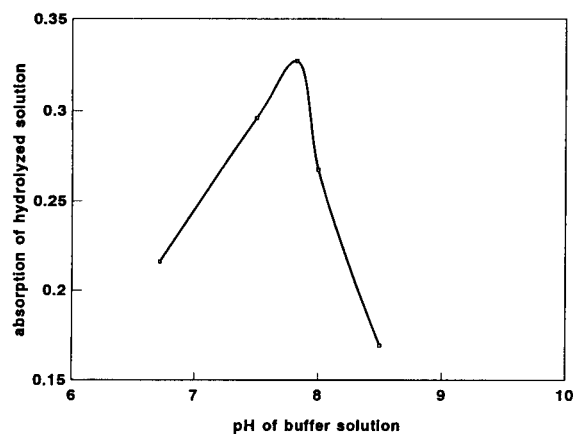


Fig. 5. Effect of pH on the immobilized enzymatic hydrolysis. Enzymatic hydrolysis of *p*-nitrophenylglucuronide (10 ppm, 10 ml) with 0.5 g immobilized enzyme at 30°C for 10 min. The hydrolysis product was detected at 397 nm.

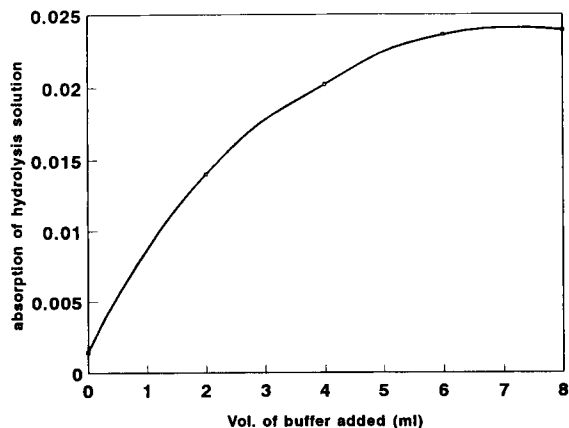


Fig. 6. Influence of urine matrix on the immobilized enzymatic hydrolysis.

enzyme. Possibly, as the enzyme was immobilized onto the LC-NH supports, the pH around the enzyme (microenvironment) decreased due to the attraction of H^+ . Thus, the pH of the bulk solution is greater than the pH experienced by the enzyme. So, the optimal pH for the immobilized-enzyme on the LC-NH₂ support was higher than those of the soluble enzymes in hydrolysis.

3.4. Effect of urine concentration

The complicated urine matrix is toxic to the enzymes and causes a decrease in enzyme activity. Because it is difficult to remove the toxic matrix, the dilution method was therefore investigated to maintain the enzyme activity. Tris buffer (0.1 M, pH 7.82) was used to dilute urine by 1 + 0, 1 + 2, 1 + 4, 1 + 6 and 1 + 8 (urine to buffer). Each 1.0 ml diluted urine sample was taken and mixed with 1.0 ml of *p*-nitrophenyl-glucuronide (10 ppm) as the hydrolyzed samples. A 0.5 g sample of immobilized enzyme (onto LC-NH₂) was used for the enzymatic hydrolysis for 20 min, and the absorbance was measured at 397 nm for *p*-nitrophenol. Fig. 6 shows the influence of dilution on the enzyme activity. As can be seen from Fig. 6, the peak UV absorbance values for the 1 + 6 and 1 + 8 dilutions are identical. Thus, a 1 + 6 dilution of urine sample is recommended.

3.5. Chromatographic separation and detection of phenol in urine

Owing to the high content of *p*-cresol in urine, the solution after enzymatic hydrolysis can not be detected by UV directly. Therefore, a chromatographic separation is necessary prior to the phenol determination. Because there are many UV detectable species in urine, there would be serious interferences if a UV detector was used. The high selectivity electrochemical detector therefore was used to detect the separated species. Fig. 7 shows the chromatogram of a urine sample after enzymatic hydrolysis by reversed-phase LC with electrochemical detection. The separated species were compared with the reference sample in retention behaviours. This was also verified with a photodiode array detector at 215 and 270 nm by scanning the peaks between 200 and 500 nm. Table 1 lists the spectrophotometric charac-

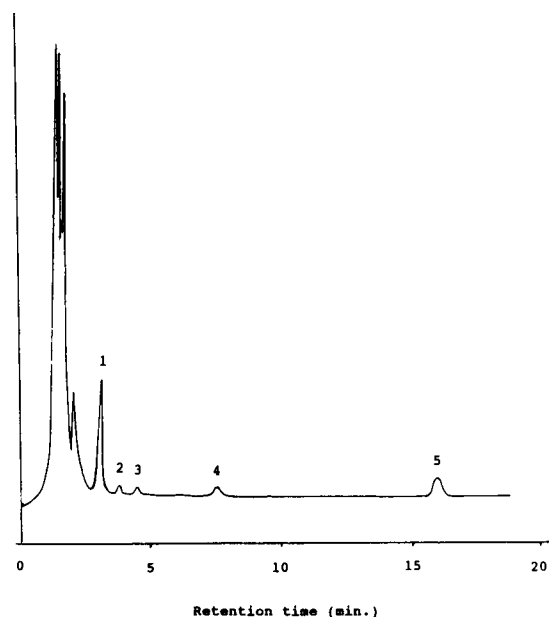


Fig. 7. The chromatogram of a urine sample after the immobilized enzymatic hydrolysis by RP-LC with electrochemical detection. Elution: 30% methanol in water at pH 4.15 adjusted by H_3PO_4 , with a Spherisorb 5 ODS column. Flow-rate, 1.0 ml/min. Detection, electrochemical at 0.85 V (vs. Ag/AgCl). Peak 4 is phenol, peak 5 is *p*-cresol, and peaks 1–3 are other electrochemically-detective species.

Table 1
Retention times and UV absorption characteristics of enzymatic hydrolysis products^a and their reference standards by LC with photodiode array detection^b

Hydrolysis products			Reference standards		
Peak no. in Fig. 7	Retention time (min)	λ_{\max} (nm)	Compound	Retention time (min)	λ_{\max} (nm)
1	2.96	220			
2	3.56	217			
3	4.22	232			
4	7.59	214, 270	Phenol	7.62	214, 270
5	15.97	232, 277	<i>p</i> -Cresol	16.02	232, 277

^a The enzymatic hydrolysis was performed as: after removing the suspended material (1000 rpm for 10 min and filtration using a 0.45- μ m filter), the urine sample was diluted with Tris buffer (1+6), and then hydrolyzed by immobilized enzyme under 30°C for 20 min.

^b Detection was at 215 and 270 nm by photodiode array, and UV-visible spectra were scanned in the 200–500 nm range.

teristics of these species. Peaks 4 and 5 in Fig. 7 were agreed well with those for phenol and *p*-cresol, respectively. Peaks 1–3 were other electrochemically detected species in the hydrolyzed urine sample. Comparison with the further oxidation products of phenol (hydroquinone, resorcinol, catechol and 1,4-benzoquinone), these peaks were found not to correspond to these species. When using the electrochemical detector, the applied potential should not too high to maintain selectivity and obtain a stable baseline. According to the cyclic voltammogram of phenol and considering the sensitivity, 0.85 V vs. Ag/AgCl was chosen as the applied potential for phenol determination. It should be noted that polymerization products from phenolic compounds adsorbed on the surface of the glassy-carbon electrode after long-time use should be removed daily to ensure the quality of detection.

3.6. Calibration graphs and detection limits

In order to test the applicability of the proposed method for the determination of phenol in hydrolyzed urine samples, a linear calibration graph for peak area was obtained for 0.1–5.0

ppm as phenol (correlation coefficient > 0.999, $n = 6$). The reproducibilities were examined with five replicate enzymatic hydrolysis of 60 and 100 ppb phenylglucuronide. After four 20 μ l injections of each hydrolyzed solution into the chromatographic system, peak areas were measured and the relative standard deviations were calculated. The R.S.D. values were 1.16 and 3.38% for 1.2 ng (60 ppb sample) and 2.0 ng (100 ppb sample) injections, respectively. The instrumental detection limit was 0.2 ng (20 μ l) based on the three times the average background noise level.

3.7. Analysis of a real urine sample from a refinery worker

A urine sample collected from a refinery worker was analyzed with the standard addition method by the proposed enzymatic hydrolysis chromatographic procedure under the optimal experimental conditions. Because phenol was readily oxidized, the enzymatic hydrolysis and other treatments were deaerated by purging with nitrogen gas. The phenol concentration in the urine was found to be 33 ng/g and the *p*-cresol concentration was 1.2 μ g/g. Compared to the creatinine content (85 mg/100 ml urine), the phenol content was 0.039 mg and the *p*-cresol content was 14.1 mg per g of creatinine.

4. Conclusions

In this study, the proposed method was proved to be an effective alternative to other hydrolysis and analytical methods for the determination of phenol in urine samples. With a cheaper LC-NH₂ material and a convenient procedure, the glucosidase was immobilized and a high efficiency of enzymatic hydrolysis was obtained. The resulting chromatographic method offered a stable baseline, high selectivity and sensitivity in urinary phenol determination. This technique can be used to determine the phenol content in urine and can thus also be used as a biological exposure index for benzene.

Acknowledgements

The authors thank the National Science Council of Taiwan for financial support under grant Number NSC 81-0421-E-005-19-Z and the financial support from Taichung Veterans General Hospital.

References

- [1] M.A. Medinsky, P.J. Sabourin, G. Lucier, L.S. Birnbaum and R.F. Henderson, *Toxicol. Appl. Pharmacol.*, 99 (1989) 193.
- [2] D.V. Parake and R.T. Williams, *Biochemistry*, 55 (1953) 337.
- [3] P.J. Sabourin, W.E. Bechtold and R.F. Henderson, *Toxicol. Appl. Pharmacol.*, 99 (1989) 421.
- [4] P.J. Sabourin, W.E. Bechtold and R.F. Henderson, *Anal. Biochem.*, 170 (1988) 316.
- [5] C.G. Hunter and D. Blair, *Ann. Occup. Hyg.*, 15 (1972) 193.
- [6] R.J. Sherwood, *Ann. Occup. Hyg.*, 15 (1972) 409.
- [7] M.K. Baldwin, M.A. Selby and H. Bloomberg, *Analyst*, 106 (1981) 763.
- [8] O. Inoue, K. Seiji, M. Kasahara, H. Nakatsuka and W. Ikeda, *Br. J. Ind. Med.*, 43 (1986) 692.
- [9] L. Drummond, R. Luck, A.S. Afacan and H.K. Wilson, *Br. J. Ind. Med.*, 45 (1988) 256.
- [10] G. Chiavari and V. Concialini, *Analyst*, 113 (1988) 91.
- [11] H.H. Weetall, *Anal. Chem.*, 46 (1974) 602A.
- [12] V.K. Boppana, R.K. Lynn and J.A. Ziemniak, *J. Pharm. Sci.*, 78 (1989) 127.
- [13] E. Rapatz, A. Travnicek, G. Fellhofer and F. Pittner, *Appl. Biochem. Biotechnol.*, 19 (1988) 223.
- [14] S. Oscarsson and J. Carlsson, *Analyst*, 116 (1991) 787.
- [15] G. Marko-Varga and E. Dominguez, *Trends Anal. Chem.*, 10 (1991) 290.
- [16] P.J. Robinson, P. Dunnill and M.D. Lilly, *Biochim. Biophys. Acta*, 242 (1971) 659.
- [17] M.M. Hossain and D.D. Do, *Biotechnol. Bioeng.*, 27 (1985) 842.
- [18] L.L. Klopff and T.A. Nieman, *Anal. Chem.*, 57 (1985) 46.
- [19] V.K. Boppana, K.-L. Fong, J.A. Ziemniak and R.K. Lynn, *J. Chromatogr.*, 353 (1986) 231.
- [20] L.D. Bowers and P.R. Johnson, *Anal. Biochem.*, 116 (1981) 111.
- [21] L.D. Bowers, *Anal. Chem.*, 58 (1986) 513A.
- [22] L. Gorton, E. Csöregi, E. Domínguez, J. Emnéus, G. Jönsson-Pettersson, G. Marko-Varga and B. Persson, *Anal. Chim. Acta*, 250 (1991) 203.

Experimental studies on the enrichment of carboxylic acids with tri-*n*-octylphosphine oxide as extractant in a supported liquid membrane

Yin Shen, Lena Grönberg, Jan Åke Jönsson *

Department of Analytical Chemistry, University of Lund, P.O. Box 124, S-221 00 Lund, Sweden

(Received 27th September 1993; revised manuscript received 24th January 1994)

Abstract

The enrichment of carboxylic acids using a supported liquid membrane was experimentally studied. A supported PTFE membrane was impregnated with a solution of tri-*n*-octylphosphine oxide (TOPO) dissolved in di-*n*-hexyl ether (DHE). TOPO was found to be an effective extractant, especially for highly polar acids. The extraction efficiency and the memory effects of the acids were investigated under various conditions of TOPO content and pH of the acceptor phase. It was observed that the pH of the acceptor phase had a great influence on the memory effect and extraction efficiency when using the TOPO-containing membrane; these effects were more pronounced for highly polar acids. The mechanisms of the extraction and the memory effects of carboxylic acids and also the influence of the co-diffusion of carbonic acid on the extraction are discussed.

Key words: Carboxylic acids; Extraction; Supported liquid membrane; TOPO

1. Introduction

Determination of carboxylic acids at low concentrations usually necessitates enrichment in order to improve the detection limit. The conventional enrichment techniques for short chain carboxylic acids from water are distillation, solvent extraction or a combination of both [1,2]. However, the conventional solvent extraction of the most polar short chain carboxylic acids is difficult because of their high degree of hydrophilicity, and hence unfavourable distribution coefficients.

Improved efficiency can be obtained by adding a second component, an extractant, to the solvent to facilitate the extraction [2].

The supported liquid membrane (SLM) technique for on-line enrichment has been used in our laboratory for a wide range of compounds in various matrices [3,4]. The principle of the enrichment is a liquid extraction and back extraction of the analytes from an aqueous donor stream, through a hydrophobic liquid membrane, into a stagnant aqueous acceptor phase. By careful choice of solvent for the impregnation of the membrane, combined with a proper composition of donor and acceptor phases, a selective preconcentration and an efficient clean-up of the sam-

* Corresponding author.

ple can be achieved simultaneously. Considering the extraction of organic acids, the selectivity in the process is achieved by adjusting pH of the two phases so the uncharged species pass the membrane by diffusion and are trapped by ionization in a stagnant acceptor phase [4].

Facilitated transport through a liquid membrane using a chemical extractant (carrier) dissolved in the membrane liquid enhances the flux of the analyte through the membrane [5–7]. This enhancement of the flux is due to a reversible reaction between the analyte and the extractant molecules [8]. It has been found that the addition of tri-*n*-octylphosphine oxide (TOPO) as a carrier to the liquid membrane promoted the flux of carboxylic acids [9,10].

TOPO is known as an efficient extractant for carboxylic acids [5]. Owing to the two lone electron pairs on the oxygen atom, TOPO has the ability to form hydrogen-bond complexes of various composition [11–14]. Therefore, it is particularly useful in the extraction of acids, especially highly polar acids. Moreover, TOPO is very stable when used in a liquid membrane, as it is soluble in organic solvents but insoluble in water.

Kue and Gregor [5] investigated the reversible reaction between acetic acid and TOPO in a liquid membrane. The phase equilibrium constants and apparent diffusion coefficients of acetic acid through these membrane were measured. The extraction rate and mechanism of volatile fatty acids transferred from the acid source across the SLM to a basic acceptor solution was measured by Nuchnoi et al. [9] and Yano et al. [10]. It was observed that only undissociated acids can penetrate into the membrane and that complex formation between TOPO and the acids (1:1 mole ratio) inside the membrane enhanced the transfer rate of the acids across the membrane. Hano et al. [15] examined the recovery of organic acids from fermented broth by the application of a liquid surfactant membrane, containing TOPO as a carrier. The solvation numbers of the acids were found to be the same as the numbers of the carboxyl groups in the each acid molecule. The permeation rate of the acids was in the order: monocarboxylic acid > dicarboxylic acid > tricarboxylic acid.

The analytical application of SLM with TOPO as a extractant for preconcentration and determination of carboxylic acids was developed in our group [16]. Air samples were enriched by means of a SLM incorporated in a flow system connected on-line to an ion exclusion column. It was observed that the memory effects, i.e., organic acids remaining in the membrane during the back extraction, was an important factor influencing the recovery of the acids.

In this paper PTFE supported membranes impregnated with solutions of TOPO dissolved in di-*n*-hexyl ether (DHE) were studied for extraction of carboxylic acids. The influence of the TOPO concentration in the membrane as well as the acceptor phase pH on the extraction efficiency and on the memory effect were investigated. The mechanisms of the extraction and the influence of the co-diffusion of carbonic acid on the extraction are discussed.

2. Experimental

2.1. Membrane and flow system

Details about the construction and operation of the flow system were as published in Ref. 16 so only a short description is given here. The PTFE membrane (TE 35 Membrane filter, Schleicher and Schuell, Dassel, Germany) with a pore size of 0.2 μm was cut to $36 \times 77 \text{ mm}^2$. The membrane was immersed in the selected organic liquid for 30 minutes and then clamped between two blocks of PVDF (polyvinylidene difluoride) with meander channels (0.1 mm deep, 2.5 mm wide and 750 mm long, 188 μl) facing each other. Thereby the membrane, containing an organic phase, separates the donor and acceptor aqueous phases. The membrane unit was incorporated in a flow system as shown in Ref. 16, connected together with PTFE tubing and screw fittings.

A peristaltic pump and pneumatic actuators were used to provide the flow. The system was controlled by a personal computer using the JCL6000 chromatography data system (Jones Chromatography).

2.2. Operation of the enrichment system

The sample is injected via a 3-ml sample loop and introduced into a water stream and mixed with 1 M HCl in a knitted tube reactor, resulting in a pH of ca. 1. The neutralized carboxylic acids diffuse into the liquid membrane, and are trapped in the acceptor side in a stagnant alkaline solution. After the entire sample has passed the membrane unit, the enriched sample is pushed into a 300- μ l injection loop and injected into the chromatographic column.

The donor and acceptor channels are washed with the corresponding solutions for 3 min before the membrane unit is used for the next extraction. The enrichment time is determined by the volume of the sample loop and the flow rate. A typical enrichment time for a 3.0-ml loop is 23 min, which is equal to the chromatographic analysis time.

2.3. Chromatographic equipment

A Dionex 4000i ion chromatographic system fitted with a HPICE-AS1 column and an anion micro membrane suppressor (AMMS-ICE) was used. Eluent and regenerant were 1 mM HCl and 5 mM tetrabutylammonium hydroxide with 0.8 ml/min and 2 ml/min flow rates, respectively. The injected volume was 300 μ l. The chromatograms were collected and handled by the JCL6000 chromatography data system.

2.4. Studies of memory effects

The overall memory effect OME is defined as the quotient $P_b/(P_b + P_s)$. P_s and P_b are the peak areas of an enriched sample and a subsequent blank, respectively.

To investigate the membrane memory effect (MME), which is the major part of the OME, caused by sample remaining in the membrane, the following procedure was undertaken.

After a sample had been enriched, the donor and acceptor channels were washed for 3 min and then the pump was stopped. After a certain time interval (stop time), the acceptor solution, which contains analyte desorbed from the membrane,

was pumped into the injection loop for analysis. With the peak area (P_m) measured in such a procedure, the MME is calculated as the ratio $P_m/(P_m + P_s)$.

2.5. Determination of extraction efficiency

The extraction efficiency (E) is defined as the fraction of the analyte extracted into the acceptor phase to the total amount of analytes in the sample:

$$E = C_a V_i / (C_d V_s)$$

where C_a is the concentration of analyte in the acceptor measured after extraction as a peak area, related to a calibration graph, V_i the volume of the injection loop, C_d the concentration of analyte in the sample before extraction. This was separately measured with manual introduction of the sample into the injection loop, and V_s is the volume of the sample loop.

2.6. Chemicals

The acids studied are listed in Table 1. Stock solutions (20 mM) of these acids were prepared in water and 0.5 ml chloroform (Merck, Darmstadt) per 100 ml was added as a biocide. The solutions were stored in a refrigerator. Di-*n*-hexyl ether (Sigma, St. Louis, MO) and tri-*n*-octylphosphine oxide (Fluka, Buchs) were used as components in the membrane. Tetrabutylammonium hydroxide (1.5 M) was also obtained from Fluka. Tris(hydroxymethyl)aminomethane (Tris), sodium carbonate and hydrochloric acid were from Merck, and sodium hydroxide from EKA

Table 1
Carboxylic acids studied

Name	Abbreviation	Source	p <i>K</i> _{a1} , p <i>K</i> _{a2} [18]
Malic acid	Ma	Sigma	3.40, 5.11
Lactic acid	La	BDH	3.08
Formic acid	Fo	Merck	3.75
Acetic acid	Ac	Merck	4.75
Propanoic acid	Pr	Aldrich	4.87
Butanoic acid	Bu	BDH	4.81
Succinic acid	Su	Merck	4.16, 5.61

(Bohus, Sweden). The water was purified with a Milli-Q/RO4-unit (Millipore, Bedford, MA).

3. Results and discussion

3.1. Influence of TOPO concentration on the extraction efficiency

The extraction of various carboxylic acids in membranes with 0–20% TOPO in DHE was studied. The extraction efficiency depended strongly on the concentration of TOPO in the membrane as can be seen in Fig. 1. The highly polar hydroxy acids (malic and lactic acid) were not extracted with the 0% TOPO membrane. With this membrane, the extraction efficiency of the other acids increased with the carbon chain length. For most acids, the extraction efficiency increased with the TOPO concentration in the whole range, only propanoic and butanoic acid showed a slight decrease at high TOPO concentrations. These acids have the lowest polarities and are less efficiently extracted with a highly polar membrane.

Comparing lactic acid with malic acid, acetic acid with formic acid and butanoic acid with

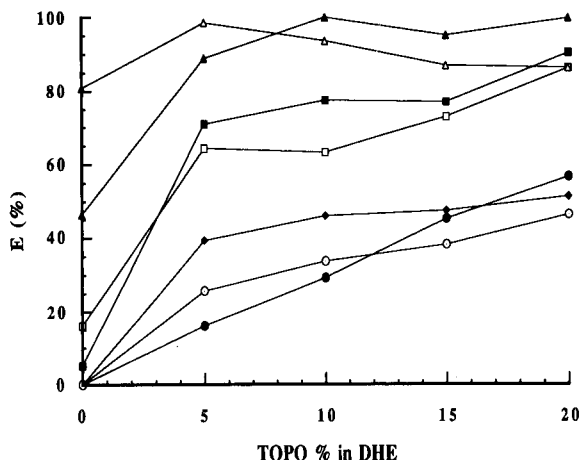


Fig. 1. Influence of TOPO content (%) in DHE on extraction efficiency (E , mean of 4 successive injections). Pyruvic, ◆; malic, ●; lactic, ○; formic, ■; acetic, □; propanoic, ▲; and butanoic acid, △. Acceptor solution: 20 mM NaOH. Sample concentration: 20 μ M.

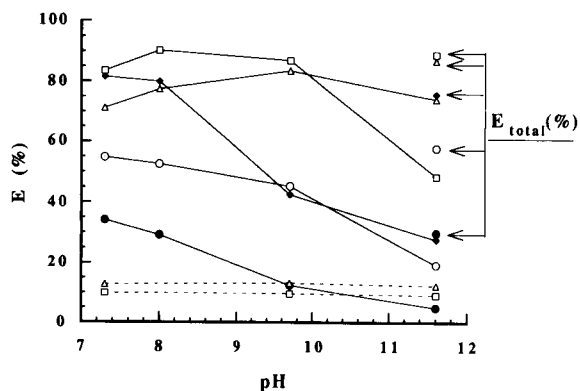


Fig. 2. Influence of acceptor pH on extraction efficiency (E). Malic, ●; succinic, ◆; lactic, ○; formic, □; acetic acid, △. Membrane: 10% TOPO in DHE (solid lines), 0% TOPO in DHE (dashed lines). Acceptor phase: 50 mM tris buffer. Sample concentration: 20 μ M. For E_{total} , see the text.

propanoic acid, respectively, it can be seen that the extraction efficiency of the more polar acid in each pair increased faster with TOPO content than the less polar acid. Pyruvic, malic and lactic acid show generally lower extraction efficiencies than the other acids. These observations are in agreement with Hano et al. [15]. A concentration of TOPO higher than 20% was found to be impractical since TOPO would precipitate within half an hour.

3.2. Influence of acceptor solution and TOPO concentration

The pH of the acceptor phase is critical for a selective and efficient trapping of the acids. According to Ref. 17, the condition of $pH > pK_a + 3.3$ is necessary to prevent the acids from re-entering the membrane.

A Tris buffer solution was chosen as acceptor phase since it was found that this buffer did not introduce any additional interfering ions into the chromatogram. Figs. 2 and 3 show the influence of the acceptor phase pH on the extraction efficiency (E) and on the overall memory effect (OME), respectively, of some carboxylic acids extracted with a 10% TOPO membrane. In the pH range 7–12, the efficiency decreased while the memory effect increased with pH. This effect was

especially pronounced for malic and succinic acid. The same experiment was performed with a membrane of 0% TOPO, but the same phenomenon was not found for formic and acetic acid (dotted lines in the figures). Since no malic, succinic and lactic acid was extracted with the DHE membrane, the effect could not be evaluated for these acids. However, the results suggest that the unexpected decrease in extraction efficiency with pH is related to the presence of TOPO.

In previous experiments [16] a NaOH solution was used as acceptor solution. It was found that the pH dropped during the extraction due to transfer of the carboxylic acids as well as HCl from the donor. This fact suggested that a high concentration of the NaOH solution should be used, but unexpectedly, the extraction efficiency was found to decrease when the NaOH concentration was too high. This effect was therefore studied in more detail.

Table 2 lists the pH of the acceptor phase as well as the E and OME values of some acids trapped in different concentrations of the NaOH solutions. The pH was measured with a universal pH indicator paper, drop by drop when the enriched sample was pumped out from the separator. The pH intervals shown in the table correspond to the lowest and highest values measured.

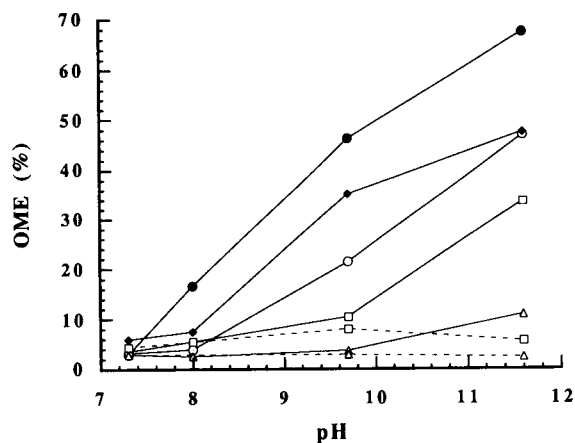


Fig. 3. Influence of acceptor pH on overall memory effect (OME). Symbols and conditions as in Fig. 2.

Table 2

Influence of acceptor phase on extraction efficiency (E) and overall memory effect (OME)

[NaOH] _{acceptor} (mM)		5	10	20	50
pH before extraction		11.5	12	12	> 12
pH after extraction		5–8	6–9	7–10	> 12
Malic acid	E (%)	22.8	31.9	23.1	19.9
	OME (%)	1.0	13.2	27.1	39.9
Lactic acid	E (%)	28.6	44.1	33.3	20.5
	OME (%)	22.2	13.5	18.0	34.2
Formic acid	E (%)	66.4	91.6	87.9	55.9
	OME (%)	5.3	7.8	7.5	27.6
Acetic acid	E (%)	35.4	73.1	70.7	49.1
	OME (%)	6.0	7.3	6.8	26.1
Butanoic acid	E (%)	47.2	88.5	93.9	87.2
	OME (%)	15	2.3	0	8.9

Membrane: 10% TOPO in DHE.

The variations of E and OME with pH show the same tendencies as with Tris buffer (see Figs. 2 and 3), except in the case of the lowest concentration of NaOH (5 mM). The relatively low efficiency for this case is a result of insufficient alkalinity.

In Table 2 it is seen that the decrease in extraction efficiency found at high pH of the acceptor phase is caused by an increased memory effect.

Another observation was that, at high pH, not only was OME increased, but so was the time required for the back extraction of the acids from the membrane. One blank was not enough to release all the remaining acids (Fig. 4). The sum of the sample peak area and the peak areas from several subsequently injected blanks was used to calculate E_{total} (Fig. 2). These values are approximately equal to the values of E found at low pH values, which indicates that the residual acids in the membrane are indeed the main reason for the decreased extraction efficiency at high acceptor pH.

In Fig. 5, it can be seen that with longer contact time between the acceptor solution and the membrane (stop time), increasing amounts of acids are released from the membrane. The membrane memory effect (MME) of malic acid increased markedly up to 23 min stop time, indicating that malic acid adsorbed more strongly in

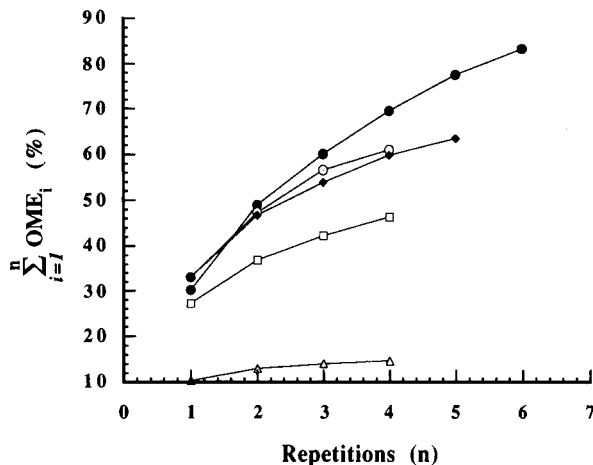


Fig. 4. Variation of the accumulated overall memory effect with repetitions (n) of blank extractions. Symbols and conditions as in Fig. 2.

the membrane than the other acids. For the least polar butanoic acid, MME was small and virtually independent on the stop time. Apparently, the residence time and the amount of adsorbed acid in the membrane increase with the polarity of the acids.

Fig. 6 demonstrates the influence of the TOPO content on MME, which increased markedly from 10 to 20% TOPO in the membrane. The result

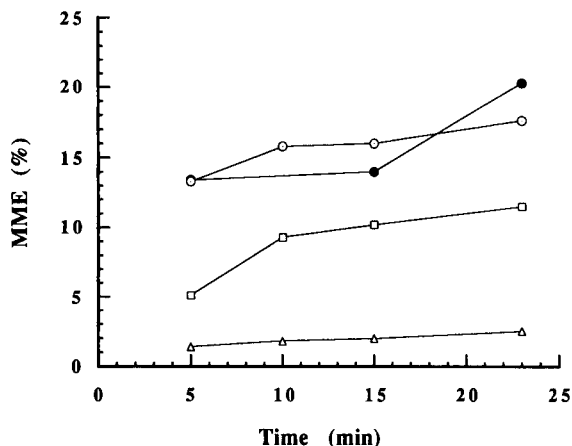


Fig. 5. Variation of membrane memory effect (MME) with stop time (see text). Malic, ●; lactic, ○; formic, □; butanoic acid, △. Membrane: 10% TOPO in DHE. Acceptor phase: 50 mM NaOH.

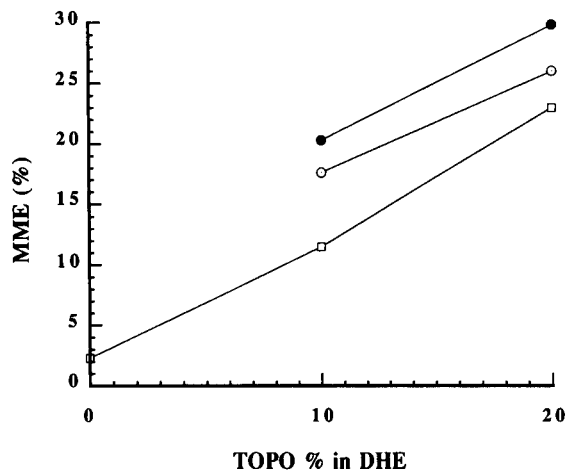


Fig. 6. Influence of TOPO content (%) in DHE on the membrane memory effect (MME). Stop time: 23 min. Symbols and conditions as in Fig. 5.

shows that TOPO content has a strong influence on the memory effect of acids in the membrane.

The mechanism of TOPO extraction has been suggested to involve hydrogen bonding between the phosphoryl oxygen of TOPO and the acidic hydrogen atoms of uncharged acids [5,9]. An acid diffuses through the membrane as a free acid or as a complex formed by a reversible reaction with TOPO. At the acceptor side of the membrane, the complex breaks and the acid is desorbed into the alkaline acceptor solution and dissociates (Fig. 7).

The whole reaction scheme can be presented as follows:

On the donor side:

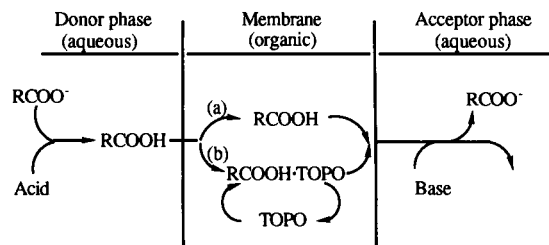
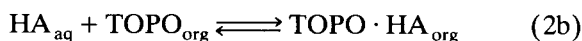
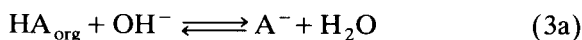


Fig. 7. Enrichment principle of carboxylic acids without (a) and with (b) TOPO as carrier in the membrane.

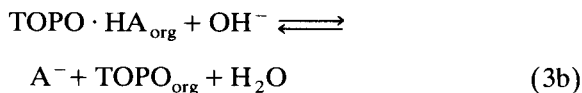
or



On the acceptor side:



or



For free acids, an acceptor $\text{pH} > \text{p}K_{\text{a}}$ is necessary to ionize the acids and trap them as soon as they arrive at the membrane–acceptor interface. A higher pH would not cause any negative effect. This is the observed case when the pure DHE membrane is used. The free acids will stay in the membrane if the acceptor solution is not alkaline enough.

In the case of a membrane containing TOPO, the dissociation of the complex is suggested to be a key step in the desorption of the acids. In the presence of TOPO, step 2b is more favourable than step 2a, but the dissociation in step 3b is less favourable than 3a. A dicarboxylic acid such as succinic acid probably forms a twin hydrogen bond, thus associating more strongly with TOPO. A hydrogen bond can also be formed between a hydroxyl group and TOPO [11,13], so lactic acid might also form a twin bond. Malic acid may even form a triple hydrogen bond. The order of the memory effects shown in Fig. 3 are in agreement with the stabilities explained in this way.

Summarizing, it is clear that the rate of acid transfer from the membrane to the acceptor phase considerably decreases with increasing pH in the presence of TOPO. The detailed reasons for this decrease remains unknown.

3.3. Influence of carbonate

Samples originating from air sampling in diluted base contain a large amount of carbonate, which interferes with the propanoic acid peak in the chromatogram. Therefore carbonate was removed from the sample before it was injected into the column [16]. On the other hand, the

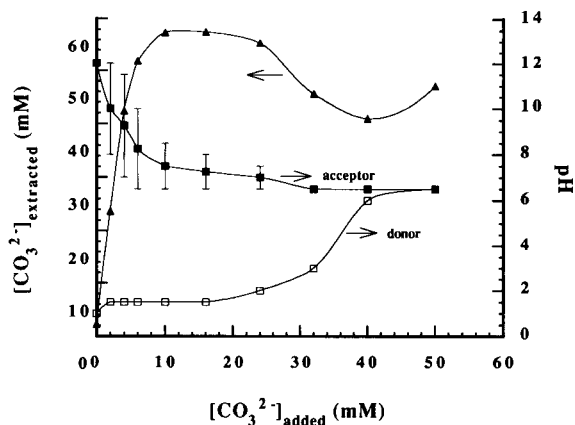


Fig. 8. Influence of the carbonate concentration added in the sample ($[\text{CO}_3^{2-}]_{\text{added}}$) on the extracted carbonate concentration ($[\text{CO}_3^{2-}]_{\text{extracted}}$), donor pH and acceptor pH after extraction. Membrane: 10% TOPO in DHE. Acceptor phase: 50 mM NaOH.

co-extraction of a certain amount of carbonate promoted the efficiency and decreased the memory effect of the carboxylic acids when NaOH was used as acceptor solution.

To investigate the influence of carbonate, different amounts of Na_2CO_3 were added to solutions of acids which were extracted with 50 mM NaOH as acceptor. The acceptor pH decreased significantly as the carbonic acid was trapped in the acceptor phase. The final pH was around 7.5 in the range 10 to 24 mM of added carbonate since a $\text{HCO}_3^-/\text{CO}_3^{2-}$ buffer solution was formed (Fig. 8). In the same range the maximal extraction efficiency and the least memory effect were obtained (Fig. 9). Further addition of Na_2CO_3 caused the donor pH to increase, thus decreasing the flux of all acids.

To clarify whether the effects of carbonate originated from the diffusion process or only from the acceptor pH adjustment, the same experiments were carried out at a given pH (7.3) which was controlled by a Tris buffer. Even then, the extraction of carbonic acid still decreased the acceptor pH slightly, as shown in Table 3. Therefore, the extraction efficiency of acetic acid decreased with increase of carbonate concentration (Fig. 10). For lactic acid, the maximum efficiency was obtained when 6 mM carbonate was added to

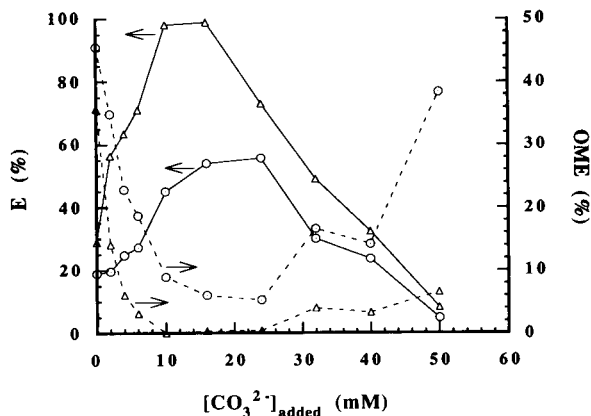


Fig. 9. Influence of the carbonate concentration added to the sample ($[\text{CO}_3^{2-}]_{\text{added}}$) on extraction efficiency (E) and overall memory effect (OME). Lactic, \odot ; acetic acid, \triangle . Conditions as in Fig. 8.

Table 3

Influence of the carbonate concentration added in the sample ($[\text{CO}_3^{2-}]_{\text{added}}$) on the extracted carbonate concentration ($[\text{CO}_3^{2-}]_{\text{extracted}}$), donor pH and acceptor pH after extraction

$[\text{CO}_3^{2-}]_{\text{added}}$ mM	0	2	6	10	16
$[\text{CO}_3^{2-}]_{\text{extracted}}$ mM	0.1	2.6	3.3	4.0	4.7
pH _{donor}	1	1	1.5	1.5	1.5
pH _{acceptor}	7	6.5	6.5	6.5	6-6.5

Membrane: 10% TOPO in DHE. Acceptor phase: 50 mM tris buffer.

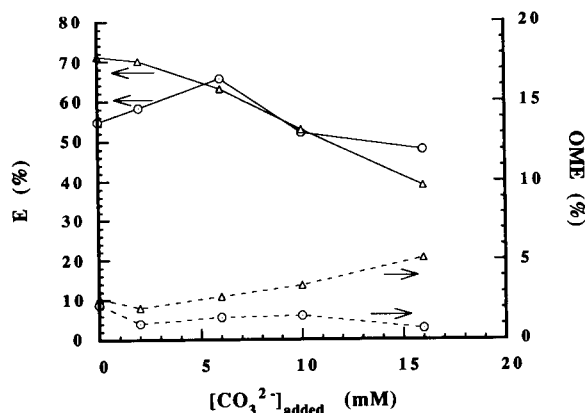


Fig. 10. Influence of the carbonate concentration added to the sample ($[\text{CO}_3^{2-}]_{\text{added}}$) on extraction efficiency (E) and overall memory effect (OME). Lactic, \odot ; acetic acid, \triangle . Membrane: 10% TOPO in DHE. Acceptor phase: 50 mM tris buffer, pH 7.3.

the sample and the memory effect was approximately constant in the whole range. The results indicate that the co-diffusion of a large amount of carbonic acid facilitates the extraction of carboxylic acids to a certain extent but the adjustment of acceptor pH to an appropriate value is a more important factor to improve E . Considering the interference of CO_3^{2-} in the chromatograms, it is worth to remove it if determination of propanoic acid is of interest.

4. Conclusions

The addition of TOPO as an extractant in the supported liquid membrane, significantly increased the extraction efficiency, especially of hydroxy, oxo and dicarboxylic acids. If the pH of the acceptor phase is increased above the pH value needed for complete trapping of the acids, the release of the acids from the membrane is considerably slowed down when TOPO is used, leading to a decreased extraction efficiency. Therefore, the pH control is of great importance.

Acknowledgements

This work was partly supported by the Swedish Environmental Protection Agency. Fruitful discussions with Dr Lennart Mathiasson are gratefully acknowledged.

References

- [1] P.R. Kiezyk and D. Mackay, *Can. J. Chem. Eng.*, 49 (1971) 747.
- [2] R.W. Helsel, *Chem. Eng. Prog.*, 73 (1977) 55.
- [3] G. Audunsson, *Anal. Chem.*, 58 (1986) 2714.
- [4] J.Å. Jönsson and L. Mathiasson, *Trends Anal. Chem.*, 11 (1992) 106.
- [5] Y. Kue and H.P. Gergor, *Sep. Sci. Technol.*, 18 (1983) 421.
- [6] I. Lau and G. Hayward, *Can. J. Chem. Eng.*, 68 (1990) 376.
- [7] J.S. Schultz, J.D. Goddard and S.R. Suchdeo, *AIChE J.*, 20 (1974) 417.

- [8] R.D. Noble and J.D. Way (Eds), *Liquid membranes, Theory and Applications* (ACS Symp. Ser. Vol. 347), ACS, Washington, DC, 1987.
- [9] P. Nuchnoi, T. Yano and N. Nishio, *J. Ferment. Technol.*, 65 (1987) 301.
- [10] T. Yano, P. Nuchnoi, N. Nishio and S. Nagai, in Fiechter, Okada and Tanner (Eds.), *Bioproducts and Bioprocesses*, Springer Verlag, Berlin, 1989, p. 281.
- [11] R. Wolny, A. Koll and L. Sobczyk, *J. Phys. Chem.*, 89 (1985) 2053.
- [12] J.J. Bucher, T.J. Conocchioli, E.R. Held, J.A. Labinger, B.A. Sudbury and R.M. Diamond, *J. Inorg. Nucl. Chem.*, 37 (1975) 221.
- [13] E.I. Matrosov and M.I. Kabachnik, *Izv. Akad. Nauk SSSR, Ser. Khim.*, 7 (1983) 1518.
- [14] C. Klofutar, Š. Paljk, M. Senegačnik and B. Jerkovič, *J. Inorg. Nucl. Chem.*, 34 (1972) 3873.
- [15] T. Hano, T. Ohtake, M. Matsumoto, K. Sasaki, F. Hori and Y. Kawano, *Proc. Symp. Solvent Extraction*, 1989, pp. 123–128.
- [16] L. Grönberg, Y. Shen and J. Å. Jönsson, *J. Chromatogr.*, 655 (1993) 207.
- [17] J.Å. Jönsson, P. Lökvist, G. Audunsson and Göran Nilvé, *Anal. Chim. Acta*, 277 (1993) 9.
- [18] R.C. Weast (Ed), *Handbook of Chemistry and Physics*, 53rd edn., CRC Press, Cleveland, OH, 1972.

Optical sensors for a wide pH range based on azo dyes immobilized on a novel support

Gerhard J. Mohr, Otto S. Wolfbeis *

Institute of Organic Chemistry, Analytical Division, Karl-Franzens University, Heinrich St. 28, A-8010 Graz, Austria

(Received 11th February 1994)

Abstract

New reactive azo dyes are described which are useful for optical determination of pH. The dyes are covalently linked (via ethylsulfonyl groups) to a novel type of transparent solid films consisting of a thin film of cellulose on top of a polyester support. The resulting membranes exhibit distinct color change when changing the pH and, in most cases, are compatible with LED light sources. Various membranes have been developed with pK_a values ranging from 0.5 to 11.28, thus practically covering the whole pH range. Because of the stability of the dyes, the covalent bond and the solid support, the new membranes exhibit storage stability over years, and operational lifetimes of weeks, good reproducibility and a fast (30–60 s) response to pH.

Key words: Sensors; Azo dyes; Immobilization; Optical sensors; pH determination

1. Introduction

Optical sensors for pH (pH optodes, from Greek *οπτοδεδε* – the optical way) are usually obtained by immobilizing pH indicators on a solid support and monitoring their optical properties [1–4]. The majority of pH optodes can be classified into two main groups. The first comprises dyes statically immobilized on solid supports such as ion exchangers [5,6], the second comprises dyes covalently bonded to hydrophilic supports such as cellulose or glass [6–10]. The former are easy to make but suffer from numerous disadvantages, the more serious ones being swelling, hysteresis,

dye leaching at high ionic strength, and inhomogeneity of the material. It is probably therefore that such materials, despite their ease of preparation, have never been incorporated into commercial instrumentation.

Covalently immobilized dyes, in contrast, do not suffer from leaching and hysteresis, and effects of swelling can be minimized. This is particularly true when extremely thin sensor membranes come to use. Cellulose membranes have the additional advantage of being rapidly penetrated by protons and, in contrast to glass-immobilized materials, can more easily be manufactured and handled.

Most indicators used so far cover the near-neutral pH range. If other pH ranges are to be covered, entirely different indicators along with

* Corresponding author.

different immobilization protocols have to be applied. In the present work, we describe a more general logic for obtaining pH optodes by applying *one* single synthon and *one* single immobilization protocol. The synthetic route presented here allows the covalent immobilization of numerous dyes (including similar ones not described here) with tailor-made optical properties and pK_a values, resulting in sensors that cover the whole pH range of interest.

2. Experimental

2.1. Instrumentation

Absorption spectra were run on a UV-2101-PC photometer (Shimadzu, Kyoto). The pK_a values were determined with the help of a flow-through

cell in a Perkin Elmer Lambda 5 photometer. Response time and reproducibility measurements were performed with an experimental arrangement [11] comprising an autosampler (Besta, Heidelberg), a peristaltic pump (Minipuls 3, Gilson Medical Electronics, Villiers-le-Bel, France), a fiber-optic photometer (Oriel 3090, Chelsea Instruments, London) with a xenon flash lamp (FX 800, Polytec, Waldbronn, Germany) pulsed at 9 Hz, a data acquisition unit (Keithley 575, Taunton, MA) and a 386 PC. pH measurements were performed with a pH meter (Metrohm, Buchs, Switzerland) calibrated with Aldrich pH standards of pH 7.00, 4.00 and 10.00 at 21°C

2.2. Reagents

All reagents were of analytical reagent grade. A buffer covering the pH 2–12 range was used which was 0.04 M in sodium acetate, 0.04 M in

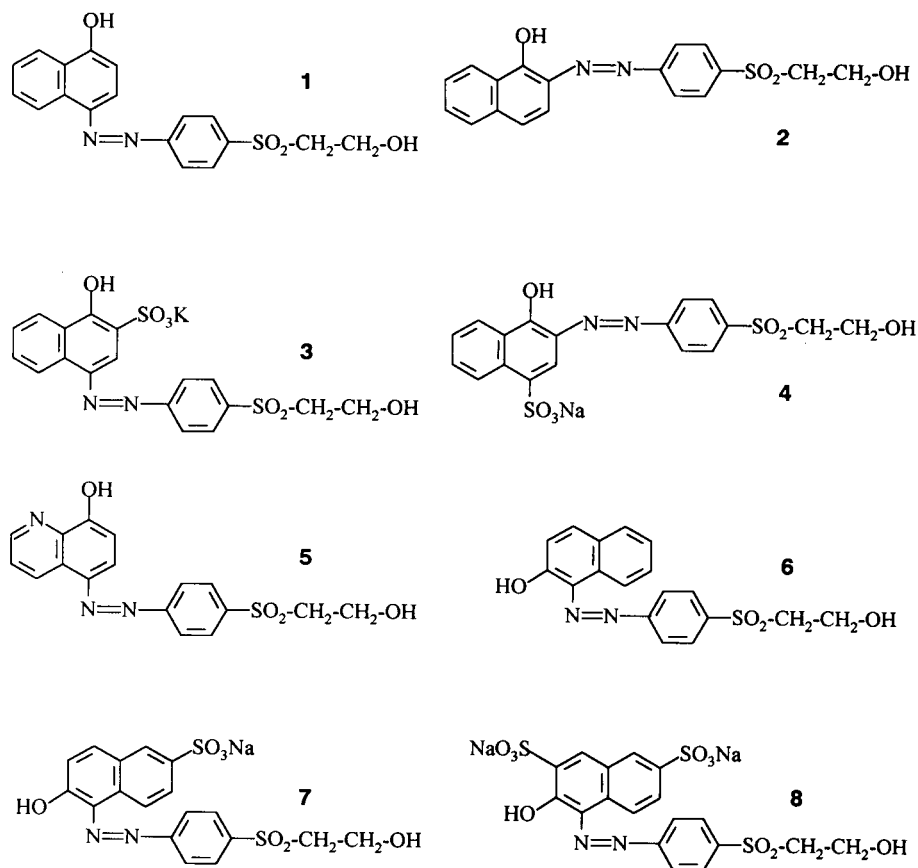


Fig. 1. Chemical structures of reactive phenolic azo dyes 1–8.

boric acid, 0.04 M in sodium dihydrogen phosphate, and 0.1 M in sodium sulfate. The pH was adjusted to the desired value by adding 1.0 M sodium hydroxide or 6 M sulfuric acid. The synthesis of dyes 1–11 has been described elsewhere [12].

2.3. Polymeric support

The dyes were immobilized on transparent overhead foils (Hewlett Packard, prod. no. 17703T), consisting of a 10- μm layer of cellulose acetate fixed onto a transparent 100- μm polyester support. The cellulose acetate is converted into cellulose under the experimental conditions of the dye immobilization. Cellulose is the preferred polymeric support for optical sensors for ions on grounds of its good permeability for ions including protons [13]. Because the cellulose membrane is very thin, the sensor exhibits fast response (30–60 s for t_{95}).

2.4. Covalent immobilization of vinylsulfonyl pH indicators

The following is a general protocol for immobilizing vinylsulfonyl dyes on cellulose. The chemical structures of the phenolic dyes used in this work are given in Fig. 1, while the indicators derived from aromatic amines and covering the low pH range are given in Fig. 2. Typically, 0.1 g of the dye is treated with 1.0 g of concentrated sulfuric acid for 30 min at room temperature. This operation converts the hydroxyethylsulfo group of dyes 1–11 into the $-\text{SO}_2-\text{CH}_2-\text{CH}_2-\text{O}-\text{SO}_3\text{H}$ group, i.e., sulfo esters are formed.

Then, the solution is poured into 1 l of distilled water and neutralized with 1.8 ml of a 32% (m/v) sodium hydroxide solution. The membranes to be colored are placed in this solution. After 5 min, 25 g of sodium carbonate and after another 5 min, 5.2 ml of a 32% (m/v) sodium hydroxide solution are added. This leads to elimination of sulfuric acid and formation of the reactive vinylsulfonyl group ($-\text{SO}_2-\text{CH}=\text{CH}_2$). Simultaneously, the cellulose acetate on the polyester support is hydrolyzed to form cellulose (Cell-OH). In strongly alkaline solution, the vinylsulfonyl group reacts with cellulose (Cell-OH) to give the dye/cellulose conjugate [dye- $\text{SO}_2-\text{CH}_2-\text{CH}_2-\text{O}-\text{Cell}$]. After 45 min, the colored membranes are removed from the dyeing bath and washed with distilled water [8–10]. The resulting membranes are ready for use.

2.5. Spectroscopic measurements

The $\text{p}K_a$ values of the sensing membranes were determined from pH-dependent absorption data at fixed wavelength. The wavelength was chosen such that the difference in the absorbances between acid and conjugate base form was largest. Buffers of defined pH were passed over the membranes mounted in a flow-through cell, and absorbance was recorded once it was constant. Plots of absorbance versus pH provided sigmoidal curves. The $\text{p}K_a$'s were calculated with the help of the following equation:

$$\text{p}K = \text{pH} + \log(A_x - A_b) / (A_a - A_x) \quad (1)$$

where A_x , A_b , and A_a are the absorbances of the immobilized dye at a defined pH near the

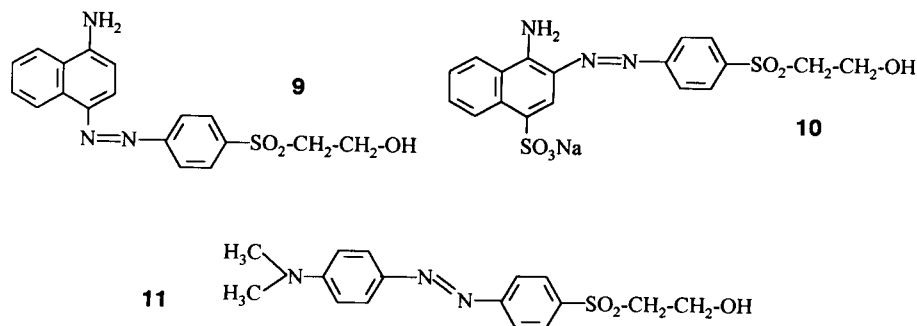


Fig. 2. Chemical structures of reactive amine azo dyes 9–11.

pK_a , of the base form, and of the acid form, respectively.

The response toward pH changes was monitored by placing the membranes in a flow-through cell and monitoring optical changes with the help of an optical fiber-optic arrangement (Oriol). After passing a 560-nm interference filter, light was guided through the input fiber bundle of a bifurcated fiber-optic onto the sensing membrane. Reflected light was guided back through a second fiber bundle to hit the photomultiplier tube. Buffer solutions were pumped through the cell at a flow-rate of 1.5 ml min^{-1} .

3. Results

3.1. Strategy for the synthesis of reactive azo dyes

The objective of this work was to provide a generally applicable scheme for making pH-sensitive membranes, resulting in a simple and generally applicable method for making sensor membranes. In addition to the widely applicable synthetic route to the reactive dyes [10], the method should be flexible enough to allow the preparation of dyes with highly different pK_a values, thus providing sensors covering almost the whole pH range.

The dyes have been synthesized by the help of the new synthon 4-(2-hydroxyethylsulfonyl)anilinium chloride [12], referred to as GM-1. In combination with various coupling components, it is capable of forming a large variety of different

dyes with different properties. GM-1 possesses two chemical functions, namely (a) an amino group which allows diazo coupling to form the azo chromophore, and (b) a 2-hydroxyethylsulfonyl group which, after activation, enables immobilization of the dye onto the cellulose support. The synthon has been coupled to various naphthols and amines allowing the development of a variety of indicators (see Figs. 1 and 2).

3.2. Dye immobilization

Immobilizing vinylsulfonyl dyes onto cellulose is an established technique in textile chemistry in case of the so-called "Remazol" dyes [14]. The method requires the use of both strong acid and strong base and therefore the support material must be resistant to both. We find the cellulose-on-polyester support to be a viable substrate because it does not undergo a detectable change in its optical properties during immobilization of the dyes, and because all dyes invariably could be coupled to this particular solid support. It should be kept in mind, however, that the support material in fact is a cellulose triacetate foil which, because of treatment with strong alkali during immobilization, is converted into cellulose. Dyes 1–11 resulted in pH sensor membranes M-1 through M-11. A schematic of the structure of membrane M-3 is given in Fig. 3.

The material chosen for dye immobilization (a cellulose-on-polyester compound foil) has a number of advantages over conventional cellulose. The cellulose film is only $10 \mu\text{m}$ thick and hence

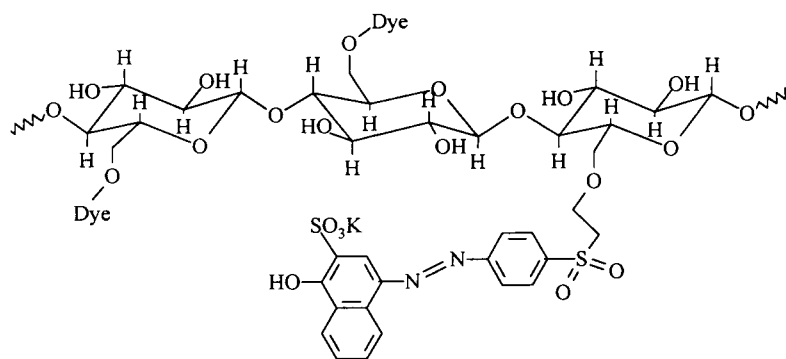


Fig. 3. Schematic of the chemical structure of the indicator-cellulose conjugate in membrane M-3.

the acid–base equilibria are established within seconds, resulting in fast response times. In addition, the membranes are fully transparent and can be easily subjected to photometric analysis, while conventional cellulose membranes (including the commercial test strips) are not transparent at all and have response times on the order of many minutes when operated near their pK_a although they respond quite quickly on changing between pH's outside the titration curve.

3.3. Spectral properties and dissociation constants

Dyes 1–8 (Fig. 1) are derived from phenolic compounds which dissociate in alkaline solutions. Their pK_a 's range from 7.34 (resulting in a pH sensor useful for measuring physiological pH's) up to pK_a 11.28, i.e., a pH range, where the glass electrode is prone to deterioration as a result of the attack of strong alkali. Sensor membranes usually are of yellow or orange color at low pH, and red to purple at high pH. The color change in going from the acid to the base form is most significant in case of the *para*-azo dyes (1, 3, 5), the color changes being from yellow to purple. There is little overlap in the absorption spectra of the acid and conjugate base forms of 1, 3 and 5 (Fig. 4). This contrasts the behavior of dyes derived from 2-naphthol (6–8), which do not display

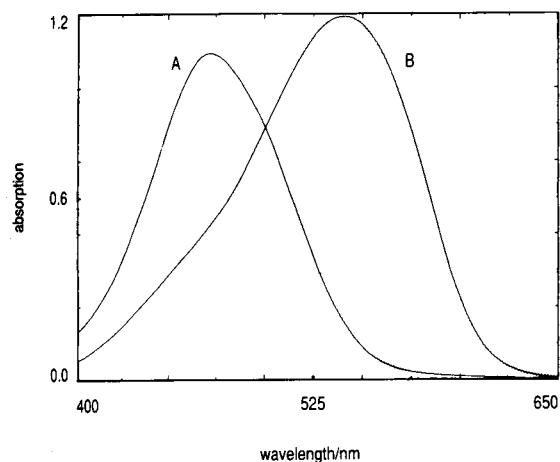


Fig. 4. Absorption spectra of M-3 in (A) the acid form, and (B) the base form.

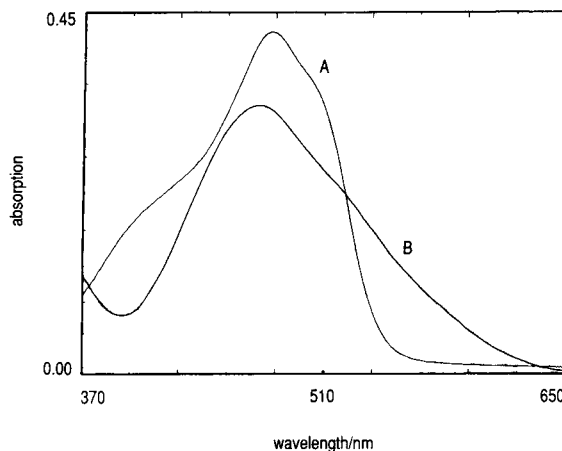


Fig. 5. Absorption spectra of M-7 in (A) acid form, and (B) the base form.

such an intense color change and have strongly overlapping spectra (Fig. 5). The absorption maxima of the sensor membranes in their acid and conjugate base forms, respectively, along with their pK_a values are summarized in Table 1.

Azo indicators 9–11 are derived from aromatic amines (Fig. 2) and show an entirely different behavior in that the absorption maxima of the amine (conjugate base) forms occur at shorter wavelengths than those of the protonated (conjugate acid) form (Fig. 6). This is in agreement

Table 1

Absorption maxima of acid and conjugate base forms, and pK_a values of dyed cellulose sensor membranes M-1 to M-11 at 21°C

Membrane	λ_{\max} (nm) (base form)	λ_{\max} (nm) (acid form)	pK_a
M-1	553	460	9.37
M-2	535	501	9.26
M-3	541	473	7.55
M-4	517	491	7.83
M-5	518	455	7.34
M-6	476	487	11.28
M-7	474	479	10.68
M-8	481	488	10.64
M-9	507	509	3.68
M-10	492	518	~ 0.5
M-11	486	503	2.24

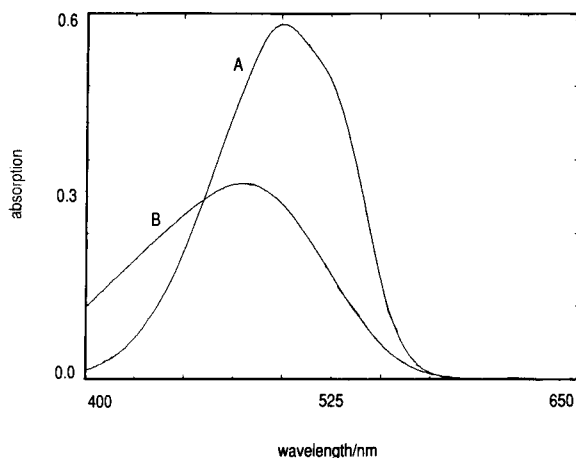


Fig. 6. Absorption spectra of M-11 in (A) the acid form, and (B) the base form

with established structure–color relationships. The respective membranes (M-9 through M-11) are orange colored in their base forms (i.e., at high pH) and turn to red or purple on protonation. The spectra overlap significantly.

3.4. Performance of the indicator membranes

Fig. 7 shows the response of membrane M-3 on exposure to buffers ranging from pH 5.0 to 9.5. The response is fast (30–40 s for t_{95}), and signal changes are fully reversible. A constant baseline is good proof that the covalent dye-to-cellulose bond (see Fig. 3) is stable. No leaching or bleaching of the immobilized dyes was observed.

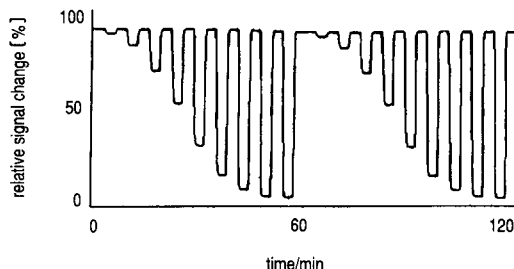


Fig. 7. Response time, relative change in the intensity of reflected light, and reversibility of membrane M-3 in the fiber optic pH meter (using the Oriel instrument) on exposure to buffer solutions of pH 5.0 (top) to 9.5 (bottom) in 0.5 pH increments.

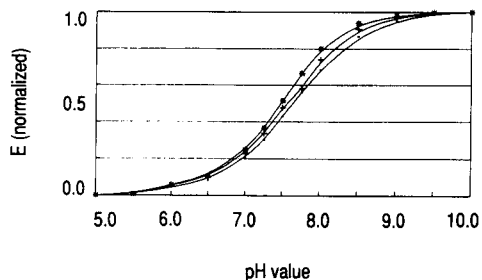


Fig. 8. pH titration plot of membrane M-3 in the presence of 0, 0.1 and 1.0 M sodium sulfate (absorption measured at 560 nm), showing the effect of ionic strength.

3.5. Effect of ionic strength (IS)

A major disadvantage of optical pH sensors is the effect of ionic strength (IS) on the dissociation constant and, consequently, the pK_a of the dye [1–4]. The effect of IS cannot be distinguished from signal changes caused by pH. Fig. 8 shows the pH titration of M-3 with different concentrations of sodium sulfate being added to the buffer (composed of 0.04 M sodium acetate, 0.04 M boric acid, 0.04 M sodium dihydrogen phosphate). The pK_a decreases from 7.64 to 7.45 in going from 0 to 1.0 M sodium sulfate. The effect of IS on the pK_a is more expressed at low IS: the shift is 0.09 units on changing from 0 to 0.1 M sodium sulfate, and 0.1 units on going from 0.1 to 1.0 M sodium sulfate (see Fig. 8).

3.6. Effect of immobilization on pK_a

Not unexpectedly, the pK_a 's are different for the dissolved and the immobilized forms. The

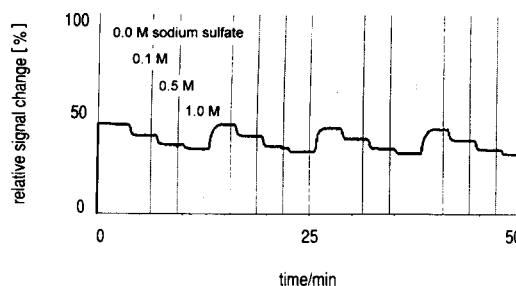


Fig. 9. Relative signal change of membrane M-4 on exposure to a buffer solution of pH 8.17 containing 0, 0.1, 0.5 and 1.0 M concentrations of sodium sulfate (absorption measured at 560 nm).

pK_a of immobilized hydroxynaphthalenes 1–8 usually is higher by around 0 to 1 unit, whereas the pK_a of immobilized aromatic amines 9–11 is lower by around one unit in the immobilized form. A similar effect has been found for dyes covalently [15] or electrostatically [16] bound to hydrolyzed cellulose acetate.

4. Discussion

The method for preparing pH-sensitive membranes by immobilizing indicator dyes via the vinylsulfonyl group to result in optical pH sensor membranes shows several advantages over existing approaches for optical measurement of pH. Dyes are covalently bound to a highly transparent sensor membrane, and both leaching and bleaching is absent. In fact, the covalent bond is stable over the whole pH range 0–13. This is in contrast with the leaching observed with surface adsorbed dyes when used over prolonged periods of time.

More recently, another type of pH-sensitive matrices have been introduced which, like the materials based on surface adsorbed materials, are highly lipophilic. The matrix is composed of plasticized PVC [17]. In order to make dyes applicable for such matrices, they have to be lipophilized which, unfortunately, does not prevent slow leaching when becoming charged by protonation or deprotonation. Furthermore, in order to improve the mobility of protons, lipophilic counterions have to be added. Notwithstanding this, such materials still can be very useful if the respective sensors are not intended for long-term use or frequent recalibration is possible.

Immobilization of pH probes on ion exchangers can solve the problem of slow response, because in this case the dye is located on the surface of the support [4]. Electrostatic binding of dyes onto ion exchangers is rather strong so that leaching is not a serious problem. However, such materials are charged even after immobilization of the dye. This results in a number of shortcomings: (a) the surface charges can act as ion exchangers; as a result, the counterion may change with each new sample, giving rise to a change in the

optical signal due to varying ionic strength near the dye; (b) ion exchangers are prone to hysteresis [18]; (c) at very high ionic strength, the dye may also be exchanged by another electrolyte; (d) Donnan potentials may be formed at the surface and may limit the diffusion of ions to the dye; (e) many ion exchangers suffer from pH-dependent swelling. Due to these limitations, neutral copolymers such as styrene–divinylbenzene (e.g., the XAD type) have also been used as supports and do not suffer from such limitations but binding of the dye to the support is too weak for long-term applications.

The transparent cellulose support, onto which dyes may be immobilized covalently by the method presented here, is uncharged, so the typical drawbacks of charged supports are not encountered. The membranes have high proton permeability, and this results in fast response times. No hysteresis was found in either case. From a manufacturing point of view it is important to know that the cellulose-on-polyester support (designed for use as a foil for graphic plotters) is easily available in constant quality. Thus, membranes can be produced with well-defined and reproducible properties. Moreover, the membrane preparation does not require the use of a toxic solvent such as chloroform or tetrahydrofuran.

The synthetic scheme allows various dyes with tailor-made optical properties and pK_a values to be made, and a wide pH range is covered. It should be mentioned here that the synthetic scheme and immobilization protocol is not limited to pH-sensitive dyes. In fact, numerous chromionophores (such as those for alkali, earth alkali, and heavy metals) conceivably may be immobilized this way [14].

The dyed membranes resist standard sterilization protocols such as steam heating or 6% hydrogen peroxide [9] and, therefore, can be used for bioreactor monitoring. In order to compensate for interferences caused by turbidity and coloration of the sample, and by fluctuations of the light source, a double-cell configuration is recommended in which the light beam split and passes through both a dyed and an undyed section of the sensor foil [19].

When coated with a layer of silicone (such as

the E-4 from Wacker, Burghausen, Germany), sensors are obtained which respond to acid or basic gases such as carbon dioxide [20] or ammonia. Sensor membranes with high pK_a may be used for monitoring highly alkaline solutions where the glass electrode is known to perform poorly. Because the sensor material is rather unexpensive, sensor spots conceivably may be used only once and evaluated visually as it is done with conventional pH test strips. Even when used in an optical pH meter, replacement of damaged pH sensor membranes is affordable.

5. Conclusion

Cellulose membranes colored with reactive indicator dyes can be applied for optical pH sensing. A general scheme for obtaining tailor-made indicators and immobilizing them onto a new kind of support is presented which results in sensor membranes covering a wide pH range, depending on whether naphthols or aromatic amines are used for diazo coupling. Dyes derived from 1-hydroxynaphthalene derivatives display the best optical properties for application in pH sensing in showing large changes in the absorption spectra in going from the acid to the base form, being compatible with the green LED and highly photostable. Because the dyes are covalently linked to the transparent cellulose membranes, no leaching is observed.

Acknowledgement

This work was supported by the Austrian National Science Foundation within project S5701-PHY, which is gratefully acknowledged.

References

- [1] J. Janata, *Anal. Chem.*, 59 (1987) 1351.
- [2] T.E. Edmonds, N.J. Flatters, C.F. Jones and J.N. Miller, *Talanta*, 35 (1988) 103.
- [3] M.J.P. Leiner and O.S. Wolfbeis, in: O.S. Wolfbeis (Ed.), *Fiber Optic Chemical Sensors and Biosensors*, Vol. 1, CRC Press, Boca Raton, FL, 1991, p. 359f.
- [4] M.J.P. Leiner and P. Hartmann, *Sensors Actuators*, 11B (1993) 281.
- [5] G.F. Kirkbright, R. Narayanaswamy and N.A. Welti, *Analyst*, 109 (1984) 15.
- [6] Z. Zhujun and W.R. Seitz, *Anal. Chim. Acta*, 160 (1984) 47.
- [7] L.A. Saari and W.R. Seitz, *Anal. Chem.*, 54 (1982) 821.
- [8] H. Offenbacher, O.S. Wolfbeis and E. Furlinger, *Sensors Actuators*, 9 (1986) 73.
- [9] A. Holobar, B.H. Weigl, W. Trettnak, R. Benes, H. Lehmann, N. Rodriguez, A. Wollschlager, P. O'Leary, P. Raspor and O.S. Wolfbeis, *Sensors Actuators*, 11B (1993) 425.
- [10] T. Werner and O.S. Wolfbeis, *Fresenius' J. Anal. Chem.*, 346 (1993) 564.
- [11] B. Weigl, *Proc. Soc. Photo Opt. Instrum. Eng. (SPIE)*, 1587 (1991) 288.
- [12] G.J. Mohr, T. Werner and O.S. Wolfbeis, *Dyes and Pigments*, in press.
- [13] J. Brandrup and E.H. Immergut, *Polymer Handbook*, Wiley, New York, 3rd ed., 1989, Chap. IV, pp. 437 ff.
- [14] P. Burba and K.H. Lieser, *Angew. Makromol. Chem.*, 50 (1976) 151.
- [15] Y. Kostov, S. Tzonkov, L. Yotovan and M. Krysteva, *Anal. Chim. Acta*, 280 (1993) 15.
- [16] T.P. Jones and M.D. Porter, *Anal. Chem.*, 60 (1988) 404.
- [17] E. Bakker, M. Lerchi, T. Rosatzin, B. Rusterholz and W. Simon, *Anal. Chim. Acta*, 278 (1993) 211.
- [18] M. Bacci, F. Baldini and A.M. Scheggi, *Anal. Chim. Acta*, 207 (1988) 343.
- [19] A. Holobar and O.S. Wolfbeis, *Anal. Methods Instrum.*, submitted for publication.
- [20] B.H. Weigl, A. Holobar, N.V. Rodriguez and O.S. Wolfbeis, *Anal. Chim. Acta*, 282 (1993) 335.

Immobilisation of photosynthetic cells based on film-forming emulsion polymers

Nicolas Martens, Elizabeth A.H. Hall *

Institute of Biotechnology, University of Cambridge, Tennis Court Road, Cambridge CB2 1QT, UK

(Received 27th September 1993; revised manuscript received 24th January 1994)

Abstract

Applications requiring the immobilisation of whole cells presents a need for rigorous control of the 'environment' of the cells more so even than in the use of isolated enzymes, since the phase must be isotonic with the cell, if the cell membrane is to remain intact. In this paper we report on an immobilisation matrix for whole cells. The preparation of film forming emulsion polymers based on methacrylates and acrylates is described. Photosynthetic bacteria were immobilised in latex films retaining nearly 100% activity of the photosynthetic electron transport chain, determined in an amperometric system. The diffusion properties of the latex films were studied in rotating disc electrode experiments.

Key words: Enzymatic methods; Film-forming emulsion polymers; Immobilisation; Photosynthetic cells

1. Introduction

The immobilisation of whole cells or intact cell components e.g. thylakoid membranes or mitochondria have attracted attention for use as a 'alternative energy source' [1,2], for the biosynthesis of organic compounds [3–5] or 'recognition systems' in biosensors. In many of these applications the activity of a highly complex biological system has to be retained. Therefore, the immobilisation presents a need for rigorous control of the 'environment', more so even than in the use of isolated enzymes, since the phase must be

isotonic with the cell, if the cell membrane is to remain intact.

Existing methods for whole cell immobilisation are often based on polysaccharides such as calcium alginate [6,7] and gelatine [8] or proteins etc., but their commercial application is limited as they do not have the right hydrating or mechanical properties where the film must be fabricated and stored for months before use. They also lack the adhesion onto metal surfaces often required in sensor technology. Nevertheless, a common and essential feature of these methods is that they maintain the aqueous cell environment. Synthetic matrices like acrylamides have also been explored, which retain water in the phase, but they are liable to deactivate the cell due to the

* Corresponding author.

toxicity of the monomers [9]. This can be circumvented by employing pre-polymerised linear polyacrylamide gels, containing functional groups to allow chemical cross linking in situ [10]. This method, however, still relies on a cross linking reaction in the presence of the biological material which may lead to loss of activity and post-fabrication treatment is required. Cells and organelles can also be entrapped in pre polymerised photocrosslinkable resins based on hydroxyethylacrylate and poly(ethylene glycol) or poly(propylene glycol) [11]. The physio-chemical nature of these matrices can be altered via changes in the network size, the hydrophilic–hydrophobic balance and the ionic nature, thus allowing optimal activity of the biocatalyst in the polymer matrix. Nevertheless, as the prepolymer is water soluble cross linking of the matrix is necessary.

The principle problem of immobilisation of sensitive biological materials is the need to form a water insoluble matrix from an aqueous solution. The key to the solution is the formation of emulsion polymers, which also have industrial applications such as paints, coatings and adhesives. Latex membranes have already been explored for the immobilisation of glucoamylase [12]. A latex polymer is an emulsion which can be defined as a stable dispersion of water insoluble polymer particles ranging in size from 1 nm to 1 μm . The word stability here means that the particles in the dispersion will remain as single entities over long periods. The forces which keep the polymer particles in solution are mainly electrostatic interactions between charged groups on the polymer chain or the surfactant and steric effects arising from the geometry and conformation of adsorbed or grafted molecules [13,14]. The process by which the polymer colloids in the dispersion are transformed into a continuous film is termed coalescence. When a latex polymer is dried by evaporation of water from its surface, the polymer particles are driven closer together until the stabilising forces keeping them apart are overcome. A soft latex (i.e. one above its minimum film forming temperature) then forms a continuous film.

Miller [12] has described a latex membrane based on butadiene for the immobilisation of the

enzyme glucoamylase. Although the enzyme was found to be stable for several hydrolysis steps, its activity subsequently decreased to zero. This was attributed to loss of enzyme into the surrounding solution. ^{60}Co γ -radiation improved the stability of the enzyme in the membrane, but this treatment decreased the initial activity of the enzyme-membrane, and is not readily compatible with the intact photosynthetic cells, which are subject of the study reported herein. In contrast to this previous work, we describe the preparation of a group of latex polymers based on different methacrylate and acrylate monomers and the incorporation of intact photosynthetic cells in films cast from these polymers, to test their application as immobilisation matrices for complex and sensitive biological materials. The activity of the immobilised cells was monitored by their ability to generate a photocurrent measured in an electrochemical cell.

2. Materials and methods

2.1. Reagents

Synechococcus (PCC 6301) was a gift from Dr. Peter Rowell (University of Dundee). All chemicals for the preparation of the BG-11 medium were of analytical grade and were supplied by BDH, Sigma and Aldrich. 3-(*N*-Morphinol)propanesulphonic acid (MOPS) was obtained from Sigma. Diaminodurene (DAD) and ammonium peroxodisulphate were used as received from Aldrich. Poly(vinyl alcohol) (PVA) was 100% hydrolysed and purchased from Aldrich, as were all monomers employed in the emulsion polymerisation.

2.2. Growth of the cyanobacteria

The cells were grown in batch cultures in 250-ml conical flasks using BG-11 medium [15], with 100 oscillations/min in an orbital shaker with warm fluorescent light at 25°C. Stock cultures were maintained using the same medium with addition of 1.5% agar. Cells were harvested in 1 ml aliquots by centrifugation for 5 min at 13000

rpm in a desk top centrifuge (Microcentaur MSE). Pellets were then frozen in liquid nitrogen and stored at -80°C without significant loss of activity over one week.

2.3. Estimating chlorophyll in whole cells

A pellet of cyanobacteria prepared as described above was thawed. The pellet was then dissolved in aqueous acetone (80%). The cells were further disrupted by three ultrasonic bursts of 5 s with 20 s cooling time on ice. The cell debris was then separated by centrifugation for 10 min at 13 000 rpm in a MSP desktop centrifuge. The absorbance of the bright green supernatant was determined at 663 nm and at 645 nm. Using these values in the MacKinney-Arnon equation the chlorophyll concentration was estimated [16].

2.4. Electrochemical measurements

All measurements were performed in a thermostatically jacketed glass vessel (15 ml capacity) coated to exclude light at 25°C . In all experiments a three-electrode set up was used with glassy carbon (0.07 cm^2) as the working electrode, a platinum flag (1.5 cm^2) and a saturated calomel electrode (SCE) as the counter and reference electrodes respectively. BG-11 medium containing MOPS (50 mmol, pH 7.0) was used as the electrolyte in all experiments. Stock solutions of DAD were freshly prepared in ethanol and the required amount added into the electrolyte. A computer controlled potentiostat (Autolab, Ecochemie, Utrecht) was used and the current–time response was recorded on an $y-t$ chart recorder (Gould BS-273). Cyclic voltammograms were recorded on an $x-y$ plotter (Philips PM 8043).

Rotating disk electrode (RDE) experiments were performed using a platinum disk electrode with a geometric surface area of 0.125 cm^2 . Reference and counter electrode were the same as described above. Rotation speed of the electrode was controlled by a EG&G PARC Model 616 controller and stand. For each rotation rate a single cycle from -0.2 V to 0.3 V was recorded at a scan speed of 5 mV/s , or the electrode was

held at a potential of $+300\text{ mV}$ on the diffusion controlled oxidation plateau for DAD.

A halogen lamp (1 W, 12 V) served as the light source for the photocurrent measurement and was fitted underneath the electrochemical cell such that direct illumination of the working electrode was achieved. During the photocurrent measurement the electrode was exposed either to constant illumination or light pulses controlled by an ‘in-house’ constructed timer producing pulses of 250 ms length with a dark period of 2.5 min.

2.5. Emulsion polymerisation

The emulsion polymerisation was carried out at 70°C in a reactor flask stirred at 500 rpm. The recipes of the polymerisation are shown in Table 1. The initial charge was prepared by dissolving PVA in deionised water. The solution was purged with nitrogen for 30 min and then transferred into the thermostated reaction vessel. After the temperature had stabilised the initiator, ammonium peroxodisulfate, was added. The monomer mixture was then added slowly over 15 min. Monomers were used without further purification. Sodium methacrylate was prepared by the neutralisation of a stoichiometric amount of methacrylic acid and sodium hydroxide in an aqueous solution and the water was then removed under reduced pressure at room temperature. The second aliquot of the initiator, dissolved in deionised water (10 ml), was then added dropwise over 10 min. The polymerisation reaction was terminated after 3 h by cooling the reactor to room temperature. The emulsion was then transferred into a storage container via a $25\text{-}\mu\text{m}$ sieve.

The emulsions were cleaned from any residual monomers or water soluble oligomers in two steps. First the emulsion was evaporated under reduced pressure to $2/3$ of the original volume to remove residual monomers and then topped up to its original volume with BG-11 medium. This was repeated twice. The emulsion was cleaned further by dialysis over night at room temperature against deionised water and a second dialysis over night against BG-11 medium. Finally the pH was adjusted to 7.0 with NaOH.

2.6. Immobilisation of the photosynthetic cells

Calcium alginate matrix

The immobilisation of the photosynthetic cells in a calcium-alginate matrix was performed as follows. The cell pellet obtained after centrifugation as described above was suspended in a sodium alginate solution (20 μ l of a 1% solution in BG-11 medium). 3 μ l of this suspension was then used to drop coat a glassy carbon electrode. This electrode was then dried for 30 min at room temperature and subsequently incubated for 30 min in BG-11 medium containing MOPS (50 mmol/l, pH 7.0) and CaCl₂ (50 mmol/l). The calcium alginate matrix thus formed was then protected using a dialysis membrane secured onto the electrode by a rubber o-ring.

Emulsion polymer

For the immobilisation of cells in films cast from emulsion polymers a cell pellet was resus-

pended in the emulsion (20 μ l). 3 μ l of this suspension was applied on to the glassy carbon electrode. The electrode was then left drying at room temperature over night or for 1 h at 40°C. The polymer matrix did not require protection by covering with a dialysis membrane.

3. Results and discussion

3.1. Emulsion polymerisation and film formation

Table 1 shows the composition of different emulsions based on the acrylate monomers, methyl methacrylate (MMA), methacrylic acid (MAA), the sodium salt of methacrylic acid (NaMAA) and butyl acrylate (BA); poly(vinyl alcohol) (PVA) was the surfactant. The emulsions were initially tested by visual inspection, in terms of film forming properties by drop coating of

Table 1

Monomer composition of the emulsion polymerisations (PVA was 100% hydrolysed and ammonium peroxodisulfate was used as the initiator. Results: +, poor; ++, satisfactory; +++, good)

	Initial charge		Initiator	Monomer Addition				Initiator	Stability	Film formation
	Volume	Surfactant		MMA	MAA	NaMAA	BA			
Poly 3	150 ml	5% PVA MW 100 000 Tween 20 4.5 g	1.82 g	0.06 M (6.0 g)	0.02 M (1.72 g)	–	–	1.82 g +PVA + Tween 20	< 1 month	+
Poly 4	150 ml	5% PVA MW 100 000	0.18 g	0.06 M (6.0 g)	0.02 M (1.72 g)	–	–	0.5 g	< 1 month	+
Poly 6	150 ml	2% PVA MW 100 000	0.18 g	0.06 M (6.0 g)	–	0.02 M (1.72 g)	–	0.5 g	> 1 year	–
Poly 7	150 ml	2% PVA MW 100 000	0.18 g	0.055 M (5.5 g)	0.02 M (1.72 g)	–	0.012 M (1.5 g)	0.5 g	> 1 year	+
Poly 10	150 ml	2% PVA MW 100 000	0.18 g	0.055 M (5.5 g)	0.013 M (1.1 g)	–	0.017 M (2.2 g)	0.5 g	> 1 year	++
Poly 12	150 ml	2% PVA MW 100 000	0.18 g	0.055 M (5.5 g)	–	–	0.030 M (3.84 g)	0.5 g	> 1 year	+++
Poly 14	150 ml	2% PVA MW 100 000	0.18	0.030 M (3.00 g)	–	–	0.056 M (7.17 g)	0.5 g	> 1 year	+++
Poly 15	150 ml	0% PVA MW 100 000	0.18 g	0.055 M (5.5 g)	–	–	0.030 M (3.84 g)	0.5 g	< 1 week	+++
Poly 16	150 ml	0.2% PVA MW 100 000	0.18 g	0.055 M (5.5 g)	–	–	0.030 M (3.84 g)	0.5 g	< 1 month	+++
Poly 17	150 ml	1% PVA MW 100 000	0.18 g	0.055 M (5.5 g)	–	–	0.030 M (3.84 g)	0.5 g	< 1 month	+++
Poly 18	150 ml	2% PVA MW 65 000	0.18 g	0.055 M (5.5 g)	–	–	0.030 M (3.84 g)	0.5 g	< 1 month	+++

electrodes and drying of the latex suspension. Secondary evaluation was made by comparing the photocurrent achieved with a comparable alginate immobilisation, to assess the activity of the immobilised cells.

Poly3 was prepared employing PVA and Tween 20 as the emulsifiers and MMA and MAA as monomers. Although the emulsion showed relatively good stability and the films cast from Poly3 appeared to give a uniform coating, this polymer was unsuitable for the immobilisation of photosynthetic cells as it was found that Tween 20 was responsible for the inactivation of the photosynthetic system, probably due to the destruction of the cell membranes. Tween 20 has been used in emulsion preparations as a non-ionic emulsifier, but as can be seen in the other polymers proposed in Table 1, its presence is not required for film formation and stability.

Better control over the polymerisation could be achieved if the initial concentration of ammonium peroxodisulfate was decreased significantly compared with Poly3. High concentration led in some cases to coagulation. Poly4 for example, exhibited good stability and film formation, but here the quality of the film cast onto an electrode was dependent on the pH of the emulsion from which the film was cast. The pH of the emulsion resulting from the Poly4 recipe was strongly acidic due to the high methacrylic acid content (pH 1.5–2) and films cast at this low pH appeared uniform. However, if the emulsion was adjusted to pH 7.0 the resultant films were inhomogeneous. Obviously, for the immobilisation of whole cells a pH as low as 2 is unsuitable, so to circumvent this problem in Poly6, MAA was replaced with NaMAA such that the pH during the polymerisation was neutral. However, although this emulsion showed good stability the film formation was strongly inhibited.

The pH dependency of the film forming properties of all emulsion polymers containing either MAA or NaMAA is probably due to the strongly charged emulsion particles. Around pH 7 the acid groups in the polymer are fully dissociated and therefore the particle carries maximum negative charge. This results in a strong repulsion force inhibiting the coagulation of the particles

when the emulsion is dried and resulting in poor quality inhomogeneous films.

The coalescence mechanism of latex polymers with a core-shell structure has been studied by Dobler et al. [17]. They found that the kinetics of coalescence was closely related to the interfacial tension at the polymer particle water interface. The rate of coalescence decreased as the amount of methacrylic acid in the shell was increased, or when sodium dodecyl sulfate was adsorbed onto the particles. The formation of homogeneous films was further inhibited when MAA in the shell was neutralised with sodium hydroxide. These findings are consistent with the results reported for Poly4 and Poly6. At low pH values the acid groups in the polymer are protonated giving the emulsion particle less charge and therefore the coalescence of particles during the drying is not hindered.

Furthermore the glass transition temperature (T_g) of MAA and NaMAA is relatively high compared to MMA. It is known that a high T_g will affect the film forming temperature (T_f) of the emulsion polymer. For the application as an immobilisation matrix for biological materials it is obvious that polymers with a high T_f , requiring curing at elevated temperature, are unsuitable, as this would lead to inactivation of the biological material. The introduction of BA into the polymer addresses this problem, as this monomer has a low T_g and thus decreases the T_f of the polymer. Poly7 shows the influence of BA, but as would be anticipated from the foregoing discussion, the films were still dependent on pH.

In order to achieve a film which can be cast at about pH 7, it is apparent that the resultant charge on the emulsion must be adjusted. Poly10 and Poly12 investigate the effect of decreasing the MAA ratio. In Poly10 the molar ratio of MAA has been decreased in favour of BA and Poly12 is a copolymer of only MMA and BA. It can be seen that the stability of the emulsion was not diminished as the MAA was replaced, but the film forming properties of the emulsion were improved and films cast from Poly12 were of good quality at a neutral pH. The introduction of BA also increased the adherence of the films to metal surfaces, a property which is required in

the application of these polymers as an immobilisation matrix in sensor technology.

Further adjustments in the molar ratio of BA and MMA allow the physical properties of the film to be manipulated. For example Poly14 resulted in an emulsion again with good stability, and films cast from this polymer appeared 'softer' compared with films cast from Poly12. In both cases the quality of the films was good at neutral pH values.

Additional tuning can be achieved by adjusting the emulsifier. In Poly15 to Poly17, for example the influence of the PVA concentration was investigated. It was found that although the polymers showed good film formation properties, the decrease in the PVA content led to a decrease in the stability of the emulsion stored at room temperature. This was most apparent in Poly15 were

no PVA was added and significant coagulation occurred after a few weeks storage.

The polymers 12 to 17 were considered suitable for further testing for their application as an immobilisation matrix for whole cells.

3.2. Photocurrent measurement

Initial apparent activity of the PET

The photosynthetic cyanobacterium *Synechococcus* sp. was immobilised as described in Materials and methods. The activity of the immobilised cells was tested by determination of the activity of the photosynthetic electron transport chain (PET) which is located in the thylakoid membrane. To retain its activity this membrane and all its components have to remain intact after the immobilisation. This can be determined by

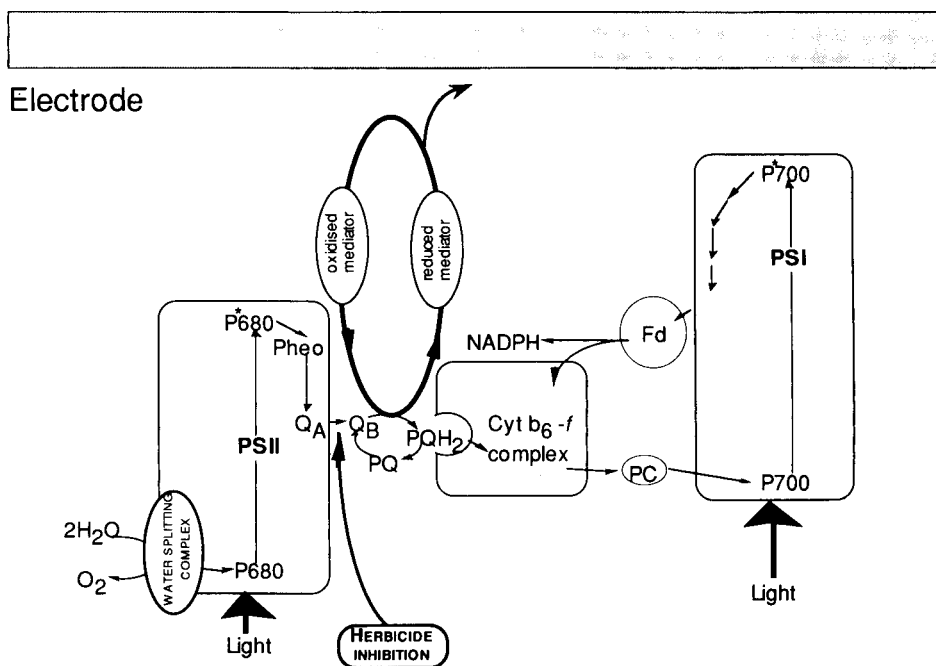


Fig. 1. Principle of the generation of a mediated photocurrent employing whole photosynthetic cells. Light energy, absorbed by the antenna pigments in the light harvesting complexes of the two photosystems PSII and PSI, is transferred to the respective reaction centre chlorophylls P680 and P700 which are in turn excited and eject electrons. The excited electrons are transported along a series of intermediates to ferredoxin (Fd), the final electron acceptor for photosystem I. The excitation of P680 is accompanied by the splitting of water and oxygen evolution, a reaction catalysed by the water splitting complex and the electrons from water are transferred to P680. A photocurrent is generated via the reduction of mediator which intercepts the electron transport between photosystem II and photosystem I and its subsequent reoxidation at the electrode. Pheo = Pheophytin, Q_a and Q_b = plastoquinones associated with PSII, PQ = plastoquinone pool, Cyt b₆-f complex = non haem iron sulphur complex, PC = plastocyanin, NADPH = nicotinamide adenine dinucleotide phosphate.

coupling the PET to an electrode employing a redox mediator (in this case DAD) which is able to accept electrons from the PET within the cell during activation by illumination. The reduced mediator is subsequently reoxidised at the electrode thus generating a photocurrent dependent on the activity of the PET. The general principal is shown in Fig. 1 and discussed in detail in a previous publication [18].

Fig. 2 shows the current response of an electrode modified with *Synechococcus* immobilised in the calcium-alginate/dialysis membrane system and in the emulsion polymers Poly12 and Poly14. The photocurrent is in all three cases of a similar magnitude although the time response varies. The steady state currents shown in Fig. 2 were normalised for the amount of chlorophyll immobilised at the electrode and compared with cells immobilised in Ca-alginate (Table 2). Ca-alginate was employed in this comparison since it is an extremely mild method of immobilisation of whole cells, as it does not involve the use of any bifunctional crosslinkers or other toxic reagents and can thus be considered as the 'standard' to relate the performance of these new latex polymers.

The composition of Poly15, Poly16 and Poly17 differ from Poly12 only in the amount of PVA present. However, although the influence of the PVA concentration on the activity of the immobilised cells is not straightforward it is apparent that a decreased signal accompanies a reduced PVA content. Poly16 and Poly17 (0.2% PVA and 1% PVA respectively) gave almost the same current response (30% of the photocurrent measured with Poly12), while with no PVA (Poly15) only 14% of the activity of Poly12 was recorded. In Poly18 a different molecular weight PVA was

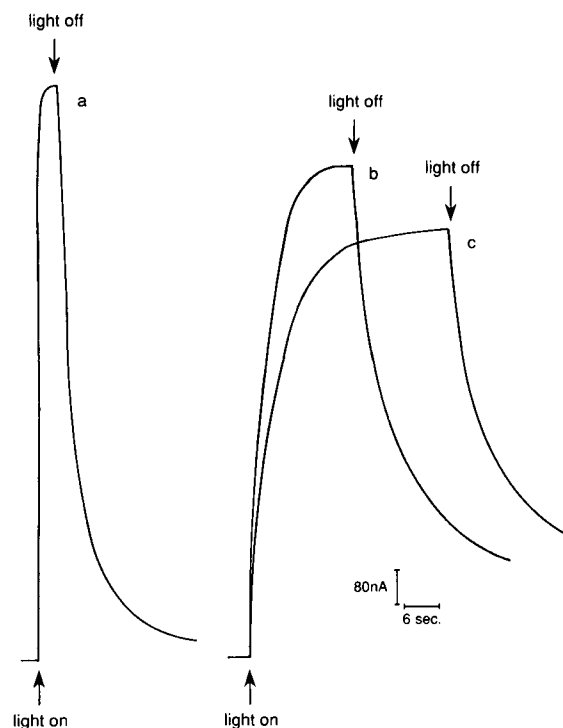


Fig. 2. Photocurrent generated by cells immobilised in calcium alginate (a), Poly14 (b) and Poly12 (c) at 0.2 V vs. SCE employing DAD as a mediator (0.2 mmol/l). The illumination period is indicated by the arrows.

added as the emulsifier: this again led to a significant decrease of the photocurrent compared to Poly12.

In conclusion therefore, the emulsion polymers could be fabricated which compared favourably with calcium alginate in their response and since unlike alginate the adherence of these films was good, no further physical support to hold the films at the electrode was necessary. The

Table 2
Activity of the PET in cells immobilised in different matrices

	Ca-alginate	Poly12	Poly14	Poly15	Poly16	Poly17	Poly18
I (μA)	3.30	2.46	2.80	0.52	1.22	1.17	1.01
ΣChl^a ($\mu\text{g}/\text{elec.}$)	0.018	0.012	0.015	0.018	0.018	0.018	0.014
I ($\mu\text{A}/\mu\text{g}$)	183.33	205.00	186.67	28.89	67.78	65.00	72.14

^a Immobilized chlorophyll (μg per electrode).

fabrication of the emulsion polymer modified electrodes was thus significantly simpler.

The current–time transient of the photocurrent measurement differs significantly for all three immobilisation matrixes shown in Fig. 2. The most obvious source of this difference would be the diffusion properties of DAD in these films and indeed the steady state photocurrent may be limited by the diffusion of the mediator. The diffusion properties of these films will be addressed later in this paper.

Long term stability

In view of the reduced stability of emulsions with lower PVA content, only Poly12 was tested over long periods. The long term stability of the immobilised photosynthetic cells was tested by measurements of the photocurrent as a response of the modified electrode to a series of light pulses. Light pulses rather than continuous illumination, were employed to minimise the deactivation of the photosynthetic system by illumination (photoinhibition). The photocurrent was measured daily, always employing the same electrode and the electrodes were stored at 4°C in fresh BG-11 medium when not in use. Fig. 3 shows the stability over a period of 10 days for cells immobilised in Poly12 and calcium alginate. In each case the behaviour was very similar, with a stable signal being recorded for three days, followed by a reduction over 3 days to a new stable level of about 80% of the original.

It must be concluded that since in the alginate electrode the cells are physically retained by a dialysis membrane, the deterioration in this instance is not due to leaching. By inference therefore, the similarity of the response from the emulsion polymer suggests that cells do not leach either, even though no retaining membrane is employed. It would be interesting to reflect on the cause of the reduction in the photocurrent since it is observed with the same pattern over the same time scale in both the Ca-alginate and the emulsion systems, but there is insufficient information from these experiments to make further conclusions.

Although the films cast from both Poly12 and Poly14 appeared uniform by visual inspection

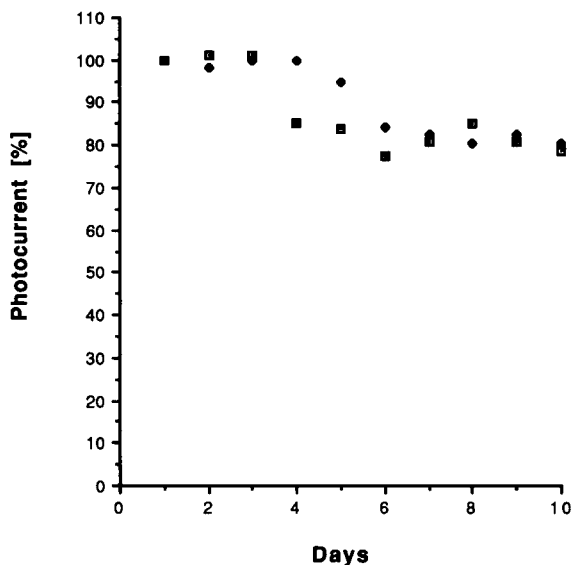


Fig. 3. Stability of the activity of the immobilised cells in calcium alginate (□) and Poly12 (◆). The electrodes were stored in fresh buffer at 4°C when not in use. The electrodes were illuminated by light flashes (250 ms) and DAD was used in a concentration of 0.2 mmol/l.

when cast onto electrodes with a small surface area (0.07 cm²) the coatings were less uniform when larger electrodes were employed. This was thought to be due to the low viscosity of the emulsions. An increase in the viscosity of the emulsion may therefore not only overcome this problem, but also make these emulsions applicable to mass production processes such as ink-jet printing or screen printing. We therefore added high molecular weight poly(ethylene oxide) (PEO, MW = 5 × 10⁶). This improved the uniformity of the coatings at larger electrodes. Fig. 4 shows the current response of electrodes modified with photosynthetic cells immobilised in Poly12 with the addition of different amounts of PEO to the casting solution. The photocurrent measured could be improved by the addition of low concentrations of PEO (up to 10% of the solid content of the emulsion polymer). However high concentrations of PEO added to the emulsion polymer led to a decrease in the measured photocurrent (e.g. 40% in Fig. 4). This may be associated with the high solubility of PEO in water, leading to a

water-soluble coating at high concentrations. It is also apparent from the time–current transient of the photocurrent measurements shown in Fig. 4, that the addition of PEO changes the time response, presumably due to the diffusion properties of the latex films. Changes in the partition of DAD in the phase next to the electrode would also modulate the steady state photocurrent.

The long term stability of the photosynthetic cell was also investigated when the electrodes prepared, as described in materials and methods, were stored in a dry state at 4°C (Fig. 5). A fresh electrode was employed for each experiment. Within the first two days the photocurrent decreased to about 50% of the original activity for both, the calcium-alginate/dialysis membrane and Poly12/PEO, but thereafter retained the same activity for up to 3 weeks. One cause of this rather large initial loss in activity of the photosynthetic system could be the maturation of the emulsion polymer film: a process in which the polymer film cast from an emulsion does not lose

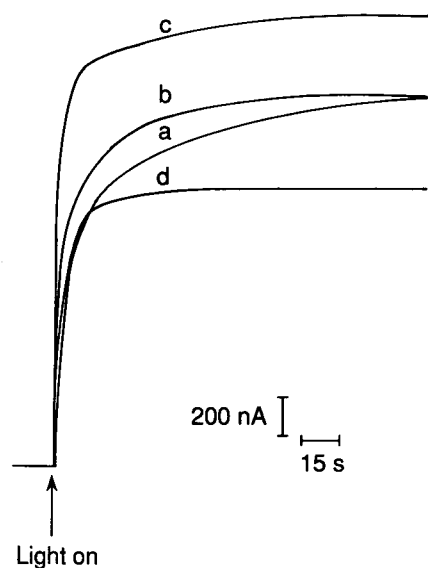


Fig. 4. Influence of the addition of PEO to Poly12 employed to immobilise the photosynthetic cells on the photocurrent generated. PEO was added to the emulsion before the film was cast at concentrations of a (0%), b (5.3%) c (10.7%) and d (42.1%) weight/weight with respect to the solid content of the emulsion polymer. Conditions of the photocurrent measurement as in Fig. 2.

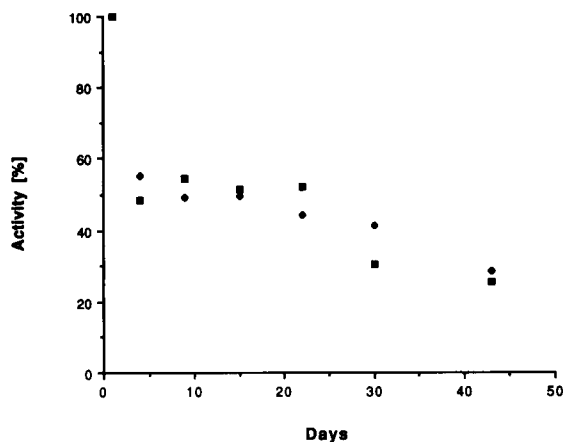


Fig. 5. Stability of the activity of immobilised cells in calcium alginate (□) and Poly12/PEO (♦). The electrodes were stored dry at 4°C, and disposed after the first use. The photocurrent was measured under constant illumination, the DAD concentration employed was 0.2 mmol/l.

significant amounts of water but changes its physical properties due to changes in the morphology of the film [19]. This can cause a change in the diffusion properties of the polymer film and therefore influence the magnitude of the photocurrent measured. Furthermore the process of maturation itself could lead to inactivation of the photosynthetic system. It seems however unlikely that the same maturation mechanism occurred in both Poly12/PEO and Ca-alginate, yet the initial drop of activity was similar for both immobilisation systems. The only commonality in the two methods lies in the identity of the cells, so that an explanation as to the cause of the decrease in activity, may lie in the rehydration properties of the cells themselves. After this initial loss of activity a slow gradual decrease of the measured photocurrent was recorded. Again Poly12/PEO and Ca-alginate gave very similar results. This decrease may reflect the deterioration of the photosynthetic system.

3.3. Investigation of the diffusion model for the emulsion polymer

Rotating disk electrode measurements allow the investigation of the mass transport of electroactive species through polymer membranes.

Gough and Leyboldt [20–22] showed that for an electroinactive polymer coated electrode the steady state current at low rotation rates is linear with the square root of the rotation rate. However, with the increase of the rotation rate the diffusion layer is confined within the polymer layer causing the steady state current to be independent of the rotation rate. Gough and Leyboldt derived the following relationship between the limiting steady state current, i_{lim} , and the rotation rate of the electrode:

$$\frac{1}{i_{lim}} = \frac{1}{0.62nFAC_{\infty}D^{2/3}\nu^{-1/6}\omega^{1/2}} + \frac{\delta}{nFAKc_{\infty}D_m} \quad (1)$$

where i_{lim} is the steady state current measured employing a rotating disc electrode modified with a polymer membrane measured at the plateau current of the oxidation wave. The first term of the equation is given by the Levich current $i_{lev} = 0.62nFACD^{2/3}\nu^{-1/6}\omega^{1/2}$ which applies for the current measured at an uncoated electrode. The second term in Eq. 1 involves the permeability of the polymer membrane given by:

$$P_m = \frac{KD_m}{\delta} \quad (2)$$

Where K is the partition coefficient, D_m the diffusion coefficient of the electroactive species in the membrane and δ is the thickness of the membrane. The other terms have their usual significance. From this it is clear that only the permeability can be extracted from RDE experiments unless both the thickness of the polymer membrane and the partition coefficient are determined by an independent measurement. Nevertheless the P_m value by itself will allow a qualitative comparison of the transport of DAD in the different emulsion polymer films prepared in this study.

Fig. 6(I) shows single sweep voltammograms of an uncoated RDE at different rotation rates. The cathodic current was almost independent of the rotation rate indicating that DAD is present in its reduced form in the bulk solution. The anodic current reached a plateau current at +100 mV and was strongly dependent on the rotation speed.

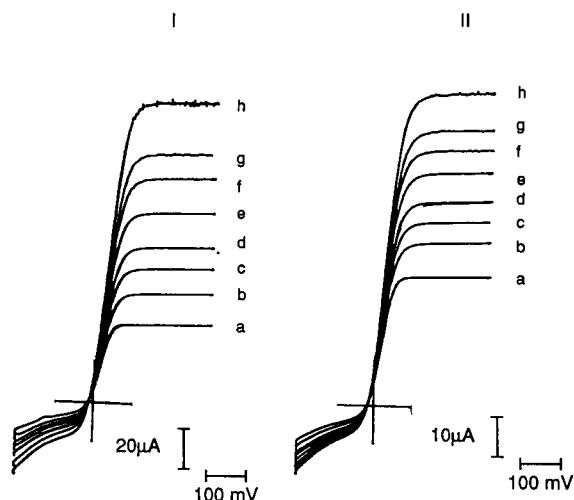


Fig. 6. Single sweep cyclic voltammograms of an uncoated (I) electrode and an electrode coated with Poly12 (II) at different rotation speeds (a = 50 rpm, b = 100 rpm, c = 150 rpm, d = 200 rpm, e = 300 rpm, f = 400 rpm, g = 500 rpm, h = 750 rpm). The concentration of DAD was 2.4 mmol/l.

In Fig. 6(II) the same experiment was performed with a coated electrode. The anodic current is again dependent on the rotation rate, however

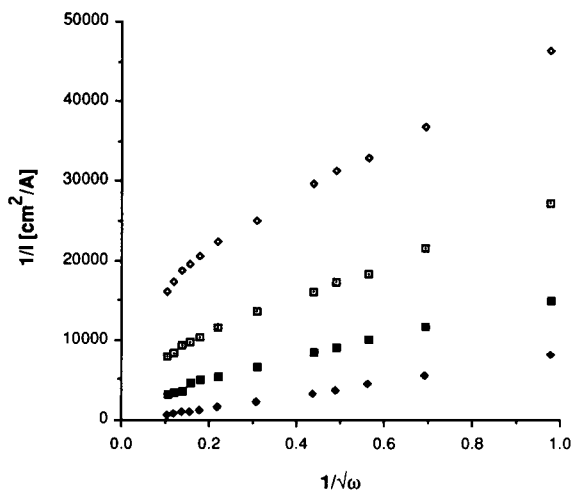


Fig. 7. Koutecky-Levich plot for electrodes coated with films cast from Poly12 with 7.24% solids (◇), 6.33% solids (□), 4.2% solids (■) and an uncoated electrode (◆). The rotation rate was varied from 10 rpm to 900 rpm, the electrolyte consisted of 0.1 mol/l KCl and 0.05 mol/l MOPS adjusted to pH 7.0. DAD was added to the electrolyte at a concentration of 2.4 mmol/l.

the magnitude of the current was greatly reduced compared with the uncoated electrode. In all further experiments the electrode was held at a positive potential of 300 mV and the steady state current was measured as a function of the rotation speed.

According to Eq. 1 a plot of i_{lim}^{-1} vs. $\omega^{-1/2}$ (Koutecky-Levich) for a polymer modified electrode should have the same slope as a similar plot for the uncoated electrode given by the Levich equation. The positive intercept is determined by the permeability of the polymer coating. Such plots for electrodes coated with different amounts of Poly12 and Poly14 are shown in Fig. 7 and Fig. 8, respectively. The amount of polymer was var-

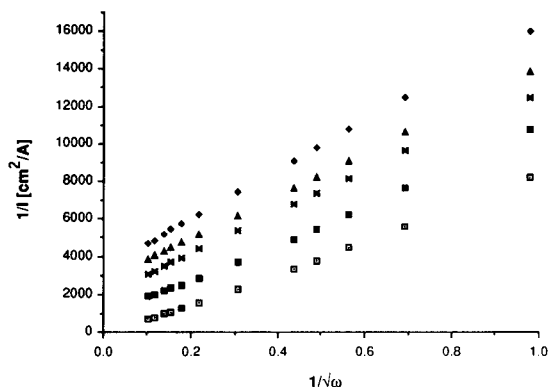


Fig. 8. Koutecky-Levich plot for electrodes coated with films cast from Poly14 with 6.33% solids (\blacklozenge), 4.22% solids (\blacktriangle), 3.16% solids ($*$), 2.11% solids (\blacksquare) and an uncoated electrode (\square). Conditions as described in the legend of Fig. 7.

Table 3

Estimated values for the permeability (P_m in cm/s) of films cast from the emulsion polymers, employing the membrane model

(a) Different solid content, Poly12 and Poly14

Solids (w/v)	2.11%	3.16%	4.22%	6.33%	7.24%
Poly12			7.4×10^{-4}	2.8×10^{-4}	1.42×10^{-4}
Poly14	30.6×10^{-4}	10.7×10^{-4}	8.0×10^{-4}	6.29×10^{-4}	

(b) Different solid content, Poly12/PEO and Poly14/PEO

Solids (w/v)	2.07%	4.22%	6.33%
Poly12/PEO	34.6×10^{-4}	17.3×10^{-4}	8.1×10^{-4}
Poly14/PEO	32.0×10^{-4}	14.7×10^{-4}	8.9×10^{-4}

(c) Different concentrations of DAD

DAD (mol/l)	0.61×10^{-6}	1.22×10^{-6}	2.44×10^{-6}
Poly12/PEO (6.33% solids)	6.3×10^{-4}	5.8×10^{-4}	6.2×10^{-4}
Poly14/PEO (4.22% solids)	18.1×10^{-4}	18.6×10^{-4}	17.2×10^{-4}

(d) Poly12 dried for different times

Drying time (h)	1	3	7	16
Poly12/PEO	9.1×10^{-4}	11.5×10^{-4}	16×10^{-4}	13.8×10^{-4}

(e) Different immobilised cell concentrations (as chlorophyll)

ΣChl (μg)	0	0.17	0.34	0.67	1.27
Poly14/PEO 6.33% solids	7.7×10^{-4}	7.5×10^{-4}	6.3×10^{-4}	5.6×10^{-4}	5.16×10^{-4}
ΣChl (μg)	0	0.09	0.22	0.45	
Poly12/PEO 6.33% solids	17.7×10^{-4}	16.1×10^{-4}	12.4×10^{-4}	11.3×10^{-4}	

ied by changing the solid content of the emulsion polymer from which the film was cast.

As would be expected, the intercept is seen to increase with solid content, allowing an estimate of P_m which decreased systematically (Table 3a). It is also apparent that deviation from the Levich slope increases with solid content and that this is greater in Poly12 (Fig. 7) than Poly14 (Fig. 8). In the former case estimates of P_m made by extrapolation, are of the same general order as Poly14. It is clear however, that adoption of the membrane model of an electroinactive matrix is not really appropriate here, since the deviation from both linearity and Levich slope is significant. As already suggested, films of Poly12 and Poly14 are not completely uniform. Indeed, this non-uniformity may be the result of 'pinholes' in the membrane. These may not be holes in the membrane in the strict sense, but areas of low density where the diffusion coefficient is of the same order of magnitude as in solution and other areas where the electrode surface is effectively inactivated. Such a model would be consistent with the coalescence mechanism idea as described earlier.

An analysis of the pinhole model has been made by Landsberg and co-workers [23–25], allowing the size and distribution of such holes to be estimated from RDE data. According to their model, diffusion to the electrode surface occurs via the pin-hole channels and not through the membrane itself.

$$\frac{1}{i_{\text{lim}}} = \frac{1.61\nu^{1/6}}{nFD_s^{2/3}c_sA\omega^{1/2}} + \frac{\sum A_n \tanh\left[\frac{x_n\delta_o}{r_2}\right]}{nFD_sAc_s} \quad (3)$$

where $\delta_o = 1.61D^{1/3}\nu_{1/6}\omega^{-1/2} = nFAD_s\text{Lev}$; $2r_2$ = distance between adjacent holes; r_1 = radius of the hole; x_n = zero point of the 1st order Bessel functions A_n is a function of r_1 , r_2 and x_n .

Since δ_o is a function of ω , a plot of $1/i_{\text{lim}}$ vs. $1/\omega^{1/2}$ will be non-linear. The two limiting cases are:

(i) $\delta_o > r_2$, $A_n \tanh[x_n\delta_o/r_2] \rightarrow A_n$. Therefore, for small rotation rates i.e. large values of δ_o

compared to r_2 , Eq. 3 will reduce to:

$$\frac{1}{i_{\text{lim}}} = \frac{1.61\nu^{1/6}}{nFD_s^{2/3}c_sA^{1/2}} + \frac{\sum A_n}{nFD_sAc_s} \quad (4)$$

According to Eq. 4 a plot of i_{lim} vs. $\omega^{1/2}$ will result in a straight line parallel to the Levich plot with a non-zero intercept. Extrapolation to $\omega = 0$ allows the estimation of A_n . According to Eq. 3 deviation from the linear relationship of i_{lim} on $\omega^{1/2}$ should occur at $\delta_o = r_2$. A working curve [24] equates the value of A_n/r_2 to the ratio of r_1 and r_2 from which the surface coverage can be calculated.

(ii) $\delta_o < r_2$, $A_n \tanh[x_n\delta_o/r_2] \rightarrow A_n x_n \delta_o/r_2$. The linear dependency of δ_o on $\omega^{1/2}$ leads to a straight line with a zero intercept and a slope as in Eq. 5:

$$\text{slope} = \frac{1.61\nu^{1/6} \left(1 + \frac{A_n x_n}{r_2}\right)}{nFD_s^{2/3}c_sA\omega^{1/2}} \quad (5)$$

Fig. 7 shows that for films cast from Poly12 with different solid contents the rotation rate at which deviation from the straight line occurred is constant. At high rotation rates where δ_o is expected to be significantly smaller than r_2 the graphs tended towards a zero intercept. The slope in the region of $\delta_o > r_2$ (low rotation rates) did change with the increase in the solid content of the emulsion. This is in disagreement with Eq. 4 and may be explained by a change in D_s in the first term. As mentioned above, the pin hole model is based on a blocked electrode with circular active sites, the diffusion coefficient in the holes is equal to that in free solution and is obviously not dependent on r_2 . In our case the increase in the solid content may decrease the mass transport rate of DAD through the low density areas which we considered to be the active area of the electrode, resulting in an increase of the slope in the Koutecky-Levich plot.

Values for r_2 , r_1 were estimated according to the method of Scheller et al. [24] and the surface coverage Ψ (Table 4) obtained from the r_1/r_2 ratio [24]. r_2 was independent of the solid content, whereas r_1 decreased with increasing solid content. The surface coverage increased, as could be expected with the increase of the solid con-

Table 4

Values for the parameters describing the 'pin-hole' model estimated according to the method developed by Landsberg and co-workers [23–25] for a film cast from Poly12

Solid content	7.24%	6.33%	4.20%
ΣA_n	16×10^{-3}	7.02×10^{-3}	2.80×10^{-3}
r_2	1.57×10^{-3} cm	1.57×10^{-3} cm	1.57×10^{-3} cm
r_1	1.09×10^{-4} cm	2.19×10^{-4} cm	4.39×10^{-4} cm
Ψ	99%	98%	92%

tent. These findings indicate that films cast from Poly12 are not uniform in their morphology.

By comparison, for Poly14 the Koutecky-Levich plot was linear over the whole range of $\omega^{1/2}$ and had a non zero intercept for all solid contents investigated (Fig. 8). Treated in the pin-hole model $d_o \gg r_2$ ($r_2 < 6.3 \times 10^{-4}$ cm) for all solid contents and therefore, case ii for Eq. 3 can be eliminated for this polymer. A_n calculated according to the model of Landsberg has a value of 3×10^{-3} cm so that if r_2 becomes less than 0.6 μ m, then r_1 is of the order of 50 nm which tends towards a "pin-hole-free" polymer. From this point of view it seems that Poly14 leads to a more uniform morphology of the film compared with Poly12. This may be a result of the difference in the monomer composition of Poly12 and Poly14. The increased BA content of Poly14 compared with Poly12 is expected to cause a decrease in the lowest film forming temperature of Poly14, as the glass transition temperature of BA is considerably lower compared with MMA. If the lowest film forming temperature for Poly12 is above 40°C, the temperature at which the films were dried, the coagulation of the polymer particles will not be complete, leading to inhomogeneous coatings cast from this polymer.

Based on these models, coagulation of the polymer particles occurs during the drying process to give high density areas in the case of Poly12 which cause "inactivation of the electrode surface" and areas of low density with relatively high transport rates of the electroactive species.

In Fig. 9 and Fig. 10, Koutecky-Levich plots for polymer coatings from both Poly12 and Poly14 with the addition of PEO also indicate a more uniform film. For both polymers the change in

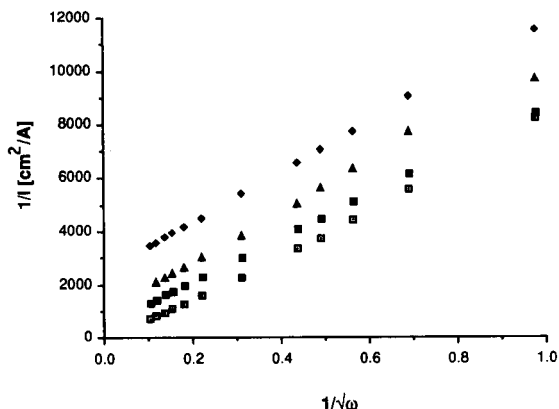


Fig. 9. Koutecky-Levich plot for electrodes coated with films cast from Poly12-PEO (10.7%, w/w) with 6.33% solids (♦), 4.22% solids (▲), 2.07% solids (■), and an uncoated electrode (□). Conditions as described in the legend of Fig. 7.

solid content of the coating did not influence the Levich slope, indicating that these coatings can be better represented by the membrane model. The permeability for both polymers increased significantly with the decrease of the solid content of the emulsion (Table 3b) and were of a similar magnitude for a given solid content. However, the addition of PEO to Poly12 and to Poly14 increased the extrapolated permeability of the resulting film and this may be responsible for the increase in the photocurrent for the PEO containing films shown in Fig. 4. PEO has been used extensively as a polyelectrolyte as it forms poly-

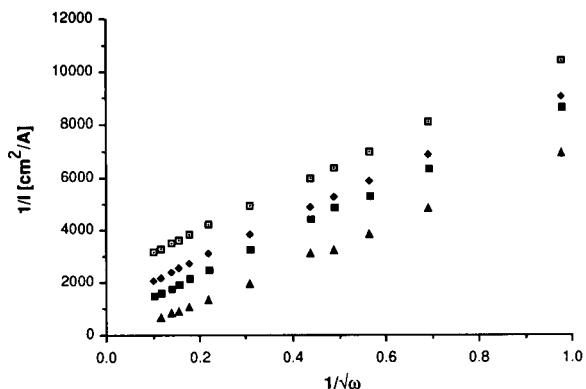


Fig. 10. Koutecky-Levich plot for electrodes coated with films cast from Poly14-PEO (10.7%, w/w) with 6.33% solids (□), 4.22% solids (♦), 2.07% solids (■), and an uncoated electrode (▲). Conditions as described in the legend of Fig. 7.

mer–salt adducts with many common alkali salts [26]. However, the salts employed in this study are unfavourable for the interaction with PEO as a polyelectrolyte and it seems unlikely therefore, that this property is responsible for the increase in the permeability of the films with PEO added to the emulsion polymer. Roulstone et al. [27] investigated the influence of the addition of a non-ionic surfactant, containing a relatively short chain of ethylene oxide, on the film forming properties of a poly(butyl methacrylate) latex. The addition caused an increase in the water vapour permeability and hydrophilicity of the film cast from the emulsion. In a similar way, PEO may act as a plasticiser when added to Poly12 and Poly14 improving both the homogeneity and the hydrophilicity of the films, yielding an increase in their permeability. The permeability for both polymers was, as expected from Eq. 1, independent of the concentration of DAD in the bulk solution (Table 3c).

The formation of a continuous film from a latex polymer can be divided into three stages [28]. During the first stage, defined as the time until the polymer particles come into irreversible contact with each other, which is due to the concentration occurring as the water evaporates, the rate of evaporation is very similar to that of water in the presence of the surfactant. In the intermediate stage the particles coagulate and fuse into a continuous film. The rate of evaporation decreases significantly during this period. The third stage, often referred to as maturation of the films describes further changes of the physical properties of the film. Distler and Kanig [29] observed that in a film cast from an acrylate latex, the boundaries between deformed latex particles were maintained even after the films were dried. Chainey et al. [19] compared the permeability of gases through films cast from different latex polymers and solvent cast films. They found that the permeability of films cast from the emulsions showed generally higher permeabilities compared with solvent cast films from the same polymer. However, the permeability for the latex film decreased significantly with the age of the polymer as the latex particles boundaries deteriorate. We therefore studied the permeabil-

ity of DAD in films cast from Poly12–PEO as a function of the drying time. The P_m did not change significantly if the film was dried for 1 h or 16 h at 40°C (Table 3d), but this PEO containing polymer did not show “pin-hole” behaviour so that one could propose that in this instance the latex boundaries had already merged. This is again an indication that the initial decline in activity of the immobilised cells when the electrodes are stored in the dry state (Fig. 5) is not due to a change in the diffusion properties of the polymer film due to maturation.

We also investigated the influence of the immobilisation of photosynthetic cells into the polymer matrix on its permeability. It was found that for both polymers the amount of cells immobilised, determined by the chlorophyll concentration (ΣCHL), had no or only little influence on the permeability of the polymer film (Table 3e).

4. Conclusions

In this paper the use of film forming emulsion polymers based on acrylates for the immobilisation of photosynthetic cells is described. Latex copolymers of methylmethacrylate and *n*-butyl acrylate were found to exhibit good stability when stored at room temperature. The activity of the photosynthetic system retained in the polymer matrix was similar to activities measured when the cells were immobilised in Ca-alginate matrixes but the emulsion polymers could be deposited in thin layers, not requiring retaining membranes. The long term stability of the cells in both the emulsion polymer films and Ca-alginate films were similar when the electrodes were stored in buffer and its dry state.

RDE experiments were performed to study the morphology and diffusion properties of the films. A modified “pin-hole” model was proposed to describe the inhomogeneity in Poly12. When the model was applied to Poly14 it led to the conclusion that the “pin-holes” tended to zero and presented a more homogeneous membrane. The addition of PEO to the emulsions generally increased the permeability and homogeneity of both the Poly12 and Poly14 films. These results are encouraging for the further develop-

ment of these polymers for the immobilisation of intact cells as they allow a rigorous control over the immobilisation conditions and are compatible with many mass production techniques such as screen or ink jet printing. However, their further exploitation must identify the nature of the aging process which lead to the signal deterioration in the model presented here.

Acknowledgements

We would like to thank the “Gottlieb Daimler und Karl Benz Stiftung” for the financial support. We would also like to thank Dr. Carl Hall for his invaluable assistance in designing emulsion recipes.

References

- [1] W.J. Aston and A.P.F. Turner, in J. Russels (Ed.), *Biotech. Genet. Eng. Rev.*, Intercept, Newcastle-upon-Tyne, Vol. 1, 1984, p. 89–120.
- [2] H.P. Bennetto, in A.M. Michelson and Bannister (Eds.), *Live Chemistry Reports* Harwood Academic, London, Vol. 2, No. 4 (1984) pp. 363–453.
- [3] N. Bernet, P. Naouri, A. Arnaud, P. Galzy and G.M. Rios. *J. Chem. Eng.*, 46 (1991) B43.
- [4] P. Linko and Y.Y. Linko, in I. Chibata and L.B. Wingard (Eds.), *Immobilized Microbial Cells*, Academic Press, New York, 1983, pp. 12–51.
- [5] I. Chibata and T. Tosa, *TIBS*, 5 (1980) 88.
- [6] W. Hartmeier, *Food-Biotechnol.*, 4 (1991) 399.
- [7] Y. Kuwada and Y. Ohta, *J. Ferment. Technol.*, 65 (1987) 597.
- [8] E. De-Alterilis, P. Parascandola, M.A. Pecorella and V. Scardi, *Biotechnol. Tech.*, 2 (1988) 205.
- [9] J. Klein and F. Wagner, in I. Chibata and L.B. Wingard (Eds.), *Immobilized Microbial Cells*, Academic Press, New York, 1983, pp. 12–51.
- [10] A.Y. Freeman and Y. Aharonowitz, *Biotechnol. Bioeng.*, 23 (1981) 2747.
- [11] S. Fukui and A. Tanaka, in A. Fichter (Ed.), *Advances in Biochemical Engineering and Biotechnology*, Springer Verlag, Berlin, 1984, pp. 1–33.
- [12] E. Miller, *J. Radioanal. Nucl. Chem.*, 158 (1992) 383.
- [13] D.H. Napper, *J. Colloid Interface Sci.*, 58 (1977) 390.
- [14] R.H. Ottewill, in I. Prima (Ed.), *Emulsion Polymerisation*, Academic Press, New York, 1982, p. 1.
- [15] R. Rippka, J. Deruelles, J.B. Waterbury, M. Herdman and R.Y. Stanier, *J. Gen. Microbiol.*, 111 (1979) 1.
- [16] M.F. Hipkins and N.R. Baker, in M.F. Hipkins (Ed.), *Photosynthesis, Energy Transduction. A Practical Approach*, IRL Press, Oxford, 1986, p. 63.
- [17] F. Dobler, T. Pith, M. Lambla and Y. Hol, *J. Colloid Interface Sci.*, 152 (1992) 1.
- [18] N. Martens and E.A.H. Hall, *Photochem. Photobiol.*, (1994) in press.
- [19] M. Chainey, M.C. Wilkinson and J. Hearn, *Sci. Polym. Chem. Ed.*, 23 (1985) 2947.
- [20] D.A. Gough and J.K. Leyboldt, *Anal. Chem.*, 51 (1979) 439.
- [21] D.A. Gough and J.K. Leyboldt, *A.I.Ch.E.J.*, 26 (1980) 1013.
- [22] D.A. Gough and J.K. Leyboldt, *Anal. Chem.*, 52 (1980) 1126.
- [23] R. Landsberg and R. Thiele, *Electrochim. Acta*, 11 (1966) 1243.
- [24] F. Scheller, S. Müller, R. Landsberg and H.-J. Spitzer, *J. Electroanal. Chem.*, 19 (1968) 187.
- [25] F. Scheller, R. Landsberg and S. Müller, *J. Electroanal. Chem.*, 20 (1968) 375.
- [26] M.B. Armand, *Ann. Rev. Matter. Sci.*, 16 (1986) 245.
- [27] B.J. Roulstone, M.C. Wilkinson and J. Hearn, *Polym. Int.*, 27 (1992) 43.
- [28] J.W. Vanderhoff, E.B. Bradford and W.K. Carrington, *J. Polym. Sci. Polym. Symp.*, 41 (1973) 155.
- [29] D. Distler and G. Kanig, *Colloid Polym. Sci.*, 253 (1975) 29.



ELSEVIER

Analytica Chimica Acta 292 (1994) 65–70

**ANALYTICA
CHIMICA
ACTA**

Total urinary protein sensor based on a piezoelectric quartz crystal

Shigeo Imai ^a, Haruyuki Mizuno ^a, Masayasu Suzuki ^b, Toshifumi Takeuchi ^b,
Eiichi Tamiya ^b, Fumiko Mashige ^c, Akiyuki Ohkubo ^c, Isao Karube ^{*,b}

^a INAX Corporation, Central Research Laboratory, 3-77 Minatomachi, Tokoname-shi, Aichi 479, Japan

^b Research Center for Advanced Science and Technology, University of Tokyo, 4-6-1 Komaba, Meguro-ku, Tokyo 153, Japan

^c Department of Laboratory Medicine, Faculty of Medicine, University of Tokyo, 7-3-1 Hongo, Bunkyo-ku, Tokyo 113, Japan

(Received 2nd August 1993; revised manuscript received 4th January 1994)

Abstract

A protein sensing system using a piezoelectric sensor with an AT-cut quartz crystal of a basic resonant frequency of 9 MHz has been developed and applied to the determination of total protein in urine. The measurement method is based on the sedimentation of proteins by a turbidimetric procedure. The amount of precipitate formed was determined as the resonant frequency change of the quartz crystal because of the mass change on the surface of the piezoelectric sensor due to the precipitation. A satisfactory correlation was observed between the protein concentration and the frequency change at the range from 50 to 1000 mg/l, and a coefficient of variation (C.V.) of 5.3% ($n = 10$) was given for 300 mg/l albumin when sulfosalicylic acid was used as the precipitation reagent. When trichloroacetic acid was used as the precipitator, the C.V. was 3.2% ($n = 12$), and the difference in results for the same concentration of albumin and globulin was much less than that when using sulfosalicylic acid. Treatment with a protease after the measurement was effective for cleaning the electrode surface, allowing the device to be repeatedly used over 300 times.

Key words: Sensors; Piezoelectric sensors; Urinary protein sensor; Quartz

1. Introduction

The need for an accurate, simple and rapid method for determining total protein in urine is quite apparent. Slightly increased excretion of protein in urine has been recognized as an early indicator of renal damage in diabetes [1]. In diabetes, urinary protein excretion increases in asso-

ciation with renal glomerular hyperfiltration; it occurs in the initial stage of disease [2]. Therefore, the measurement of proteins in urine is significantly important in the field of renal pathology.

Urinary proteins have been determined by colorimetric methods [3,4], and automated assays employing these methods have been used in clinical laboratories. Although the colorimetric methods can be easily performed, they are sometimes problematic because these methods give different

* Corresponding author.

absorbances depending upon proteins to be tested. Turbidimetric methods using precipitants are also used and the sensitivity is acceptable for practical use [5–7]. An advantage of this technique is that the differences in results among various proteins is less than those in the colorimetric methods, thus, more precise levels of total protein could be determined more precisely.

In this study, we employed a microbalance system based on the measurement of small mass changes on the surface of a piezoelectric quartz crystal caused by sedimentation of proteins in urine, instead of using a conventional optical detection systems. The piezoelectric quartz crystal is well-known as a nanogram-sensitive mass detector [8]. It has been applied in chemical analysis to the direct determination of metal ions [9], microbes [10], immunoglobulins [11,12] and gases [13,14]. It has also been found that piezoelectric quartz crystals can oscillate in solution [15].

In this paper, two precipitation reagents, sulfosalicylic acid (SSA) and trichloroacetic acid (TCA) were used for the quantitative precipitation of proteins, and the mass precipitated was determined by the piezoelectric sensor. The effectiveness of the sensor is demonstrated by the determination of total urinary protein and the reusability of the sensor is discussed.

2. Experimental

2.1. Reagents and materials

SSA, TCA, bovine serum albumin (BSA), human γ -globulin and a kit for measuring total protein (MICRO TP-TEST WAKO; pyrogallol red method) were obtained from Wako (Osaka). Human serum albumin (HSA, Fraction V), protease (Type 1, crude) and Triton X-100 were obtained from Sigma (St. Louis, MO). Quantitative urine controls (Lyphochek, normal and abnormal) manufactured from pooled human urine were obtained from Bio-Rad (Richmond, CA). Other reagents were of analytical grade and distilled water was used for all procedures.

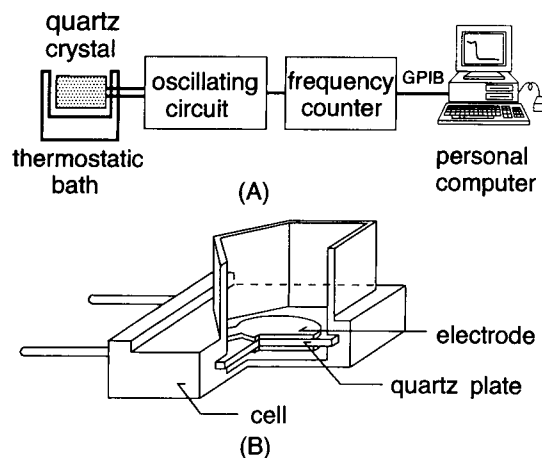


Fig. 1. Schematic diagram of the sensor system (A) and the well-type cell (B). The quartz crystal plate is set at the bottom of the cell.

A protein stock solution (1 g/l) was dissolved in 0.1 M glycine buffer solution (GBS, pH 3.0), and was standardized by the pyrogallol red method. It was stored at 4°C and prepared freshly in each month. The working standards were prepared by diluting the stock solution with GBS to yield the appropriate concentrations (50, 100, 200, 300 and 500 mg/l).

Urine samples collected from healthy volunteers were preincubated at 30°C in a water bath before the determination. Quantitative urine controls (normal and abnormal) are also used in the same way.

2.2. Apparatus

Fig. 1 shows a schematic diagram of the sensing device. Quartz crystals were obtained from Seiko (Tokyo). The piezoelectric quartz crystals used in this study consist of AT-cut quartz with a basic resonant frequency of 9 MHz. The crystal surface was coated with silver by vapour deposition to form silver electrodes and in order to protect the electrode surface palladium layers were deposited on the surface by electrochemical plating. The quartz crystal was fixed to the cell with silicon gum in which only one side of the quartz crystal electrode was allowed to contact with liquid phase (Fig. 1B). An oscillator circuit

constructed from a TTL-IC (SN7400, Texas Instruments) was directly connected to the quartz crystal electrodes and the crystal frequency was monitored with a universal counter (Iwatsu SC-7201, Tokyo). An NEC microcomputer (PC-9801 RX, Tokyo) was used to record resonant frequency data. The cell, sample and precipitant solutions (SSA and TCA) were kept at 30°C in a thermostated water bath during the experiments.

Response of piezoelectric crystals to changes in mass at the surface is given by the following equation [8]:

$$\Delta F = -K\Delta m$$

where ΔF is the frequency change (Hz), Δm is the change in mass at the crystal surface (g). The constant K depends upon the resonant frequency, thickness, electrode area and density of the crystal.

2.3. Standard procedures

Four hundred μl of sample or a standard solution is pipetted into the cell. The steady resonant frequency (F_1) was measured after 200 s from the injection, and 71 μl of 0.79 M SSA is pipetted into the cell (the final SSA concentration is 0.12 M). The resonant frequency (F_2) after 250 s from the injection of SSA was measured. A frequency change is calculated by $\Delta F = F_1 - F_2$. When TCA is used as the precipitate, 100 μl of sample solution and 300 μl of 0.31 M TCA were injected into the cell. All the measurements were carried out by the batch process. The quartz crystal was stored in distilled water.

2.4. Cleaning procedure of the electrode surface

Four solutions, (a) 1 M HCl, (b) 5 g/l protease dissolved in 0.1 M phosphate buffer at pH. 7.0, (c) 1% Triton X-100, and (d) 0.1 M NaOH, were examined for cleaning the electrode surface. After measuring the protein standard solution (300 mg/l), the cell is washed five times with distilled water, then 200 μl of treatment solution is injected into the cell. After 200 s, the cell was then washed five times with distilled water. Distilled

water (400 μl) is poured into the cell, and after 200 s the resonant frequency is measured.

3. Results and discussion

3.1. Protein determination with SSA

When a protein solution was injected into the cell, the frequency decreased rapidly and after 200 s from injection the frequency became constant (F_1). When SSA was added to the cell, the resonant frequency (F_2) became stable after 10 min from injection. The frequency change caused by the addition of the precipitation reagent was 137 Hz in the SSA system. Fig. 2 shows typical responses of the sensor for BSA with SSA as the precipitate. As can be seen the extent of the frequency change depended on the concentration of BSA. It was found that the values of F_2 after 250 s from injection showed good reproducibility although the precipitation reaction had not yet reached equilibrium, therefore this time period (250 s) was used for further experiments.

A relationship between protein concentrations and the resonant frequency changes is shown in Fig. 3. Linear calibration graphs were obtained for BSA and HSA in the range 50–1000 mg/l. The amplitude of the frequency change depended on the concentration of each protein. For human

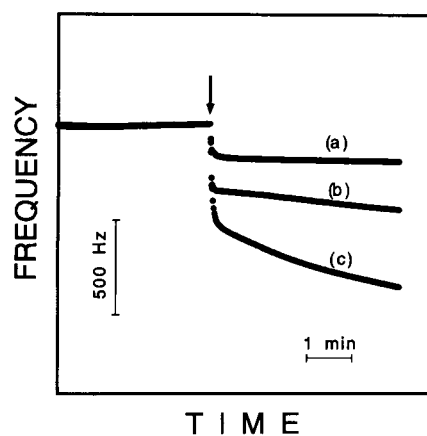


Fig. 2. Resonant frequency responses to 100 (a), 500 (b) and 1000 (c) mg/l BSA standard solutions at 30°C. The downward arrow shows the injections of SSA.

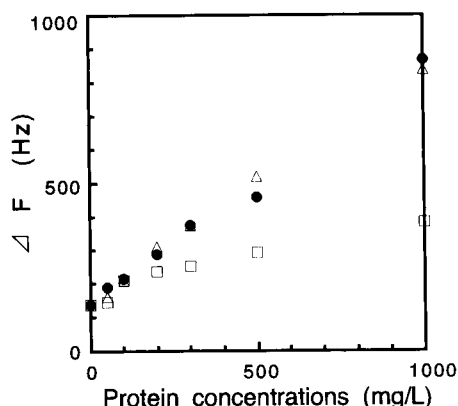


Fig. 3. Relationship between protein concentration and the resonant frequency change with SSA at 30°C. The frequency change (ΔF) was measured after 250 s from the injection of SSA; (Δ) BSA, (\bullet) HSA, (\square) human γ -globulin.

γ -globulin, no linear relationship was observed and the sensitivity appeared to be approximately half that of HSA and BSA. It was reported that there was a great discrepancy between the total protein found and calculated for an artificial mixture of albumin and globulin when SSA was used because of the difference in turbidity produced by SSA with albumin and globulin [7]. The same tendency was observed in the present piezoelectric sensor system.

Proteins are ordinarily present in human urine at a low concentration level, < 100 mg/l, therefore when a sustained value is about 150 to 300 mg/l or more, it is usually regarded as abnormal [2]. Because the detection limit of the system using SSA was 50 mg/l, the sensitivity is high enough to apply to the determination of urinary protein for initial screening.

The system was applied to the determination of urinary proteins in order to examine the effect of the urine matrix. Two healthy urine specimens and a quantitative urine control were analyzed by the present method and a conventional colorimetric method using pyrogallol red. A good linear correlation was observed between the frequency changes using the present method and the concentration of total protein measured using the pyrogallol red method: ΔF (Hz) = 5.94 [protein] (mg l^{-1}) + 214 ($r = 0.993$, $n = 4$) for these three

samples over the range 0–600 mg l^{-1} . The results demonstrate the technical feasibility of this system; however, more detailed investigation may be necessary for further practical applications because factors such as pH, viscosity and the ionic strength of the urine sample may affect the formation of precipitate and the sedimentation rate.

3.2. Effect of the protein removal treatment

When the sensor was used repeatedly, the resonant frequency became unstable and eventually a low sensitivity and a poor reproducibility were observed. The major reason for these phenomena could be the adsorption of proteins onto the surface of the quartz crystal, because the resonant frequency gradually decreased. In order to improve the poor reusability, we examined four treatments, (a) 1 M HCl, (b) 5 g/l protease, (c) 1% Triton X-100, and (d) 0.1 M NaOH for the removal of impurities on the surface. The treatment was carried out each time after measuring the protein standard solution (300 mg/l BSA; $n = 10$). As shown in Fig. 4, no improvement was observed with treatments (c) and (d), while the resonant frequency gradually increased with treatment (a). Treatment (b) gave the most satisfactory results because the sensor gave the most stable responses among the four treatments.

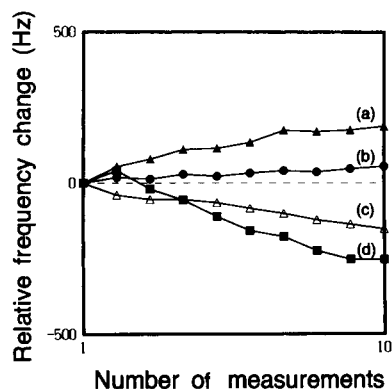


Fig. 4. Resonant frequency responses by the effect of BSA adsorption measured in the water after the rinsing with (a) 1 M HCl; (b) 5 g/l protease; (c) 1% Triton X-100; (d) 0.1 M NaCl.

Table 1
Effect of the protease treatment

ΔF	Without protease	With protease
mean (Hz)	256	334
S.D. (Hz)	40.6	17.7
C.V. (%)	15.8	5.3

Sample: BSA 300 mg/l

From these results, it appears that the sensor could be used repeatedly if the protease treatment was performed between measurements. Within-day precision of the frequency change was determined by repeated assays of 300 mg/l BSA ($n = 10$), and the resulting arithmetic means, standard deviations and coefficients of variation are listed in Table 1.

The quartz crystal device was found to be reusable for at least 300 analyses in 3 months if the protease cleaning treatment was used. Although the resonant frequency decreased by 100 Hz in 3 months, the device still showed a good performance. Without the protease treatment, the device showed an unstable response after 20–50 repetitive measurements. These results show that this treatment removes the adsorbed protein from the quartz crystal, so that the sensor can be reused after treatment with the protease solution.

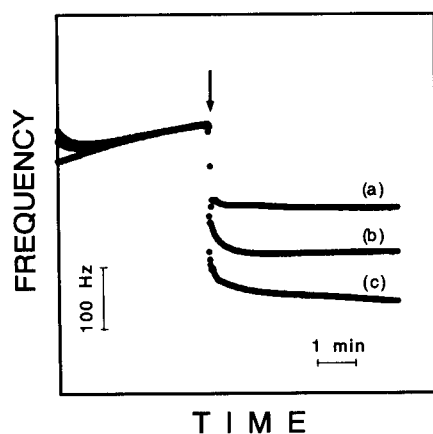


Fig. 5. Resonant frequency responses to 100 (a); 500 (b); 1000 mg/l (c) BSA standard solutions with TCA at 30°C. The upward arrow shows the injections of TCA.

Table 2
Comparison of relative resonant frequency change after the injection of TCA or SSA

	50 s	100 s	150 s
TCA (%)	96.6	98.9	100
SSA (%)	88.2	93.4	100

Sample: BSA 300 mg/l

3.3. Protein determination with TCA

Fig. 6 shows typical sensor responses for BSA with the use of TCA. The frequency changes depended on the concentration of BSA. Reproducibility of the measurement in the TCA system was evaluated by within-day repetitive analyses involving the protease treatment. The resulting arithmetic means, 192 Hz, and standard deviation, 6.17 Hz, were obtained by assaying a BSA standard (300 mg/l; $n = 12$), and a C.V. value was calculated to be 3.2%. The time to equilibrium in the TCA system was found to be shorter (Table 2) than that in the SSA system. The relationship between protein concentrations and frequency changes (ΔF) at 250 s after the injection of TCA is shown in Fig. 6. The results indicate that TCA gives almost identical turbidity for HSA, BSA and human γ -globulin. A value of A/G ratio, which is defined as a ratio of frequency change in albumin and γ -globulin at 1000 mg/l,

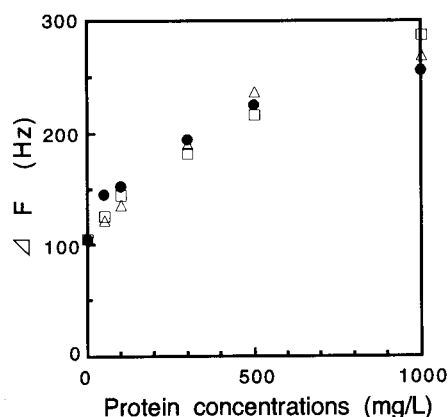


Fig. 6. Relationship between protein concentration and the resonant frequency change with TCA at 30°C. The frequency change (ΔF) was measured after 250 s from injection of SSA; (Δ) BSA, (\bullet) HSA, (\square) human γ -globulin.

was calculated to be 2.14 in the SSA system, while that in the TCA system was 0.96. Such small differences were also reported in a spectrophotometric method [6]. These results suggested that the difference in turbidity between albumin and globulin could be improved by using TCA.

In conclusion, the proposed method requires only a sample size of 100–400 μ l and gives reliable results for protein concentrations between 50 and 1000 mg/l. The sensitivity and calibration graphs for this method were comparable to those in the turbidimetric procedure. In nephelometry, the intensity of scatter depends not only on the protein concentration but also on the size of the precipitate particles or the colour of the urine. Different proteins may therefore give different turbidities even if their concentrations are equal. Because the proposed method is based on the piezoelectric mass sensor, such interference may be avoidable. Although the sensitivity was not greater than that of other sensitive methods such as the dye-binding procedure, an advantage of the present system is its simplicity, so that the system may be easily automated by developing a flow-injection system, extending the capability for continuous and repeated assays. This end-point determination may be completed within 5 min. We have demonstrated that the relatively cheap piezoelectric quartz crystal can be effectively applied to the determination of total urinary protein. This simple method appears to be feasible and practical for the analysis of total urinary protein, and expected for use not only in basic

researches and clinical practice but also in health screening and home care.

Acknowledgement

The authors thank Hiroshi Muramatsu and Masayuki Suda of Seiko Instruments Inc. (Tokyo, Japan) for providing the quartz crystals and helpful discussion.

References

- [1] C.E. Mogensen, *New Engl. J. Med.*, 310 (1984) 356.
- [2] Z.K. Shihabi, J.C. Konen and M.L. O'Connor, *Clin. Chem.*, 37 (1991) 621.
- [3] L.A. McElderry and I.F. Tarbit, *Clin. Chem.*, 28 (1982) 356.
- [4] M.M. Bradford, *Anal. Biochem.*, 72 (1976) 248.
- [5] F.B. Kingsbury, C.P. Clark, G. Williams and A.L. Post, *J. Lab. Clin. Med.*, 11 (1926) 981.
- [6] R.J. Henry, C. Sobel and M. Segalove, *Proc. Soc. Exp. Biol. Med.*, 92 (1956) 748.
- [7] O. Meulemans, *Clin. Chim. Acta*, 5 (1960) 757.
- [8] G. Sauerbrey, *Z. Phys.*, 155 (1959) 206.
- [9] T. Nomura and M. Iijima, *Anal. Chim. Acta*, 131 (1982) 97.
- [10] H. Muramatsu, K. Kajiwara, E. Tamiya and I. Karube, *Anal. Chim. Acta*, 188 (1986) 257.
- [11] M. Thompson, C.L. Arthur and G.K. Dhaliwal, *Anal. Chem.*, 58 (1986) 1206.
- [12] H. Muramatsu, J.M. Dicks, E. Tamiya and I. Karube, *Anal. Chem.*, 59 (1987) 2760.
- [13] W.H. King, *Anal. Chem.*, 36 (1964) 1735.
- [14] J. Hlavay and G.G. Guilbault, *Anal. Chem.*, 49 (1977) 1890.
- [15] K.K. Kanazawa and J.G. Gordon, *Anal. Chim. Acta*, 175 (1985) 99.

New anaerobic thin-layer spectroelectrochemical cell

T.B. Jarbawi *, M.T. Stankovich

Chemistry Department, Birzeit University, P.O. Box 14, West Bank, Israel

(Received 28th June 1993; revised manuscript received 13th January 1994)

Abstract

An anaerobic thin-layer spectroelectrochemical cell design and fabrication is described. The cell's anaerobicity and spectroelectrochemical response is demonstrated using methyl viologen dye and flavodoxin. A comparison between the new cell and bulk spectrocoulometric cells provides the following attractive features: (1) results for spectroelectrochemical characterization of methyl viologen agree very well; (2) no mediator dye is needed for the reduction of flavodoxin; and (3) the time of analysis is considerably shortened (12 min compared to 12 h).

Key words: Voltammetry; Thin-layer spectroelectrochemical cell

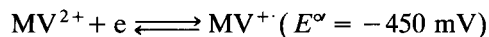
1. Introduction

In 1967, Heineman et al. [1] first reported a design for an optically transparent thin-layer electrode (OTTLE) [1]. Since then, many advancements have been made in order to increase the applicability of thin-layer cells. These include studies in the infrared [2], visible and ultraviolet [3–7]. Special designs were also made to ease the process of deoxygenation [8] and for studies in nonaqueous solvents [9]. A flow through cell had also been designed to electrochemically monitor the eluent in a chromatographic column [10].

Stankovich and co-workers [11–13] have successfully used an anaerobic bulk cell to perform spectrocoulometric titrations of flavodoxin and glucose oxidase using mediator dyes. Mediators

are necessary to rapidly transfer electrons from the electrodes to the proteins. The process of choosing the optimum mediator is time consuming. Even in the presence of the mediators, the spectrocoulometric titrations still required 4–12 h to complete the redox process. Also, an interference in the last step of the titration was observed.

Methyl viologen dye (MV^{2+}) is one of the best known electron transfer mediators. It is reduced according to the following equation:



The reduced form (MV^{+}) is extremely sensitive to oxygen. Therefore, it serves as a good compound to test the anaerobicity and spectroelectrochemical response of our cell.

Flavodoxin is an electron transfer protein with a molecular weight of approximately 15 000. It contains one molecule of flavin mononucleotide and substitutes for the iron-sulfur protein ferredoxin in pyruvate metabolism [14].

* Corresponding author. Current address: Department of Chemistry, University of Cincinnati, Cincinnati, OH 45221-0172, USA

Thin-layer cells have several attractive features; among these are the speed of coulometric titration, the requirement of a very small volume of analyte [15] and the capability of electrochemical characterization of a large variety of electrochemically active compounds [16–20]. The fabrication of an anaerobic thin-layer cell in which rapid coulometric reduction of methyl viologen can be performed with nearly 100% current efficiency is described here. Using this cell, we were able for the first time to perform a direct (unmediated) spectrocoulometric titration of flavodoxin with a current efficiency near 100%.

2. Experimental

2.1. Cell construction

A diagram of the thin layer spectroelectrochemical cell used is shown in Fig. 1A. The OTTLE (the bottom part of the cell) was fabricated by sandwiching a 500 wires-per-inch gold minigrad (Buckbee-Mears, St. Paul, MN) and a PTFE tape (0.30 mm) between two quartz slides (40 × 9.5 × 1 mm). The sandwiched minigrad has

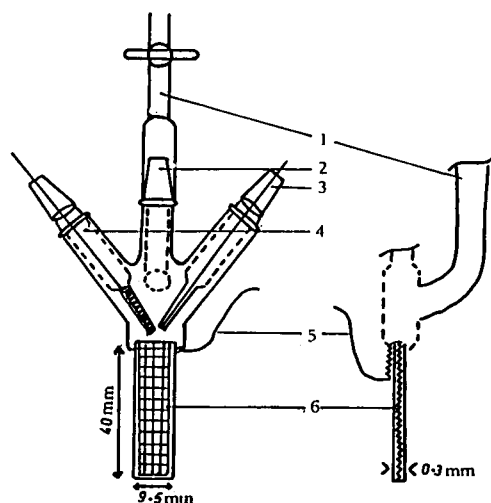


Fig. 1. Thin-layer spectroelectrochemical cell for coulometric titrations. (A) Front view; (B) side view; (1) main connection of nitrogen line; (2) sample inlet; (3) silver–silver chloride reference electrode; (4) silver–silver chloride auxiliary electrode; (5) copper wire; (6) gold minigrad working electrode.

dimensions of 50 × 9.5 mm so that it covers the length of the slides and extends beyond it where the connection with a copper wire is then made as shown in Fig. 1B. The OTTLE is then attached to the top part of the cell by means of Elmer epoxy glue (Borden, Columbus, OH).

The top part of the cell is fabricated from glass. The auxiliary and reference electrode compartments end with long ground (7/15") female joints to isolate the cell from the outside oxygen. The sample inlet ends with a long ground male (7/15") joint which is covered by the female (7/15") after introducing the sample.

The reference electrode is a silver–silver chloride electrode. Electrical contact is made to the solution through a piece of thirsty glass. The auxiliary electrode is a coiled silver wire contained in a fritted compartment which is sealed by a piece of thirsty glass and filled with 0.1 M KCl. Both electrodes were pretreated according to the method of Stankovich [11].

2.2. Reagents

Methyl viologen was purchased from BDH. A buffer of pH 7.25 was made from 0.1 M sodium phosphate. Flavodoxin, isolated from *Megasphaera* was a gift of Dr. Jed Fisher.

2.3. Instrumentation

Electrochemical experiments were performed with a BAS 100 electrochemical analyzer. A Varian Cary 219 UV–visible recording spectrophotometer was used to record spectra.

2.4. Procedure

A 5×10^{-4} M solution of methyl viologen in phosphate buffer pH 7.25 was deoxygenated in a separate cell for 0.5 h. This is a heart-shaped flask with two stopcocks, one for connection to a nitrogen line and one through which the needle is inserted for the withdrawal of sample. Approximately, 0.5 ml was then drawn out by means of a No. 1750 gas tight syringe (Hamilton, Reno, NV) and transferred to the previously nitrogen-flushed cell. The sample inlet joint was closed by means

of its male joint and another 30 min of evacuation and nitrogen equilibration was applied to the cell. The auxiliary and reference electrodes were then inserted in the cell under positive nitrogen pressure. The cell was then ready for electrochemical or spectroelectrochemical experiments. The potential of the reference electrode was checked before and after each experiment against the hexacyanoferrate(II)/(III) redox couple [21].

3. Results and discussion

3.1. Cyclic voltammetry

A typical cyclic voltammogram of 5×10^{-4} M methyl viologen is shown in Fig. 2. The cycle has a cathodic peak potential of -505 mV vs. SHE and an anodic potential of -410 mV at a scan rate of 10 mV/s. The formal potential of methyl viologen is -450 mV vs. SHE. In thin layer cells, the peak potential for both the oxidative and reductive processes should be identical. There is a 95 mV separation indicating the presence of an iR drop in this cell as is found with most other thin layer cells [1].

3.2. Spectrocoulometric titration

In this technique, the potential of the system is controlled at a value (-480 mV) negative enough to reduce MV^{2+} during the coulometric titration. The resulting current is then integrated and the number of coulombs Q is accurately determined.

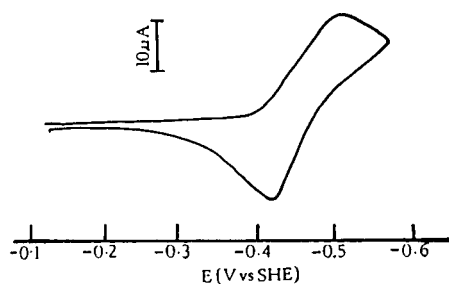


Fig. 2. Thin-layer cyclic voltammogram at a gold minigrad optical transparent thin-layer electrode for 5×10^{-4} M methyl viologen, phosphate buffer pH 7.25. Scan rate, 10 mV s^{-1} .

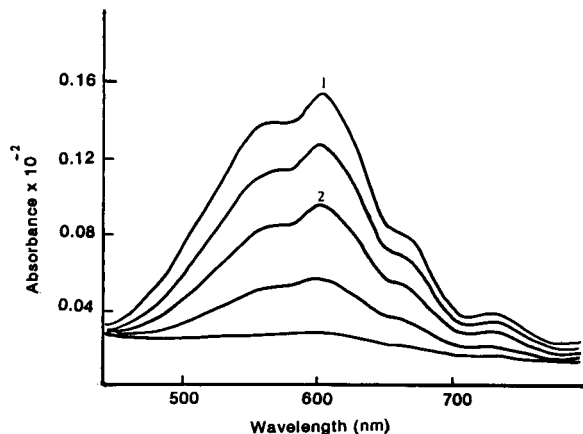


Fig. 3. Controlled potential thin-layer coulometric titration of methyl viologen. $E = -480$ mV. Methyl viologen 5×10^{-4} M, phosphate buffer pH 7.25. (1) Reduced methyl viologen; (2) $n = 0.6$ electrons per mol methyl viologen.

Spectra are periodically recorded throughout the reduction; thus absorbance (A) can be obtained as a function of Q . As a result, two pieces of information can be directly obtained: (a) the molar absorptivity of all species, oxidized and reduced; (b) the number of electrons (n) transferred to the system [22].

Fig. 3 shows a typical spectrocoulometric plot of 5×10^{-4} M methyl viologen in pH 7.25 phosphate buffer. This titration was used to test the anaerobicity of the cell as well as the speed of titration. At 602 nm, the absorbance increases as a function of charge added. A plot of A_{602} versus number of moles (n) was linear with a non-zero intercept (Fig. 4). The non-zero intercept corresponds to the amount of current consumed by oxygen initially present in the cell. This was calculated to be 2.4×10^{-6} M oxygen. The slope yielded a molar absorptivity of $(12\ 176\ M^{-1}\ cm^{-1})$. When the absorbance of 50% reduced methyl viologen was monitored as a function of time, the oxygen leak rate was found to be $0.07\ nmol\ min^{-1}$. The reductive titration of methyl viologen took 12 min to complete.

Fig. 5 shows the spectral change which occurred upon coulometric reduction of 2.3×10^{-5} M flavodoxin in pH 7.25 phosphate buffer. No mediator dye was used. The concentration of flavodoxin was calculated from the measured ab-

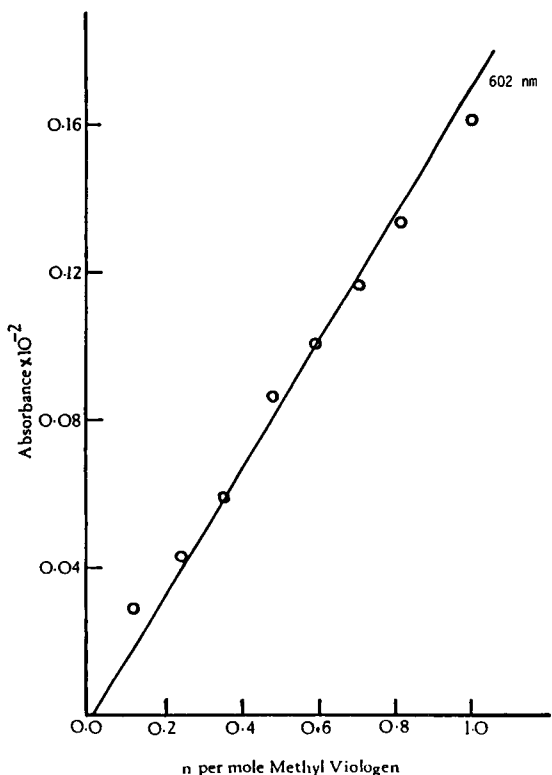
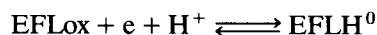


Fig. 4. Controlled potential thin-layer coulometric titration of methyl viologen. Plot of absorbance at 602 nm vs. amount of charge added to the system (n equal equivalents of charge). The non-zero intercept is due to residual O_2 in the system.

sorbance and the molar absorptivity [14]. The maximum absorbance at 445 nm corresponds to the oxidized form of flavodoxin (EFLox). The decrease in absorbance at this wavelength corresponds to the gradual reduction of (EFLox)



to the one electron reduced form (EFLH⁰). Its spectrum is shown in Fig. 3. From A vs. Q plots, the molar absorptivity of EFLox is calculated to be $9250 \text{ M}^{-1} \text{ cm}^{-1}$. The rest of the spectra represents the transfer of the second electron to produce $\text{EFLH}_{\text{red}}\text{H}^-$. At 580 nm, where EFLox absorbs least ($\epsilon = 1850 \text{ M}^{-1} \text{ cm}^{-1}$), the solid lines represent the increase in absorbance as EFLox is reduced to EFLH⁰. The broken lines represent the decrease in absorbance as EFLH⁰ is further reduced to $\text{EFL}_{\text{red}}\text{H}^-$. Fig. 6 is a plot of A_{580} and A_{445} as a function of the number of reducing equivalents added per flavin molecule. The non-zero intercept corresponded to the residual oxygen in the system $7.8 \times 10^{-6} \text{ M}$. The value of A_{580} increased linearly with the number of equivalents added to the system up to $n = 1$ equivalent/FMN. Between $n = 1$ and $n = 2$, it decreased linearly. A_{445} decreased linearly with the number of equivalents added up to $n = 1$ equivalent.

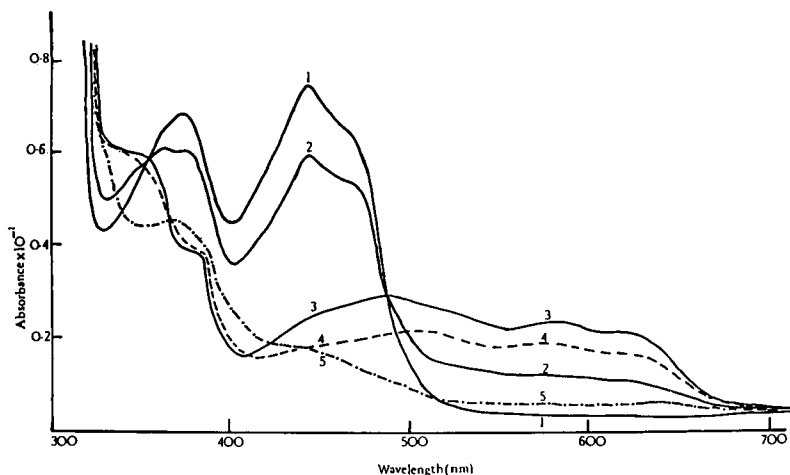


Fig. 5. Controlled potential thin-layer coulometric titration of flavodoxin. $E = -380 \text{ mV}$. Flavodoxin $2.3 \times 10^{-5} \text{ M}$ in phosphate buffer pH 7.25 without any mediator. (1) Oxidized flavodoxin; (2) $n = 0.4$ electrons per mol flavodoxin; (3) $n = 1$ electron per mol flavodoxin; (4) $n = 1.3$ electrons per mol flavodoxin; (5) $n = 2.03$ electrons per mol flavodoxin.

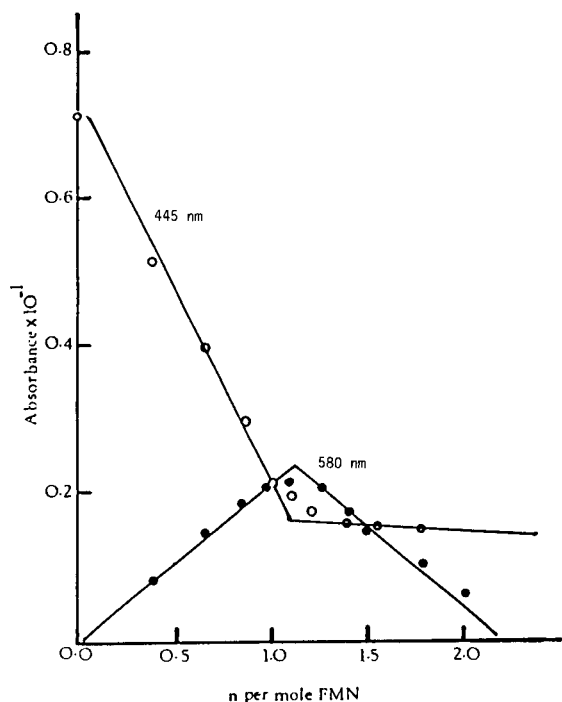


Fig. 6. Controlled potential thin-layer coulometric titration of flavodoxin. Plot of absorbance at 445 and 580 nm vs. amount of charge added to the system (n equal equivalents of charge). The non-zero intercept is due to residual O_2 in the system.

lents as well as from $n = 1$ up to $n = 2$, with a less steep slope. The A_{480} maximum occurred at the same value of n as did the inflection in the A_{445} plot. The spectral data are in agreement with those previously obtained in a bulk cell with the mediator dye methyl viologen [11].

The region $n = 0-1$, represents the equilibrium between $EFLox$ and $EFLH^0$. This is reflected in the spectra of Fig. 5 and in the plots of Fig. 6. That is, A_{580} increases from $n = 0$ to $n = 1$ while A_{445} decreases. This equilibrium is broken at $n = 1$. From $n = 1$ to $n = 2$ the equilibrium is between $EFLH^0$ and $EFL_{red}H^-$. A_{580} as well as A_{445} decreases from $n = 1$ to $n = 2$.

From the plots of Fig. 6, it can be seen that 100% $EFLH^0$ was formed at $n = 1.09$ equivalents of FMN, an error of 9%. The two-electron reduction was complete at $n = 2.16$, an overall error of 8%.

To discuss the utility of the new cell, the following points should be considered:

- (1) Ease of construction. The two major components of the cell are easily constructed within a short period of time. The top part is fabricated in the glass shop in less than 30 min; cutting and sandwiching the gold minigrid requires less than 10 min. The complete unit assembly (attaching the top part to the slide-minigrid using epoxy resin) requires 20 min. An additional 2 h are required for complete drying of the resin.
- (2) Ease of cleaning. The cell is cleaned through one of its electrode compartments. It is flushed several times with soap and water followed by cyclohexane.
- (3) Life time. In aqueous media, the cell can be used for complete spectroelectrochemical characterization of electroactive compounds regardless of the number of experiments performed. If cross-contamination is suspected, the cell components can easily be disassembled by soaking the cell in formic acid for 30 min. A new slide-minigrid is then easily attached to the previous top (which can be reused).
- (4) Oxygen leakage. Once the solutions are deoxygenated and the electrodes are pretreated, the cell proves to be easily protected from oxygen, at least within the short time (12 min for methyl viologen and 1 h for flavodoxin) needed for the experiment to be completed.

4. Conclusions

We have constructed an anaerobic thin-layer spectroelectrochemical cell and demonstrated that it can be used successfully for the coulometric titrations of methyl viologen and flavodoxin. The reduction of flavodoxin can be performed directly without a mediator dye and with a shorter time of analysis (1 h) than the 12 h required for bulk spectroelectrochemical cells. The oxygen leak rate is 3-fold lower than reported by Hawkrige and Kuwana [22]. In addition, the cell is easy to construct and maintain. The accuracy of our measurements has been demonstrated by reproducing values of ϵ and n for the previously

well characterized methyl viologen and flavodoxin.

References

- [1] W.R. Heineman, R.W. Murray and G.W. O'Dom, *Anal. Chem.*, 39 (1967) 1666.
- [2] W.R. Heineman, J.N. Burnett and R.W. Murray, *Anal. Chem.*, 40 (1968) 1974.
- [3] W.R. Heineman, J.N. Burnett and R.W. Murray, *Anal. Chem.*, 40 (1968) 1970.
- [4] A. Mills, Q. Chang and N. McMurray, *Anal. Chem.*, 64 (1992) 1383.
- [5] M. Collinson and E.F. Bowden, *Anal. Chem.*, 64 (1992) 1470.
- [6] T.B. Jarbawi and W.R. Heineman, *J. Electroanal. Chem.*, 132 (1982) 323.
- [7] J.Y. Gui, G.W. Hance and T. Kuwana, *J. Electroanal. Chem.*, 309 (1991) 73.
- [8] G.M. Tom and A.T. Hubbard, *Anal. Chem.*, 43 (1971) 671.
- [9] R.K. Rhodes and K.M. Kadish, *Anal. Chem.*, 53 (1981) 1539.
- [10] T.C. Pinkerton, H. Hajizadeh, E. Deutsch and W.R. Heineman, *Anal. Chem.*, 52 (1980) 1542.
- [11] M.T. Stankovich, *Anal. Biochem.* 109 (1980) 308.
- [12] C.W. Fink, M.T. Stankovich and S. Soltysik, *Biochemistry*, 25 (1986) 6637.
- [13] M.T. Stankovich and S. Soltysik, *Biochemistry*, 26 (1987) 2627.
- [14] S.G. Mayhew, G.P. Foust and V. Messey, *J. Biol. Chem.*, 244 (1969) 803.
- [15] T.P. DeAngelis and W.R. Heineman, *J. Chem. Educ.*, 53 (1976) 594.
- [16] Y.Y. Huang and T. Kimura, *Anal. Biochem.*, 133 (1983) 385.
- [17] D.F. Rohrbach, R.W. Heineman and E. Deutsch, *Inorg. Chem.*, 18 (1979) 2536.
- [18] D. Lexa, J.M. Saveant and J. Zickler, *J. Am. Chem. Soc.*, 99 (1977) 2786.
- [19] T.B. Jarbawi, W.R. Heineman and G.J. Patriarcho, *Anal. Chim. Acta*, 126 (1981) 57.
- [20] T.B. Jarbawi and W.R. Heineman, *Anal. Chim. Acta*, 186 (1986) 11.
- [21] J.E. O'Reilly, *Biochim. Biophys. Acta*, 292 (1973) 509.
- [22] F.M. Hawkrige and T. Kuwana, *Anal. Chem.*, 45 (1973) 1021.

Chromium(VI) determination at a rotating disc electrode

Neil G. Smart^{a,1}, Michael L. Hitchman^{b,*}, Ray O. Ansell^a, J. Duncan Fortune^a

^a Department of Physical Sciences, Glasgow Caledonian University, Cowcaddens Road, Glasgow G4 0BA, UK

^b Department of Pure and Applied Chemistry, University of Strathclyde, 295 Cathedral Street, Glasgow G1 1XL, UK

(Received 21st October 1993; revised manuscript received 12th January 1994)

Abstract

Results are given for a method of determination of Cr(VI) by amperometry at a solid electrode. By using a fluoride containing electrolyte at a controlled pH and an amalgamated gold electrode, previously reported problems of electrode passivation by Cr(III) have been overcome. The method gives reproducible results and can be used for monitoring Cr(VI) with a detection limit of 0.9×10^{-9} mol cm⁻³ at the 95% confidence level.

Key words: Amperometry; Chromium; Amalgamated gold; Solid electrode

1. Introduction

During the course of studying the corrosion mechanisms of stainless steels, we have needed to determine low levels of Cr(VI) in solution. Trace level determination of this species has been the subject of various investigations [1]. Traditionally a spectrophotometric method involving the complexing agent diphenyl carbazide in acid solution to produce a clear, intense violet colour with trace amounts of Cr(VI) has been used [2–4]. This technique is, though, not particularly suitable for in situ analysis during corrosion studies. Differential pulse polarography (DPP) at a drop-

ping mercury electrode (DME) has also been developed for Cr(VI) analysis [5,6]. Analysis is usually carried out in neutral or basic solution since in acidic solution Cr(VI) readily oxidises the mercury. Electrolytes which have been investigated include ammonium tartrate [5,6] ammonium acetate [6,7], sodium phosphate [8], sodium hydroxide [5] and sodium fluoride [7]. Although the last of these electrolytes, sodium fluoride, has been found to be particularly useful for the determination of Cr(VI) down to $\sim 10^{-8}$ M, which is comparable to the sensitivity achievable with the spectrophotometric method, a DME is again not very practicable for in situ monitoring of the very dilute solutions that will be produced by the corrosion and dissolution of stainless steels.

What would be useful for this application is a solid material that could form either a ring detecting electrode around a corroding stainless steel disc or a monitoring electrode downstream

* Corresponding author.

¹ Present address: Company Research Laboratory, British Nuclear Fuels plc, Springfield Works, Salwick, Preston PR4 0XJ, UK

from a generating electrode. This would then allow detection of the Cr(VI) within the diffusion layer at a low level [9]. However, the amperometric determination of Cr(VI) at solid electrodes is hindered by the formation of films of Cr(III) which passivate the electrode surface [10,11]. Some modified electrodes have been developed to try and overcome this problem. For example Cox and Kulesza [12,13] have used a protonated film of poly(4-vinylpyridine) into which Cr(VI) is preconcentrated by ion exchange, and then they have measured the amount of metal incorporated into the film by cathodic voltammetric stripping. In this case it was thought that passivation of the electrode surface was prevented by the ejection of the Cr(III) species during the stripping step and that this was facilitated by the use of fluoride ions in solution. This type of electrode, though, may not be readily adaptable to the fabrication of a ring detector electrode. Larochelle and Johnson [14] have also used a different type of modified electrode for monitoring Cr(VI) eluting from an ion chromatography column. They have adsorbed iodine onto a platinum electrode and have suggested the adsorbate exerts an electrocatalytic effect on the Cr(VI)/Cr(III) couple and this presumably prevents irreversible film formation on and passivation of the electrode surface. On the basis of the results obtained with a DME it has occurred to us to try an alternative approach for in situ monitoring of Cr(VI) by using an amalgamated metal electrode. This paper presents results for the amperometric determination of Cr(VI) on an amalgamated gold electrode for concentrations as low as ca. 10^{-9} mol cm $^{-3}$.

2. Experimental

All experiments were carried out using solutions in doubly distilled water. A Cr(VI) stock solution was prepared by dissolving K₂Cr₂O₇ (AnalaR) in 0.05 M H₂SO₄. The background electrolyte solution of NaF (0.15 M) at pH 3.5 was prepared by dissolving 6.5 g of NaF in 950 ml of water and adjusting the pH to the required value by dropwise addition of dilute HCl (4 M Proanalysis). The solution was then made up to

1000 ml. A Hg(II) stock solution for plating the gold electrode was prepared by dissolving Hg(NO₃)₂ (BDH) in water.

An Oxford Electrodes potentiostat was used, in conjunction with an Oxford rotating disc electrode (RDE) system. Current–voltage curves were recorded on a Bryans X–Y recorder. A three-electrode cell configuration with a main compartment volume of 150 ml was used. The cell was maintained at 25°C by circulating water from a thermostat through a jacket around the cell. The main compartment of the cell had a lid with an opening for the RDE and for a degassing tube. The solution was deoxygenated with nitrogen prior to the voltammetric experiments and nitrogen gas was blown over the solution during the experiments. The reference electrode was connected to the main cell via a Luggin capillary. A 7 mm diameter gold disc surrounded by a 20 mm diameter epoxy resin insulator (Oxford Electrodes) was used as the working electrode (WE). A large surface area platinum foil served as the counter electrode. A saturated calomel electrode (SCE) was used as the reference electrode and all potentials are reported with respect to the SCE.

Prior to experiments, the gold RDE was polished using a 600 grit paper followed by 1 μm diamond paste. The polished gold electrode was electrolytically cleaned by cycling at a sweep rate of 50 mV s $^{-1}$ in degassed 0.15 M NaF from –0.2 V to +1.0 V for 50 to 100 cycles. The electrode was then held in the hydrogen evolution region for 3 min to reduce any oxide on the surface. To plate mercury onto the gold electrode, 1.5 ml of 400 mg dm $^{-3}$ Hg(II) solution was added to the cell. The electrode was rotated at 10 Hz in this solution and was amalgamated at a potential of –0.4 V for 15 min. For Cr(VI) determination, initially a blank scan was run in the supporting electrolyte over the potential range 0.6 V to –0.1 V at a rate of 50 mV s $^{-1}$ with the electrode rotating at 10 Hz. Standard additions from a 1 g dm $^{-3}$ Cr(VI) stock solution were then made and after each addition the electrode potential was scanned as for the case of the blank. The diffusion limited current was measured as the difference between the blank and the standard at a potential of 0.1 V (cf. Fig. 1). A constant elec-

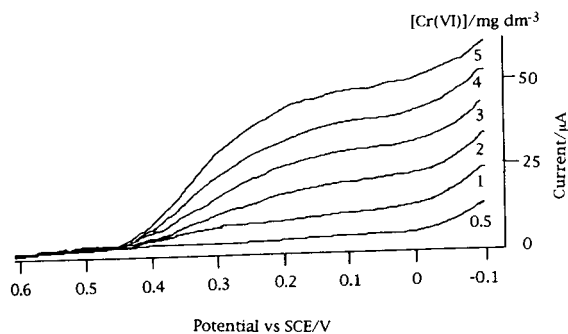


Fig. 1. Reduction waves for Cr(VI) reduction at the various concentrations shown, on a Au/Hg RDE. Rotation rate, 10 Hz; scan rate, 50 mV s^{-1} ; scan range, $+0.6 \text{ V}$ to -0.1 V ; supporting electrolyte, 0.15 M NaF at pH 3.5.

trode rotation speed of 10 Hz was maintained throughout.

3. Results and discussion

In preliminary experiments it was found that, in agreement with other published results [10,11], determination of Cr(VI) at a clean gold or platinum RDE in both acidic and basic solutions was not possible due to electrode passivation. However, using a mercury plated gold RDE well defined reduction curves for Cr(VI) over the concentration range 0.5 to 5 mg dm^{-3} , were obtained using linear sweep voltammetry with a NaF supporting electrolyte. Typical current–voltage curves are shown in Fig. 1. The calibration graph obtained from these results had a slope of $(9.15 \pm 0.24) \mu\text{A (mg dm}^{-3})^{-1}$ and an intercept of $(1.62 \pm 0.74) \mu\text{A}$, where the errors have been calculated at the 95% confidence level. Using a statistical procedure based on that suggested by Caultt and Boddy [15], the limit of detection was estimated as $0.92 \times 10^{-9} \text{ mol cm}^{-3}$. Repeating the procedure on a freshly prepared electrode resulted in a calibration curve within the given errors. With repeated scans of the electrode in Cr(VI) solution there was no sign of electrode passivation and reproducible reduction curves were obtained. The electrode amalgam could, though, be removed electrochemically or by gentle polishing. On carrying out a cyclic voltammo-

gram of the gold RDE in $0.5 \text{ M H}_2\text{SO}_4$ after removal of the amalgam, a scan typical of gold [16] was obtained, indicating the amalgam was only on the very top surface layers of the electrode.

As mentioned above, the fluoride anion has been found [7] to assist in the determination of Cr(VI) at a DME. It has been suggested [12] that this occurs because of the high coordinating power of the anion and that this accelerates dissolution of Cr(III) and so prevents electrode passivation. This is apparently the case as well for an amalgamated electrode. A pH of 3.5 has also been suggested [11] as minimising the precipitation of Cr(III), and again this seems to have been a successful ploy for an amalgamated electrode. The amalgamation also, of course, minimises any interference from H^+ ion reduction.

For the determination of Cr(VI) from a corroding alloy it would be necessary to extend the technique to a double electrode system with a stainless steel electrode as a central disc or as an upstream electrode, and an amalgamated gold electrode as a concentric ring or a downstream electrode. The required test solution of pH 3.5 and a background electrolyte of 0.15 M F^- could have an influence on the corrosion process. The system of a double electrode in a flow channel [17] would more readily lend itself to overcoming this problem than a rotating ring disc electrode [9] by having a small injection port for the analytical solution between the upstream corroding electrode and downstream detection electrode. The application of the technique to the monitoring of corrosion processes is being investigated further.

Acknowledgement

We acknowledge financial support from Glasgow Caledonian University for NGS.

References

- [1] G. Fang and C. Miao, *Analyst*, 110 (1985) 65.
- [2] A.I. Vogel, *Quantitative Inorganic Analysis*, Longmans, London, 3rd edn., 1961, p.791.

- [3] R. Belcher, A.J. Nutten and A.M.G. MacDonald, *Quantitative Inorganic Analysis*, Butterworths, London, 3rd edn., 1970, p. 306.
- [4] T.L. Allen, *Anal. Chem.*, 30 (1958) 447.
- [5] Princeton Applied Research Corporation, Application Brief C-2, New Jersey.
- [6] S.T. Crosnum and T.R. Mueller, *Anal. Chim. Acta*, 75 (1975), 199.
- [7] J.A. Cox, J.L. West and P.J. Kulesza, *Analyst*, 109 (1984) 927.
- [8] C. Harzendorf and G. Janser, *Anal. Chim. Acta*, 165 (1984) 201.
- [9] W.J. Albery and M.L. Hitchman, *Ring-Disc Electrodes*, Clarendon Press, Oxford, 1971.
- [10] J.J. Lingane and I.M. Kolthoff, *J. Am. Chem. Soc.*, 62 (1940) 852.
- [11] T. Heumann and H.S. Panesar, *J. Electrochem. Soc.*, 110 (1963) 628.
- [12] J.A. Cox and P.J. Kulesza, *J. Electroanal. Chem.*, 159 (1983) 337.
- [13] J.A. Cox and P.J. Kulesza, *Anal. Chim. Acta*, 54 (1983) 71.
- [14] J.H. Larochele and D.C. Johnson, *Anal. Chem.*, 50 (1978) 240.
- [15] R. Caulcutt and R. Boddy, *Statistics for Analytical Chemists*, Chapman and Hall, London, 1983, Chap. 13.
- [16] H. Angerstein-Kozłowska, in E. Yeager, J. O'M. Bockris, B.E. Conway and S. Soragnaponi (Ed.), *Comprehensive Treatise of Electrochemistry*, Vol. 9, Plenum Press, New York, 1984, p. 25.
- [17] K. Aoki and H. Matsuda, *J. Electroanal. Chem.*, 94 (1978) 157.

Differential pulse polarographic study of the degradation of H^+/K^+ ATPase inhibitors SK&F 95601 and omeprazole in acidic media and the subsequent reactions with thiols

S. McClean, E. O’Kane, V.N. Ramachandran, W.F. Smyth *

Department of Applied Physical Sciences, University of Ulster, Coleraine, Co. Derry BT52 1SA, UK

(Received 4th October 1993; revised manuscript received 27th January 1994)

Abstract

Differential pulse polarography (DPP) has been used to monitor the degradation of benzimidazole sulphoxide antiulcer drugs SK&F 95601 and omeprazole in 10^{-2} mol dm⁻³ HCl to two main products, i.e., the sulphenamide and the benzimidazole sulphide. It is also used to follow the reactions of 2-mercaptoethanol with the respective products of these degradations, as simulations of their believed reactions in vivo. These reactions are also followed by UV spectrophotometry, spectrofluorimetry and liquid chromatography. DPP can also be used to selectively determine nanomolar concentrations of these antiulcer drugs and their degradation products, of value in formulation and body fluid analysis.

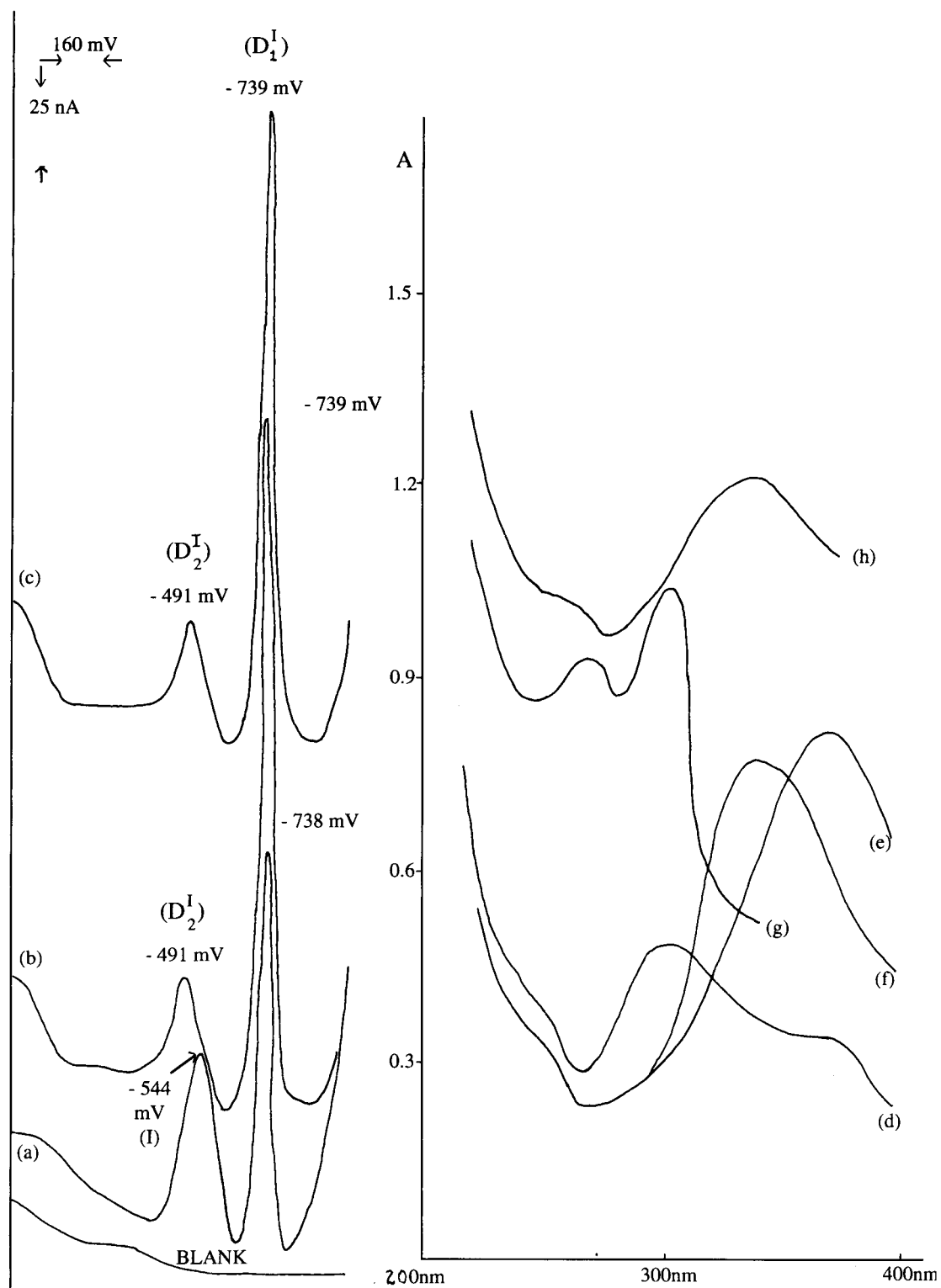
Key words: Differential pulse polarography; ATPase inhibitors; Thiols; Omeprazole

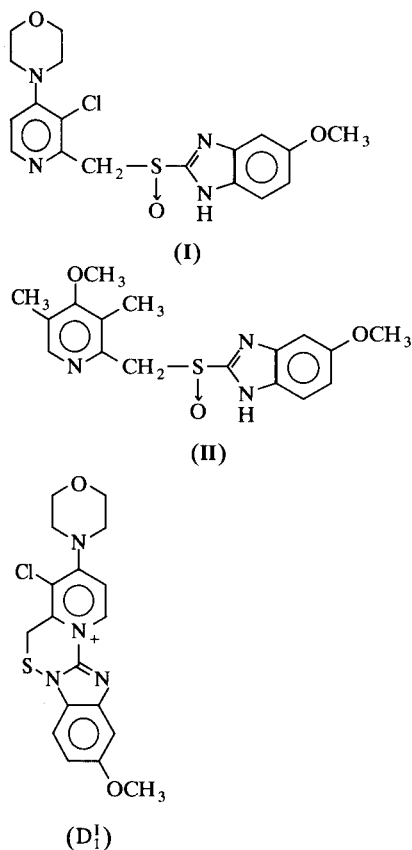
1. Introduction

H^+/K^+ ATPase inhibitors such as SK&F 95601 (**I**) and omeprazole (**II**) are effective in stomach ulcer treatment due to their acid catalysed rearrangement to form sulphenamides such as (**D**₁) for SK&F 95601. The sulphenamide then irreversibly inhibits the H^+/K^+ ATPase enzyme which is part of the “proton pump” located in the

parietal cell of the stomach wall [1] by reaction with a thiol residue [2–4]. This paper is concerned with the use of differential pulse polarography (DPP) to monitor the degradation of **I** and **II** in acidic media, pH 2 and the reaction of a thiol (i.e., 2-mercaptoethanol) with the respective products of these degradations, as simulations of the believed reactions in vivo. These reactions are also followed by UV spectrophotometry, spectrofluorimetry and liquid chromatography (LC). Limits of detection (LODs) for **I** and **II**, and their respective degradation products are also assessed using DPP.

* Corresponding author.





2. Experimental

The degradation of benzimidazole sulphoxides **I** and **II** was followed by differential pulse polarography using the Metrohm 646 VA processor. The mercury drop size was 0.40 mm², the voltage step for the sweep 8 mV, the pulse amplitude was 50 mV and the time step for the measurement interval 500 ms. To a 20 ml solution of 1 × 10⁻² mol dm⁻³ HCl was added 200 μl of a 1 × 10⁻³ mol dm⁻³ solution of the benzimidazole sulphoxide in methanol. The time from this addition, i.e., start of the degradation, to the appearance of the

D₁ peak was noted and this designated the particular reaction time *t*. Scans were initiated every few minutes for first 30 min then every 15 min for the next 2 h. During the remainder of the 5-day studies, scans were initiated every 3–4 h.

The reaction of 2-mercaptoethanol with the benzimidazole sulphoxides **I** and **II** was carried out as follows. **I** was allowed to degrade in 10⁻² mol dm⁻³ HCl for 3 min, together with deaeration. 1 × 10⁻⁵ mol dm⁻³ mercaptoethanol (0.08 g of thiol/100 ml of methanol is 10⁻² mol dm⁻³) was added to the degrading solution and the sample vessel deaerated with nitrogen for 1 min. A DPP cathodic scan was then initiated at ca. +100 mV, terminating at -1.050 V approximately 5 min after addition of the thiol. Similar experiments were carried out in which **I** was allowed to degrade for increasing lengths of time up to 7.5 h prior to 2-mercaptoethanol addition. In the case of **II**, omeprazole was allowed to degrade for 30 min up to 2 h prior to 2-mercaptoethanol addition.

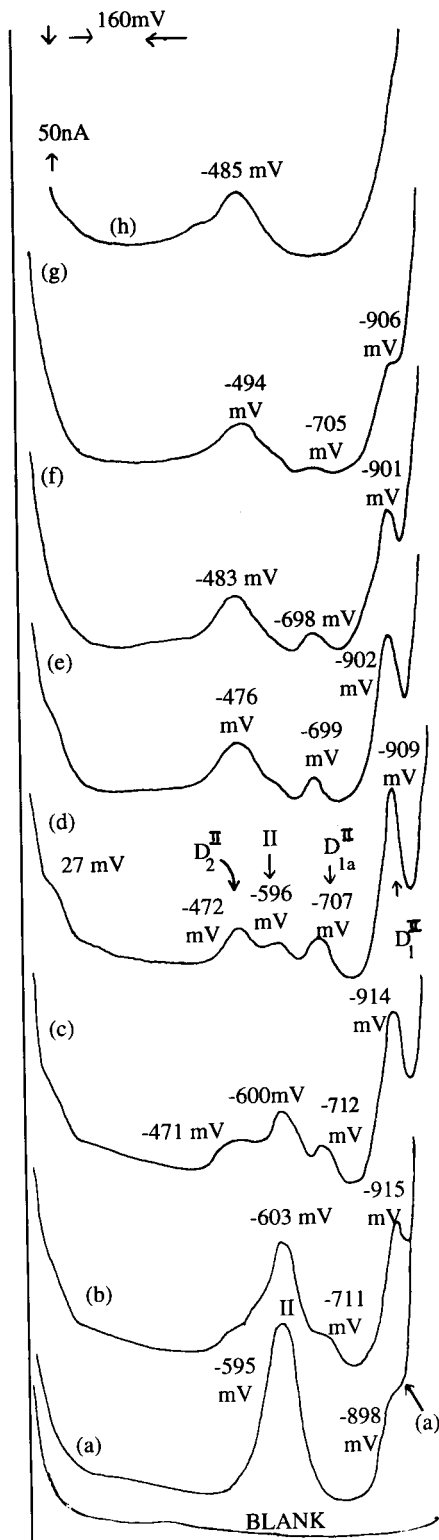
Supporting data on degradation of **I** and **II** in acidic media and subsequent reactions with 2-mercaptoethanol was obtained by UV spectrophotometry using a Perkin-Elmer Lambda 5 spectrophotometer and LC using a C₁₈ Novapak column, a mobile phase of acetonitrile and water (50:50, v/v) and a UV detector set at 300 nm. Fluorescence spectrophotometry was carried out with a Perkin-Elmer LS-5B instrument.

3. Results and discussion

3.1. The degradation of **I** and **II** in acidic media (pH 2.0)

The degradation of 1 × 10⁻⁵ mol dm⁻³ **I** in 10⁻² mol dm⁻³ HCl was monitored by DPP (Fig 1). **I** gives a cathodic peak at -544 mV which rapidly decays and is replaced by a new cathodic

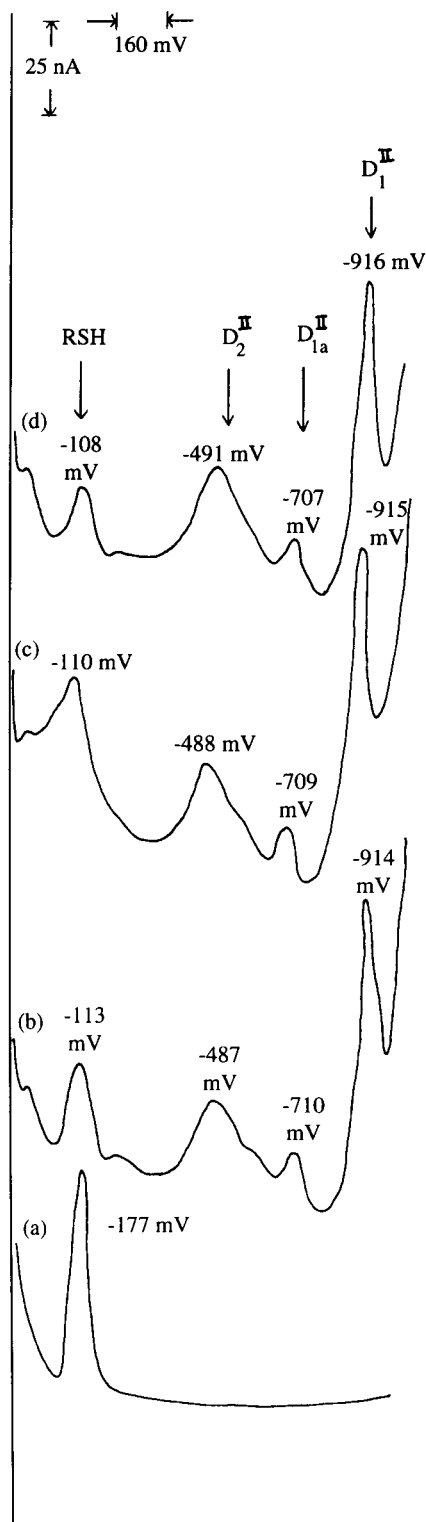
Fig. 1. DPP and UV study of degradation of **I** in 10⁻² mol dm⁻³ HCl. DPP study for 10⁻⁵ mol dm⁻³ **I** with starting potential +100 mV, end potential -1000 mV (a) after 2 min 39 s degradation, (b) after 18 min degradation and (c) after 60 min degradation. The quoted times in a, b and c refer to the exact time at which the D₁⁺ peak is observed. UV study for 5 × 10⁻⁵ mol dm⁻³ **I** with scan speed 120 nm min⁻¹, scan initiated at 400 nm (d) immediately on addition of **I** to 10⁻² mol dm⁻³ HCl, (e) after 18 min degradation and (f) after 108 min degradation. (g) UV spectrum of D₂⁺ following its separation from the degradation mixture by LC [6], (h) UV spectrum of the degradation product of D₁⁺ following the separation of D₁⁺ from the degradation mixture by LC [6]. Both spectra g and h have been elevated on the absorbance axis by 0.5 absorbance units for visualisation purposes.



peak at -491 mV (D_2^I) with only one composite peak ever being observed. Its peak height reaches a constant value by about 10 min and remains so for the rest of the 5-day study. A new peak (D_1^I) is also rapidly formed at -739 mV and this reaches a constant peak height in about 10 min, maintaining this for approximately 1 h, prior to decreasing to one third of its maximum value after two days. The D_1^I peak height then remains constant till the end of the 5-day study. A third cathodic peak (D_3^I) is observed at -891 mV after two days and its height remains essentially constant for the remainder of the study. The rate of appearance of D_1^I and its partial disappearance after approximately 1 h is matched in a study of the degradation of 5×10^{-5} mol dm $^{-3}$ **I** in 10^{-2} mol dm $^{-3}$ HCl using UV spectrophotometry (Fig. 1), i.e., **I** gives its major UV absorption peak at 305 nm (Fig. 1d) which in a pH 2 medium rapidly changes to a major UV absorption peak at 380 nm (Fig. 1e). The half life of this transformation can be calculated at 1.2 min, in agreement with other data [5]. The absorbance of this 380 nm peak reaches a maximum in ca. 10 min, its wavelength and absorbance remaining constant for ca. 60 min. After this time the 380 nm peak gradually disappears giving rise to a new peak at 340 nm (Fig. 1f).

It is possible, therefore to postulate that the D_1^I peak in polarography and the 380 nm peak in UV spectrophotometry are due to the one and the same degradation product, i.e., the sulphenamide D_1^I . This long wavelength band at 380 nm can be attributed to the sulphenamide on the grounds that coplanarity of the aromatic entities in D_1^I is achieved by virtue of the S-containing ring which allows for greater conjugation/delocalisation. This assignment is in agreement with a report by Sturm [5]. Further evidence in support of coplanarity of the aromatic entities in

Fig. 2. DPP study of degradation of 10^{-5} mol dm $^{-3}$ **II** in 10^{-2} mol dm $^{-3}$ HCl with starting potential 100 mV, end potential -1.050 V, (a) after 4 min 37 s, (b) after 10 min 39 s, (c) after 20 min 9 s, (d) after 35 min, (e) after 3 h 10 min, (f) after 5 h 10 min, (g) after 24 h, (h) after 73 h. The quoted times in a to h refer to the exact time at which the D_1^I peak at ca. -900 mV is observed.



sulphenamides such as D_1^I can be obtained from the following spectrofluorimetric data. SK&F 95601 (**I**) and omeprazole (**II**) at concentrations of 3.3×10^{-5} M were each allowed to degrade to their respective sulphenamides in acetonitrile–water (83 + 17) (pH 2) for 15 min after which time the fluorescence emissions in the range 420 to 700 nm were recorded following excitation at optimum wavelengths 400 and 390 nm, respectively. Significant fluorescent signals were observed for SK&F 95601 and omeprazole at 554 and 552 nm respectively with a ratio of emission intensities of 11.1:14.0 arbitrary units. It should also be noted that when the sulphenamide of SK&F 95601 (D_1^I) is prepared in pH 2 media and is then subjected to LC conditions [6] which degrade it to a compound in which coplanarity of the aromatic entities is lost, the resulting eluting compounds (i.e., **I**, degraded D_1^I and D_2^I) gave no fluorescence emission when monitored by an on-line fluorescence detector. The significant fluorescent emissions of the sulphenamides of **I** and **II** are to be expected for such coplanar molecules with electron donating groups such as morpholino, methoxy (for D_1^I) and methyl, methoxy (for D_1^{II}).

In both DPP and UV studies of the degradation of **I**, the sulphenamide D_1^I itself begins to degrade after ca. 1 h. This is manifested in DPP by a partial loss of the peak at -739 mV and in UV spectrophotometry by a move of the λ_{\max} from 380 to 340 nm. It is likely then that the sulphenamide D_1^I has its S-containing ring broken to yield a product which still gives a DPP signal at -739 mV and which possesses more conjugation/delocalisation than the parent compound **I** or the degradation product D_2^I , both of which give their primary absorption maxima at 305 nm. (Fig. 1d and g, respectively). Possible candidates

Fig. 3. Reaction of 10^{-5} mol dm^{-3} 2-mercaptoethanol (RSH) with 10^{-5} mol dm^{-3} omeprazole **II**. (a) 10^{-5} mol dm^{-3} RSH. After 40 min degradation of **II** in 10^{-2} mol dm^{-3} HCl then addition of 10^{-5} mol dm^{-3} RSH and DPP recording (b) after 7 min 11 s, (c) after 17 min, and (d) after 27 min 50 s. The quoted times in b, c and d refer to the exact time at which the D_1^{II} peak at ca. -915 mV is observed.

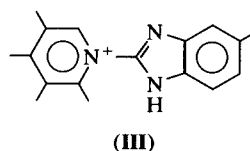
are disulphides noted in the paper by Senn-Bilfinger et al. [4]. It should also be noted that when the sulphenamide D_1^I is prepared in pH 2 media and is then subjected to LC-UV [6], it is unstable in the LC mobile phase of acetonitrile– H_2O (50 + 50) and degrades to a compound whose UV spectrum is given in Fig. 1h also with maximum absorbance at 340 nm.

The degradation of 1×10^{-5} mol dm^{-3} omeprazole in 10^{-2} mol dm^{-3} HCl was monitored by DPP (Fig. 2). **II** gives a cathodic peak at ca. –600 mV which decays less rapidly than SK&F 95601 to a cathodic peak at ca. –900 mV. This latter peak has a similar kinetic profile to D_1^I in that it reaches a maximum DPP peak height (in this case after 35 min degradation), remains at this value for a period of time (in this case ca. 3 h degradation) and then decreases until after 48 h degradation, it has disappeared completely. The half life of 1×10^{-5} mol dm^{-3} **II** in 10^{-2} mol dm^{-3} HCl can be estimated as 10 min by DPP. This can be compared to data by Ife et al. [7] in which the $t_{1/2}$ of **II** in pH 1.0 using acetonitrile–buffer (1 + 3) at ambient temperature was quoted as 2 min compared to a value of 1 min for **I** under identical conditions. The degradation of **II** can also be followed by UV spectrophotometry in that the principal absorption bands of the parent molecule at 278 and 300 nm are replaced by one at 270 nm and a long wavelength absorption band at 362 nm, when recorded in acetonitrile–water (50 + 50) (pH 2) for 1×10^{-4} M **II**. The –900 mV cathodic DPP peak is believed to be due to the omeprazole sulphenamide which in addition possesses a long wavelength UV absorption peak at 362 nm when recorded in the above medium. It is therefore ascribed the appropriate symbol D_1^{II} . At the same time the **II** peak is disappearing and D_1^{II} is forming two new cathodic DPP peaks appear. One occurs ca. –480 mV and this reaches a maximum current value after 40 min degradation, remaining constant for the remainder of the study (i.e., 73 h). These kinetic characteristics, combined with its relative ease of reduction, would suggest its similarity to the D_2^I species in the case of SK&F 95601. It is therefore labelled D_2^{II} . Another DPP peak appears at ca. –700 mV, reaching its maximum current value after 35 min.

After 3 h at this maximum value, it then decreases and totally disappears after 48 h degradation. This peak possesses none of the kinetic characteristics of D_3^I but seems to follow the profile of D_1^{II} (see Fig. 2). It is therefore labelled D_{1a}^{II} .

3.2. Mechanism of degradation / electrode reactions

Using the conditions described in this paper, SK&F 95601 and omeprazole degrade somewhat similarly, as monitored by DPP. This is illustrated in Fig. 1 where the 4e and 2e reductions of benzimidazole sulphoxide and sulphide respectively have been observed for similar model compounds [8]. It should be noted that in an earlier paper [6], it was presumed that the sulphenamide D_1^I , due to its particularly large DPP peak height in comparison to those of **I** and D_2^I , gives rise to catalytic hydrogen evolution with D_1^I as the catalyst, adsorbed on the Hg surface, with its unshared electron pairs picking up protons prior to reduction and catalytic generation of H_2 . It is now believed that the signals for sulphenamides D_1^I and D_1^{II} and related molecules are due to reduction of entities such as **III**

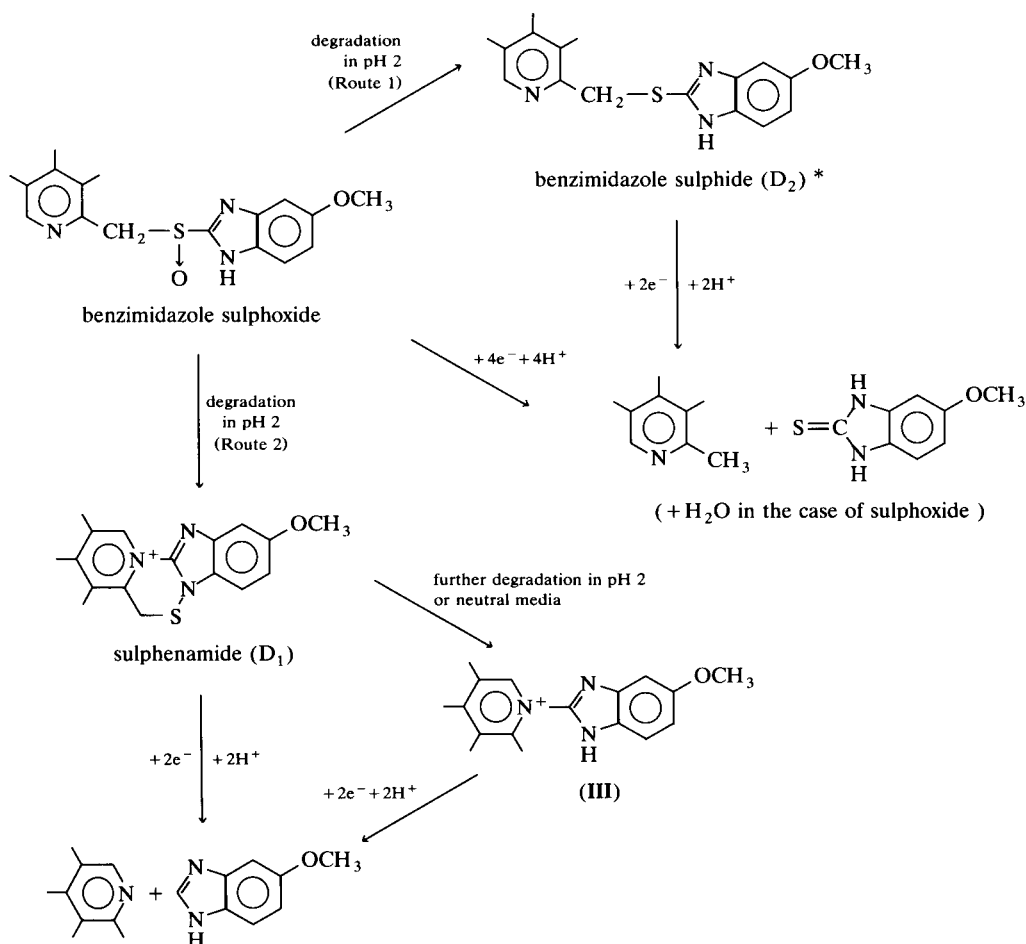


as opposed to catalytic hydrogen evolution. These entities are adsorbed on the Hg surface with the electrostatic attraction of the negatively charged Hg surface for the positively charged quaternary nitrogen atom assisting in this adsorption process. The DPP peak height for D_1^I is therefore relatively large due to the effect of this reactant adsorption. This is further illustrated in a stripping voltammetric study of **I** and its degradation products in pH 2 supporting electrolyte where the strong reactant adsorption of D_1^I allows it to be determined down to a limit of detection of 1×10^{-8} mol dm^{-3} [9]. The DPP peak height for D_1^{II} is relatively small due to a lesser degree of reactant adsorption. Further evidence to negate cat-

alytic hydrogen evolution as an explanation of the DPP signals of a sulphenamide such as D_1^1 and related molecules which contain the molecular entity **III** is that D_1^1 shows DPP behaviour over the pH range 1–9 more characteristic of electron transfer leading to reduction, i.e., it has a more or less constant peak height in this pH range with an E_p varying from -0.66 to -1.20 V. It should be noted that D_1^1 will degrade in neutral media to a molecule which also contains the reducible molecular entity **III**. The height of signals corresponding to catalytic hydrogen evolution are particularly influenced by variation in pH for example.

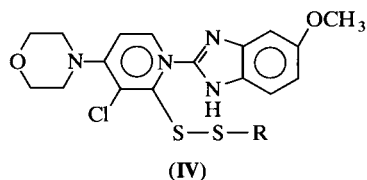
3.3. Reaction of 2-mercaptoethanol with degrading **I** and **II** in solution at pH 2

DPP has been used to follow in situ the reaction between a thiol such as 2-mercaptoethanol and **I** in pH 2 supporting electrolyte as a simulation of its believed reaction in vivo [6]. It was found that the thiol signal at ca. -100 mV (due to reduction of the Hg salt of the thiol) practically disappeared as **I** degraded to give the D_1^1 and D_2^1 signals in a 30 min time scale. No new peaks appeared and the pattern of D_1^1 and D_2^1 signal production was essentially the same as in the absence of the thiol. This is still consistent with



Scheme 1. Mechanism of degradation/electrode reactions as monitored by DPP. * Structure determined for SK&F 95601 in an earlier paper [6] by preparative TLC + mass spectrometry.

the sulphenamide D_1^I reacting with the thiol to produce a disulphide **IV** since a structure such as this disulphide can still give rise to a reduction peak at the same potential observed for D_1^I .



As has already been stated in this text, an unsuccessful attempt was made to isolate a sample of D_1^I by LC using a mobile phase of acetonitrile– H_2O (50 + 50). Instead D_1^I degraded to a compound whose UV spectrum is given in Fig. 1h with a λ_{max} of 340 nm, believed to be a disulphide of similar structure to **IV**. When this degradation product of D_1^I with a DPP peak at -720 mV was mixed with 1×10^{-5} mol dm^{-3} 2-mercaptoethanol in 10^{-2} M HCl the thiol peak did not decrease. The same event occurred when a sample of D_2^I , prepared in a previous paper [6], was mixed with 2-mercaptoethanol, i.e., the thiol peak did not decrease and the D_2^I peak at -493 mV was unaltered.

Since the D_1^I /sulphenamide signal at -739 mV attains its maximum peak height between 10 min and 1 h of the initiation of its degradation in pH 2 media prior to decreasing to one third of its maximum value after two days (this residual signal at -739 mV being due to a sulphenamide degradation product such as a disulphide rather than the sulphenamide), it would therefore be supposed that the reaction of the thiol and the sulphenamide would be maximised between 10 min and 1 h of the initiation of the degradation reaction. 1×10^{-5} mol dm^{-3} **I** was therefore allowed to degrade for various times in 1×10^{-2} mol dm^{-3} HCl prior to introduction of 1×10^{-5} mol dm^{-3} of 2-mercaptoethanol into the polarographic cell and immediate recording of the polarogram. Since it takes 25 s from the start potential of $+100$ mV to reach the thiol peak at -100 mV plus 1 min deaeration time then the reaction time allowed between generated sulphenamide D_1^I and 2-mercaptoethanol is 85 s.

Table 1

Effect of degradation time at pH 2 on the height of the thiol peak at ca. -100 mV

Time allowed for I to degrade in 10^{-2} mol dm^{-3} HCl (min)	Thiol peak height at ca. -100 mV with running of DPP (arbitrary units) after a delay period of 1 min
I absent	26.0
3	7.0
9	5.5
15	4.5
30	7.5
40	6.5
50	6.5
60	6.0
80	12.0
120	15.0
160	18.0
200	20.0
240	22.0
360	26.5
450	28.0

Results in Table 1 show that between 9 and 60 min of degradation of **I** in pH 2 medium prior to introduction of the thiol is optimum from the view point of maximum reaction of the sulphenamide D_1^I and the thiol, as expected. It also suggests that with a reaction time of 85 s the reaction between D_1^I and 2-mercaptoethanol in 10^{-2} mol dm^{-3} HCl is relatively rapid. The reaction of SF&K 95601 **I** with 2-mercaptoethanol in 10^{-2} mol dm^{-3} HCl was also followed by UV spectrophotometry in that the long wavelength absorption band at 380 nm due to the sulphenamide (D_1^I) was moved to 340 nm upon addition of the thiol. This is to be expected of the disulphide reaction product **IV** from the preceding discussion in this paper.

The reaction of 1×10^{-5} mol dm^{-3} omeprazole **II** and 1×10^{-5} mol dm^{-3} 2-mercaptoethanol was also studied by DPP after allowing **II** to degrade for various times prior to introduction of 2-mercaptoethanol into the polarographic cell. Lowest thiol peak heights of 10 arbitrary units were found (compared to 6 units for SK&F 95601) when omeprazole was allowed to degrade for 30 min to 1 h prior to thiol addition as already predicted since omeprazole's sulphenamide D_1^{II} is

generated more slowly than D_1^I . This is illustrated in Fig. 3 after allowing **II** to degrade for 40 min prior to thiol addition. As with SK&F 95601, the cathodic phenomena, i.e., D_2^{II} , D_{1a}^{II} and D_1^{II} are essentially unaffected by the presence of 2-mercaptoethanol (RSH) but the thiol peak is noticeably reduced due to its reaction with sulphenamide D_1^{II} generated in the degradation of **II** in pH 2 media.

3.4. Limits of detection of **I**, **II** and their respective degradation products using DPP

Not only has DPP proved itself to be a very useful tool in monitoring the degradation of **I** and **II** in acidic media, pH 2 and in following the reactions of 2-mercaptoethanol with the respective products of these degradations, it can also be used to selectively determine trace levels of these compounds at nanomolar concentrations. This could then be applied to the analysis of such molecules in formulations or in the analysis of biological fluids. SK&F 95601 in Britton-Robinson (BR) buffer (pH 9) shows linear calibration in the range $(1-10) \times 10^{-7}$ mol dm⁻³ with a correlation coefficient of 0.9974 as calculated by linear regression analysis. A limit of detection (LOD) can be calculated from this latter analysis by taking the intercept on the signal axis as the blank signal and adding three times the standard deviation of the blank signal to this to give a signal which corresponds to the LOD. For **I**, this LOD corresponds to 0.7×10^{-7} mol dm⁻³. The reproducibility of measurement at a concentration of 4×10^{-7} mol dm⁻³ **I** is calculated as 6.11% relative standard deviation (R.S.D.) ($n = 6$). Calibration is linear for **I** up to a concentration of 1×10^{-4} mol dm⁻³ where the reproducibility of measurement is 1.15% R.S.D. ($n = 6$). Omeprazole in BR buffer (pH 9) also gives a linear calibration in the range $(1-10) \times 10^{-7}$ mol dm⁻³ with a correlation coefficient of 0.9992. The LOD, calculated as for **I**, is 0.8×10^{-7} mol dm⁻³. Reproducibility for **II** at a concentration of 4×10^{-7} mol dm⁻³ is calculated as 4.38% R.S.D. ($n = 6$) and at a concentration of 1×10^{-4} mol dm⁻³ **II** up to which linearity for **II** is achieved, a

value of 0.55% R.S.D. ($n = 6$) was calculated. In the absence of complete kinetic pictures of the respective degradations of **I** and **II** in 1×10^{-2} mol dm⁻³ HCl, it is impossible to calculate absolute LODs for degradation products D_1^I and D_2^I (for **I**) and D_1^{II} and D_2^{II} (for **II**) in this supporting electrolyte. However, bearing in mind that the actual concentrations of the degradation products are less than the parent compounds from which they are derived in 1×10^{-2} mol dm⁻³ HCl the LODs for D_2^I and D_2^{II} would be expected to be comparable to the LODs of **I** and **II** whereas the LODs for sulphenamides D_1^I and D_1^{II} , which produce relatively large DPP signals, would be expected to be lower than the LODs of **I** and **II**.

Acknowledgements

The authors wish to thank Smith Kline and Beecham Pharmaceuticals for provision of a sample of SK&F 95601 and Astra Pharmaceuticals for provision of a sample of omeprazole. Dr. E. Sturm of Byk Gulden is thanked for his helpful communication (Ref. 5) on subject matter contained in this publication.

References

- [1] S.P. Clissold and D.M. Campoli-Richards, *Drugs*, 32 (1986) 15; and references cited therein.
- [2] K. Klemm, *J. Chem. Soc., Chem. Commun.*, (1986) 125.
- [3] P. Lundberg, *J. Med. Chem.*, 29 (1986) 1327.
- [4] J. Senn-Bilfinger, V. Kruger, E. Sturm, V. Figala, J. Klemm, B. Kohl, G. Rainer, H. Schaeffler, T.J. Blake, D.W. Darkin, R.J. Iffe, C.A. Leach, R.C. Mitchell, E.S. Pepper, C.J. Salter, N.J. Viney, G. Huttner and J. Zsolnai, *J. Org. Chem.*, 52 (1987) 4573 and 4582.
- [5] E. Sturm, Byk Gulden, personal communication.
- [6] E. O'Kane, V.N. Ramachandran, S. McClean and W.F. Smyth, *Analyst*, 118 (1993) 511.
- [7] R.J. Iffe, C.A. Dyke, D.J. Keeling, E. Meenan, M.L. Meeson, M.E. Parsons, C.A. Price, C.J. Theobald and A.H. Underwood, *J. Med. Chem.*, 32 (1989) 1970.
- [8] B.-L. Johansson, PhD Thesis, Uppsala University, 1983.
- [9] S. McClean, T.J. Maxwell, V.N. Ramachandran, E. O'Kane and W.F. Smyth, *Electroanalysis*, in press.

Adsorptive stripping voltammetry of trace uranium: critical comparison of various chelating agents

Jianyan Wang^a, Joseph Wang^{a,*}, Jianmin Lu^a, Khris Olsen^b

^a Department of Chemistry and Biochemistry, New Mexico State University, Las Cruces, NM 88003, USA

^b Geochemistry Section, Environmental Sciences Department, Battelle PNL, Richland, WA 99352, USA

(Received 25th October 1993; revised manuscript received 8th February 1994)

Abstract

A critical and systematic evaluation of four chelating agents for adsorptive stripping voltammetric measurements of trace uranium is reported. The utility of propyl gallate (PG) and *N*-benzoyl-*N*-phenylhydroxylamine (BPA) is illustrated for the first time and compared to that of previously used cupferron and oxine. All ligands offer convenient quantitation of low $\mu\text{g/l}$ uranium concentrations, following short adsorption times. The sensitivity pattern is: PG > cupferron > oxine > BPA. A large difference in the selectivity (in the presence of co-existing metals) is observed, according to the following selectivity order: PG \approx cupferron > BPA > oxine. Applicability to rapid assays of groundwater and sediments is illustrated. Such comparison of the analytical performance of various ligands should serve as a guide for selecting the most appropriate adsorptive stripping scheme for other target metals.

Key words: Adsorptive stripping voltammetry; Propyl gallate; *N*-Benzoyl-*N*-phenylhydroxylamine; Uranium

1. Introduction

Considerable interest has developed (upon the end of the cold war) in highly sensitive and reliable analytical procedures for monitoring trace uranium in contaminated nuclear energy sites. Because of their portable character and low power needs, voltammetric techniques are highly suitable for the task of on-site characterization, and have been used for the determination of uranium in various matrices. In particular, highly sensitive (and yet inexpensive) adsorptive stripping proce-

dures – based on the formation and adsorptive accumulation of various uranium chelates – have been developed in past years [1–6]. Such procedures offer extremely low (subnanomolar) detection limits, coupled to different degrees of selectivity.

This paper reports a systematic comparison of several (new and old) chelating agents for adsorptive stripping measurements of uranium. It attempts to critically evaluate the analytical utility of four such ligands, and to compare all aspects of the adsorptive stripping performance (and not only the detection limits). While the utility of cupferron and oxine for stripping measurements of uranium has been described previously [1,2],

* Corresponding author.

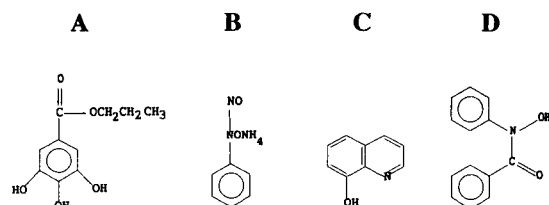


Fig. 1. Chemical structure of chelating agents used for adsorptive stripping measurements of trace uranium: (A) propyl gallate; (B) cupferron; (C) oxine; (D) *N*-benzoyl-*N*-phenylhydroxylamine.

the use of propyl gallate (PG) and *N*-benzoyl-*N*-phenylhydroxylamine (BPA) for the same task is reported here for the first time. Fig. 1 displays the structure of the ligands used in this comparative study. It is hoped that such comparison will serve as a guide for the selection of the most appropriate procedure for uranium. In addition, since numerous ligands are now available for adsorptive stripping measurements of various trace metals [6], we hope that such critical comparison will be adopted as a general approach for choosing an adsorptive stripping scheme for a given target metal.

2. Experimental

2.1. Apparatus and reagents

An EG & G PAR 264A voltammetric analyzer, a PAR 303A static mercury drop electrode (SMDE), and a PAR 0073 X–Y recorder were used to obtain the voltammograms. A medium-size hanging mercury drop electrode (with an

area of 0.016 cm²) was employed. The potentiometric stripping response was obtained with a TraceLab unit (PSU 20, Radiometer) and an IBM PS/2 55SX computer. All solutions were prepared from doubly-distilled water. The stock solution (1000 mg/l) of uranium (atomic absorption standard, Aldrich) was diluted daily as required. The ligands cupferron, oxine and BPA were received from Aldrich, while propyl gallate was obtained from Sigma. Various acetate buffer, PIPES and HEPES solutions served as supporting electrolytes (see Table 1). The groundwater and soil samples were collected at the Hanford site (Richland, WA). The soil sample (1.0 g) was microwave digested for 10 min in 20 ml of a (1 + 1, v/v) Ultrex nitric acid solution, filtered through a 0.45- μ m cellulose acetate syringe and diluted with 100 ml Milli-Q water.

2.2. Procedure

The supporting electrolyte solution (10 ml), containing the desired level of the chelating agent was pipetted into the cell and deaerated by nitrogen for 8 min. The preconcentration potential was applied to a fresh mercury drop while the solution was stirred. Following the preconcentration step, the stirring was stopped and after 15 s the voltammogram was recorded by applying a negative-going linear potential scan (with 100 mV/s scan rate). Aliquots of the uranium standard solution were introduced after recording the background voltammograms. Throughout this operation, nitrogen was passed over the solution. All data were obtained at room temperature.

Table 1
Experimental conditions used in the adsorptive stripping procedures for uranium

Conditions	Chelating agent			
	PG	Cupferron	Oxine	BPA
Media	0.05 M acetate buffer (pH 4.5)	0.1 M acetate buffer (pH 4.5)	2×10^{-3} M PIPES (pH 7.1)	0.05 M HEPES (pH 8.1)
Ligand conc. (M)	5×10^{-5}	5×10^{-6}	2×10^{-4}	5×10^{-5}
E_{acc} (V)	-0.15	-0.10	-0.40	-0.10
E_{final} (V)	-0.60	-0.60	-0.80	-0.80
Waveform	DC	DC	DC	DC
Scan rate (mV/s)	100	100	100	100

Details of the specific procedures used for each chelating agents are given in Table 1.

Potentiometric stripping measurements were made on a preplated mercury film, covering the glassy carbon electrode. The film was obtained by plating mercury from a 800 mg/l Hg^{+2} (in 1.3 M HCl) solution at -0.9 V for 15 min following a 2 min 'cleaning' at -0.1 V. A constant current ($-20 \mu\text{A}$) was used during the stripping step, followed by a one-min 'cleaning' at -1.40 V.

3. Results and discussion

The strong interfacial accumulation of the U-PG and U-BPA complexes is indicated from Fig. 2, which shows repetitive cyclic voltammograms for 50 $\mu\text{g/l}$ uranium in unstirred solutions containing 5×10^{-5} M PG (A) or BPA (B). For both ligands, progressive increases of the cathodic and anodic peaks are observed upon repetitive scans, until saturation is achieved. The cathodic peaks are observed at -0.38 (A) and -0.62 (B) V, while the anodic ones are at -0.14 (A) and -0.26 (B) V. The peaks at saturation remained stable upon continuous scanning, with no desorption over prolonged periods. The maximum charges obtained by integrating the reduction current (at saturation) were found to be 88 (A) and 53 (B) nC, i.e., surface coverages of 2.87×10^{-11} and 1.73×10^{-11} mol cm^{-2} , respec-

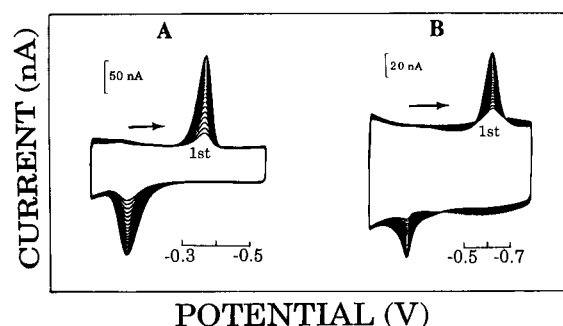


Fig. 2. Repetitive cyclic voltammograms for 50 $\mu\text{g/l}$ uranium in the presence of 5×10^{-5} M propyl gallate (A) and 5×10^{-5} M *N*-benzoyl-*N*-phenylhydroxylamine (B). Scan rate, 100 mV/s; electrolyte, 0.05 M acetate buffer (pH 4.5) (A) and 0.05 M HEPES buffer (pH 8.1) (B).

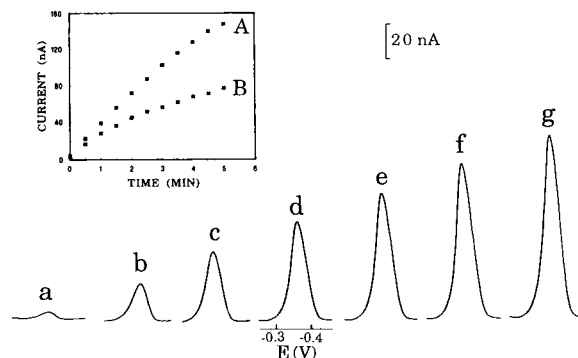


Fig. 3. Stripping voltammograms for 10 $\mu\text{g/l}$ uranium, in the presence of 5×10^{-5} M propyl gallate, following different adsorption times 0 (a) 30 (b), 60 (c), 90 (d), 120 (e), 150 (f) and 180 (g) s. Linear scan at 100 mV/s; acetate buffer solution (pH 4.5, 0.05 M). Also shown (inset) current–time plots in the presence of propyl gallate (A) and BPA (B). See Experimental section for details.

tively. For both ligands, plots of \log (peak current) vs. \log (scan rate) were linear over the 5–100 mV/s range. The resulting slopes of 0.88 (PG) and 0.73 (BPA) indicate deviations from a behaviour expected for an ideal surface-bound redox couple (i.e., slope of 1.0).

The spontaneous adsorption of the U-PG and U-BPA complexes can be used as an effective preconcentration step, prior to the voltammetric measurement. In this way, highly sensitive adsorptive stripping measurements of uranium can be achieved. For example, Fig. 3 displays stripping voltammograms for 10 $\mu\text{g/l}$ uranium, in the presence of 5×10^{-5} M PG, after different accumulation periods (0–180 s, a–g). The longer the preconcentration time, the more U-PG chelate is adsorbed, and the larger the current response. For example, with 180 s accumulation there is a 24-fold enhancement of the peak relative to that obtained without accumulation (a vs. g). Such current enhancements offer convenient quantitation of low ($\mu\text{g/l}$) uranium levels. Also shown in Fig. 3 (inset) are plots of peak current vs. accumulation time for BPA (A) and PG (B) over the 0–5 min range. For both ligands, the current rises linearly with time first, and then more slowly.

While experimental conditions have been optimized earlier [1,2] for the use of oxine and cup-

ferron, it is essential to examine the influence of various variables upon the uranium response in the presence of BPA and PG. Fig. 4 displays the effect of solution pH (A), ligand concentration (B), and accumulation potential (C) upon the uranium peak current. The U–BPA peak increases gradually upon raising the pH between

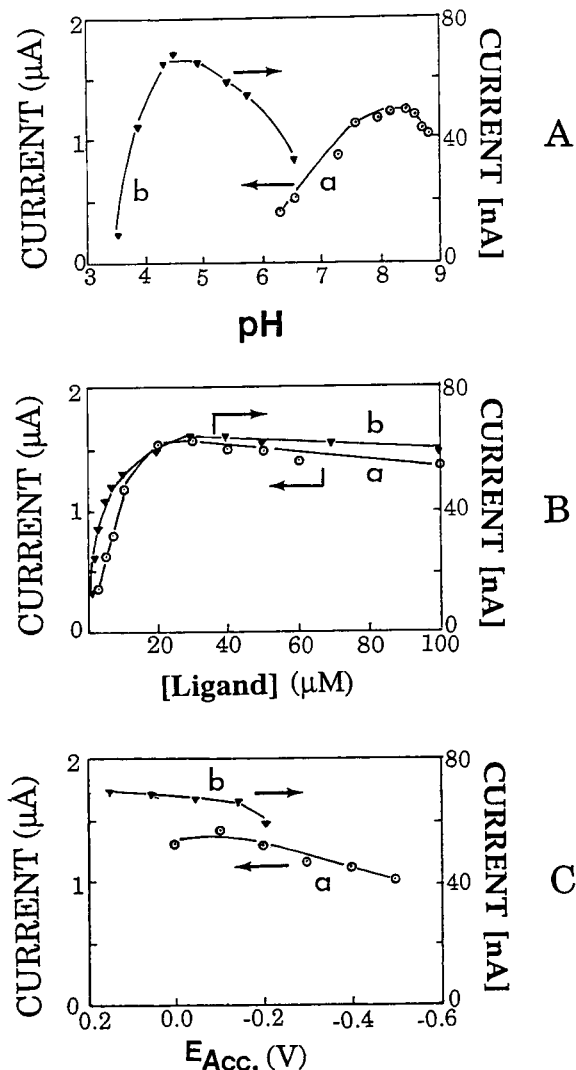


Fig. 4. Effect of solution pH (A), ligand concentration (B) and accumulation potential (C) upon the adsorptive stripping response $10 \mu\text{g/l}$ uranium in the presence of BPA (a) and PG (b). Preconcentration for 120 (a) and 90 (b) s. Differential pulse scan with 20 mV/s rate (a). Other conditions are in the Experimental section and Table 1.

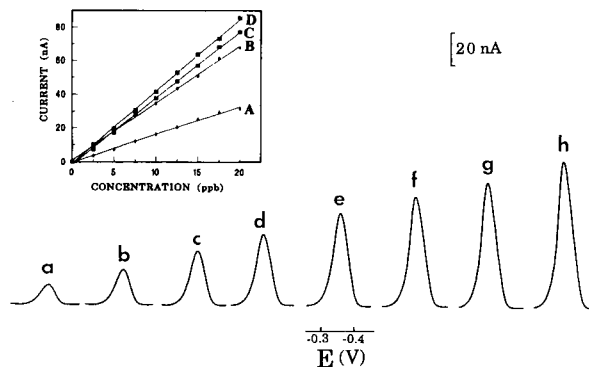


Fig. 5. Voltammograms obtained with increasing uranium concentration in steps of $2.5 \mu\text{g/l}$ (a–h). Ligand, PG; preconcentration for 60 s. Also shown (inset) are calibration plots over the same range using BPA (A), oxine (B), cupferron (C) and PG (D). Conditions, as in Table 1.

6.3 and 7.6, and then more slowly up to 8.3 (a); a sharp decrease is observed at higher pH values. Similarly, the pH of the acetate buffer strongly influences the U–PG response (b). This peak rapidly increases between pH 3.6 and 4.5, and gradually decreases at higher values. The ligand concentration has a similar effect upon the U–BPA and U–PG peaks, with a sharp increase up to $2 \times 10^{-5} \text{ M}$, and a levelling off at higher concentrations. The accumulation potential has a minor effect upon the resulting response. Yet, most favourable signal-to-background characteristics were obtained following accumulation at -0.15 V (PG) and -0.10 V (BPA). Such conditions offer also good reproducibility, as indicated from the relative standard deviations (2.2 (PG) and 2.4 (BPA)%) for 12 repetitive measurements of $10 \mu\text{g/l}$ uranium (90 s accumulation; not shown).

Fig. 5 displays stripping voltammograms for PG solutions of increasing uranium concentration ($2.5\text{--}20 \mu\text{g/l}$, a–h). Well-defined peaks over a flat baseline, are observed at this low level following a short (60 s) preconcentration time. A linear relationship exists between the peak height and uranium concentration over the entire range (see inset, D). Also shown, are calibration plots, recorded under similar conditions, but in the presence of BPA (A), oxine (B) and cupferron (C). All ligands exhibit high linearity, reflecting

conditions of low surface coverage (linear isotherm conditions). Least squares treatment of these data yielded slopes of 1.7 (BPA), 3.4 (oxine), 3.9 (cupferron) and 4.3 (PG) $\text{nA} \cdot \text{l}/\mu\text{g}$. Additional calibration experiments with PG over the 5–100 $\mu\text{g}/\text{l}$ range indicated a linear response up to 80 $\mu\text{g}/\text{l}$ (not shown); high linearity over the entire range was obtained for a shorter (30 s) adsorption period. Detection limits of 0.06, 0.05, 0.15 and 0.22 $\mu\text{g}/\text{l}$ uranium were estimated based on the standard deviation ($3 \times$) of repeated measurements of 0.25 $\mu\text{g}/\text{l}$ uranium in the presence of cupferron, PG, oxine and BPA (10 min adsorption; not shown).

While the various chelating agents offer remarkable sensitivity and convenient quantitation of low $\mu\text{g}/\text{l}$ concentrations, it is as important (for practical environmental surveillance work) to achieve high degree of selectivity. Coexisting metal ions may compete for the ligand binding, thus influencing the uranium response. The effect of large excess of common metal ions upon the adsorptive stripping response of various uranium complexes is illustrated in Table 2. Both PG and cupferron result in high selectivity, with no interference in the presence of a 10-fold excess of copper, thallium, cobalt, cadmium, manganese, chromium, antimony, thorium, iron, lead or zinc. In contrast, additions of 100 $\mu\text{g}/\text{l}$ iron and lead

resulted in a 78% decrease and 14% increase, respectively of the uranium–BPA peak. (The increase in the presence of lead is attributed to an overlapping response.) Similarly, the uranium–oxine peak disappeared in the presence of 10-fold excess of iron and cadmium, and decreased by nearly 30, 40 and 82% in the presence of cobalt, lead and manganese, respectively. The presence of molybdenum masked the uranium–cupferron peak, and caused a 20% decrease of the uranium–PG response (with a large molybdenum–PG peak appearing at -0.27 V). Only excess titanium severely affected the uranium peak of all four ligands. Such interference can be addressed by addition of EDTA. Overall, the trend in selectivity is cupferron \approx PG $>$ BPA $>$ oxine. Other potential interferences (as in all adsorptive stripping schemes) include natural surface active organic materials and uranium complexing agents in the sample.

The highly sensitive and selective response of the adsorptive stripping procedures allows direct assays of relevant environmental samples. Fig. 6 demonstrates their suitability for monitoring uranium in an untreated and diluted groundwater sample. With a 1 min preconcentration time, three of the ligands (PG (A), cupferron (B) and BPA (D)) display a well defined response for the (1:20 diluted) sample (a), thus permitting convenient quantitation following standard additions of 10 $\mu\text{g}/\text{l}$ uranium (b, c). In contrast, because of severe interference problem, oxine cannot be used for such assay (C). The resulting standard additions plots (also shown, inset) yield similar values (147 (PG), 153 (cupferron) and 166 (BPA) $\mu\text{g}/\text{l}$) following correction for the dilution. The three ligands were also found useful for the determination of uranium in a contaminated sediment sample (that was microwave digested and 1:100 fold diluted; not shown). The large dilution, accrued from the inherent sensitivity towards uranium, greatly minimizes potential matrix effects.

Potentiometric stripping procedures may be advantageous over their voltammetric counterparts in connection with on-site (field) assays of groundwater or sediments. In particular, the potentiometric stripping approach eliminates the need for a time-consuming sample deaeration

Table 2
Effect of coexisting ion upon the response for 10 $\mu\text{g}/\text{l}$ uranium, in the presence of various chelating agents (100 $\mu\text{g}/\text{l}$)

Coexisting ion	Change in response (%)			
	PG	Cupferron	Oxine	BPA
Cd(II)	0	0	-100	0
Cr(VI)	0	0	0	0
Cu(II)	0	0	0	0
Fe(III)	0	0	-100	-78
Pb(II)	0	0	-39	+14
Zn(II)	0	0	0	0
Th(IV)	0	0	0	0
Sb(III)	0	0	0	0
Co(II)	0	0	-70	0
Mn(II)	0	0	-82	0
Tl(I)	0	0	0	0
Ti(IV)	-100	-100	-30	-100
Mo(VI)	-20	+150	0	0

Conditions as in Table 1, with 60 s accumulation.

step, and should minimize concerns related to field handling of mercury (as it relies on a pre-plated thin mercury film, rather than fresh mercury drops). Fig. 7 displays stripping potentiograms, in the presence of cupferron (A) and PG (B), for a contaminated groundwater sample (a), and following two standard additions of $10 \mu\text{g/l}$ uranium (b, c). Convenient quantitation is indicated from the well-defined potentiometric stripping response, and the resulting standard additions plots (also shown). Both ligands yielded similar uranium values (148 (cupferron) vs. 143 (PG) $\mu\text{g/l}$). Yet, cupferron exhibits more favourable response characteristics. Similar to the voltammetric scheme, the inherent sensitivity of

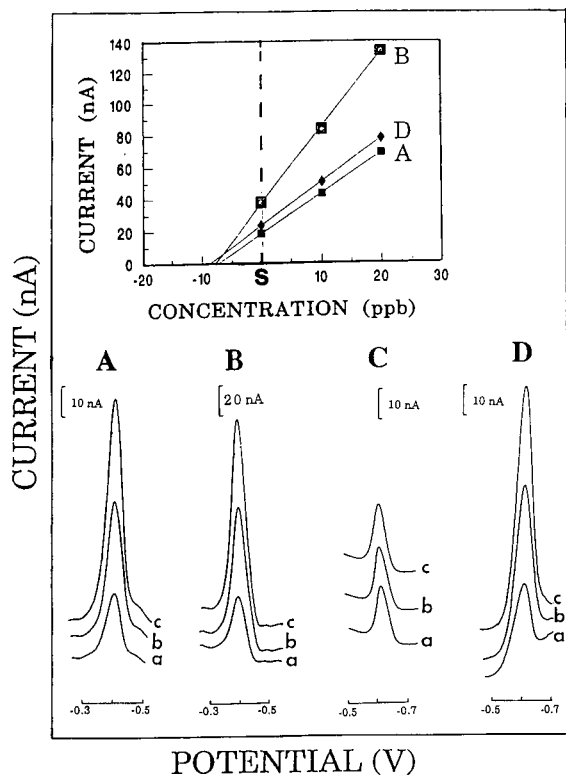


Fig. 6. Voltammograms for a groundwater sample (a) and successive concentration increments of $10 \mu\text{g/l}$ uranium (b, c). Sample was diluted (1:20) with the supporting electrolyte. Ligands, PG (A), cupferron (B), oxine (C) and BPA (D). Preconcentration for 60 s. Also shown (inset) are the resulting standard addition plots for BPA (D), cupferron (B) and PG (A). Conditions, as in Table 1, except that the cupferron concentration was 1×10^{-4} M.

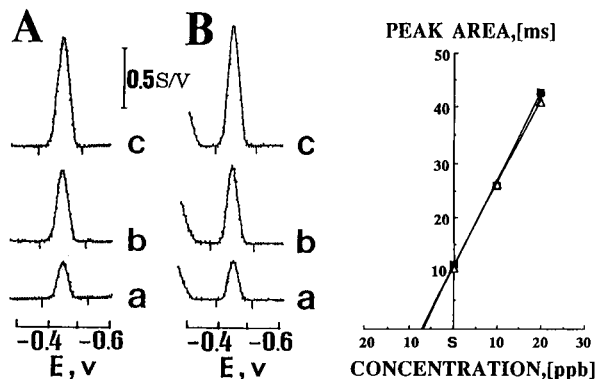


Fig. 7. Stripping potentiograms for a (1:20 diluted) groundwater sample (a), and following additions of $10 \mu\text{g/l}$ uranium (b, c). Accumulation for 1 min at -0.05 V, following a constant-current ($-20 \mu\text{A}$) stripping, and 1 min 'cleaning' at -1.4 V. Ligands, 5×10^{-6} M cupferron (A); 5×10^{-5} M PG (B).

the potentiometric approach permits significant (20-fold) dilutions and short preconcentration times. Fig. 8 demonstrates a potentiometric stripping assay of a contaminated sediment sample. The sediment was microwave digested and the leachate was diluted (50-fold) in the cell. The resulting uranium value (1.16 mg/l) is in good agreement with the value (1.21 mg/l) obtained by ICP-MS.

In conclusion, the utility of new chelating agents for adsorptive stripping measurements of

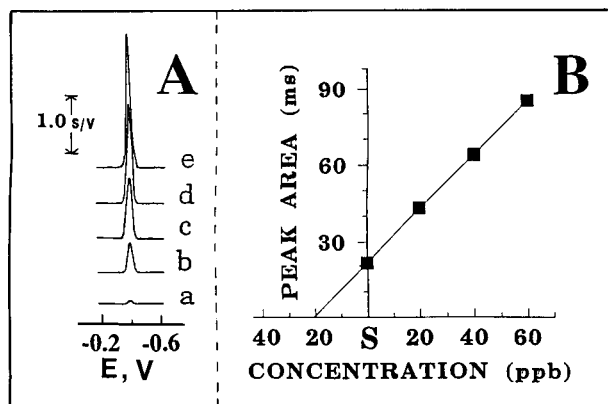


Fig. 8. Stripping potentiograms for a soil sample. (a) Response for the electrolyte; (b) same as (a) but after adding $400 \mu\text{l}$ of the leachate; (c–e), same as (b), but after additions of $20 \mu\text{g/l}$ uranium. Conditions, as in Fig. 7A, but using 1×10^{-4} M cupferron.

trace uranium has been demonstrated, and systematically compared to other ligands used for the same task. Particularly attractive is the use of PG which offers remarkable sensitivity as well as high selectivity. This ligand, along with cupferron, appear to be most suitable for the task of field screening for uranium. Details of such on-site operations will be reported in the near future. The use of a family of ligands, of varying coordination strength may open the door for uranium speciation studies (via displacement of different fractions from natural complexes). In addition, important information relevant to the oxidation state is expected using cupferron, which displays peaks for different oxidation states of uranium [2]. It is hoped that future selection of the most appropriate chelating agent for a given target metal will rely on a similar critical comparison of their overall analytical performance.

Acknowledgements

This work was supported by a grant from Battelle PNL (Contract 152891) and the U.S. Department of Energy (Waste Management Education and Research Consortium, WERC).

References

- [1] C.M.C. van den Berg and M. Nimmo, *Anal. Chem.*, 59 (1987) 924.
- [2] J. Wang and R. Setiadji, *Anal. Chim. Acta*, 264 (1992) 205.
- [3] J. Wang and J. Zadeii, *Talanta*, 34 (1987) 247.
- [4] J. Wang, R. Setiadji, L. Chen, J. Lu and S. Morton, *Electroanalysis*, 4 (1992) 161.
- [5] C. Hua, D. Jagner and L. Renman, *Anal. Chim. Acta*, 197 (1987) 265.
- [6] M. Pandi and A. Voulgaropoulos, *Electroanalysis*, 5 (1993) 355.

Static and flow-injection voltammetric determination of periodate by reduction at a rotating platinum wire electrode

H.İ. Gökçel^a, G. Nişli^{b,*}

^a Chemical Engineering Department, Faculty of Engineering

^b Chemistry Department, Faculty of Science, Ege University, 35100 Izmir, Turkey

(Received 24th September 1993; revised manuscript received 20th December 1993)

Abstract

A method for periodate determination was developed as a result of static and flow-injection voltammetric investigations where a rotating platinum wire electrode was employed. In the static system, 4.0×10^{-5} – 4.2×10^{-4} M periodate could be determined in the cell in pH 7.0–7.5 phosphate buffer. In the flow-injection system, periodate solutions of 20–100 μ l were injected into the carrier stream of a phosphate buffer solution at pH 7.0. The flow rates were in the range of 1.0–1.7 ml min⁻¹. The peak currents were measured at -0.07 V against a saturated calomel electrode. The determination of periodate concentrations in the range 1.0×10^{-5} – 1.0×10^{-4} M was possible with a throughput of 15–40 samples per hour.

Key words: Flow injection; Voltammetry; Periodate

1. Introduction

Periodate is used as a strong and selective oxidant for the determination of vicinal polyhydroxy compounds such as carbohydrates and polyols [1]. Quantitation of these compounds depends on either the determination of the oxidation products of the organic compounds, the measurement of IO_3^- formed or of the excess of IO_4^- .

The kinetics and mechanism of oxidation pathways of such compounds have also been described, and were determined by means of spec-

trophotometric and/or titrimetric methods [2–7].

The determination of such compounds could also be based on the detection of periodate by spectrophotometric methods [8–12] or by electro-metric methods, employing a periodate-selective electrode or measuring the polarographic reduction current of periodate [13–16]. In recent years, continuous-flow and flow-injection techniques have been employed in the periodate oxidation methods [17–21].

In the present article, the behaviour of periodate at a rotating platinum wire electrode (RPWE) was studied as a function of pH and concentration of periodate in a static system. The developed voltammetric procedure was then applied to the flow-injection amperometric determi-

* Corresponding author.

nation of the periodate under optimum pH and flow conditions.

2. Experimental

2.1. Apparatus

All experiments were performed with a Tacussel UAP1 polarograph and a Tacussel PRT 500LC potentiostat, in conjunction with a GRSO Tacussel recorder. The three-electrode system consisted of an RPWE (Metrohm EA 222), an auxiliary platinum electrode (Metrohm EA 201) and a saturated calomel reference electrode (SCE, Tacussel C5). A rotation speed of 750 rpm was obtained, using a Metrohm GCY 82 × M rotator.

A Metrohm E 510 pH meter was used for pH measurements with a combined glass electrode. The temperature was maintained at $25 \pm 1^\circ\text{C}$ with a Heto Ultrathermostat, 05 E 623.

In the static system, a conventional electrolytic cell with a water jacket was used.

The manifold used for flow experiments is shown in Fig. 1. The supporting electrolyte (as eluent) was pumped by a mini-peristaltic pump with six rollers (Ergun Medical, Turkey) through the flow cell. The sample was introduced into the system by means of a Rheodyne 7125 sample injection valve with 20, 50 and 100 μl loop volumes. A 50 cm \times 0.51 mm i.d. PVC tubing was employed as a delay coil.

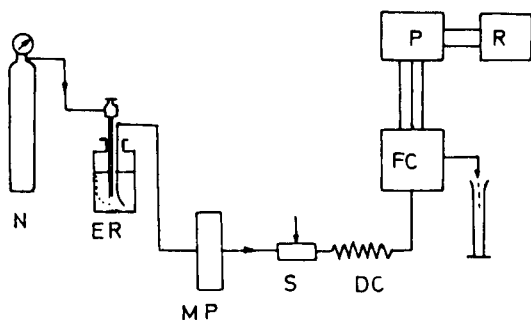


Fig. 1. Flow-injection manifold for the determination of periodate. N = nitrogen gas; ER = eluent reservoir; MP = mini-peristaltic pump; S = sample injection valve; DC = delay coil; FC = flow cell; P = potentiostat; R = recorder.

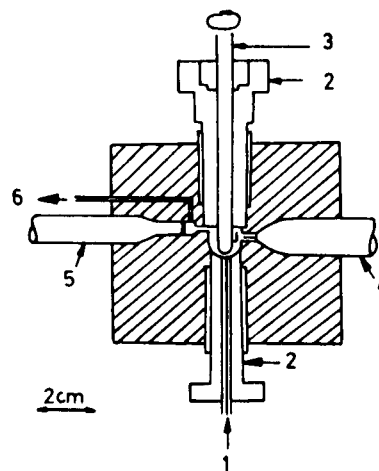


Fig. 2. Cross-section of flow-through three-electrode cell. 1 = inlet; 2 = PTFE elements; 3 = RPWE; 4 = Pt electrode; 5 = SCE; 6 = outlet.

A new flow cell with a volume of 0.6 ml was constructed from PTFE and plexiglas (Fig. 2). All interconnections were made with 0.51 mm i.d. and 2.30 mm o.d. PVC tubing and fitting.

2.2. Reagents and solutions

Doubly distilled water and analytical-reagent grade chemicals (BDH or Merck) were used. Potassium metaperiodate (KIO_4) stock solution (1.0×10^{-2} M) was prepared by dissolving the salt in water and diluting to 100 ml. Lower concentrations of solutions of periodate were prepared by further dilution of this solution.

Acetate buffer (pH 5.59): 10.7 ml of 1.250 M acetic acid was added to 100 ml of 0.125 M sodium hydroxide. Phosphate buffers (pH 6.10–7.50): 50.0, 11.5 or 3.4 ml of 1.000 M sodium dihydrogenorthophosphate (NaH_2PO_4) solutions were added respectively to 100 ml of 0.125 M dipotassium hydrogenorthophosphate (K_2HPO_4). Borate buffers (pH 8.48–9.64): 65.4, 13.0 or 3.85 ml of 0.500 M boric acid (H_3BO_3) were added respectively to 100 ml of 0.330 M sodium borate. All buffer solutions were diluted to 250 ml and their final pH values were measured by a pH meter at 25°C . These solutions were used as

supporting electrolyte after deaerating with nitrogen.

2.3. Procedure

The electrode was preconditioned in the conventional voltammetric manner by repeated scans of the applied potential in the range +1.3 V to -0.7 V versus SCE until identical current-potential (i - E) curves for each buffer solution were obtained in consecutive runs. The RPWE was also cleaned by polishing with alumina, when required.

In the static system, the concentration of periodate (C) in the cell was increased from 4.0×10^{-5} to 4.2×10^{-4} M by successive addition of 0.2 ml of the stock periodate solution into 50 ml of supporting electrolyte. After each addition, the corresponding i - E curves were recorded.

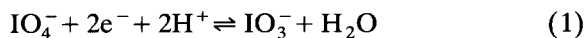
In the flow system, the supporting electrolyte (pH 7.00) was first pumped through the cell. After a steady background current at -0.07 V was obtained, the periodate solutions in increasing concentrations were injected and the cur-

rent-time (i - t) curves were recorded. Injection of each solution was repeated 2 to 5 times. Flow rates were measured volumetrically.

3. Results and discussion

3.1. Investigation of the reduction of periodate in the static system

Periodate gives two reduction signals in aqueous buffered solutions (Fig. 3). The height of the first peak (i_1), related to the first reduction step of periodate (Eq. 1), increased linearly with increasing periodate concentration in the pH range 5–10. The values of the slopes of the graphs $i = f(C)$ in Fig. 4 were greatest in the pH range 6.10–7.50, indicating the highest sensitivity for analysis.



Various pH-dependent equilibria exist in aqueous periodate solutions [14,15]. The higher values of the slopes of the graphs were, therefore,

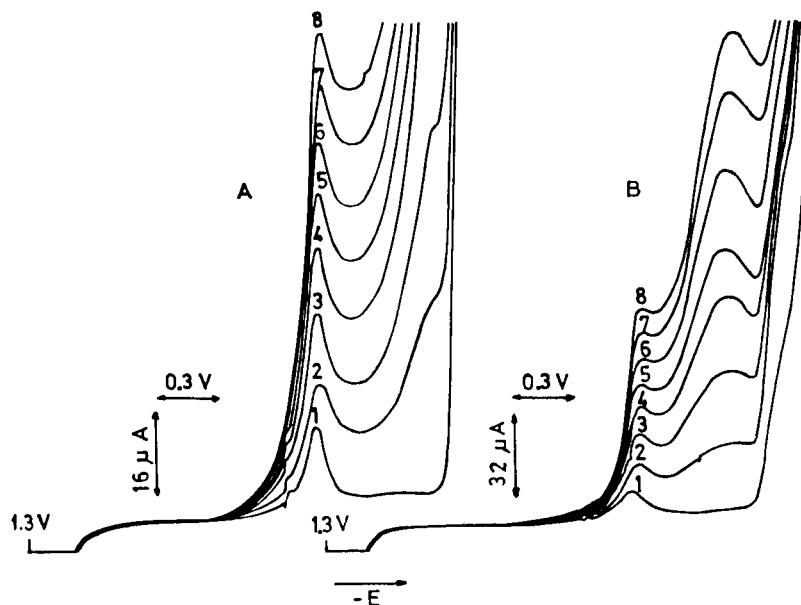
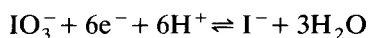


Fig. 3. i - E curves for periodate in the static system. (A) pH 7.00, (B) pH 7.93, at (1) 0.00, (2) 0.40, (3) 0.80, (4) 1.20, (5) 1.57, (6) 1.96, (7) 2.32, (8) 2.72×10^{-4} M cell concentrations of periodate.

attributed to the relatively high concentration of reducible species, possible metaperiodate (IO_4^-), in this pH range.

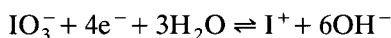
The peak current of periodate (i_1) was measured after subtracting the peak for the supporting electrolyte (Fig. 3), which was attributed previously to oxide formation on the platinum electrode [22]. Since the oxide peak potential and the reduction potential of periodate slightly differ at different pH values, and the $i = f(C)$ graphs are linear for up to 10^{-3} M periodate, the current for periodate cannot be attributed to catalysis by platinum oxide.

The second signal (i_2) in the $i-E$ curves is related to the second reduction step of periodate (Eq. 2) [23]. This was confirmed by comparing the $i-E$ curve of KIO_4 at the same pH with that of KIO_3 , and also by polarographic measurements [15].



(in acidic medium)

or



(in alkaline medium) (2)

Both the potential of the first (E_1) and that of second reduction step (E_2) of periodate shift

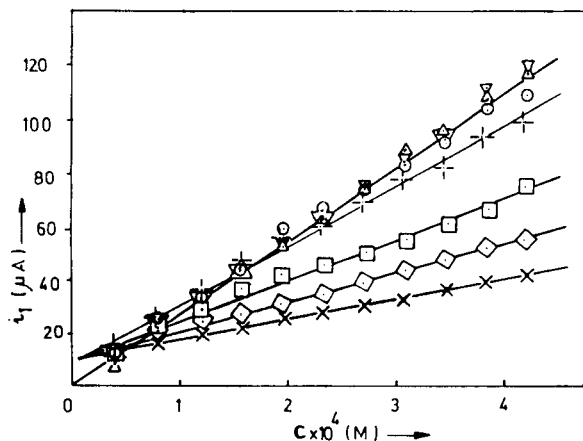


Fig. 4. Currents of periodate (i_1) against concentration (C) as a parameter of pH. pH values: 5.59 (+); 6.10 (○); 7.00 (Δ); 7.50 (▽); 8.48 (□); 9.28 (◇); 9.64 (×).

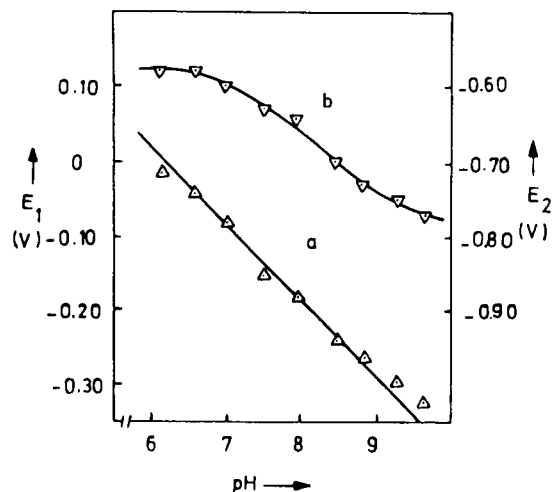


Fig. 5. Dependence of potentials of periodate reduction on pH. $C = 1.0 \times 10^{-4}$ M. (a) E_1 , (b) E_2 .

towards the negative potential values with increasing pH values (Fig. 5), because protons are consumed during each reaction (Eqs. 1 and 2). From curve a in Fig. 5, the value of the slope is ca. 100 mV/pH unit, indicating the involvement of 2 protons in Eq. 1, whereas the slope of curve b does not have any definite value because of the changes in the mechanism shown in Eq. 2 with pH. Similar shifts in the half-wave potentials with pH were also observed in a previous polarographic study [15].

The current obtained by the RPWE was greater than that established by polarography, because of the faster mass transfer to the electrode surface and different surface area of the electrodes involved. Thus, the sensitivity increased as expected according to the Levich equation [22] which explains that the limiting current increases by effects of rotation and surface area of the electrode. The first reduction step can be used for the determination of periodate in the range 4.0×10^{-5} – 4.2×10^{-4} M, at pH 7.0–7.5. This procedure is more sensitive than the conventional polarographic methods. The correlation coefficient of the regression line is 0.998 and the limit determination is 4.0×10^{-5} M (Fig. 4). Taking into account the results of the static system, the second reduction step of periodate at the RPWE

was not found suitable for the determination of periodate.

3.2. Investigation of the reduction of periodate in a flow system by an amperometric method

In view of the results of the above voltammetric studies, the experiments in a flow system would best be carried out at pH 7.0–7.5. However, as the buffer capacity is higher at pH 7.0, this pH was preferred and $i-t$ curves were recorded at a constant potential of -0.07 V (Fig. 5a).

Effects of flow rate and concentration

The mass transport to the electrode surface determines the current and varies greatly with the hydrodynamic conditions in the cell. In general the limiting current (i_1) is related to the bulk concentration of the electroactive species (C_0) and the flow rate (v) as represented by Eq. 3, where n , F and A have their usual electrochemical significance, k is a constant related to the diffusion coefficient and geometric parameters, and β is a function which is a characteristic of the electrode geometry and fluid dynamics [24].

$$i_1 = knFAC_0v^\beta \quad (3)$$

In this work, the dependence of the current on the flow rate was first studied with solutions of periodate from 1.0×10^{-3} to 7.0×10^{-3} M and

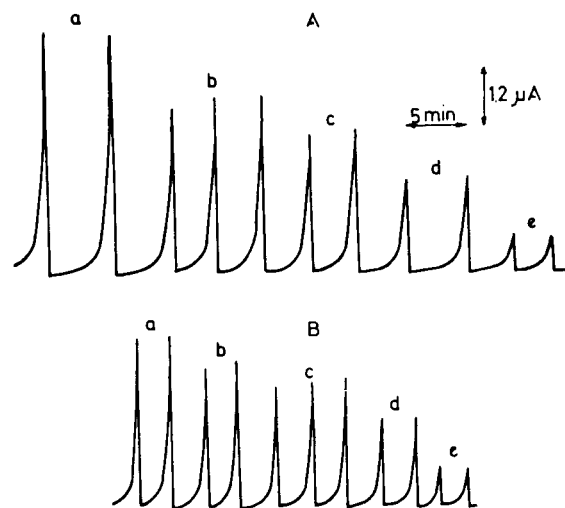


Fig. 6. $i-t$ curves for periodate in the flow system. pH 7.00; $E = -0.07$ V; $V_s = 20$ μ l; v (ml min^{-1}): (A) 1.0; (B) 1.7. Concentrations (injected): (a) 7.0, (b) 5.5, (c) 4.0, (d) 2.5, (e) 1.0×10^{-3} M.

with a sample volume of 20 μ l (Fig. 6). For a flow rate of 1.0 ml min^{-1} , the current changed linearly with concentration (Fig. 7a). However, when 1.7 ml min^{-1} was used, the current increased linearly at the same rate with increasing concentration of periodate up to 2.5×10^{-3} M, but the increase was not linear above this concentration (Fig. 7b). Moreover, the areas of the peaks, which are directly proportional to concentration, decreased

Table 1

Change of periodate peak currents with concentration and sample volume (pH 7.00, $E = -0.07$ V, $v = 1.0$ ml min^{-1} , injection series is numbered I–X)

$C \times 10^5$ (M)	Sample volume (μ l)									
	100				50				20	
	I	II	III	IV	V	VI ^a	VII	VIII	IX	X
1.0	0.180	0.148	0.100	0.076	0.036	0.112	0.084	0.068	0.020	0.015
3.0	0.284	0.198	0.136	0.116	0.060	0.168	0.130	0.116	0.038	0.028
5.0	0.358	0.256	0.194	0.172	0.092	0.236	0.192	0.176	0.056	0.049
7.0	0.424	0.294	0.240	0.212	0.112	0.288	0.248	0.228	0.080	0.064
10.0	0.506	0.360	0.308	0.280	0.148	0.374	0.332	0.308	0.116	0.085
m^b	3565	2354	2362	2288	1251	2923	2793	2690	1070	797
r^b	0.991	0.998	0.998	0.999	0.998	0.999	0.999	0.999	0.997	0.997

^a The RPWE was cleaned.

^b Slopes (m) and correlation coefficients (r) were calculated for $i_p = mC + b$.

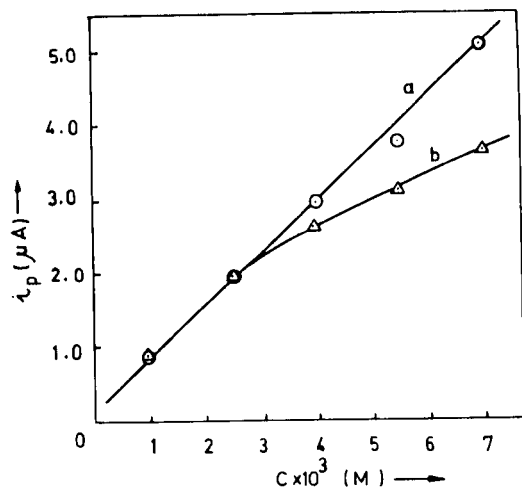


Fig. 7. Dependence of the peak current of periodate on flow rate and concentration. pH 7.0; $E = -0.07$ V; $V_s = 20$ μ l; v (ml min^{-1}); (a) 1.0, (b) 1.7.

with increasing flow rate for the same concentration.

Thus, although the sampling rate increases with increasing flow rate, because of the faster removal of periodate from the cell, the sensitivity of measurement decreases.

Effects of sample volume and concentration

The influence of the sample volume was investigated using more dilute periodate solutions (1.0×10^{-5} – 1.0×10^{-4} M) at a flow rate of 1.0 ml min^{-1} . Each series of solutions in Table 1 was injected in order of increasing concentration. During the measurements in the series I–IV, the RPWE was not cleaned. When the peak currents obtained by injection of $100 \mu\text{l}$ of the same solution in different series, the peaks decreased with series number, i.e., as the electrode was used, the sensitivity decreased. However, when the electrode surface was cleaned as described above, the peak intensities increased once again, as can be seen by comparing column V and VI.

The peak intensities also decreased almost linearly with sample volume, as shown in Table 1. For $20 \mu\text{l}$ injections, the calibration graph was linear (regression equation: $i_p = 796.7C + 6.77 \times 10^{-3}$; correlation coefficient = 0.997) in the range 1.0×10^{-5} – 1.0×10^{-4} M periodate.

The increase in peak currents with changes in concentration was greater when the flow rate was smaller (1.0 ml min^{-1}) and the sample volume was larger ($100 \mu\text{l}$). When the sample volume increased, the rate of sampling decreased due to the longer retention time of periodate in the cell. 15–40 injections per hour could be achieved depending on the flow rate and sample volume.

4. Conclusions

Periodate can be determined in the range 4.0×10^{-5} – 4.2×10^{-4} M and 1.0×10^{-5} – 1.0×10^{-4} M by the static and flow systems, respectively. If it is taken into consideration that 4.0×10^{-5} M periodate is the diluted sample concentration in the cell of the static system and 1.0×10^{-5} M is the original sample concentration in the flow system, it is evident that the sensitivity is much higher in the flow system.

The method developed is more sensitive than the reported direct potentiometric [13] and chemiluminescence methods [20].

As the peak current changes linearly with concentration of periodate even at high concentration (7.0×10^{-3} M) the flow-injection amperometric methods described can be applied to the indirect determination of some organic and inorganic compounds based on the measurement of the excess periodate after periodate oxidation of such compounds. This has already been proved by application to the determination of adrenaline [21].

Acknowledgements

The authors are grateful for careful reading of the manuscript by Prof. Dr. E. Henden and Prof. Dr. D. Balköse.

References

- [1] J.A. Fatiadi, *Synthesis*, (1974) 229.
- [2] E. Pelizzetti, E. Mentasti and E. Pramauro, *J.C.S. Perkin II*, (1976) 1651.

- [3] D.G. Graham, *Mol. Pharmacol.*, 14 (1978) 633.
- [4] L.R. Sherman, V.L. Trust and H. Hoang, *Talanta*, 28 (1981) 408.
- [5] M.E. El-Kommos, F.A. Mohamed and A.S. Khedr, *Talanta*, 37 (1990) 625.
- [6] G. Nişli and A. Townshend, *Talanta*, 15 (1968) 1377.
- [7] A.M. El-Wakil, A.B. Farag and M.S. El-Shahawi, *Talanta*, 36 (1989) 783.
- [8] R. Belcher and A. Townshend, *Anal. Chim. Acta*, 41 (1968) 395.
- [9] M.C. Mochon and J.A.M. Leyva, *Analyst*, 109 (1984) 951.
- [10] A. Garrido, M. Silva and D. Perez-Bendito, *Anal. Chim. Acta*, 184 (1986) 227.
- [11] K.K. Verma, D. Gupta, S.K. Sanghi and A. Jain, *Analyst*, 112 (1987) 1519.
- [12] E. Kavlentis, *Analisis*, 16 (1988) 253.
- [13] A.K. Jain, M. Jahan and V. Tyagi, *Analyst*, 114 (1989) 1155.
- [14] A.M. Shams El Din, T.M.H. Saber and H.A. El Shayeb, *J. Electroanal. Chem.*, 36 (1972) 411.
- [15] H.İ. Sapmaz (Gökçel) and G. Nişli, E.Ü. Mühendislik Fakültesi Dergisi, C 1 (1984) 61.
- [16] M.M. Kamal, *Anal. Lett.*, 24 (1991) 485.
- [17] E.P. Diamandis and T.P. Hadjiioannou, *Analyst*, 107 (1982) 1471.
- [18] S.R. Varma, J.M. Calatayud and H.A. Mottola, *Anal. Chim. Acta*, 233 (1990) 235.
- [19] C.M. Lozano, T.P. Ruiz, V. Tomas and E. Yagüe, *Analyst*, 113 (1988) 1057.
- [20] N.P. Evmiridis, *Talanta*, 36 (1989) 357.
- [21] H.İ. Gökçel, Ph.D. Thesis, Chem. Eng. Dept., Ege University, İzmir, 1990, pp. 71–78.
- [22] R.N. Adams, *Electrochemistry at Solid Electrodes*, Marcel Dekker, New York, 1969, pp. 80 and 191.
- [23] B.K. Gupta, D.S. Jain and J.N. Gaur, *Electrochim. Acta*, 22 (1977) 479.
- [24] D. MacKoul, D.C. Johnson and K.G. Schick, *Anal. Chem.*, 56 (1984) 436.

Catalytic oxidation and flow detection of acetaminophen at a dicyanobis(1,10-phenanthroline)iron(II)-modified electrode

Huimei Li ^a, Rile Ge ^b, Erkang Wang ^{*,a}

^a *Laboratory of Electroanalytical Chemistry, Changchun Institute of Applied Chemistry, Chinese Academy of Sciences, Changchun 130022, China*

^b *Department of Chemistry, Beijing University, Beijing, China*

(Received 23rd August 1993; revised manuscript received 17th December 1993)

Abstract

Dicyanobis(1,10-phenanthroline)iron(II)-modified glassy carbon electrodes were shown to exhibit an electrocatalytic response for the oxidation of acetaminophen with a decrease of 100 mV in the potential required. It can also inhibit the oxidation of ascorbic acid and uric acid. When used for amperometric monitoring of acetaminophen in a flowing stream, the coated electrode may permit detection at lower potentials compared with the naked surface. The method gives a linear range from 0.05 to 100 $\mu\text{g ml}^{-1}$ and a detection limit of 0.02 $\mu\text{g ml}^{-1}$ (signal-to-noise ratio = 2). The application of the method to the determination of acetaminophen in urine by LC is briefly described.

Key words: Amperometry; Flow injection; Liquid chromatography; Acetaminophen; Catalytic oxidation; Chemically modified electrodes; Dicyanobis(1,10-phenanthroline)iron(II); Pharmaceuticals

1. Introduction

The scope of electrochemical detection in liquid chromatography (LC) has been greatly increased by the development of chemically modified electrodes (CMEs), which offer great potential for alleviating fouling of the electrode surface and lowering the overpotential (with otherwise slow electron-transfer kinetics). Such acceleration of the desired reaction can offer a significant lowering of detection limits in addition to improved selectivity, which is highly desirable to meet new challenges posed by clinical samples.

Much effort has been devoted to developing detectors based on CMEs for biologically important species [1–5].

Acetaminophen is a commonly used analgesic drug that has been detected at more than 0.7 V at glassy carbon electrodes [6,7]. Zhou and Wang [8] described the detection of acetaminophen in urine by HPLC using dual electrodes with an upstream electrode (oxidation $E_1 = 0.7$ V) and a downstream electrode (reduction $E_2 = 0.12$ V). The detection limits of all above methods were more than 0.2 $\mu\text{g ml}^{-1}$. Wang and Golden [5] demonstrated that metalloporphyrin-modified electrodes can produce a catalytic electrode response towards acetaminophen, but gave no detailed data for its determination or practical analysis.

* Corresponding author.

Analogues of dicyanobis(1,10-phenanthroline)iron(II) (DBPI) such as tris(4,7-diphenyl-1,10-phenanthroline)iron(II) have been used to modify electrodes and to detect NO_2 [9]. However, to our knowledge, there has been no previous report on DBPI-modified electrodes. In the present work, it was found a DBPI-based CME exhibits the electrocatalytic oxidation of acetaminophen, and moreover it can inhibit the oxidation of co-existing compounds such as ascorbic acid and uric acid in urine. A detailed examination was made of the behaviour and analytical advantages of DBPI-modified electrodes for voltammetric and amperometric measurements of acetaminophen, ascorbic acid and uric acid with both flow-injection analysis (FIA) and LC. This paper reports the construction of a DBPI-modified CME intended to provide a stable response to acetaminophen. In addition, the electrode was applied to the measurement of acetaminophen in urine.

2. Experimental

2.1. Reagents

DBPI was obtained from Sigma and was used as received. Acetaminophen was of pharmaceutical grade from Harbin Medicine (Harbin, China). Other chemicals were of analytical-reagent grade and were used as received. All solutions were prepared with doubly distilled water.

2.2. Apparatus

Voltammetric experiments were performed with a laboratory-built voltammeter. All experiments were done by using a three-electrode cell configuration with a modified or unmodified glassy carbon working electrode, a saturated Ag/AgCl reference electrode and a platinum wire auxiliary electrode.

Flow-injection analysis and liquid chromatographic (LC) experiments were performed with a Gilson Model 306 pump (Gilson Medical Electronics, France) and a Model 7125 injector

(Rheodyne, Berkeley, CA) with a 20- μl sample loop. A Model 400 electrochemical detector with a MP 1303 glassy carbon electrode (EG & G PAR, Princeton, NJ, USA) was used for detection. The stationary phase for the chromatographic separations was Nucleosil C_{18} (10 μm) in a 200 \times 4 mm i.d. column. The mobile phase was 0.04 M potassium phosphate buffer (pH 4.2), containing 15% (v/v) methanol, and was delivered at a constant flow-rate of 1.0 ml min^{-1} . The mobile phase was filtered through filter-paper and was briefly degassed in an ultrasonic bath before use. The experiments were carried out at room temperature.

2.3. Procedure

A stock standard solution was prepared by dissolving 100 mg of acetaminophen (weighed accurately) in ethanol in a 100-ml volumetric flask and diluting to volume with ethanol, and was stored at 4°C in the dark. An aliquot was diluted to the appropriate concentration with mobile phase before an actual analysis.

A drug-free urine sample from a healthy subject who had been fasting for the preceding 12 h was taken and immediately filtered through a G-4 glass filter (2–5 μm pore size) and was kept at 4°C in the dark.

2.4. Electrodes

Prior to surface modification, the glassy carbon electrode was polished successively using 1-, 0.3-, and 0.05- μm alumina powder suspension on a smooth cloth, thoroughly ultrasonicated in a water-bath and ethanol-bath alternately and then rinsed with water. This electrode is referred to as a fresh bare glassy carbon electrode (GCE). The CME was prepared by dipping in 10 μl of 1 mmol l^{-1} DBPI solution in ethanol containing 1% Nafion, allowed to dry under an IR lamp, and then cycled in 0.1 mol l^{-1} potassium phosphate buffer (pH 4.0) between –0.2 and 1.1 V at a scan rate of 100 mV s^{-1} for 6 min to obtain a steady current–potential profile. This electrode is referred to as the DBPI-CME and was subjected to further experiments.

3. Results and discussion

3.1. Electrochemistry of acetaminophen

The cyclic voltammograms (CVs) in a conventional cell obtained for a DBPI-CME immersed in $0.1 \text{ mol l}^{-1} \text{ KH}_2\text{PO}_4$ solution (pH 4.0) are shown in Fig. 1. The CVs exhibit a reversible process. The reduction and oxidation peaks of DBPI-CME at about 0.55 and 0.60 V vs. Ag/AgCl (saturated KCl) are due to the redox reaction of dicyanobis (1,10-phenanthroline)iron(II)/-iron(III) couple. Good voltammograms with sharp peaks and a steady response were obtained after potential scanning for 6 min from -0.2 to 1.1 V in the above solution. The DBPI-CME can allow 1000 cycles at a scan rate of 100 mV s^{-1} in the same potential range with a slight decrease in peak current (11%). This indicates that the DBPI-CME prepared with adsorption is very stable.

CVs obtained in $0.1 \text{ mol l}^{-1} \text{ KH}_2\text{PO}_4$ (pH 4.0) for a $1 \times 10^{-3} \text{ mol l}^{-1}$ solution of acetaminophen, ascorbic acid and uric acid are shown in Fig. 2 for both GCE and DBPI-CME. The modified electrode exhibits a dramatic improvement in the response for acetaminophen. The overvoltage for the oxidation process for acetaminophen is 100 mV lower than that at the

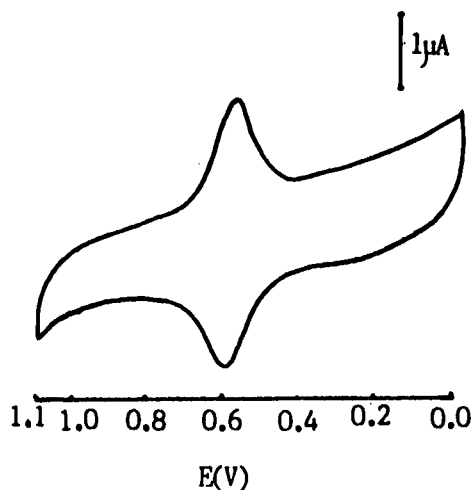


Fig. 1. Cyclic voltammogram of DBPI-CME in $0.1 \text{ mol l}^{-1} \text{ KH}_2\text{PO}_4$ solution (pH 4.0). Scan rate, 100 mV s^{-1} ; electrode diameter, 2.5 mm.

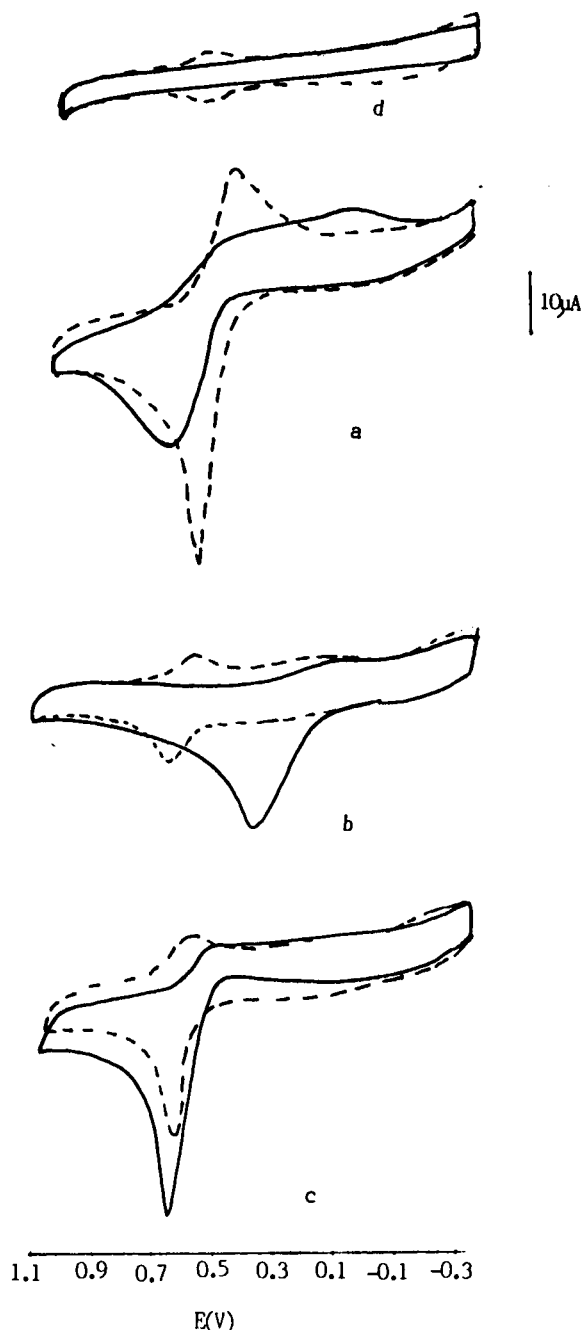


Fig. 2. Cyclic voltammograms of $10 \mu\text{g ml}^{-1}$ (a) acetaminophen, (b) ascorbic acid, (c) uric acid and (d) blank solution at (solid lines) GCE and (dashed lines) DBPI-CME in $0.1 \text{ mol l}^{-1} \text{ KH}_2\text{PO}_4$ solution (pH 4.0). Scan rate, 100 mV s^{-1} .

Table 1
Comparisons of peak current and oxidation potentials of acetaminophen on DBPI-CME and GCE

Parameter	Electrode	pH				
		2.0	3.5	4.0	5.0	7.3
E_{p_a}	GCE	0.84	0.72	0.70	0.70	0.66
	CME	0.74	0.63	0.60	0.60	0.56
E_{p_c}	GCE	0.60	0.20	0.11	0.08	0.0
	CME	0.58	0.46	0.50	0.10	0.06
$\Delta E_{p,GCE}$		0.24	0.52	0.59	0.62	0.66
$\Delta E_{p,CME}$		0.18	0.17	0.10	0.50	0.50
$i_{p_a,CME}/i_{p_a,GCE}$		1.2	1.2	1.6	1.6	1.4

Experimental conditions as in Fig. 2.

bare GCE. Also, there is a significant improvement in the magnitude and sharpness of the anodic peaks. The effect of pH on the catalytic peak current and oxidation wave towards acetaminophen is presented in Table 1. It can be seen that both the oxidation potential peak and current peak (not shown here) increase with decrease in pH from 7.0 to 2.0 on both the naked and modified electrodes. The catalytic effect remained unchanged. Note that the increased background charging current was enveloped at the DBPI-modified electrode. This, however, does not affect analytical measurements commonly made by fixed-potential amperometry. The cyclic voltammetric peak potentials are not affected by the solute concentration. The current observed is directly proportional to the square root of scan rate in the range 10–250 mV s^{-1} , as shown in Fig. 3, indicating that the catalytic reaction is very fast with respect to diffusion and the catalytic currents are proportional to concentration. This suggests that DBPI may work as a charge-transfer mediator. It also shows that the oxidation peak of ascorbic acid and uric acid was greatly restrained, which may be due to the Nafion on the DBPI-CME. This can help to improve the selectivity in the determination of acetaminophen in biological and pharmaceutical samples.

3.2. Flow detection

On the basis of voltammetric data described above, it appeared likely that amperometric monitoring of acetaminophen in a flow system might

be greatly improved. The DBPI-CME allows amperometric detection at a lower operating potential and hence yields improved selectivity and signal-to-noise characteristics, and the large catalytic current permits a high sensitivity of detection of acetaminophen. Hydrodynamic voltammograms (HDVs) for acetaminophen with GCE and DBPI-CME are shown in Fig. 4. A substantial decrease in the half-wave potentials was observed at the coated electrode and the response to acetaminophen was greatly enhanced. The optimum response in terms of sensitivity, i.e., operation on the plateau region, occurred at 0.62 V compared with 0.88 V at the ordinary electrode. The relative standard deviation (R.S.D.) of the peak currents (i_p) with 20 repeated injections of 10 $\mu\text{g ml}^{-1}$ acetaminophen within 20 min was 5.0%. The response of the DBPI-CME was stable. The calibration graph was linear for acetaminophen from 0.05 to 0.1 ng ml^{-1} (slope 60.4 $\text{nA } \mu\text{g}^{-1}$, with a correlation coefficient of 0.982). The detection limit was 0.02 $\mu\text{g ml}^{-1}$ (signal-to-noise ratio = 2), which extends the assay sensitivity at least 100-fold [10,11] to allow the measurement of concentrations necessary for pharmacokinetic studies. Ascorbic acid and uric acid were chosen as potential interferents and the chromatograms of 10 $\mu\text{g ml}^{-1}$ each of ascorbic, uric acid and

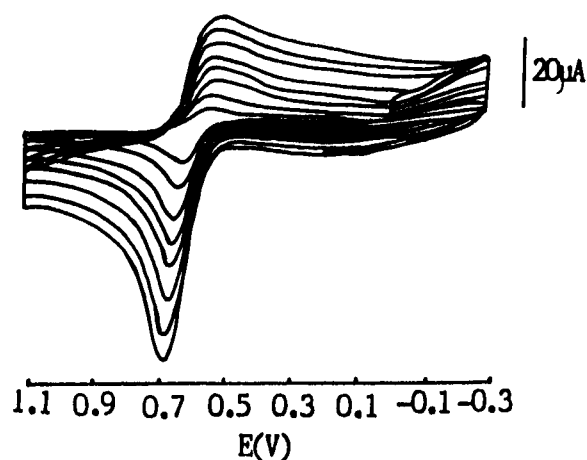


Fig. 3. Cyclic voltammograms of 10 $\mu\text{g ml}^{-1}$ acetaminophen at DBPI-CME in 0.1 mol l^{-1} KH_2PO_4 solution (pH 4.0) at scan rates of 10, 25, 50, 75, 100, 150, 200 and 250 mV s^{-1} .

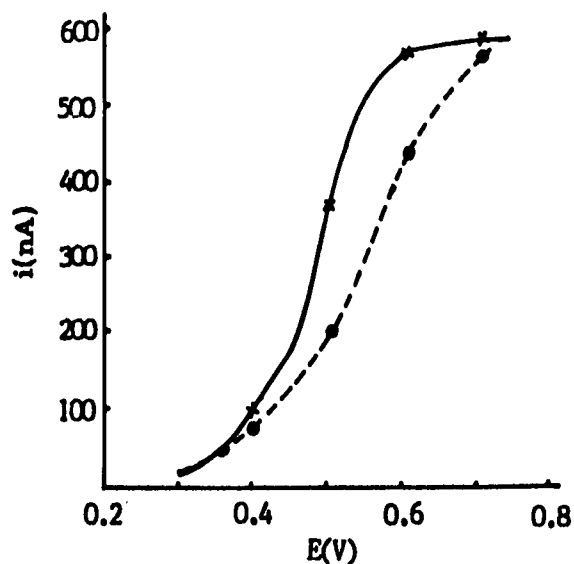


Fig. 4. Hydrodynamic voltammogram of $10 \mu\text{g ml}^{-1}$ acetaminophen at (x) DBPI-CME and (o) GCE. Mobile phase, $0.04 \text{ mol l}^{-1} \text{ KH}_2\text{PO}_4$ buffer (pH 4.2) at a flow-rate of 0.1 ml min^{-1} .

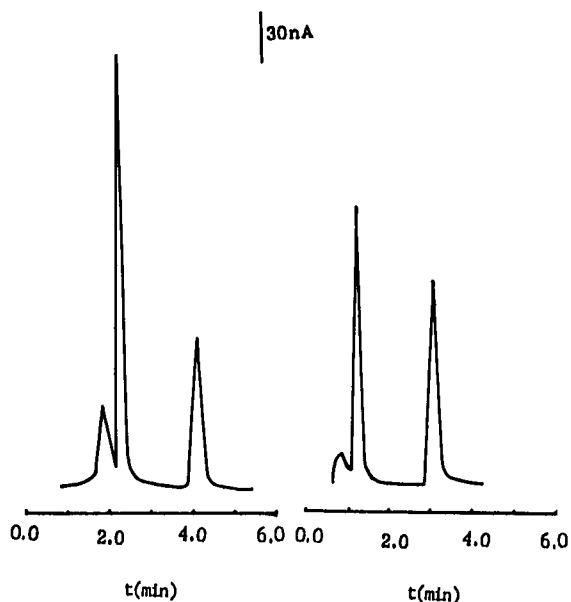


Fig. 6. Chromatograms for diluted (1:15) urine sample with $2.5 \mu\text{g ml}^{-1}$ acetaminophen added obtained at (left) GCE and (right) DBPI-CME. Conditions as in Fig. 4.

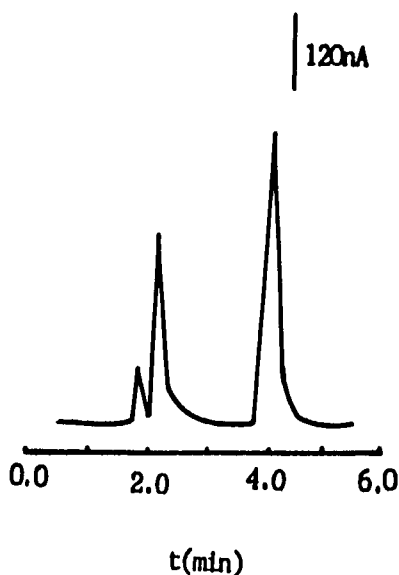


Fig. 5. Chromatogram for $10 \mu\text{g ml}^{-1}$ (left peak) acetaminophen, (middle peak) uric acid and (right peak) ascorbic acid at DBPI-CME. Conditions as in Fig. 4.

acetaminophen are shown in Fig. 5. LC separation and detection of urinary acetaminophen was done roughly. The chromatograms of a drug-free diluted urine (1:15) sample with $2.5 \mu\text{g ml}^{-1}$ acetaminophen added are shown in Fig. 6. The advantage of the selected detection model is clearly demonstrated by the high sensitivity of acetaminophen and the low sensitivity of ascorbic acid and uric acid. A high sensitivity and selectivity can certainly be achieved with application of the proposed method to the accurate determination of the drug in urine.

4. Conclusions

It has been demonstrated that a GCE with adsorbed DBPI can catalyse the electrooxidation of acetaminophen, and an additional advantage was achieved by coupling the catalytic features of DBPI with the permselective function of Nafion, that is, Nafion could exclude anions such as ascorbic acid and uric acid anions that co-exist in urine samples. The modified electrode is easy to prepare, inexpensive and stable. The use of this

modified electrode offers the possibility of detecting acetaminophen in biological samples with high sensitivity and selectivity.

Acknowledgement

The support of the National Natural Science Foundation of China is greatly appreciated.

References

- [1] M.K. Halbert and R.P. Baldwin, *Anal. Chem.*, 57 (1985) 591.
- [2] L. Santos and R.P. Baldwin, *Anal. Chem.*, 59 (1987) 1766.
- [3] J.A. Cox and T.J. Gray, *Anal. Chem.*, 61 (1989) 2462.
- [4] J. Zhou and E. Wang, *Electrochim. Acta*, 37 (4) (1992) 595.
- [5] J. Wang and T. Golden, *Anal. Chim. Acta*, 217 (1989) 343.
- [6] K.S. Pang, A.M. Taburet, J.A. Hinson and J.R. Gillette, *J. Chromatogr.*, 174 (1979) 165.
- [7] J.W. Munson, R. Weierstall and H.B. Kostenbauder, *J. Chromatogr.*, 145 (1978) 328.
- [8] J. Zhou and E. Wang, *Anal. Chim. Acta*, 236 (1990) 293.
- [9] C.J. Hynes, M. Bonakdar and H.A. Mottola, *Electroanalysis*, 1 (1989) 155.
- [10] C.G. Fletterick, T.H. Grove and D.C. Hohnadel, *Clin. Chem.*, 25 (1979) 409.
- [11] J.N. Buskin, R.A. Upton and R.L. Williams, *J. Chromatogr.*, 230 (1982) 443.

Disproportionation and thermal lens effects produced by Ar⁺ laser radiation on silver halide suspensions

M.A. Rius Revert, M.C. García Alvarez-Coque, G. Ramis Ramos *

Departamento de Química Analítica, Facultad de Química, Universitat de València, 46100 Burjassot, València, Spain

(Received 12th November 1993; revised manuscript received 7th February 1994)

Abstract

The thermal lens spectrometric (TLS) signal increases when Ag⁺ is added to a halide solution or vice versa. The change in the TLS signal is due to the disproportionation and darkening of the surface of the silver halide particles produced by the Ar⁺ laser pump radiation. The change in the TLS signal depends on the nature of the ions in excess. The injection of an excess Ag⁺ into chloride and bromide solutions gives the fastest and largest responses, respectively. TLS monitoring of titrations of chloride solutions with Ag⁺ is also possible. Absorbance is effectively discriminated from scattering in the slightly turbid silver halide suspensions.

Key words: Disproportionation; Lasers; Silver halides; Thermal lens spectrometry

1. Introduction

Very low absorbances can be accurately measured using thermal lens spectrometry (TLS). Ultratrace concentrations of metal ions [1–3] and other inorganic [4] and organic species [5–8] have been determined. Together with the photothermal effect, other effects such as thermal convection [9,10], photolysis [11,12] and transport of small particles [12] can also be produced by the intense pump radiation.

We study here the effect of the TLS Ar⁺ pump radiation on a solution containing a suspended precipitate of a silver halide. In the presence of the suspended particles loss of radiation

by scattering is produced and the TLS background noise increases noticeably. According to the theory, the noise should increase, but the net TLS signal should not be modified by the presence of the particles [13]. However, due to the disproportionation and darkening of the precipitate, a positive change in the TLS signal was observed when a silver halide suspension was illuminated by Ar⁺ laser radiation.

2. Experimental

2.1. Apparatus

The coaxial pump–probe TLS setup was constructed using a 4-W Ar⁺ laser (Spectra-Physics, Model 2016, Mountain View, CA) and a 5 mW He–Ne laser (Spectra-Physics, Model 105). The

* Corresponding author.

pump beam was modulated at 4 Hz using a chopper (Stanford, Model SR540, Sunnyvale, CA). Data acquisition and treatment was performed with a PC/AT computer through a DAS-8 interface (MetraByte, Taunton, MA). The TLS measurements were generated at a rate of one point every two seconds. Other details were as published before [10,14].

A standard quartz cell of 1 cm optical path length was used. The cell was cleaned after every measurement series with 2 M ammonia and 3.3% H_2O_2 , and rinsed with water and ethanol, to eliminate any residue of silver halide. The measurements were normalized against a potassium dichromate solution to assure inter-series reproducibility. All the experiments were carried out in an inner room where the sunlight was absent.

2.2. Reagents

Solutions of $\text{BaCl}_2 \cdot 2\text{H}_2\text{O}$, anhydrous Na_2SO_4 , KI and KBr (analytical grade, Probus, Barcelona), AgNO_3 (analytical grade, Panreac, Barcelona) and NaCl (analytical grade, Merck, Darmstadt) were used. Silver and iodide solutions were kept in the darkness. Distilled, deionized water (Barnstead deionizer, Sybron, Taunton, MA) was used throughout.

2.3. Procedures for the direct injection experiments

For the direct injection experiments, 2 ml of a 1×10^{-4} M NaCl, KBr, or KI solution, or alternatively, 2 ml of a 1×10^{-4} M AgNO_3 solution were introduced into the cell. The cell was located into the beam path, and 225 μl of 1×10^{-3} M AgNO_3 , or the same volume of a 1×10^{-3} M halide solution, were added with an automatic pipette. The TLS signal was continuously monitored.

Triplicate injections at increasing halide or silver concentrations were made to obtain the calibration curves. For the determination of chloride, the difference between the signal before and 30 s after the injection of the excess Ag^+ was measured. For the determination of Ag^+ , the signal was measured before and 2 min after the injection of the excess Cl^- .

2.4. Procedures for the titrations

The 2 ml aliquots of 1×10^{-4} M halide solutions were titrated with Ag^+ with continuous monitoring of the TLS signal. For this purpose, 20 μl aliquots of a 1.03×10^{-3} M AgNO_3 solution were successively added to the cell.

3. Results and discussion

3.1. Addition of an excess Ag^+ to a halide solution

The change in the TLS signal produced when an excess Ag^+ was added to a cell containing halide, is shown in Fig. 1. After the injection, a rapid increase in the signal followed by a slower drift was observed. The noise also increased. In the case of chloride, the AgCl suspension together with an increase in the radiation scattering was visually observed. Blanks performed in the absence of halide gave only a very small change in the TLS signal and associated noise.

Scattering from the suspended particles introduces random noise in the signal, and also produces some loss of intensity in both the pump and probe beams. When the intensity of the pump beam decreases, a weaker thermal gradient is formed and the sensitivity also decreases. The scattered energy cannot contribute to an increase in the thermal gradient; on the contrary, if a sufficiently large amount of energy is scattered, some loss of sensitivity of the TLS signal should be produced.

On the other hand, the TLS signal is obtained as the average of the relative variations of intensity at the probe beam center produced by the pumping cycles. Therefore, no changes in the TLS signal should be expected when intensity variations of the probe beam are produced at a frequency which is different from the pumping frequency, or at frequencies which are not multiples of the pumping frequency. A given amount of scattering produces a permanent decrease in the intensity of the probe beam, and therefore, this should not affect the TLS sensitivity. Sometimes in TLS experiments, the TLS signal is obtained from the absolute variations of the inten-

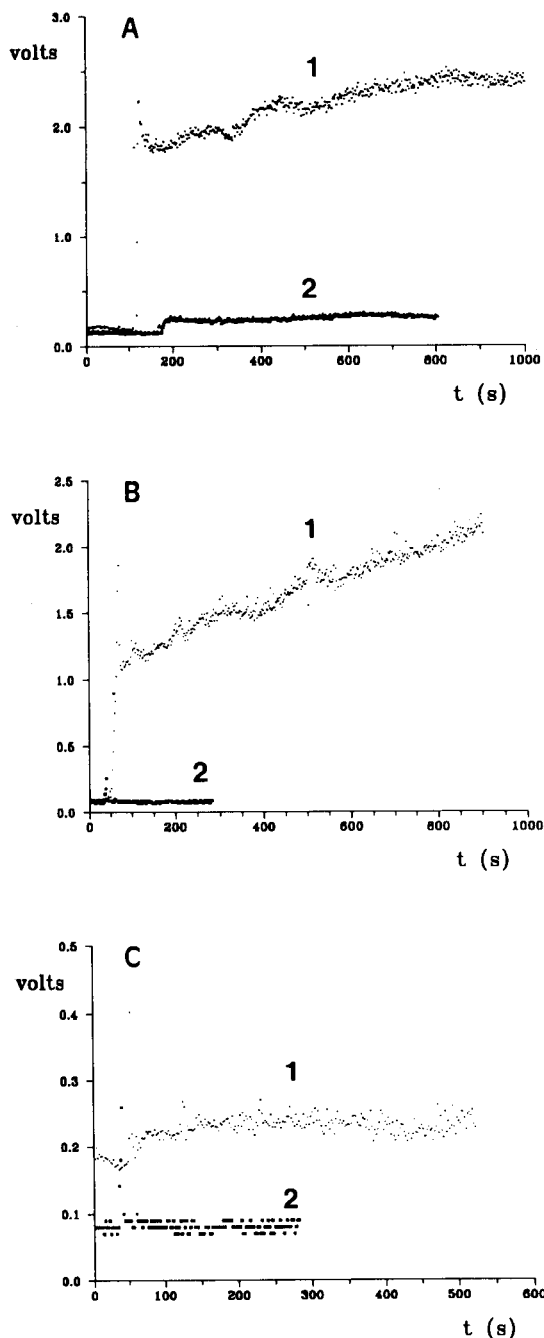


Fig. 1. Change in the TLS signal produced by injecting an excess Ag^+ into a halide solution: (A) NaCl, (B) KBr, (C) KI; (1) 1×10^{-4} M halide solution, (2) blank.

sity at the probe beam center. In this case, the reduction of the intensity of the probe beam produced by scattering will also appear as a loss of sensitivity.

Therefore, the net change in the TLS signal should be produced by absorption of the pump beam, with a loss of sensitivity if the scattered energy is large. Scattering cannot positively contribute to the TLS signal. This was confirmed by mixing barium chloride and sodium sulphate solutions at several concentrations. The BaSO_4 suspensions gave rise to a higher background noise, but the average TLS signal was not modified significantly by the presence of this precipitate.

When illuminated by the intense pump radiation, the halide colloidal particles become dark due to the photocatalyzed disproportionation reaction which produces free halogen and reduced silver [15,16]. Absorption of the pump radiation by the darkened particles followed by transfer of the thermal energy to the medium could explain the increase in the TLS signal.

To achieve an adequate understanding of the effect, other considerations should be made. The diameters of the pump and probe beams within the cell were of about 0.2 mm and, therefore, only a very small part of the ca. 2 ml sample was illuminated. In the absence of an absorbing species other than the solvent, the thermal lens effect was very small and the solution in the illuminated region was relatively calm, but a convective stream crossing the illuminated region increased when the TLS signal increased [11]. The upwards movement of the precipitate at the beam region could be visually observed using a microscope tube (enlargement $56 \times$) and a polarizing filter to reduce the scattered radiation. The particles quickly crossed through the irradiated region, and the movement stopped when the pump radiation was shut off.

The initial jump of the signals, which is produced immediately after the injection of Ag^+ , should be explained as due to darkening reactions which were much faster than the process of establishment of the dynamic equilibrium between thermal gradient and convection. In the case of chloride, all the injections performed showed a small minimum immediately after the

signal jump. This minimum, which should be distinguished from the noise produced by the mixing of the reagents, can be explained by the establishment of a dynamic equilibrium in which convection sweeps off the initially darkened particles, and introduces new particles into the beam path. The new particles are also darkened and the intensity of the thermal lens effect, together with the associated convective stream, are maintained constant.

In the presence of thermal convection, the colloidal particles which are present in the beam path are continuously renewed, and the pump beam works as a continuous reactor which progressively darkens the whole precipitate. The positive drift of the signals after the initial jump can be explained as due to the increase in the concentration of dark particles, although it could also be produced by a higher darkening rate. The slow negative drift of the TLS signals which is finally observed in all cases (not shown in the figure), can be attributed to the ageing of the precipitates, including recrystallization and flocculation of the colloidal particles.

When the volume of the NaCl solution initially introduced into the cell was decreased (from 2 ml to 1.5, 1.0, 0.75 and 0.50 ml), the height of the initial TLS signal jump was approximately constant, but the positive drift period was reduced and was not produced for a NaCl volume of 0.50 ml. In the latter case, a negative signal drift was produced immediately after the signal jump. This suggested that ageing of the precipitate was faster in the reduced volume.

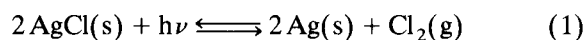
Curiously, no variation of the TLS initial signal was observed when an Ag^+ solution which was 0.06 M in HNO_3 was injected into an NaCl solution. This could be due to the substitution of the adsorbed hydrogen ions by the silver ions on the AgCl surface in the presence of the much larger H^+ concentration.

3.2. Addition of an excess halide to an Ag^+ solution

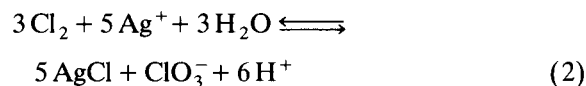
The properties of colloidal solutions strongly depend on the charge and nature of the adsorbed ions. When an excess of a halide solution was

added to an AgNO_3 solution, an initial jump of the TLS signal was never produced, but the signal increased slowly up to a maximum value after ca. 12 min for Cl^- and Br^- , and after 1 min for I^- (Fig. 2). The differences between the curves in Figs. 1 and 2 should be attributed to the substitution of the halide ions by the silver ions in the primary adsorption layer.

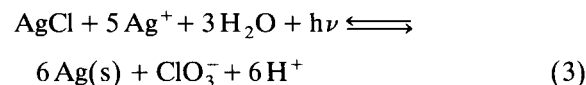
In comparison with the fast reactions shown in Fig. 1, slower darkening processes, carried out always under convection quasi-equilibrium conditions, can explain the absence of the initial peak and the shape of the curves in Fig. 2. The AgCl precipitate undergoes the disproportionation reaction:



This reaction produces darkening of the precipitate formed in the presence of an excess halide. In addition, when the precipitate is formed in a solution containing an excess Ag^+ , the following reaction could also be produced [17]:



From Eqs. 1 and 2, we have:



which indicates that the contribution of the adsorbed Ag^+ ions to the darkening of the precipitate can be very effective. In the presence of an excess of halide ions only disproportionation of the silver halide contributes to the signal, while in the reverse experiment, an additional contribution produced by the conversion of chlorine or bromine into chlorate or bromate and silver halide can also occur. This can explain the larger change in the signal, which was produced when the ions in excess were Ag^+ , when compared to the results obtained in an excess of chloride or bromide ions. Kinetic effects may also exist, that is, the darkening of the precipitate may be more rapid with adsorbed silver ions than with adsorbed halide ions.

Finally, the smaller change and faster drift of the signal obtained with iodide in Fig. 2 sug-

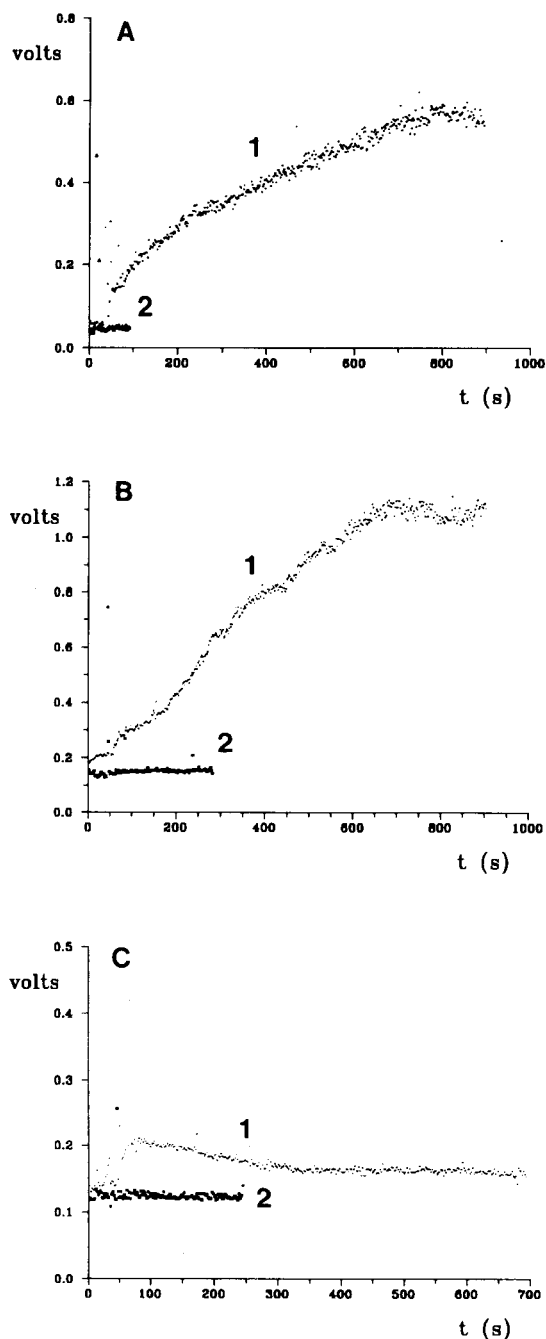


Fig. 2. Change in the TLS signal produced by injecting an excess halide into an Ag^+ solution: (A) NaCl, (B) KBr, (C) KI; (1) 1×10^{-4} M AgNO_3 , (2) blank.

gested a faster ageing of the AgI precipitate, which agrees with the prevailing tendency of this precipitate to flocculate [17].

3.3. Halide titrations with TLS monitoring

Fig. 3, part A, shows a TLS titration curve of a chloride solution with Ag^+ . The linearity of the curve before the equivalence point suggested that the sensitivity of the TLS measurements was approximately constant and that the signal was directly proportional to the amount of suspended AgCl. The linear part after the equivalence point showed also a positive slope. This can be explained by the additional AgCl produced by the common ion effect, but also by the higher sensitivity which is achieved in the presence of an excess Ag^+ , compared to the solutions containing an excess Cl^- .

The final point of the titration was calculated from the intercept of the two regression straight lines obtained after removing the points located within the region where the slope changed. The final volume was found to be 0.203 ml, which deviated 1.5% from the theoretical value (0.200 ml).

Titration curves of Br^- and I^- solutions with Ag^+ are shown in Fig. 3, parts B and C. The curves indicate a large change in the properties of the precipitates before the equivalence point. At the beginning of the titrations the sensitivity was low, but it increased in the vicinity of the equivalence point. Therefore, before the equivalence point the TLS signal was not proportional to the amount of silver halide formed. Probably, this change in sensitivity was due to the early adsorption of silver ions, which, as shown above, increased the darkening rate of the precipitates. After the equivalence point the sensitivity was approximately constant and did not depend on the excess Ag^+ . For I^- the background noise increased noticeably in this region.

3.4. Determination of the solubility product of silver chloride

If a directly proportional relationship between the TLS signal and the concentration of colloidal

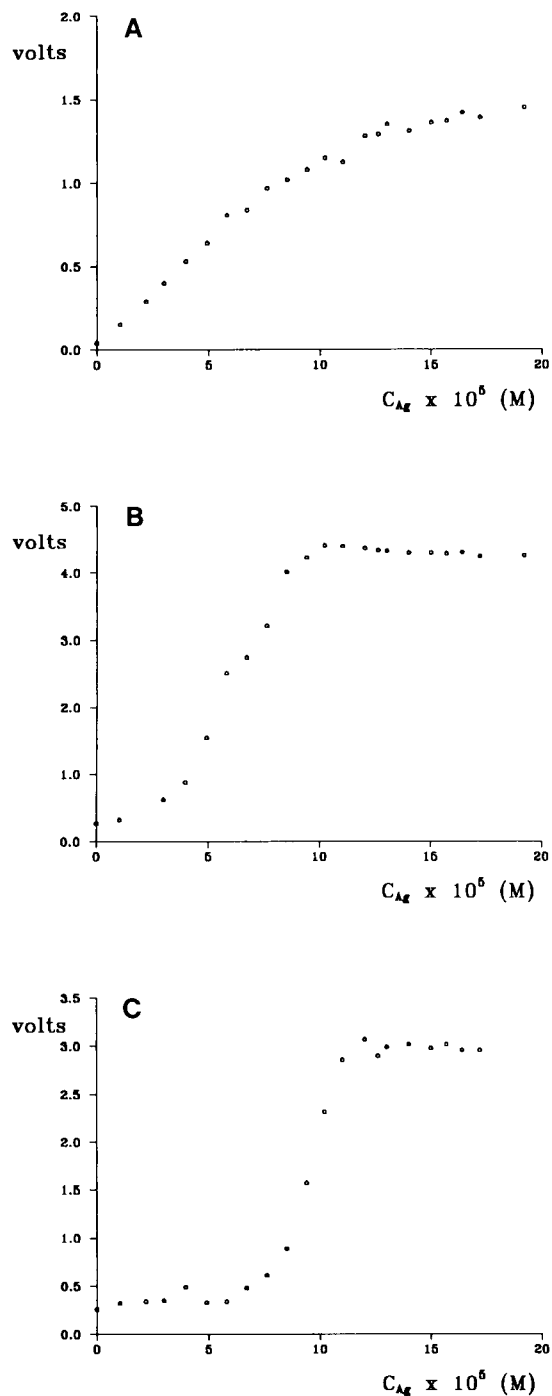


Fig. 3. Titration of 2 ml of a 1×10^{-4} M halide solution with Ag^+ and TLS monitoring: (A) NaCl, (B) KBr, (C) KI.

AgCl is assumed, the chloride titration data can be used to determine the AgCl solubility product. The following expression can be deduced:

$$K_s = \left(C_{\text{Ag}} - \frac{S_i - S_0}{k} \right) \left(C_{\text{Cl}} - \frac{S_i - S_0}{k} \right) \quad (4)$$

where C_{Ag} and C_{Cl} are the analytical concentrations of the silver and chloride ions, S_0 and S_i are the TLS signals before the addition of Ag^+ and at any moment, respectively, and k is the sensitivity. The value of k can be obtained by least-squares fitting of the points located before the equivalence point, and at some distance of the equivalence point. Using the data located in the vicinity of the equivalence point resulted $\text{p}K_s = 9.8 \pm 0.3$ (4 titrations, $\sim 25 \pm 2^\circ\text{C}$), which agreed with the literature value ($\text{p}K_s = 9.81$ at 25°C) [18].

The accurate value of K_s confirmed that the TLS signal was proportional to the AgCl concentration, and that the sensitivity was maintained approximately constant from the beginning of the titration to at least some distance after the equivalence point. The calculation of the AgBr and AgI solubility products was not possible due to the sensitivity changes along the titration curves.

3.5. Calibration curves for the halides and Ag^+ by direct injection with TLS monitoring

The possible analytical value of the direct injection experiments for the determination of both halide and silver ions was studied. Fig. 4 shows a calibration curve for chloride in the 2×10^{-5} – 1×10^{-4} M range. From the solubility product it may be calculated that the AgCl precipitate was formed for chloride concentrations over 2×10^{-6} M. However, the calibration curves performed at chloride concentrations within the 1×10^{-6} – 2×10^{-5} M range were very noisy and did not show a positive slope. Therefore, at chloride concentrations below 2×10^{-5} M the signal was not proportional to the suspended AgCl concentration.

With 8.1×10^{-5} M Cl^- the coefficient of variation was 13% (8 injections). The use of mechanical stirring of the solution to improve repeatability was tried. For this purpose, a miniature flattened glass rod was rotated at several rates with a d.c. motor. Stirring was stopped about 30 s after

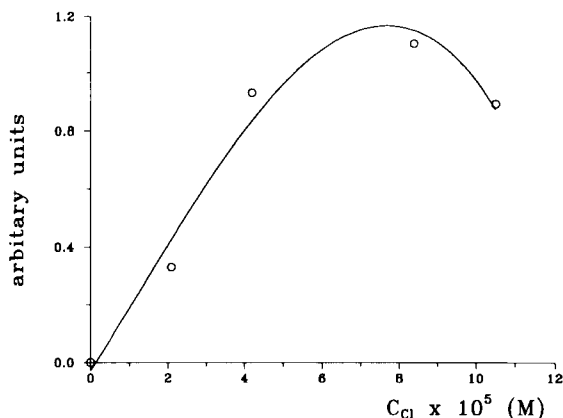


Fig. 4. Calibration curve of chloride obtained by direct injection of an excess Ag^+ (averages of triplicate points).

the injection to take the TLS measurement under static conditions. The sensitivity was lower and the repeatability was worse than without stirring the solution. The lower sensitivity suggested that mechanical stirring promoted the coagulation of the colloid.

Similar experiments performed without stirring the solution, and with $4.4 \times 10^{-5} \text{ M Br}^-$ and $5.9 \times 10^{-5} \text{ M I}^-$, gave a coefficient of variation of 14% and 22%, respectively (6 injections, signal measured 150 s after the injection of Ag^+). Compared to chloride, sensitivity ratios were 2.4 and 0.4 for bromide and iodide, respectively. Therefore, the sensitivity was not correlated to the solubility of the silver halides. The sensitivity could be a function of many parameters other than the solubility, including the shape, size and number of the particles initially produced, the flocculation rate, the rate of the darkening process, and the rate of convective transport of the particles through the illuminated region.

The calibration curve obtained by injecting an excess chloride into an Ag^+ solution was fairly linear, with $r = 0.993$. This agreed with the linearity of the chloride titration curves before the equivalence point, where Cl^- was also in excess. The coefficient of variation for $5.1 \times 10^{-5} \text{ M Ag}^+$ was 14% (7 injections). When bromide instead of chloride was injected, the coefficient of variation was 32% (7 injections, signal measured

200 s after the injection). Sensitivity was slightly lower than with chloride.

4. Conclusions

When an Ag^+ solution is added to a halide solution, or vice versa, the continuous disproportionation of the precipitate which enters the pump beam, followed by absorption of the pump radiation by the darkened surface of the particles, makes the TLS signal to increase. The rate and extent of the change in the TLS signal depends on the nature of the adsorbed ions. Thus, the injection of an excess Ag^+ into chloride and bromide solutions gives the fastest and largest responses, respectively. When the ions in excess are halides, much slower responses are obtained. Only in the latter case, calibration curves were linear. The TLS monitoring of titrations of chloride solutions with Ag^+ is also possible.

From the viewpoint of the determination of the halides and Ag^+ , the TLS procedures studied here lack reproducibility, and cannot be used at concentrations where the solubility product of the silver halide is approached. However, the experiments have shown how the TLS signal behaves in the presence of fast and slow chromogenic reactions produced by the pump radiation. It has also been shown that TLS can be used to discriminate absorbance from scattering in slightly turbid media. This point has also been studied recently [13].

Acknowledgement

Thanks are due to the DGICYT of Spain for financial support (Project PB90/425).

References

- [1] N.J. Dovichi and J.M. Harris, *Anal. Chem.*, 51 (1979) 728.
- [2] K. Miyaishi, T. Imasaka and N. Ishibashi, *Anal. Chim. Acta*, 124 (1981) 381.

- [3] G. Ramis Ramos, M.C. García Alvarez-Coque, B.W. Smith, N. Omenetto and J.D. Winefordner, *Appl. Spectrosc.*, 42 (1988) 341.
- [4] V.P. Grishko, V.I. Grishko and I.G. Yudelevich, *Zh. Anal. Khim.*, 44 (1989) 434.
- [5] T.G. Nolan and N.J. Dovichi, *Anal. Chem.*, 59 (1987) 2803.
- [6] J.F. Power and C.H. Langford, *Anal. Chem.*, 60 (1988) 842.
- [7] S.R. Erskine and D.R. Bobbitt, *Anal. Chem.*, 61 (1989) 910.
- [8] J.M. Sanchis-Mallols, R.M. Villanueva-Camañas and G. Ramis-Ramos, *Analyst*, 117 (1992) 1367.
- [9] L.E. Buffett and M.D. Morris, *Appl. Spectrosc.*, 37 (1983) 455.
- [10] E.F. Simó Alfonso, M.A. Rius Revert, M.C. García Alvarez-Coque and G. Ramis Ramos, *Appl. Spectrosc.*, 44 (1990) 1501.
- [11] R.J. Roach and R.D. Snook, *Anal. Chim. Acta*, 262 (1992) 231.
- [12] R.M. Villanueva-Camañas, J.M. Sanchis-Mallols, E.F. Simó-Alfonso and G. Ramis-Ramos, *Anal. Chim. Acta*, 257 (1992) 217.
- [13] J.B. Thorne and D.R. Bobbitt, *Appl. Spectrosc.*, 47 (1993) 360.
- [14] E.F. Simó Alfonso, M.C. García Alvarez-Coque, G. Ramis Ramos, A. Cladera Forteza, M. Estela Ripoll and V. Cerdá Martín, *Anal. Lett.*, 25 (1992) 573.
- [15] D.T. Burns, A. Townshend and A.H. Carter, in R.A. Chalmers and M. Masson (Eds.), *Inorganic Reaction Chemistry*, Horwood, Chichester, 1981, p. 389.
- [16] L. Erdely, in I. Buzás (Ed.), *Gravimetric Analysis, Part III*, Pergamon, Oxford, 1965, p. 3.
- [17] I.M. Kolthoff, E.B. Sandell, E.J. Meehan and S. Bruckenstein, in *Análisis Químico Cuantitativo*, 5th ed., Nijar, Buenos Aires, 1979, pp. 744 and 826.
- [18] R.C. Weast and M.J. Astle (Eds.), *Handbook of Chemistry and Physics*, 60th ed., CRC, Boca Raton, FL, 1980, p. B-220.



ELSEVIER

Analytica Chimica Acta 292 (1994) 121–132

**ANALYTICA
CHIMICA
ACTA**

Multi-wavelength analysis of synchronous fluorescence spectra of the complexes between a soil fulvic acid and Cu(II)

Adélio A.S.C. Machado *, Joaquim C.G. Esteves da Silva, José A.C. Maia

CIQ(UP), Chemistry Department, Faculdade de Ciências, P-4000 Porto, Portugal

(Received 17th November 1992)

Abstract

The variations observed in the synchronous fluorescence spectra of a soil fulvic acid, collected in the north of Portugal, with pH (between 2 and 7) and with Cu(II) concentration (at pH 3, 4, 5 and 6 and total copper concentrations between 0.005 and 4 mM depending on the pH) were studied by SIMPLISMA, a self-modelling mixture analysis technique. Three components were detected when varying the pH, corresponding to three acid–base equilibria with pK_a values around 3.0, 5.0 and 6.0, and their individual spectra were obtained. Two components were detected when varying the Cu(II) concentration, corresponding to two different ligand sites, and their spectra and concentration profiles (based on the two detected pure variables) were obtained. The spectrum of one binding site is similar to the component associated with the acid–base equilibrium with $pK_a = 3.0$ and that of the other binding site is similar to the sum of the spectra of the components associated with the other two acid–base equilibria. Using a 1:1 stoichiometry for complex formation, complexation capacities (C_1) and stability constants (K) were calculated for the two binding sites at the four pH values. The calculated stability constants were $\log K_1 = 3.42(4)$, $\log K_2 = 3.05(5)$ at pH 3, $\log K_1 = 4.17(3)$, $\log K_2 = 3.71(1)$ at pH 4, $\log K_1 = 4.51(3)$, $\log K_2 = 3.95(2)$ at pH 5 and $\log K_1 = 4.57(3)$, $\log K_2 = 4.03(1)$ at pH 6.

Key words: Fluorimetry; Copper; Fulvic acid; Soils; Self-modelling mixture analysis (SIMPLISMA)

1. Introduction

Fluorescence spectrometry has been used to study the complexation of metal ions by fulvic acids (FA) [1–7], alone or combined with ion-selective electrode potentiometry [4,6]. From fluorescence data obtained for a fixed set of experimental conditions, if a 1:1 stoichiometry is as-

sumed for complex formation, the stability constant and complexing capacity of the ligand can be calculated. In these calculations, only one type of binding site is defined and only one fluorescence intensity value, the maximum of the emission fluorescence spectrum, is used, because the excitation and emission fluorescence spectra of FA usually show only one band.

More recently, synchronous fluorescence (SyF) spectra were obtained for FA, which are characterized by several overlapped bands [9,10], and the information was treated by multi-wavelength

* Corresponding author.

chemometric techniques of soft modelling, namely principal component analysis (PCA) [10,11] and evolving factor analysis (EFA) [12,13]. With PCA, a qualitative tool was developed for the study of the quenching induced in the SyF spectra of FA by metal ions [9]. PCA and EFA of SyF spectra obtained when varying the pH in the presence and absence of metal ions allowed the calculation of the ionization constants of a soil and a marine FA and the observation of the effect of the metal ions on the acid–base distribution diagrams [10]. These results open up new perspectives for the understanding of the structure of FA, and the use of soft modelling techniques in this field deserves further investigation.

SIMPLISMA [14–17], a simple-to-use interactive self-modelling mixture analysis based on the pure variable concept, can be used to find the number of components that cause variations in spectral data, their pure spectra and concentration profiles. Following the strategy of soft modelling spectroscopic data of FA (FT-IR and SyF), successfully used in previous work [10,18], this paper reports a study of the application of the SIMPLISMA approach to SyF spectra of a soil FA obtained when varying the pH (between 2 and 7) and when varying the Cu(II) concentration at constant pH (3, 4, 5 and 6) (quenching experiments). The purpose of the work was to determine and characterize the components that cause variations in spectral data by obtaining their spectra and concentration profiles. In addition, for the quenching experiments, after isolation of the variations due to the different components (different binding sites), stability constants and complexing capacities were calculated assuming 1:1 complex formation.

2. Theory

The self-modelling multi-wavelength analysis strategy used in the first part of this work, SIMPLISMA, was recently developed by Windig and co-workers [14–17] and is briefly described in this section.

The first step of the SIMPLISMA procedure is the determination of the pure variables. In the

present case, a pure variable is a wavelength of the SyF spectrum of which the intensity value is due to only one component of the mixture. In this process, the spectra under analysis [represented by a matrix D , size $nv \times ns$, where nv is the number of variables (wavelengths) and ns is the number of spectra) are reduced to three vectors or spectra, named the mean spectrum, m , standard deviation (SD) spectrum, s , and purity spectrum, p . The elements of the mean spectrum are defined by

$$m_i = (1/ns) \sum_{j=1}^{ns} d_{i,j} \quad (i = 1, \dots, nv) \quad (1)$$

the elements of the SD spectrum by

$$s_i = \left[(1/ns) \sum_{j=1}^{ns} (d_{i,j} - m_i)^2 \right]^{1/2} \quad (i = 1, \dots, nv) \quad (2)$$

and the elements of the purity spectrum by

$$p_i = s_i/m_i \quad (i = 1, \dots, nv) \quad (3)$$

For small m_i values, where information is small and the noise is relatively large, the p_i values may become large. In order to remove this unwanted effect, an offset is added to the data.

The visualization of vectors s and p in the form of a spectrum will be crucial for the detection of pure variables. The wavelength with the highest intensity in the purity spectrum is the first pure variable. The SD spectra can be used to check the validity of the selected pure variable. The variations that are associated with the selected pure variable are removed from the standard deviation and purity spectra and the second pure variable is determined. This process is repeated until these spectra show only noise, i.e., when all the useful information is removed. If the determination of the rank of the system (the number of independent species, np , that are including variance in the data) is not visually sharp after determining j pure variables, two error functions, R_s (relative total intensity of the SD spectra) and R_r (ratio of the relative total intensi-

ties of the j SD and the $j + 1$ SD spectra), can be helpful:

$$R_{sj} = 100 \sum_{i=1}^{nv} s_{i,j} / \sum_{i=1}^{nv} s_{i,1} \quad (4)$$

$$R_{rj} = R_{sj} / R_{s(j+1)} \quad (5)$$

The second step of the SIMPLISMA procedure is the resolution of the data into spectra (matrix S , size $np \times nv$) and concentration profiles (matrix C , size $ns \times np$) for the number of detected species. Assuming that all the components have the same fluorescence efficiencies, the concentration profiles are equal to the fluorescence intensities of the corresponding pure variables after normalization. If the data matrix is expressed as

$$D^T = CS \quad (6)$$

the spectra and concentration profiles can be calculated by a least-squares procedure:

$$S = (C^T C)^{-1} C^T D^T \quad (7)$$

$$C = D^T S^T (S S^T)^{-1} \quad (8)$$

In Eq. 7, the intensities of the pure variables in the D spectra matrix are used in C .

The components found in the analysis of the varying pH experiments are related to the groups involved in the acid–base transformations that occur in the FA molecules, because the variations observed in the SyF spectra are a macroscopic view of that phenomenon. As the concentration profiles are related to the variation of the concentrations of the acid–base groups as a function of pH, the 50% ionization point provides an estimate of the ionization constant, which is equal to the pH of that point, if monoprotic acids are considered.

The concentration profiles obtained from the analysis of the quenching effect observed on the SyF spectra give different fluorescence intensity (I) variations that correspond to binding sites with different metal ion complexation capacities. If the stoichiometry of the complex formation between the metal ion and the ligand (binding site type) is 1 : 1, the conditional stability constant

K (at fixed pH) for each binding site is calculated by

$$K = [ML] / ([M][L]) \quad (9)$$

where $[ML]$ is the concentration of the complex, $[M]$ is the uncomplexed metal ion concentration and $[L]$ is the total concentration of uncomplexed ligand (charges omitted). The relationship between I , K , C_L (total ligand concentration or complexation capacity), C_M (total metal ion concentration), I_{ML} (fluorescence intensity when no more quenching occurs), with data adjusted so that the fluorescence intensity before quenching begins (before any metal ion is added to the FA solution) is equal to 100, is [2]

$$I = [(I_{ML} - 100) / (2KC_L)] \left\{ (KC_L + KC_M + 1) - \sqrt{[(KC_L + KC_M + 1)^2 - 4K^2 C_L C_M]} \right\} + 100 \quad (10)$$

This equation can be solved for K , C_L and I_{ML} by non-linear regression analysis using simplex optimization. In this work, the modified simplex method [19] was used. A large initial simplex with a step size of 0.8 was built so that all the information of the domains of the chosen factor was used [20]. Different factor domains were tried to check the validity of the found optimum.

The results obtained with the above data treatment of FA data should always take into consideration that FA is a highly complex mixture of low-molecular-weight polymers. Stability constants and complexation capacities of these substances, even if different binding sites are detected, must always be considered as mean values that are characteristic of more or less well defined classes of reactive chemical structures.

3. Experimental

3.1. Reagents

The sample of FA was isolated from a Portuguese forest soil collected at Louros, Famalicão (30 km from Porto) by the procedure recommended by the IHSS [21].

Solutions of 150 mg l^{-1} were prepared in 0.1 M potassium nitrate. In the titrations at varying pH and those at pH 3 and 4, standard 0.1 M nitric acid was added to the titrated FA solutions. A solution of decarbonated potassium hydroxide was used as the titrant in the varying pH titrations and to adjust the pH to a constant value in the other experiments. A standard copper nitrate solution (Radiometer) was used as the titrant in the constant pH titrations. The following ranges of Cu(II) concentrations were covered: pH 3, 0.01–4 mM; pH 4, 0.005–3 mM; pH 5, 0.005–1 mM; and pH 6, 0.005–0.5 mM.

3.2. Instrumentation

Potentiometric titrations with pH measurement were conducted with a PC-controlled system, assembled with a Crison MicropH 2002 pH-meter, a Crison MicroBU 2030 microburette, a Crison MicroBU 2031 microburette, a Philips GAT 130 glass electrode and a Radiometer K711 (double-junction) reference electrode. The experiments were done under nitrogen at $25.0 \pm 0.2^\circ\text{C}$. The cell was calibrated with three buffer solutions with ionic strength adjusted to 0.1 M [22].

Fluorescence measurements were made with a Perkin-Elmer LS-50 luminescence spectrometer

with a flow cell. A Gilson Minipuls 2 peristaltic pump forced the displacement of the titrated solution into the flow cell after each addition of titrant and, when required, after pH adjustment. During pH and fluorescence intensity measurements, the pump was turned off. Synchronous fluorescence spectra were recorded with the following settings: between 280 and 550 nm; 0.5-nm resolution between points; 7.5-nm excitation and emission slit widths; wavelength difference of 20 nm; and scan rate 200 nm min^{-1} . Emission fluorescence spectra were recorded with the following settings: between 350 and 600 nm; 320 nm as the excitation wavelength; 5.0-nm emission slit width and 15-nm excitation slit width; 0.5-nm resolution between points; and scan rate 200 nm min^{-1} . After the subtraction of the reference spectrum (0.1 M potassium nitrate solution), data spectra were stored on disk, converted into ASCII format with LAB CALC software (Galactic Industries) and reduced to a version with 5-nm resolution (55 points per spectrum) to be used in the calculations.

3.3. Programs and data treatment

All calculations were done with software developed in this laboratory and written and com-

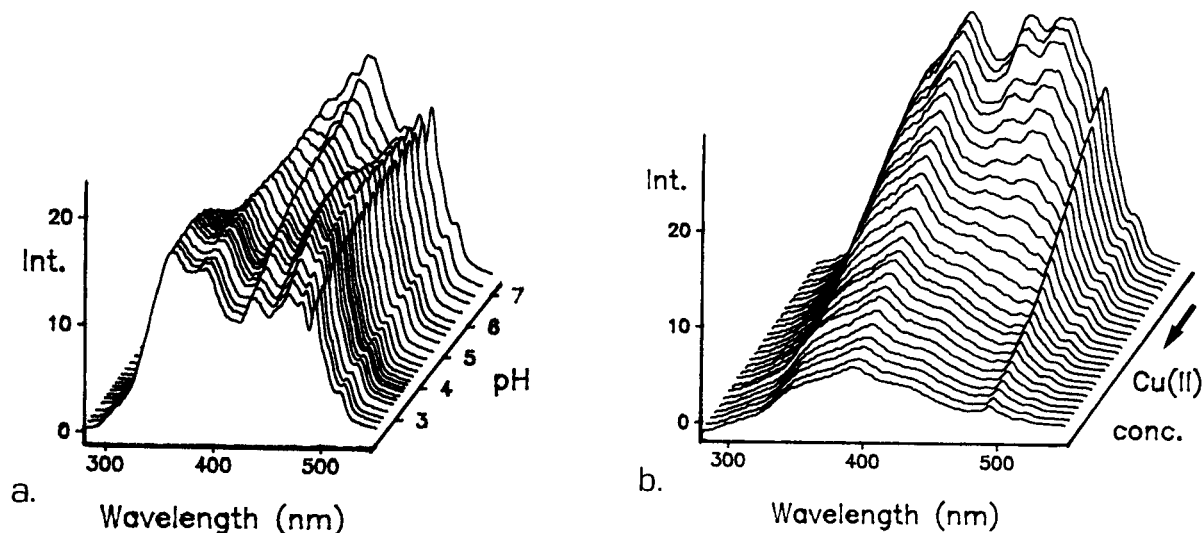


Fig. 1. Synchronous fluorescence spectra of a soil fulvic acid (a) as a function of pH and (b) at pH 5 as a function of Cu(II) concentration.

piled with Turbo Pascal 5.0 (Borland International). An IBM AT-compatible computer with math coprocessor was used for calculations.

4. Results and discussion

4.1. Preliminary analysis

Synchronous fluorescence spectra of FA as a function of pH and as a function of Cu(II) concentration at pH 5 are shown in Fig. 1a and b, respectively. Several bands are observed in these spectra that can be identified by peak positions: 360, 392, 435, 469, 481 and 494 nm. Varying the pH leads to different variations (increases and decreases) in the intensities of these peaks, while the expected quenching is observed with increasing Cu(II) concentration.

The quenching effect at the four pH values studied can be observed in more detail in Fig. 2.

Before Cu(II) ion is added to the FA solution (spectra a, c, e and g), the bands of the SyF spectra show markedly different intensities at different pH values, but after sufficient Cu(II) ion has been added no further quenching is observed and the SyF spectra obtained for different pH values are similar (spectra b, d, f and h). Nevertheless, the simple observation of the quenching on the SyF spectra, exemplified in Fig. 1b for the four pH values shown in Fig. 2, gives no indication of whether there is one or more than one component inducing variations in these spectra. Multi-wavelength mixture analysis techniques must be used to extract more information from a set of spectra such as these.

4.2. SIMPLISMA analysis of the pH effect

The SD and purity spectra that correspond to the selection of four pure variables are shown in

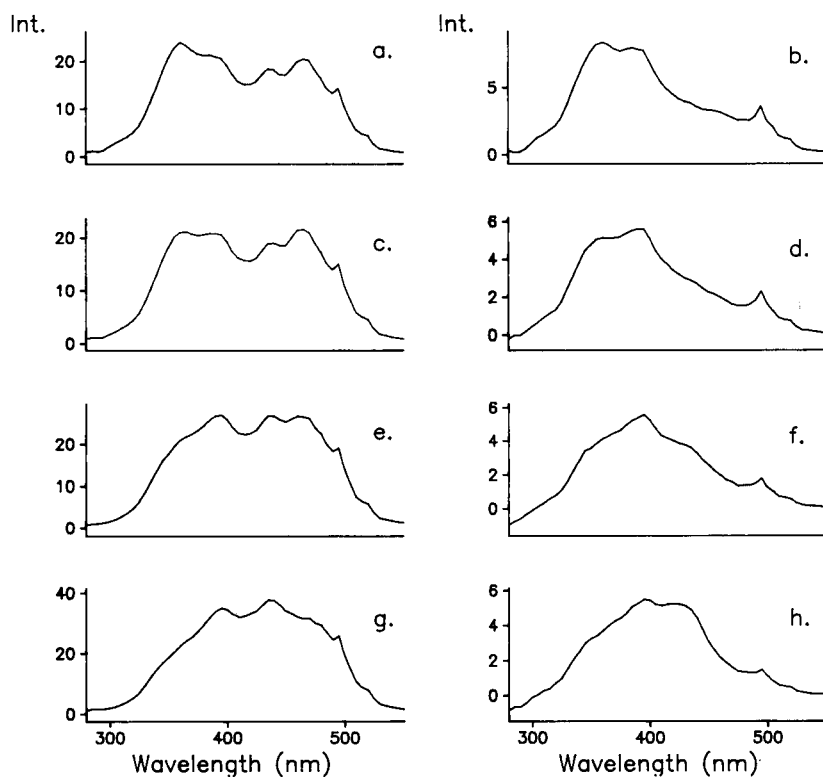


Fig. 2. Synchronous fluorescence spectra of a soil fulvic acid at (a, b) pH 3, (c, d) pH 4, (e, f) pH 5 and (g, h) pH 6, (a, c, e, g) without Cu(II) and (b, d, f, h) after no further quenching is observed on addition of Cu(II).

Table 1
Values of the error functions to determine the number of components in the varying pH experiment

N^a	R_s	R_r
1	100.0	19
2	5.1	334
3	1.5×10^{-2}	988
4	1.6×10^{-5}	4507
5	3.5×10^{-9}	

^a Number of the pure variable.

Fig. 3 (the arrows in the purity spectra show the selected pure variables) and the error functions for this process in Table 1. The R_s error function (Table 1) shows a marked decrease ($R_r = 988$) on passing from the third to the fourth SD spectrum (from 1.5×10^{-2} to 1.6×10^{-5}) and the fourth SD and purity spectra (Fig. 3g and h) are almost zero. These results show that there are three components with influence on the data.

With the three pure variables found (355, 420 and 465 nm), the spectra (Fig. 4a–c) and normalized concentration profiles (Fig. 5a) were calculated for the three components. The analysis of the concentration profiles shows different be-

haviours for the three components: the first component decreases the concentration and reaches 50% transformation at $\text{pH} \approx 5.0$; the second increases the concentration and reaches 50% transformation at $\text{pH} \approx 6.0$; and the third component increases the concentration up to $\text{pH} \approx 5.0$, with 50% transformation at $\text{pH} \approx 3.0$, but for pH values > 5.0 decreases the concentration, with 50% transformation at $\text{pH} \approx 6.0$ as with the second component. These results show that the acid–base properties of the present FA sample are characterized by three types of acid–base systems with ionization constants around 3.0, 5.0 and 6.0.

These SIMPLISMA results are very similar to those obtained for the same sample with a more rigorous and different approach in which PCA and EFA were used [10]. In the latter study, the same number of acid–base systems were obtained and their SyF spectra (characterized by main peaks at 465, 420 and 355 nm, the pure variables detected in this study) were similar to those found here with SIMPLISMA and represented in Fig. 4a–c. The three acidity constants determined with the EFA approach ($\text{p}K_{a1} = 3.0$, $\text{p}K_{a2} = 4.6$ and $\text{p}K_{a3} = 6.4$) are close to the estimates obtained

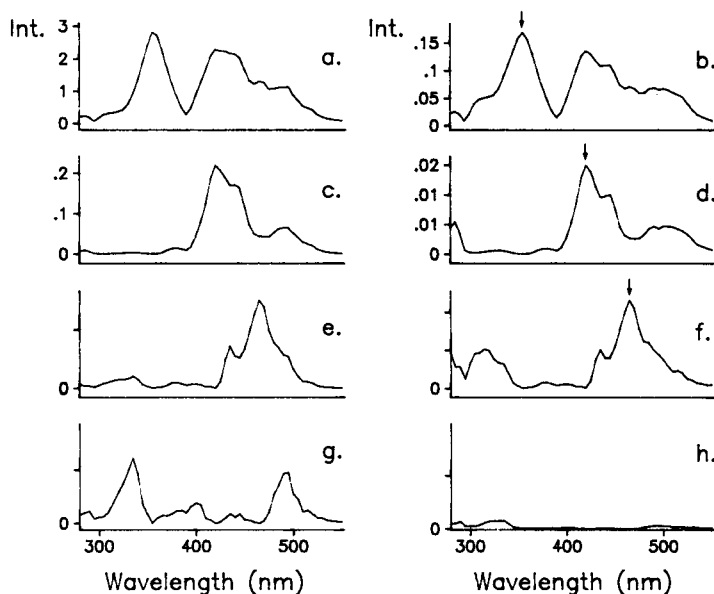


Fig. 3. Standard deviation (a, c, e, g) and purity (b, d, f, h) spectra resulting from the SIMPLISMA analysis of the varying pH experiment: (a, b) first set; (c, d) second set; (e, f) third set; and (g, h) fourth set. Maximum intensities of the third (e) and fourth (g) standard deviation spectra are 8×10^{-4} and 6×10^{-7} , respectively.

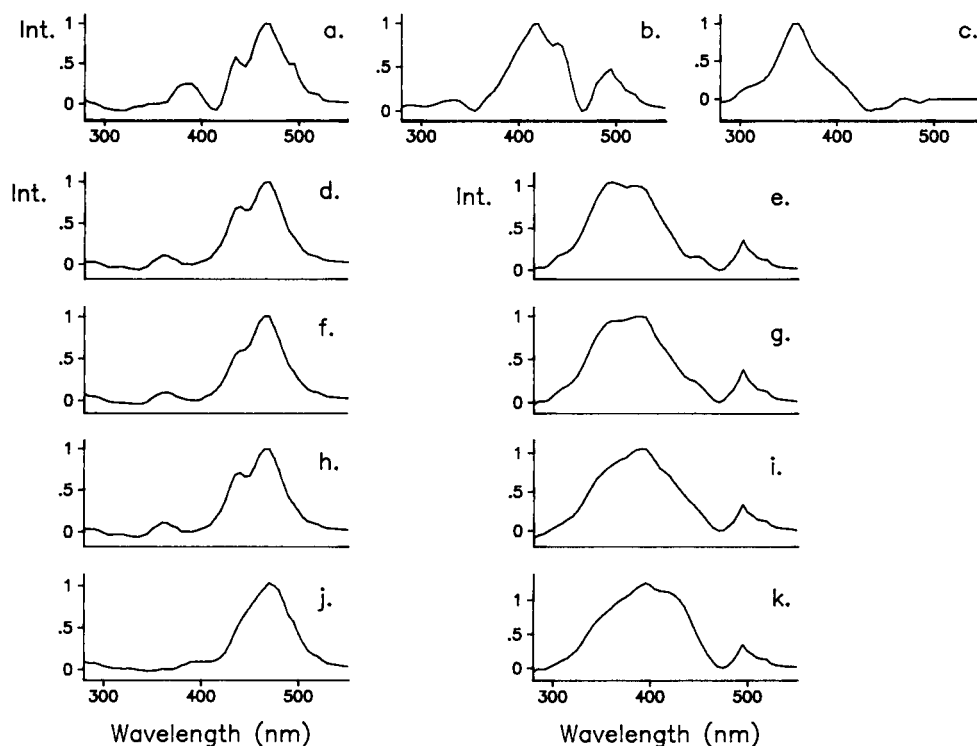


Fig. 4. Spectra based on the pure variables as extracted by the SIMPLISMA analysis: (a, b, c) varying pH experiment; (d, e) pH 3; (f, g) pH 4; (h, i) pH 5; (j, k) pH 6.

from the representation of the concentration profiles (Fig. 5a).

Carboxylic acid groups in an *ortho* position relative to a hydroxylic or a carboxylic group in aromatic structures of the salicylic and phthalic acid types are responsible for the first acid–base constant. Carboxylic acid groups free from strong interactions with neighbouring groups (benzoic acid type) are responsible for the second. The third acid–base system is constituted by a mixture of weakly acidic carboxylic acid groups and/or by

strongly acidic hydroxylic groups, probably also in an aromatic structure.

4.3. SIMPLISMA analysis of the quenching effect

The SD and purity spectra that correspond to the selection of four pure variables are shown in Fig. 6 for pH 3 and in Fig. 7 for pH 6 (the arrows in the purity spectra show the selected pure variables), and the error functions for these processes are given in Table 2. These results show that the

Table 2

Values of the error functions to determine the number of components in the constant pH experiments

N^a	pH 3		pH 4		pH 5		pH 6	
	R_s	R_r	R_s	R_r	R_s	R_r	R_s	R_r
1	100.0	31	100.0	27	100.0	28	100.0	24
2	3.2	1905	3.9	1235	3.5	773	4.1	909
3	1.7×10^{-3}	3168	3.1×10^{-3}	1837	4.5×10^{-3}	1108	4.5×10^{-3}	2294
4	5.3×10^{-7}		1.7×10^{-6}		4.1×10^{-6}		2.0×10^{-6}	

^a Number of the pure variable.

number of components that induce independent variations (quenching) of data is only two for the four pH values. The same criterion as for the varying pH data is followed here: the third SD spectrum has an R_s lower than -100 , the second SD an R_r of almost 1000 or greater, and the third SD and purity spectra are almost zero (maximum intensity lower than 10^{-5}). The band observed in Fig. 7e–h at the left-hand extreme of the wavelength range in the third and fourth SD and purity spectra is due to noise and, therefore, was not selected as a pure variable. These results show that there are two types of binding sites in the FA molecules responsible for the observed quenching.

With the two pure variables found, which were similar for the experiments at the four pH values (ca. 470 and ca. 380 nm), the spectra of the two

components were calculated (Fig. 4d–k). The four pairs of spectra are similar, showing that the same two types of binding sites are active and are responsible for the complexation between pH 3 and 6.

The comparison of the pure variables (wavelengths) and the spectra found for the varying pH [without Cu(II)] and for the constant pH experiments [with Cu(II)] (Table 3 and Fig. 4) shows two identical features: the third pure variable of the varying pH experiments (465 nm) is similar to the first pure variable of the constant pH experiments (470 nm); and the spectrum that corresponds to the third pure variable of the varying pH experiments is very similar to the first spectrum of the constant pH experiments. This is an interesting result because it shows that the most important binding site, which induces more varia-

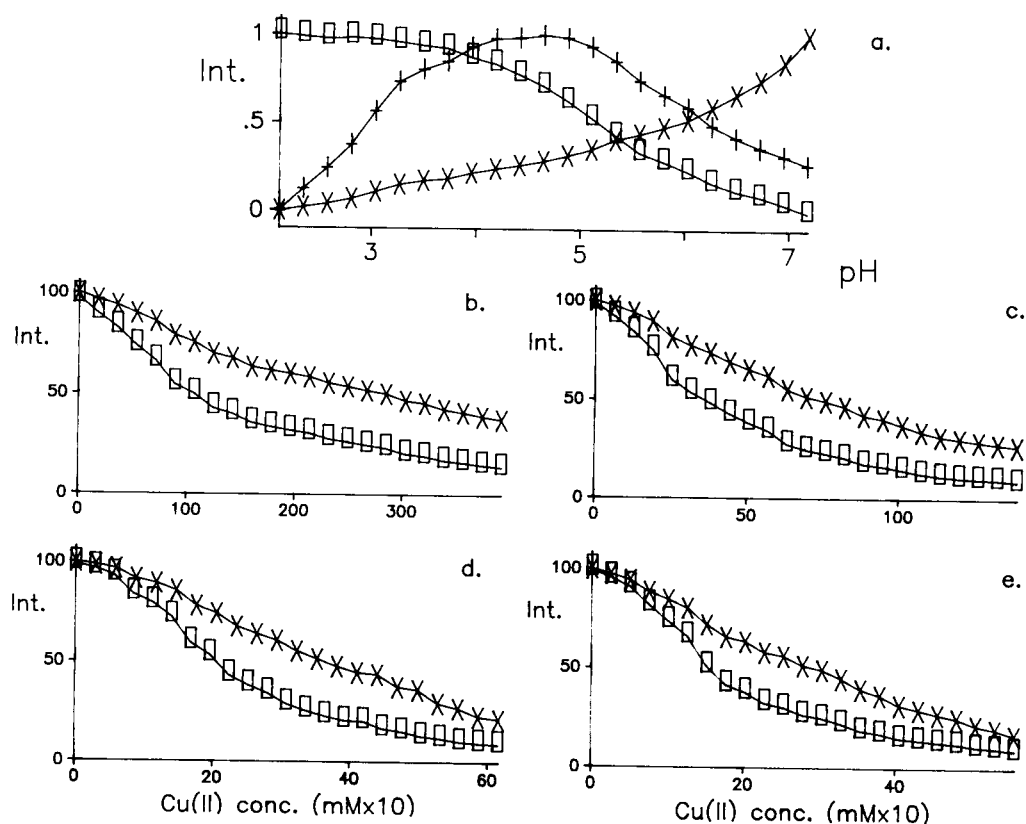


Fig. 5. Concentration profiles for the pure variables (\square = first; \times = second; $+$ = third) as extracted by the SIMPLISMA analysis: (a) varying pH experiment; (b) pH 3; (c) pH 4; (d) pH 5; (e) pH 6.

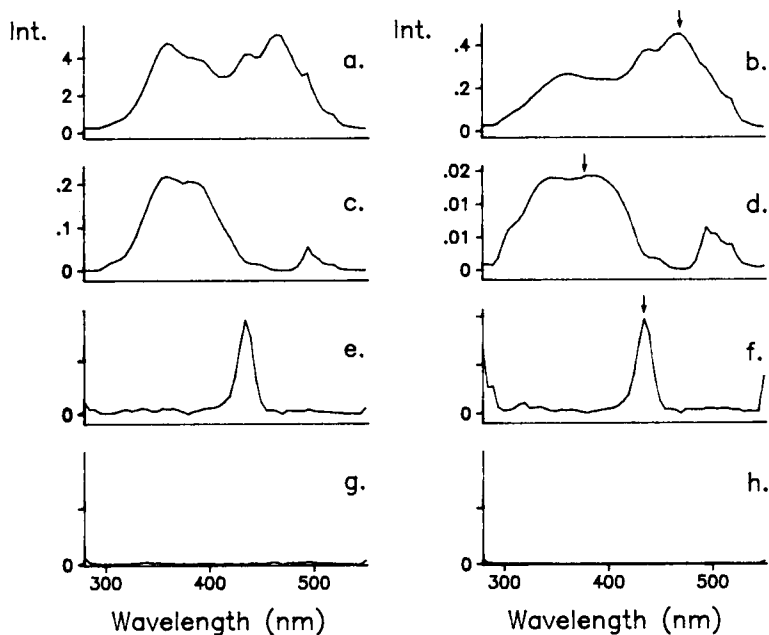


Fig. 6. Standard deviation (a, c, e, g) and purity (b, d, f, h) spectra resulting from the SIMPLISMA analysis of the constant pH 3 experiment: (a, b) first set; (c, d) second set; (e, f) third set; and (g, h) fourth set. Maximum intensities of the third (e) and fourth (g) standard deviation spectra are 4×10^{-4} and 6×10^{-8} , respectively.

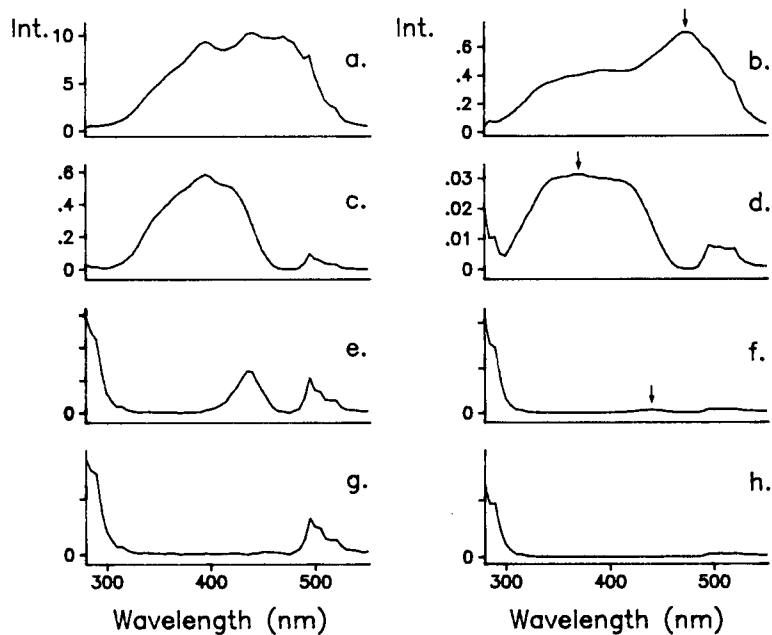


Fig. 7. Standard deviation (a, c, e, g) and purity (b, d, f, h) spectra resulting from the SIMPLISMA analysis of the constant pH 6 experiment: (a, b) first set; (c, d) second set; (e, f) third set; and (g, h) fourth set. Maximum intensities of the third (e) and fourth (g) standard deviation spectra are 6×10^{-4} and 3×10^{-7} , respectively.

Table 3
Pure variable (wavelength, nm) detected by the SIMPLISMA analysis in the varying and constant pH experiments

N^a	pH				
	Varying	3	4	5	6
1	355	470	470	470	475
2	420	380	390	380	370
3	465				

^a Number of the pure variable.

tion in the SyF spectra, is the same as that defined by a ionization constant around 3.0. This binding site [denoted No. 1, BS1(SyF)], must correspond to a class of chemical structures having very similar acid–base and complexation properties because the same spectra were obtained from two different experiments. These results show that BS1(SyF) is constituted by structures of the salicylic and/or phthalic acid types and that they are the most important in the complexation of the Cu(II) ion.

The second binding site [BS2(SyF)] spectrum corresponds to a mixture of the other two spectra

found in the varying pH experiments, indicating a binding site with a higher degree of mixing of chemical structures and complexity of the binding process.

Fluorescence intensity profiles extracted using the two pure variables are shown in Fig. 5b–e. Comparison of the curves that correspond to the quenching associated with the BS1(SyF) (\square) and BS2(SyF) (\times), shows that, for all pH values, BS1(SyF) is a stronger binding site than BS2(SyF). The fluorescence intensity for BS1(SyF) decreases more rapidly at lower Cu(II) concentrations whereas for BS2(SyF) it decreases slowly during the whole titration.

The existence of two components in the data for quenching experiments is a fact, but it might wondered whether the two pure variables are really “pure”. This question is not easy to answer. The fact that the results obtained for the varying and constant pH experiments, which are experimentally distinct, were highly compatible, and also with those obtained with the EFA method [10], which is a different data treatment approach, strongly suggests that the pure variables have a high degree of purity. As the use of

Table 4
Average results of the non-linear adjustment of the SyF spectral data

Binding site	Parameter ^a	pH			
		3	4	5	6
BS1(SyF)	Log K	3.42 (0.04)	4.17 (0.03)	4.51 (0.03)	4.57 (0.03)
	C_L	0.028 (0.014)	0.053 (0.017)	0.033 (0.016)	0.071 (0.008)
	I_{ML}	9(1)	4(1)	1(1)	0
	N_p	11	16	17	18
	ΔCu	0.61–2.38	0.076–1.2	0.016–0.53	0.016–0.35
	ΔE	0.33	0.46	0.32	0.30
	SSR	1.74	4.28	3.60	2.21
	N_e	3	2	3	3
	BS2(SyF)	Log K	3.05 (0.05)	3.71 (0.01)	3.95 (0.02)
C_L		0.016 (0.006)	0.019 (0.004)	0.031 (0.026)	0.13 (0.03)
I_{ML}		28 (3)	16 (2)	5 (1)	0
N_p		13	11	14	15
ΔCu		0.65–2.92	0.23–1.1	0.059–0.53	0.076–0.49
ΔE		0.45	0.45	0.25	0.29
SSR		3.87	2.82	1.62	1.84
N_e		3	2	3	3

^a Log K = logarithm of the stability constant (standard deviation in parentheses); C_L = complexing capacity (μM for experiments at pH 3 and 4; mM for experiments at pH 5 and 6); I_{ML} = fluorescence intensity value when no further quenching is observed; N_p = number of points used in calculations; ΔCu = Cu(II) concentration interval used in calculations (mM); ΔE = average deviation of the estimates; SSR = sum of squares of residuals; N_e = number of experiments.

derivatives minimizes the problems due to band overlapping, one further test of the purity of the variables is to work with the second-derivative SyF spectra [17]. However, the second-derivative transformation of the SyF spectra markedly lowered its intensity and the variations shown in the raw spectra almost disappeared.

4.4. Non-linear adjustment of data

Table 4 shows the results obtained by non-linear adjustment of data for the two binding sites detected in the SyF spectra, BS1(SyF) and BS2(SyF). In Table 5, for comparison, similar results calculated from the maximum of the emission fluorescence spectra (420 nm after excitation at 320 nm), for one binding site, BS(emission), obtained from the same experiments in which SyF spectra were determined, are presented.

The non-linear adjustment process always gave an average deviation from the experimental value for the calculated fluorescence intensity (I) of < 0.7 , which was less than the experimental error of the measurement of I . Also, the sum of the squares of the residuals was always ≤ 6 . These results show that the adjustment was good. Nevertheless, the complexation capacity (C_L) showed variations with the factor domain, while the stability constant (K), I_{ML} and the quality of the adjustment showed no such variations, particularly for the experiments at pH 3 and 4, and therefore the value of the C_L parameter should be considered as a rough estimate. This problem in the determination of C_L by this procedure has

been discussed previously [2] and appears when K and C_L are relatively small.

As expected from the analysis of Fig. 5, the stability constants for BS1(SyF) are larger than those for BS2(SyF); the difference between log K values is ca. 0.5. The C_L values for BS1(SyF) are similar to those for BS2(SyF) at pH 3 and 5, larger at pH 4 and smaller at pH 6. These variations show that groups associated with BS2(SyF) are weaker acids than BS1(SyF), because a large increase in C_L relative to the variation that occurs for the BS1(SyF) was observed only at pH 6. These results agree with what was said above about the relationship of the binding sites and the acid–base systems.

The variation of the K values with pH is as expected, i.e., an increase in K occurs with increase in the extent of neutralization of the ligand. For BS1(SyF) and BS2(SyF), the variation between pH 3 and 6 is ca. one log K unit, whereas for BS(emission) it is ca. two log K units. This larger variation for BS(emission) is due to a more unrealistic model in the analysis of data which ignores that more than one binding site is present and that these show different variations of K and C_L with pH.

The comparison of the K values obtained for BS1(SyF) and BS2(SyF) (Table 4) with those obtained for BS(emission) (Table 5) shows that there is no clear relationship between the two sets of results, although they all are in the same range: for pH 3 and 4, the K values for BS(emission) are close to the K values for BS2(SyF); for pH 5, the K value for BS(emission) is between the two

Table 5

Average results of the non-linear adjustment of the emission fluorescence spectra data

Parameter ^a	pH			
	3	4	5	6
Log K	2.90 (0.03)	3.63 (0.02)	4.11 (0.03)	5.03 (0.01)
C_L	0.021 (0.003)	0.031 (0.031)	0.17 (0.01)	0.27 (0.01)
I_{ML}	29(1)	20(1)	6(2)	16(1)
N_p	12	12	16	18
ΔCu	0.61–2.5	0.090–0.82	0.020–0.48	0.010–0.34
ΔE	0.33	6.06	0.96	0.3
SSR	1.85	0.61	0.17	3.60
N_e	3	2	2	2

^a See footnote to Table 4.

values for BS1(SyF) and BS2(SyF); and for pH 6, the K value for BS(emission) is larger than the two values for BS1(SyF) and BS2(SyF). These results are due to the unpredicted overall response to the different variations of the complexation parameters of different binding sites with pH for the one binding site model.

Acknowledgements

Willem Windig (Eastman Kodak, Rochester, NY) is acknowledged for providing a copy of the SIMPLISMA package. Financial support from INIC (Lisbon), through Research Line 4 of CIQ(UP), is acknowledged, in addition to a PhD grant (to J.C.G.E.S.). The Perkin-Elmer LS-50 luminescence spectrometer was acquired through Project CIENCIA 27/M/90 awarded by JNICT (Lisbon).

References

- [1] R.A. Saar and J.H. Weber, *Anal. Chem.*, 52 (1980) 2095.
- [2] D.K. Ryan and J.H. Weber, *Anal. Chem.*, 54 (1982) 986.
- [3] D.K. Ryan, C.P. Thompson and J.H. Weber, *Can. J. Chem.*, 61 (1983) 1505.
- [4] S.E. Cabaniss and M.S. Shuman, *Anal. Chem.*, 58 (1986) 398.
- [5] P. Blaser and G. Sposito, *Soil Sci. Soc. Am. J.*, 51 (1987) 612.
- [6] S.E. Cabaniss and M.S. Shuman, *Anal. Chem.*, 60 (1988) 2418.
- [7] L.S. Ventry, D.K. Ryan and T.R. Gilbert, *Microchem. J.*, 44 (1991) 201.
- [8] T.M. Miano, G. Sposito and J.P. Martin, *Soil Sci. Soc. Am. J.*, 52 (1988) 1016.
- [9] S.E. Cabaniss, *Environ. Sci. Technol.*, 26 (1992) 1133.
- [10] A.A.S.C. Machado and J.C.G. Esteves da Silva, *Chemometr. Intell. Lab. Syst.*, 19 (1993) 155.
- [11] E.R. Malinowski and D.G. Howery, *Factor Analysis in Chemistry*, Wiley, New York, 1980.
- [12] H. Gampp, M. Maeder, C.J. Meyer and A.D. Zuberbuhler, *Talanta*, 32 (1985) 1133.
- [13] H. Gampp, M. Maeder, C.J. Meyer and A.D. Zuberbuhler, *Talanta*, 33 (1986) 943.
- [14] W. Windig and J. Guilment, *Anal. Chem.*, 63 (1991) 1425.
- [15] W. Windig, C.E. Heckler, F.A. Agblevor and R.J. Evans, *Chemometr. Intell. Lab. Syst.*, 14 (1992) 195.
- [16] W. Windig, in P.C. Jurs (Ed.), *Computer-Enhanced Analytical Spectroscopy*, Vol. 3, Plenum, New York, 1992, Chap. 4.
- [17] W. Windig, personal communication.
- [18] A.A.S.C. Machado and J.C.G. Esteves da Silva, *Chemometr. Intell. Lab. Syst.*, 17 (1992) 249.
- [19] S.L. Morgan and S.N. Deming, *Anal. Chem.*, 46 (1974) 1170.
- [20] L.A. Yarbrow and S.N. Deming, *Anal. Chim. Acta*, 73 (1974) 391.
- [21] E.M. Thurman (Rapporteur), in F.H. Frimmel and R.F. Christman (Eds.), *Humic Substances and Their Role in the Environment*, Wiley-Interscience, New York, 1988, pp. 31–43.
- [22] M.T.S. Vasconcelos and A.A.S.C. Machado, *Talanta*, 33 (1986) 919.

Study of the Eu(III)–tetracycline–thenoyltrifluoroacetone system by using the stopped-flow mixing technique: Determination of tetracycline in serum

P. Izquierdo, A. Gómez-Hens, D. Pérez-Bendito *

Department of Analytical Chemistry, Faculty of Sciences, University of Córdoba, E-14004 Córdoba, Spain

(Received 2nd November 1993; revised manuscript received 26th January 1994)

Abstract

The enhancing effect of thenoyltrifluoroacetone on the fluorescence intensity of the Eu(III)–tetracycline system in the presence of Triton X-100 was studied by using equilibrium and kinetic measurements. This ligand significantly improves the sensitivity of equilibrium methods for tetracycline determination based on energy-transfer processes. Kinetic methodology implemented by means of the stopped-flow mixing technique allows analytical data to be acquired within 5 s after the reactants are mixed, thereby minimizing manipulation and enabling ready application of the proposed method to routine analyses for tetracycline in serum samples. The calibration graph was linear over the range 20–1000 ng ml⁻¹, but can be expanded up to 10000 ng ml⁻¹ by increasing the reagent concentrations. The within- and between-assay relative standard deviations were close to 1%. The mean recovery obtained in the analysis of serum samples was 98.8%.

Key words: Fluorimetry; Kinetic methods; Energy-transfer processes; Europium; Serum; Stopped-flow technique; Tetracycline

1. Introduction

The intramolecular energy-transfer process from tetracycline to europium ions has been widely studied and used for the determination of the antibiotic [1,2], with a very low detection limit (10 ng ml⁻¹). Tetracycline excited at 392 nm undergoes intersystem crossing to its triplet state and the associated energy is transferred to the 4f

level of the europium ion, which yields a characteristic line-type emission at 612 nm. Analytical methods for tetracycline based on this system have also been developed by using liquid chromatography (LC) and flow-injection analysis [3]. Recently, Georges and Ghazarian [4] reported that the sensitivity can be increased by adding Triton X-100 to the aqueous solution. The detection limit thus obtained is ca. three-fold lower than that obtained in the absence of micelles. The positive effect of surfactants on the fluorescence of lanthanide chelates is well known [5]. The micellar environment cancels the quenching

* Corresponding author.

of coordinated water molecules, which tend to create an efficient deactivation route. Also, the non-aqueous environment provided by the surfactant protects the chelate against non-radiative processes. Although these chelates usually fluoresce maximally at a surfactant concentration above its critical micelle concentration (c.m.c.), some of them only require the formation of submicellar aggregates.

Analytical methodologies involving the formation of lanthanide chelates and decay time measurements have been widely used in time-resolved fluorescence spectroscopy, particularly in immunoassays [6]. However, formation rate measurements of these lanthanide chelates have scarcely been used for analytical purposes [7]. Because the Eu(III)–tetracycline system provides a very low detection limit for tetracycline, we choose to use it in this work with the aim of extending the scope of application of kinetic methodology to systems involving energy-transfer processes. Use of the stopped-flow mixing technique is essential here in order to obtain kinetic data for this system since the formation rate of the chelate is very high, so it cannot be determined by the batch technique. Moreover, this approach allows the method to be automated for routine analyses, which is quite an interesting advantage over the equilibrium method.

Only two kinetic methods for the determination of tetracycline have previously been reported. One is based on the inhibitory effect of tetracycline on the Mo(VI)-catalysed oxidation of Azorubin S by hydrogen peroxide [8], with a linear calibration graph over the range 18–160 $\mu\text{g ml}^{-1}$. The other is based on measurements of the rate of degradation of tetracycline to its anhydrous derivative [9]; the linear dynamic range for this method is 0.8–4.0 mg%. The high determination levels of these methods led us to develop a sensitive, kinetic, automatic alternative for the determination of tetracycline.

The tetracycline molecule contains several sites at which chelation with metal cations is possible of which the β -diketone group is the most important portion; through it, tetracycline can act as a bidentate ligand to form six-membered rings with metal ions. Since the stoichiometry of the

Eu(III)–tetracycline chelate is reportedly 1 : 1 [1,4] and europium ion has nine available coordination sites [10], water molecules can be admitted into the coordination sphere of the ion, which is deleterious to europium emission. Water molecules can be displaced from the chelate either by using a surfactant, as stated above, or by adding a second ligand to displace water molecules from the ligand field. The formation of ternary lanthanide complexes has been widely studied and used for analytical purposes (e.g. the determination of lanthanide ions [11,12] and time-resolved fluoroimmunoassays [5]). One of the ligands is usually a β -diketone, which absorbs the excitation light and efficiently transfers the energy to the chelated ion, whereas the second ligand has a merely synergistic effect (it removes water molecules from the coordination sphere of the lanthanide ion). Thenoyltrifluoroacetone (TTA) is the most commonly used β -diketone in this respect, as are 1,10-phenanthroline (phen) and trioctylphosphine oxide as synergistic ligands.

In this work, the Eu(III)–tetracycline–TTA system was studied in the presence of Triton X-100 for two main purposes: (1) to determine the kinetic behaviour of the system and develop a fast, simple, automatic method for tetracycline determination by kinetic methodology with the aid of the stopped-flow mixing technique and (2) to improve the sensitivity of previous equilibrium methods for tetracycline determination involving energy transfer by using a ternary complex formation reaction and a micellar medium.

2. Experimental

2.1. Instrumentation

A Hitachi F-2000 fluorescence spectrophotometer fitted with a stopped-flow module [13] supplied by Quimi-Sur Instrumentation was used. The module, furnished with an observation cell of 1 cm path length, was controlled by the associated electronics and an Ataió 640 microcomputer running a linear regression program for application of the initial-rate method. The solutions in the stopped-flow module and cell compartment

were thermostated by means of a circulating water-bath.

2.2. Reagents

All chemicals used were of analytical-reagent grade. A standard solution of tetracycline (2×10^{-4} M) was made by dissolving the appropriate amount of its hydrochloride salt (Sigma) in distilled water. A stock aqueous solution of europium (10^{-3} M) was prepared from europium (III) nitrate pentahydrate (Aldrich). A 4.5×10^{-3} M solution of thenoyltrifluoroacetone (TTA) (Sigma) was prepared by dissolving the appropriate amount of reagent in the minimum volume of ethanol and making up to volume with distilled water. Finally, a 0.1% Triton X-100 (Serva) aqueous solution and a Tris [tris(hydroxymethyl)aminomethane] buffer solution (0.1 M, pH 7.4) were also used.

2.3. Procedure

Two solutions (A and B) were used to fill the two 2-ml drive syringes of the stopped-flow module. Solution A contained TTA (5.4×10^{-6} M), europium(III) (2×10^{-5} M) and tris buffer (10^{-2} M). Solution B contained tetracycline at a final concentration between 20 and 1000 ng ml⁻¹, Triton X-100 (0.01%) and Tris buffer (10^{-2} M). In each run, 0.15 ml of each solution was mixed in the mixing chamber and the variation of the fluorescence intensity throughout the reaction was monitored at $\lambda_{\text{ex}} = 342$ nm and $\lambda_{\text{em}} = 612$ nm. Fluorescence values were obtained for 10–15 s and processed by the microcomputer, furnished with a linear-regression program for application of the initial-rate method. The reaction rate was determined in ca. 5 s and each sample was assayed in triplicate. All measurements were made at 30°C. The blank signal was found to be negligible.

2.4. Determination of tetracycline added to serum

No sample pretreatment was required for these analyses. Serum samples were spiked with appropriate amounts of tetracycline to obtain a final

concentration of the antibiotic within the therapeutic range (1–5 $\mu\text{g ml}^{-1}$). Each determination was carried out by using 0.4 ml of sample and treating it as described above. The concentration of tetracycline in the samples was determined by interpolation on the calibration graphs constructed by adding 0.4 ml of a previously prepared serum pool to each tetracycline standard. The graph was linear over the range 0.050–1.0 $\mu\text{g ml}^{-1}$.

3. Results and discussion

As shown elsewhere [1], tetracycline forms a very stable 1:1 complex with Eu(III) that gives rise to an intensely fluorescent signal ($\lambda_{\text{ex}} = 392$, $\lambda_{\text{em}} = 612$ nm) as a result of energy transfer from tetracycline to europium ion. At europium concentrations above the stoichiometric ratio, the fluorescence intensity decreases owing to the quenching effect of the excess probe ion. However, in the presence of excess Triton X-100 (1%), such a quenching effect is changed into an enhancing effect [4]: micelles shelter the chelate from free europium ions in the aqueous phase. While the excitation wavelength does not change, the emission peak is higher than in the absence of surfactant. This enhances the sensitivity of tetracycline determination. Adding a second ligand such as TTA to the Eu(III)–tetracycline system in the absence of surfactant results in no change in its fluorescence. However, if Triton X-100 is added together with TTA, the results are rather different, as can be seen in Fig. 1, which compares the excitation and emission spectra obtained under such conditions with those recorded under optimal conditions in previous work [2,4]. The band at 392 nm in the excitation spectrum, characteristic of tetracycline excitation, overlaps with a shoulder at ca. 375 nm and a very tall peak at 342 nm. Excitation at this wavelength gives rise to an emission intensity at 612 nm (curve 4') that is ca. 30 times higher than that obtained for tetracycline in the presence of Eu(III) alone (curve 1') and ca. 5 times higher than that for the system in the presence of Triton X-100 (curve 2'), with excitation at 392 nm in both cases. The

excitation band at 342 nm, the intensity of which depends on the tetracycline concentration, suggests an interaction between TTA and tetracycline which only takes place when Triton X-100 is present in the solution at a suitable concentration that is given below. As shown elsewhere [14], Eu(III) forms ternary complexes with TTA and some substituted ammonium cations and neutral ligands such as 1,10-phenanthroline. Thus, the Eu(III)–TTA–phen system in the presence of Triton X-100 exhibits maximum excitation and emission wavelengths at 371 and 612 nm, respectively, and its stoichiometry is 1:3:1 [15]. Although TTA is assumed to be the species which undergoes excitation and transfers its energy to Eu(III), the presence of the second ligand is essential in order to obtain the fluorescent signal at 612 nm [14]. Similarly, the Eu(III)–tetracycline–TTA system studied here provided no fluorescent signal in the absence of tetracycline at $\lambda_{\text{ex}} = 342 \text{ nm}$, which shows that a ternary complex needs to be formed. As both ligands are β -diketones in this case, the excitation at this wavelength can be attributed to a different arrange-

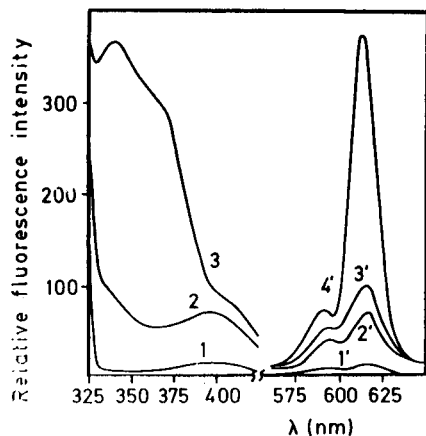


Fig. 1. Excitation (1–3) and emission (1'–4') spectra for the Eu(III)–tetracycline system in the absence (1,1') and presence of Triton X-100 (2,2') and TTA + Triton X-100 (3,3',4'). All excitation spectra were obtained at $\lambda_{\text{em}} = 612 \text{ nm}$. λ_{ex} was 392 nm for emission spectra 1'–3' and 342 nm for 4'. [Tetracycline] = $1 \mu\text{g ml}^{-1}$. [Eu(III)] = $3.3 \times 10^{-4} \text{ M}$ (curves 1,1'), $2.5 \times 10^{-5} \text{ M}$ (curves 2,2') and 10^{-4} M (curves 3,3',4'). [Triton X-100] = 1% (curves 2,2') and 0.01% (curves 3,3',4'). [TTA] = $2.7 \times 10^{-5} \text{ M}$ (curves 3,3',4').

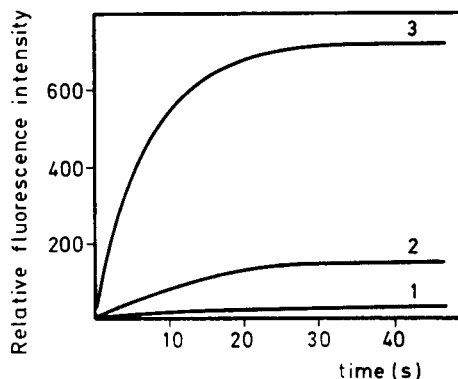


Fig. 2. Kinetic curves obtained for: (1) Eu(III) + tetracycline, (2) Eu(III) + tetracycline + 1% Triton X-100, (3) Eu(III) + tetracycline + TTA + 0.01% Triton X-100. [Tetracycline] = $1 \mu\text{g ml}^{-1}$. [Eu(III)] = $6.6 \times 10^{-4} \text{ M}$ (curve 1), $5 \times 10^{-5} \text{ M}$ (curve 2) and $2 \times 10^{-4} \text{ M}$ (curve 3). [TTA] = $5.4 \times 10^{-5} \text{ M}$ (curve 3).

ment and orientation of the ligand molecules in the ternary complex when the surfactant is present. Several assays were carried out in order to determine the stoichiometry of the Eu(III)–tetracycline–TTA fluorescent system, which was found to be 1:1:3 and hence similar to that reported for the Eu(III)–TTA–phen system.

In order to apply kinetic methodology to the proposed fluorescent system by using the stopped-flow mixing technique, the distribution of the reactants between the two syringes of the module was first studied and the following conclusions were drawn: (1) The best results were obtained by placing Eu(III) and TTA in one syringe and tetracycline plus Triton X-100 in the other, with which the reaction rate of the blank solution was negligible. (2) Placing tetracycline and TTA in a syringe and Eu(III) alone in the other, resulted in very poor reproducibility of the kinetic curves and a non-linear relation between the reaction rate and the tetracycline concentration. Fig. 2 shows the kinetic curves obtained for the Eu(III)–tetracycline system in the absence and presence of TTA and Triton X-100. While the reaction rate was very low in the first case (curve 1), the rate in the presence of TTA and surfactant (curve 3) was ca. 10 times higher than that obtained in the absence of TTA (curve 2). These results show that the combined use of TTA

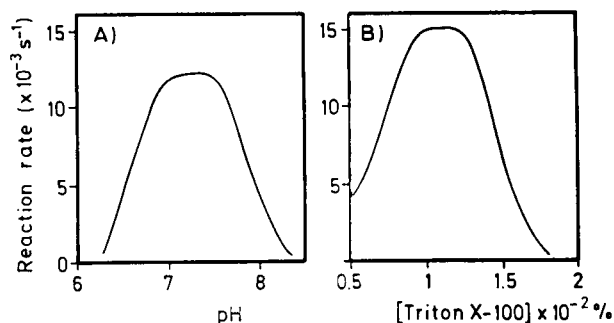


Fig. 3. Effect of pH (A) and the Triton X-100 concentration (B) on the Eu(III)–tetracycline–TTA system.

and Triton X-100 significantly increases the complex formation rate, so kinetic methodology implemented by means of the stopped-flow mixing technique is suitable for this system.

3.1. Effect of variables

Variables affecting the performance of the proposed kinetic method for the determination of tetracycline were optimized by the univariate method. All stated concentrations are initial concentrations in the syringes (twice the actual concentrations in the reaction mixture at time zero after mixing). Each kinetic result was the mean of three measurements.

The effect of pH on the system is shown in Fig. 3A. The maximum fluorescence intensity was obtained at pH 8.0–9.0 in the absence of TTA and Triton X-100 [1], at pH 7.0–8.5 in the presence of the surfactant [4] and at pH 7.0–7.5 in the presence of both TTA and Triton X-100, which also resulted in the maximum reaction rate. A Tris buffer of pH 7.5 was chosen to adjust the sample pH. The optimum buffer concentration was in the range 8×10^{-3} – 1.5×10^{-2} M.

The Eu(III) and TTA concentrations were found to have a critical effect on the reaction rate of the system as their optimum values were dependent on the tetracycline concentration in the solution. A similar influence was previously reported for the Eu(III) concentration in equilibrium methods: the optimum analytical signal in the absence of TTA and surfactant was obtained at an Eu(III)–tetracycline ratio of 1 : 1 [1], whereas

the maximum signal in the presence of Triton X-100 was reached at a ratio of 1:6 for an analyte concentration of 10^{-5} M and 1:20 for 10^{-6} M [4]. The increased optimum Eu(III) concentration in the presence of the surfactant can be ascribed to the micellar environment, which prevents the complex from colliding with free Eu(III) ions and favours energy transfer between the complex and free ions. We thus assayed various tetracycline concentrations and found 2×10^{-5} M Eu(III) and 5.4×10^{-6} M TTA to result in a good linear relationship between the reaction rate and tetracycline concentration. Fig. 3B shows the effect of the Triton X-100 concentration on the system. The reaction rate was independent of this variable over the range 1.00×10^{-2} – $1.25 \times 10^{-2} \%$. Below this range the blank signal was negligible, but above, the reaction rate of the blank solution increased with increasing surfactant concentration; thus, at $2.0 \times 10^{-2} \%$ (twice that in the reaction mixture), the reaction rate of the blank was the same as that of the sample. Therefore, increased surfactant concentrations favour the interaction between TTA and Eu(III) and hence the energy-transfer process, and cancels the effect of the tetracycline. With regard to the temperature, the reaction rate was maximal and independent of this variable over the range 30–35°C.

3.2. Figures of merit

In order to determine to which extent the presence of TTA can enhance the sensitivity of equilibrium methods for tetracycline determination [1,4], equilibrium measurements on solutions prepared under the above-described optimum conditions and containing different tetracycline concentrations (batch technique) were made. The equation obtained for the calibration graph was $I_F = 1.09 [\text{tetracycline (ng ml}^{-1})] - 1.2$, with a Pearson's correlation coefficient $r = 0.997$ ($n = 6$). The equation for the calibration graph in the absence of TTA and surfactant [1] obtained by using the same instrument was $I_F = 0.36 [\text{tetracycline (ng ml}^{-1})] + 0.5$, with $r = 0.998$ ($n = 6$). The detection limit, as defined by IUPAC [16] was 1.4 ng ml^{-1} in the former case and 3.2 ng

ml⁻¹ in the latter. Similarly, the slope of the calibration graph obtained in the presence of Triton X-100 and absence of TTA [4] was 2.6-times lower than that obtained under our working conditions. These results show that the presence of TTA significantly improves the sensitivity of the equilibrium determinations.

The kinetic curves obtained at different tetracycline concentrations by using the above-described procedure, were processed by the initial-rate method. The calibration graph was linear over the range 20–1000 ng ml⁻¹ and conformed to the equation $v \text{ (s}^{-1}\text{)} = 7.0 \times 10^{-5} [\text{tetracycline (ng ml}^{-1}\text{)}] - 3.4 \times 10^{-3}$, with $r = 0.996$ ($n = 6$). By increasing the TTA and Eu(III) concentration 10 times (5.4×10^{-5} M and 2×10^{-4} M, respectively) the linear range can be expanded to 10 $\mu\text{g ml}^{-1}$. Unlike the equilibrium methods, where all measurements need to be corrected for the blank background fluorescence, the blank signal is negligible in the kinetic method. The detection limit was 6.5 ng ml⁻¹, which is higher than that afforded by the equilibrium method [4]. This can be ascribed to the nature of the stopped-flow mixing technique, where the analyte concentration in the reaction mixture is half that in the initial sample held in the syringe; also, because of the way the observation cell is arranged, the portion of exciting radiation which impinges on the sample solution is smaller than with a conventional cell. However, the stopped-flow mixing technique offers some advantages such as reduced reactants manipulation and the ability to make measurements shortly after mixing (a mere 5 s is needed to obtain analytical data, which facilitates automation of the method).

The calibration data and detection limit given for the kinetic method were obtained by using standards prepared in water, similarly as in the equilibrium methods. The slope of the calibration graph decreased by ca. 30% on addition of 0.4 ml of a previously prepared serum pool to each tetracycline standard. Under these conditions, the detection and quantification limits of the kinetic method in the presence of serum matrix were increased to 15 and 50 ng ml⁻¹, respectively. However, these concentrations are low enough for tetracycline to be determinable at its thera-

Table 1
Recovery of tetracycline added to serum samples

Sample	Tetracycline ($\mu\text{g ml}^{-1}$)		Recovery (%)
	Added	Found ^a	
1	2.5	2.75	110
	5	4.57	91.4
	10	9.20	92
2	2.5	2.47	98.8
	5	4.97	99.4
	10	10.3	103.0
3	2.5	2.35	94
	5	4.91	98.1
	10	10.3	103.0

^a Average of three determinations.

peutic levels in serum (1–5 $\mu\text{g ml}^{-1}$).

The precision of the proposed method was evaluated by assaying replicates of serum samples containing 2 $\mu\text{g ml}^{-1}$ tetracycline. The within-day relative standard deviation ($n = 10$) was 0.9% and the between-day relative standard deviation 1.1% ($n = 5$). The selectivity of the method was studied by assaying several antibiotics. None of the penicillins (ampicillin, amoxycillin, cloxacillin and dicloxacillin) or cephalosporins tested (cephradin, cephalexin and cephaloridin) interfered with the determination of tetracycline at least at concentrations 5 times higher than that of the analyte. However, other tetracyclines such as oxytetracycline, chlortetracycline and doxycycline interfered at the same concentration level as the analyte.

3.3. Analysis of serum samples

The proposed kinetic method was applied to the determination of tetracycline in three spiked human serum samples: a volume of 0.4 ml was analysed with no pretreatment (precipitation of serum proteins was not required). Table 1 summarizes the results and analytical recoveries obtained. The mean recovery was 98.8%.

4. Conclusions

The results obtained in the equilibrium and kinetic study of the effect of TTA on the

Eu(III)–tetracycline system in the presence of Triton X-100 reveals that: (1) the sensitivity of the equilibrium method for tetracycline is significantly increased, and (2) application of kinetic methodology to this system, via the stopped-flow mixing technique allows the method to be automated, thereby avoiding the need for blank background fluorescence corrections and providing analytical results within a few seconds. One other inference is that kinetic methodology can be applied to complex-formation reactions involving energy-transfer processes, which has so far been scarcely explored for analytical purposes.

Acknowledgement

The authors acknowledge financial support from the CICyT (Grant No. PB91-0840).

References

- [1] L.M. Hirschy, E.V. Dose and J.D. Winefordner, *Anal. Chim. Acta*, 147 (1983) 311.
- [2] L.A. Files, L. Hirschy and J.D. Winefordner, *J. Pharm. Biomed. Anal.*, 3 (1985) 95.
- [3] T.J. Wenzel, L.M. Collette, D.T. Dahlen, S.M. Hendrickson and L.W. Yarmaloff, *J. Chromatogr.*, 433 (1988) 149.
- [4] J. Georges and S. Ghazarian, *Anal. Chim. Acta*, 276 (1993) 401.
- [5] X.Y. Xu, I.A. Hemmilä and T.N.E. Lövgren, *Analyst*, 117 (1992) 1061.
- [6] E. Soini and H. Kojola, *Clin. Chem.*, 29 (1983) 65.
- [7] S. Panadero, A. Gómez-Hens and D. Pérez-Bendito, *Anal. Chim. Acta*, 280 (1993) 163.
- [8] M.A.F. Sekheta, G.A. Milovanovic and T.J. Tomislav, *Glas. Hem. Drus. Beograd*, 44 (1979) 447.
- [9] M.A.H. El-Sayed, M.H. Barary and H. Mahgoub, *Anal. Lett.*, 18 (1985) 1357.
- [10] C.C. Bryden and C.N. Reilley, *Anal. Chem.*, 54 (1982) 610.
- [11] M. Morin, R. Bador and H. Dechaud, *Anal. Chim. Acta*, 219 (1989) 67.
- [12] G. Zhu, Z. Si, P. Liu and W. Jiang, *Anal. Chim. Acta*, 247 (1991) 37.
- [13] A. Loriguillo, M. Silva and D. Pérez-Bendito, *Anal. Chim. Acta*, 199 (1987) 29.
- [14] Z.K. Si, G.Y. Zhu and J. Li, *Analyst*, 116 (1991) 309.
- [15] J.H. Yang, G.Y. Zhu and B. Wu, *Anal. Chim. Acta*, 198 (1987) 287.
- [16] G.L. Long and J.D. Winefordner, *Anal. Chem.*, 55 (1983) 712A.

Towards a quantitative determination of retinoids complexed to cyclodextrin: the diphenyl polyene model

J.-C. Guilleux, K.N. Barnouin, D.A. Lerner *

Laboratoire de Chimie Physique et Informatique, Ecole Nationale Supérieure de Chimie, 8 Rue de l'Ecole Normale, 34053 Montpellier Cédex 1, France

(Received 12th May 1993; revised manuscript received 13th January 1994)

Abstract

Retinoids are prone to oxidation or isomerization and are therefore difficult to quantify in complex media. It is expected that their inclusion in cyclodextrins would increase their stability and maintain or improve their emission properties. It seems then that such complexed retinoids would lend themselves to a better quantification. A methodology has been developed with 1,6-diphenyl-1,3,5-hexatriene (DPH), a model molecule for retinoids, to follow the formation of the complex. The latter is insoluble in cold water and soluble in acetonitrile–water (1:3, v/v) mixtures. The complexes were detected by fluorescence on thin-layer chromatography plates. Free DPH and the inclusion complex are so well separated that the quantification of the unbound molecule was carried out without interference by means of a charge-coupled device camera. Differences in the absorbances of the free and totally solubilized DPH are used to determine the quantity of included DPH. Preliminary kinetic studies suggest that the oxidation or isomerization of DPH is decreased in the inclusion complex.

Key words: Fluorimetry; UV–Visible spectrophotometry; Cyclodextrins; Inclusion complexes; Retinoids; 1,6-Diphenyl-1,3,5-hexatriene

1. Introduction

Vitamin A is especially known for its anticancerous properties and for its role as a visual pigment. However, molecules of this family are easily oxidized and isomerized. These properties render their quantification in complex media difficult. It is expected that complexation of retinoids with cyclodextrins would increase their stability and maintain their emission properties. Such

complexed retinoids would then be more easily quantified.

Cyclodextrins are cyclic oligosaccharides belonging to a class of sugars also known as Schardinger dextrans. These sugars are degradation products produced by the bacterium *Bacillus macerans* [1]. They are generally composed of 6, 7, or 8 D-glucose units linked by α -1,4 glycosidic bonds and are respectively named α -, β -, and γ -cyclodextrin.

The cyclic form of cyclodextrin and its partially hydrophobic interior and hydrophilic exterior have many uses. In pharmaceuticals it can be used to include hydrophobic drugs such as retinoic

* Corresponding author.

acid to increase their bioavailability [2]. In chemistry, cyclodextrins are used as catalysts [3] and as separating agents in chromatography [4].

β -Cyclodextrin (BCD) was chosen instead of the α - or γ -oligomer for several reasons. α -Cyclodextrin is more strained and less flexible than the β -conformer. Although the cavity of γ -cyclodextrin is larger than that of β -cyclodextrin, the inclusion driving force for the guest molecules obtained by water expulsion from their cavities is greater for β - than for γ -cyclodextrin. Complex formation with BCD is therefore thermodynamically more favourable. Thus, BCD's structure allows a deeper penetration and a better inclusion of the guest molecule [5].

1,6-Diphenyl-1,3,5-hexatriene (DPH), a fluorescent probe used to monitor membrane dynamics [6], is a symmetrical, fluorescent molecule. As it is more stable than retinoids and bears some similarity with the latter (presence of a conjugated chain ending in a six-membered ring and almost the same size as retinol), DPH was chosen for the development of a method to quantify these molecules.

Since DPH is poorly soluble in water, it should be attracted to the hydrophobic cavity of cyclodextrins. Complexation of these two molecules should therefore be energetically favourable. However, our attempts to complex these two molecules via solubilization (using water as solvent and a DPH film) or a solid grinding method were unsuccessful. A second water-miscible solvent, acetonitrile, which dissolves DPH better (solubility ≈ 0.56 g/l CH_3CN at 20°C), was chosen to increase DPH's solubility in a predominantly aqueous environment.

UV-visible electronic absorption spectrometry, thermogravimetric analysis and thin-layer chromatography (TLC) were used to detect the formation of DPH-BCD complexes.

2. Experimental

2.1. Solubilization procedure

All solubilization techniques used are based on those described by Higuchi and O'Connors [7].

In all the following experiments purified Roquette β -cyclodextrin, Lancaster 1,6-diphenyl-1,3,5-hexatriene, SDSTM 99.5% acetonitrile and trice distilled water were used.

Acetonitrile-water (25:75, w/w) solvent. 3 ml of 0.4×10^{-2} , 0.8×10^{-2} , 1.2×10^{-2} , 1.6×10^{-2} and 2.0×10^{-2} mol/l BCD in $\text{CH}_3\text{CN-H}_2\text{O}$ (25:75, w/w) were added to 10 mg solid DPH. One control consisted of 2.0×10^{-2} mol/l β -cyclodextrin only. A second control contained 10 mg DPH in 3 ml $\text{CH}_3\text{CN-H}_2\text{O}$ (25:75, w/w) only. The flasks were sealed, protected from light and agitated at 60°C for 48 h in a thermally controlled shaker. All samples contained excess solid DPH which was filtered off without cooling with a Millipore filter holder and filter paper (Ederol no. 4) prior to analysis by UV electronic absorption or TLC coupled to fluorescence.

Acetonitrile-water (38:62, w/w) solvent. Samples with the same concentrations of BCD as above were prepared in $\text{CH}_3\text{CN-H}_2\text{O}$ (38:62, w/w) and treated as above. The increase in acetonitrile content in this mixture represents a 50% increase as compared to the set using 25:75 (w/w) acetonitrile-water as solvent.

2.2. Crystallization

In view of analysis by thermogravimetric methods (TGA) the sample containing 2×10^{-2} mol/l BCD was prepared again in larger quantities but under the same conditions as for the solubilization of DPH with 38:62 (w/w) $\text{CH}_3\text{CN-H}_2\text{O}$. 40 ml of a solution containing 2×10^{-2} mol/l BCD in 38:62 (w/w) $\text{CH}_3\text{CN-H}_2\text{O}$ with 30 mg DPH were agitated in the dark at 60°C for 48 h. The unsolubilized DPH was then filtered off and the filtrates were set to crystallize at 0°C for 24 h.

The crystals were separated from the solvent and left to dry for 24 h in air in a dark room. They gave, when deposited on a quartz slide, a fluorescence typical of DPH. Part of these crystals were analysed by TGA. The remaining crystals were resuspended in pure cold water to determine whether they were soluble in water or not. They were found to be soluble in water at 60°C . The solution thus obtained was cooled to 0°C and the resulting crystals were separated

from the water, left to dry in air in a dark room and analysed by TGA. This last recrystallization also ensured that no acetonitrile was left in the samples.

2.3. Analytical techniques

2.3.1. Electronic absorption spectrophotometry

Absorption spectra were measured with a Pye Unicam SP8-400 UV–visible double-beam spectrophotometer in 10-mm quartz cells. The reference was the solvent mixture used in each set.

2.3.2. Thin-layer chromatography

The following experiment was performed in a dark room.

Merck Art. 5553 silica gel TLC plates (0.2 mm thickness) without fluorescent indicator were activated 5 min at 105°C. The TLC plates were spotted with 1 μ l (Nichiryo capillary pipette) of the samples in 25:75 or 38:62 (w/w) acetonitrile–water kept at 60°C. They were eluted with hexane–ether–ethanol (95:5:1, v/v/v). This eluent allows the visualization of separate free and complexed DPH since the complex remains at $R_f = 0$. A second eluent, isobutanol–water–acetic acid (12:5:3, v/v/v) used on a separate plate, was chosen to completely dissociate complexed DPH molecules from their cyclodextrin

hosts. Here only BCD remains at $R_f = 0$. After elution, all the plates were left to dry in air for 3 min at room temperature and were immediately observed with a Camag TLC illuminator cabinet with excitation at 366 nm.

Since little DPH was solubilized by BCD and $\text{CH}_3\text{CN}-\text{H}_2\text{O}$, the free form was quantified by comparison with standards consisting of 20, 50, 80 and 100 pmol DPH entirely dissolved in pure CH_3CN . A Sony 705 charge-coupled device (CCD) camera was used to quantify and record the results. The TLC plates were filmed through two superimposed 400-nm (Corning 3-72) and 420-nm (Corning 3-73) cut-off filters. The filmed data was transferred onto a compatible 486 PC computer by means of a Vitec Videomaker card. The data were first converted to 8 bit and 256 indexed grey scale images. The latter were then transformed with the Floyd–Sternberg algorithm into 2-bit images which conserve light energy. The densities of the spots were then determined with a computer program written by one of us. This program also enables the subtraction of background light from the spots to obtain a more accurate quantification.

2.3.3. Thermogravimetric analysis

Purified Roquette β -cyclodextrin crystals, and solids separated from 38:62 (w/w) acetonitrile–

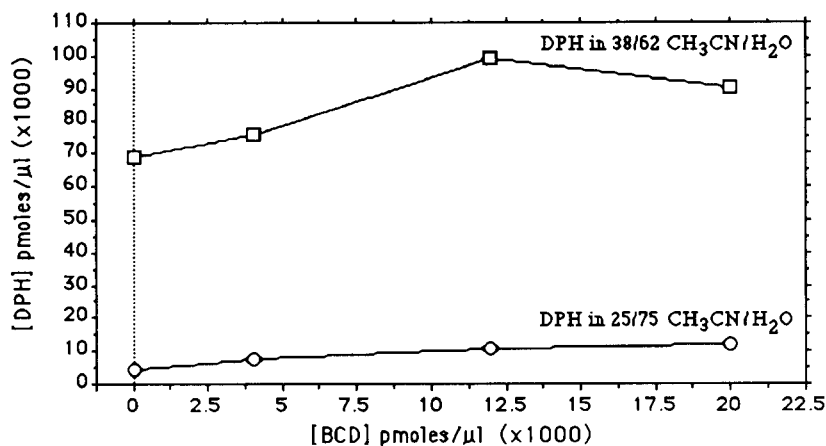


Fig. 1. Solubility curves of the total amount of DPH solubilized by BCD in the 25:75 and 38:62 (w/w) $\text{CH}_3\text{CN}-\text{H}_2\text{O}$ solvent systems. Application of Beer's law and DPH's molar absorptivity in $\text{CH}_3\text{CN}-\text{H}_2\text{O}$ of 66400 was used to determine the concentration of solubilized DPH in each sample.

water and from water were analysed by thermogravimetric methods. All samples were heated up to total combustion (900°C) at the rate of 300°C/h. The thermogravimetric analyses were performed with either a Setaram Model TG and a Setaram B85 weighing balance or with a setup assembled in the laboratory. This setup consists of a Mettler AC100 balance and a Eurotherm 818 regulator piloted by an AT286 computer using a program written by one of us.

3. Results and discussion

3.1. Electronic absorption spectrophotometry

A molar absorptivity of 66 400 at 355 nm was found for DPH in both 38:62 and 25:75 (w/w) CH₃CN–H₂O solutions. It was used to determine the concentration of solubilized DPH in each sample. Data for totally solubilized DPH in both solvent mixtures plotted versus BCD concentrations is summarized in Fig. 1. The solubility of DPH in the 25:75 (w/w) acetonitrile–water solvent system slightly increases with increasing concentrations of BCD. In the 38:62 (w/w) acetonitrile–water solvent system the increase in the solubility of DPH with augmenting BCD concentrations is more pronounced.

In the presence of BCD in solution, an equilibrium of DPH should be established as schematically represented by the following equation:



The most probable value for n is 1 or 2. However, in solution, no detectable difference between the free or complexed form was found in the UV electronic absorption spectra of DPH. It was then expected that by using thin-layer chromatography, the presence of the two separate forms could be established and their respective amounts quantified.

3.2. Thin-layer chromatography

3.2.1. General observations

Isobutanol–water–acetic acid (12:5:3, v/v/v). This eluent dissociates any complex present

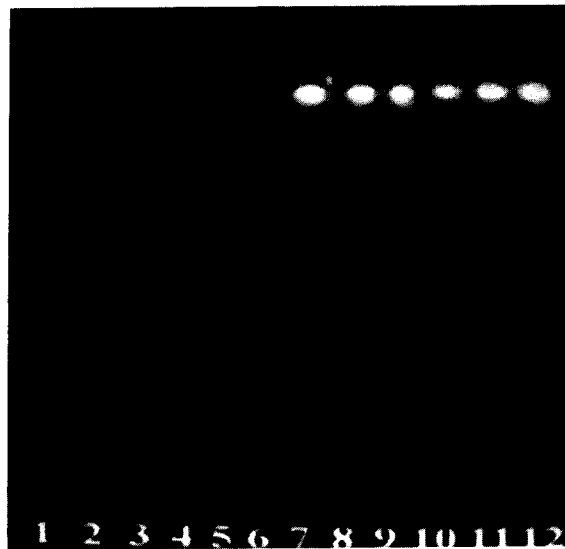


Fig. 2. Reproduction of CCD filmed view of TLC plates eluted with isobutanol–water–acetic acid (12:5:3, v/v/v). (1) BCD in acetonitrile–water (25:75, w/w). (2) BCD in acetonitrile–water (38:62, w/w). (3) DPH in acetonitrile–water (25:75, w/w). (4) DPH + 4×10^3 pmol BCD in acetonitrile–water (25:75, w/w). (5) DPH + 12×10^3 pmol BCD in acetonitrile–water (25:75, w/w). (6) DPH + 20×10^3 pmol BCD in acetonitrile–water (25:75, w/w). (7) DPH + 4×10^3 pmol BCD in acetonitrile–water (38:62, w/w). (8) DPH + 12×10^3 pmol BCD in acetonitrile–water (38:62, w/w). (9) DPH + 20×10^3 pmol BCD in acetonitrile–water (38:62, w/w). (10) 50 pmol DPH standard. (11) 80 pmol standard. (12) 100 pmol standard. All DPH standards are in pure acetonitrile.

and induces all DPH molecules to migrate at an R_f value of 0.8 (Fig. 2). So it can be used to quantify the total solubilized DPH. On heating the plate, BCD becomes carbonized and its location at the start becomes apparent.

Hexane–ether–ethanol (95:5:1, v/v/v). This eluent induces DPH standards in pure acetonitrile as well as free DPH from the sample under study to migrate at an R_f value of 0.5 where it leaves a fluorescing spot. Samples of DPH with increasing BCD concentrations leave spots of increasing fluorescence intensity at the start. This eluent does not dissociate the DPH–BCD complex and allows the quantification of the free form of DPH (Fig. 3). Attention should be paid to the fact that even if complexed DPH is separated from the free form of DPH, it cannot be

directly quantified since the quantum yield of emission of the bound form may be very different from that of the complexed one. It is well known that many flexible fluorescent molecules show an increase in fluorescence following binding to a solid, a large molecule or by inclusion. The explanation lies in the fact that in the bound species vibrational or torsional modes are hindered and a greater planarity is obtained. This lowers the efficiency of deactivation of their emitting state [8]. One such example relevant to our study concerns cyclodextrin spray reagents. The latter cause fluorescence enhancements on solid supports in the densitometric analysis of polycyclic aromatic hydrocarbons [9]. The eluted fluorescent spots of free DPH from both 25:75 and 38:62 (w/w) acetonitrile–water solvents (at R_f 0.5) display intensities which change in opposite directions with the increase in BCD. In the 25:75 solvent mixtures the emission intensities increase and in the 38:62 solvent mixtures they decrease. BCD alone in both solvent mixtures does not fluoresce (Fig. 3).

Results from the TLC studies referred to above point to the existence of a complex which must be bound by Van der Waals forces. They show also that the complexation between DPH and BCD is maintained in non-polar environments such as in hexane–ether mixtures and that the complex is dissociated in polar mixtures like isobutanol–acetic acid–water mixtures.

At this stage nothing can be said about the stoichiometry of the complex. The presence of the cosolvent may even lead to the formation of a ternary complex in which DPH could be included together with one or more acetonitrile molecules. Complexes of this type have been described before [10].

3.2.2. Densitometry study of the spots

Two problems prevent a precise quantification of solubilized DPH. First, the CCD detector is rapidly saturated with increasing fluorescence intensity of the spots. DPH's emission intensity on the TLC plates depends on the quantity spotted and on its diffusion on the plate [11]. The satura-

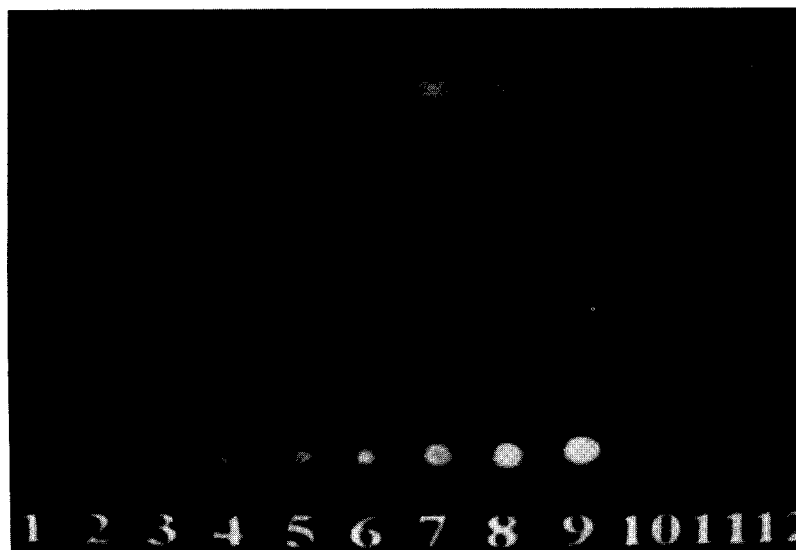


Fig. 3. Reproduction of a CCD view of a TLC plate eluted with hexane–ether–ethanol (95:5:1, v/v/v). (1) BCD in acetonitrile–water (25:75, w/w). (2) BCD in acetonitrile–water (38:62, w/w). (3) DPH in acetonitrile–water (25:75, w/w). (4) DPH + 4×10^3 pmol BCD in acetonitrile–water (25:75, w/w). (5) DPH + 12×10^3 pmol BCD in acetonitrile–water (25:75, w/w). (6) DPH + 20×10^3 pmol BCD in acetonitrile–water (25:75, w/w). (7) DPH + 4×10^3 pmol BCD in acetonitrile–water (38:62, w/w). (8) DPH + 12×10^3 pmol BCD in acetonitrile–water (38:62, w/w). (9) DPH + 20×10^3 pmol BCD in acetonitrile–water (38:62, w/w). (10) 50 pmol DPH standard. (11) 80 pmol standard. (12) 100 pmol standard. All DPH standards are in pure acetonitrile.

tion effect is further demonstrated by the data which were transferred to the computer and by the pixel representations of the spots. The analysed data show that signals due to the non-eluted spots containing high concentrations of DPH and to DPH eluted by isobutanol–water–acetic acid (12:5:3, v/v/v) are over-saturated and hinder the quantification of complexed DPH. On the other hand, DPH in free form from the samples prepared in the 38:62 acetonitrile–water solvent is present on the plates in quantifiable amounts. Secondly, samples with too low amounts of DPH (as free DPH from 25:75 acetonitrile–water samples) gave visually detectable fluorescence signals which could not be quantified because the signal-to-noise ratio was too low. It was also observed that TLC plates give a background emission under UV excitation which contributes to the overall noise and lowers the dynamic range.

Plates eluted with hexane–ether–ethanol. The amounts of free DPH were determined by comparison with DPH standards of 0, 50, 80 and 100 pmol spotted on the TLC plates. The points taken from Fig. 3 for the standards fit on a regression line determined with four points where

the slope is 0.484 ± 0.051 , the correlation coefficient 0.966, and the intercept, -4.02 ± 4 . It must be noted that the standards must be on the same plate as the other samples and that each regression, although similar to others, is unique for each plate. This limits the space available on each TLC plate and consequently the number of standards and samples which can be spotted.

The behaviour of free DPH separated from the complex is depicted in Fig. 4. The amount of free DPH tends to decrease as BCD concentrations increase. This behaviour differs from the one observed for the detailed complexation of cinnamic acid [12] in which a plateau is obtained. However, this is not unexpected since in our case the complexes are solubilized in a mixed solvent containing 38% of an organic component. The observed decrease is probably due to a salting-out effect induced by the increasing amount of solubilized BCD which is not seen in the absence of an organic cosolvent.

Complexed DPH was determined by subtracting the value for free DPH concentrations obtained from the TLC data from the total solubilized DPH obtained by UV absorption spec-

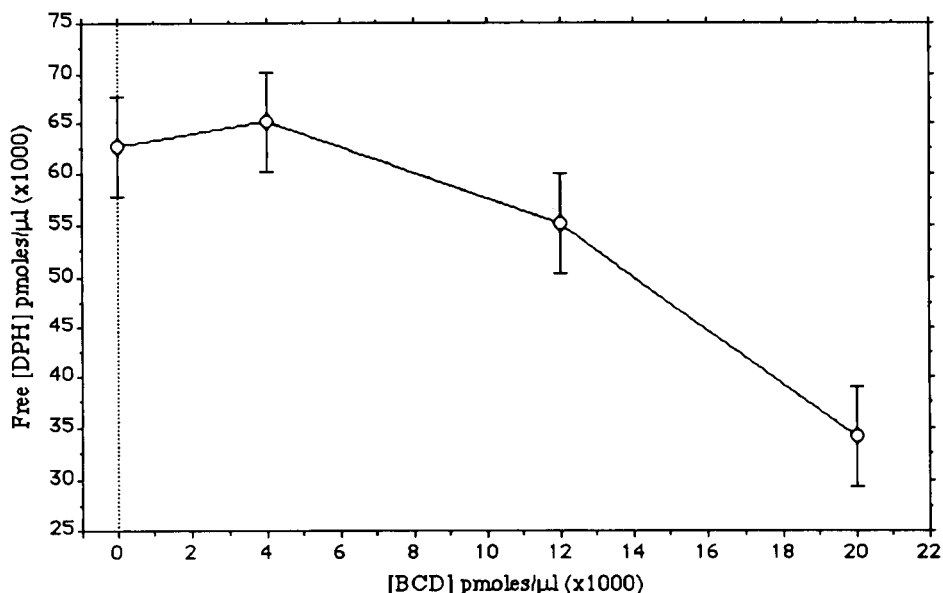


Fig. 4. Free DPH or unbound DPH versus increase of BCD concentration as quantified on TLC plates eluted with hexane–ether–ethanol. Free DPH tends to decrease with increasing BCD concentrations.

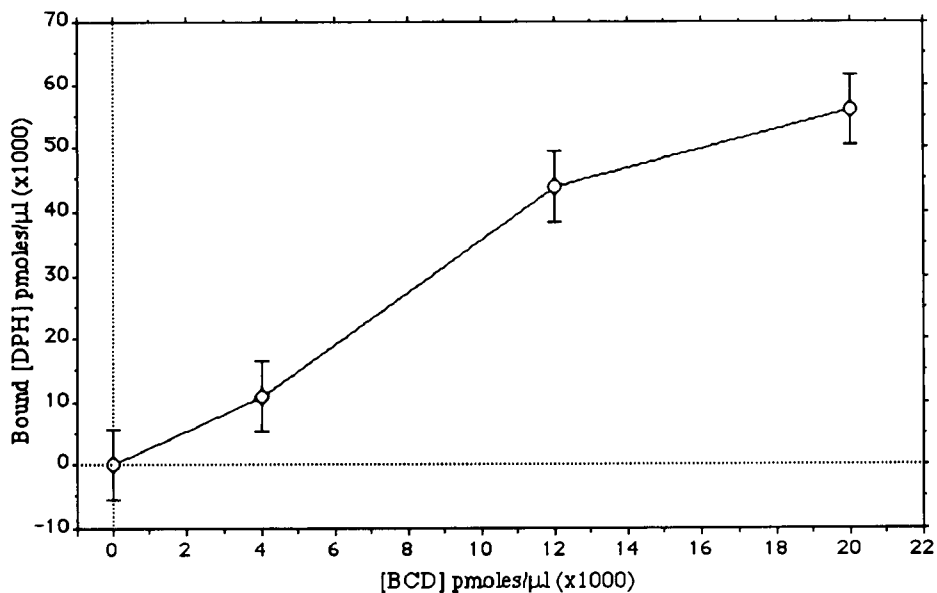


Fig. 5. Bound DPH in 38:62 $\text{CH}_3\text{CN}-\text{H}_2\text{O}$ per increasing concentrations of BCD were determined by subtracting free DPH values obtained by TLC from total solubilized DPH quantified by UV-visible absorption spectroscopy.

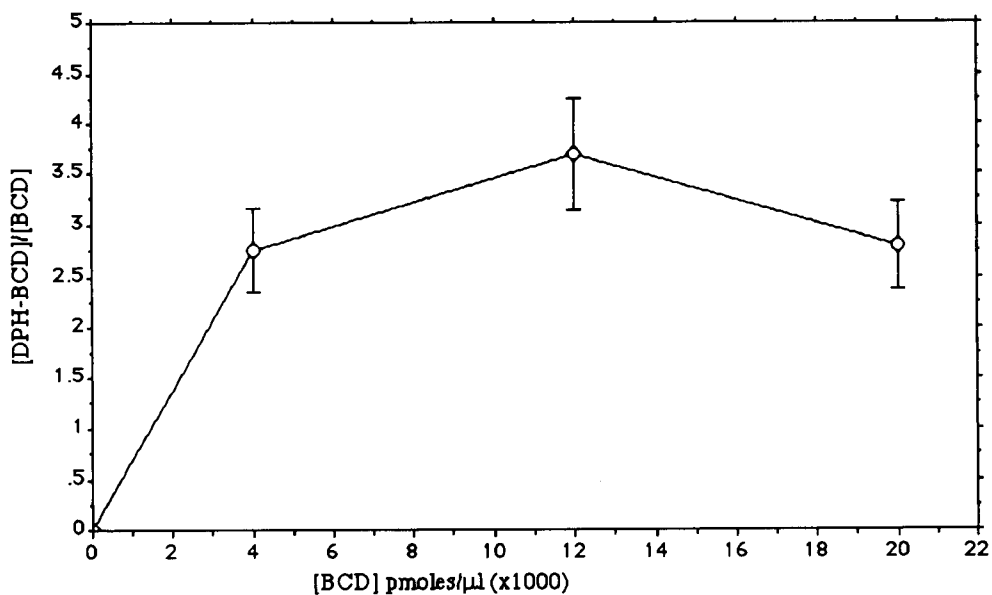


Fig. 6. This graph depicts the complexation tendencies of BCD and DPH in the acetonitrile-water (38:62, w/w) solvent for each BCD concentration. On the ordinate are the number of DPH molecules per BCD. On the abscissa are BCD concentrations in solution. The data used to plot this graph were calculated from the values of free and bound DPH in 38:62 acetonitrile-water solvent in Table 1.

Table 1

Values for totally solubilized DPH and free DPH (prepared with BCD and 38:62 CH₃CN–H₂O) were respectively obtained by UV–visible electronic absorption spectroscopy and CCD camera transferred TLC data

[BCD] (pmol/ μ l)	[DPH] (pmol/ μ l) (38:62 CH ₃ CN–H ₂ O)		
	Total	Free	Bound
0	68 \pm 3	63 \pm 70	0
4000	76 \pm 4	65 \pm 7	11 \pm 7
12000	99.5 \pm 5	55 \pm 6	44 \pm 6
20000	91 \pm 4.5	34 \pm 4	56 \pm 4

Bound DPH = total [DPH] – free [DPH].

troscopy of the samples. This data is summarized in Table 1 and in Fig. 5. The amount of totally solubilized DPH by the 38:62 acetonitrile–water solvent obtained by UV absorption spectroscopy (68 \pm 3 pmol/ μ l) is similar to the value read from the TLC plates (63 \pm 7), thus demonstrating that complexed DPH can, within error limits, be quantified by this method. Total DPH tends to increase from 68 \pm 3 pmol/ μ l without BCD to an approximate maximum of 99.5 \pm 5 pmol/ μ l when 12000 pmol/ μ l BCD is added to the solution. These results demonstrate that more DPH is complexed as BCD is added to the solution.

Another representation of complex formation tendencies is shown in Fig. 6, in which DPH–BCD:BCD ratios are plotted against BCD concentrations in solution. DPH–BCD:BCD complex ratios tend to increase to a maximum around 12000 pmol/l of BCD with 3.5 \times 10^{–3} DPH molecules per BCD.

Table 1 demonstrates that free DPH is present in solution in greater quantities than complexed DPH–BCD. However, the spots' fluorescence on the TLC plates gives the impression that the opposite is true. Comparison of the dot pixels of the free DPH containing 12000 pmol BCD with the bound DPH containing 20000 pmol BCD (Fig. 3), where the value of the latter is underestimated because of over-saturation, demonstrates that the quantum yield of included DPH is in fact higher than that for the free form. This explains



Fig. 7. A view reproduced from CCD of the TLC plate eluted in hexane–ether–ethanol solvent refilled five days after first exposure to excitation at 360 nm light and air. The spots at the start from left to right are (1) BCD in acetonitrile–water (25:75, w/w); (2) BCD in acetonitrile–water (38:62, w/w); (3) DPH in acetonitrile–water (25:75, w/w); (4) DPH + 4 \times 10³ pmol BCD in acetonitrile–water (25:75, w/w); (5) DPH + 12 \times 10³ pmol BCD in acetonitrile–water (25:75, w/w); (6) DPH + 20 \times 10³ pmol BCD in acetonitrile–water (25:75, w/w); (7) DPH + 4 \times 10³ pmol BCD in acetonitrile–water (38:62, w/w); (8) DPH + 12 \times 10³ pmol BCD in acetonitrile–water (38:62, w/w); (9) DPH + 20 \times 10³ pmol BCD in acetonitrile–water (38:62, w/w); (10) 50 pmol DPH standard. (11) 80 pmol standard. (12) 100 pmol standard. All DPH standards are in pure acetonitrile.

why the spots at the start, which correspond to very polar complexes of high molecular mass, are much brighter than those corresponding to the same quantity of free DPH. The quantum yield of fluorescence of DPH is seen to increase on complexation.

3.2.3. Aging study of DPH on TLC plates

Comparison of freshly spotted TLC plates (Fig. 3) and the same plate, kept in the dark and wrapped in aluminium foil, filmed five days later (Fig. 7) demonstrates that free DPH, including free DPH in the standards, is completely quenched in an unknown oxidative process. DPH

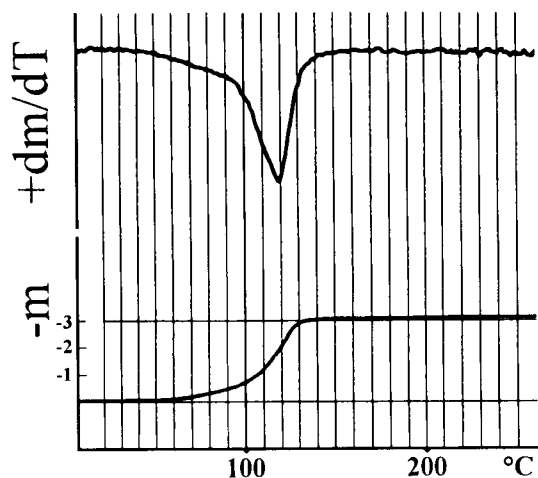


Fig. 8. TGA of BCD–DPH crystals separated from acetonitrile–water (38:62, w/w) solvent.

in the complex, on the other hand, is still visible and appears to be protected by BCD from quenching.

3.3. Thermogravimetric analysis

The graph in Fig. 8 demonstrates that each β -cyclodextrin includes approximately 11.5 water molecules. The two solids which display fluorescence and ought to contain the complexes release no detectable DPH or acetonitrile but only water. Even in the crystals which were simply separated from the 38:62 (w/w) acetonitrile–water the presence of acetonitrile is not apparent. These results concord with the ones obtained in UV absorption spectroscopy and TLC where stoichiometric ratios up to 3.5:1000 DPH:BCD were obtained. These values are well below the sensitivity limit of TGA.

4. Conclusion

Free and complexed fluorescent BCD guest molecules can easily be detected and separately quantified by a combination of TLC, UV absorption spectroscopic and fluorescence methods. This technique allows also a quantitative determination of the stabilization resulting from inclusion as well as a kinetic study of the stability of the inclusion complex at various temperatures or in the presence of actinic light. Further work is presently under way to obtain the same quantification using only fluorescence analysis on TLC.

References

- [1] D. French, M.L. Levine, J.H. Pazur and E. Norberg, *J. Am. Chem. Soc.*, 71 (1949) 353.
- [2] D. Amididouche, H. Darrouzet, D. Duchêne and M.-C. Poelman, *Int. J. Pharm.*, 54 (1989) 175.
- [3] M. Bender and M. Komiyama, *Cyclodextrin Chemistry*, Springer-Verlag, Berlin, 1978, p. 33.
- [4] J. Ho, *J. Chromatogr.*, 508 (1990) 375.
- [5] J. Szejtli (Ed.), *Cyclodextrin and their Inclusion Complexes*, Akadémiai, Budapest, 1982, p. 95.
- [6] R.B. Gennis, *Ann. Rev. Biochem.*, 37 (1985) 235.
- [7] T. Higuchi and K. O'Connors, *Adv. Anal. Chem. Instrum.*, 4 (1965) 117.
- [8] J.D. Winefordner (Ed.), *Spectrochemical Methods of Analysis*, Wiley-Interscience, New York, 1971.
- [9] A. Alak, E.E. Heilwell, W.L. Hinze, H. Oh and D.W. Armstrong, *J. Liq. Chromatogr.*, 7 (1984) 1273.
- [10] A. Muñoz de la Peña, T.T. Ndou, J.B. Zung, K.L. Greene, D.H. Live and J.M. Warner, *J. Am. Chem. Soc.*, 113 (1991) 1572.
- [11] V.A. Pollak, *J. Chromatogr.*, 393 (1987) 143.
- [12] K.A. Connors and T.W. Rosanske, *J. Pharm. Sci.*, 69 (1980) 173.



ELSEVIER

Analytica Chimica Acta 292 (1994) 151–157

**ANALYTICA
CHIMICA
ACTA**

Catalytic effect of rhodium(III) on the chemiluminescence of luminol in reverse micelles and its analytical application

Imdadullah, Terufumi Fujiwara, Takahiro Kumamaru *

Department of Chemistry, Faculty of Science, Hiroshima University, 1-3-1 Kagamiyama, Higashi-Hiroshima 724, Japan

(Received 18th October 1993; revised manuscript received 4th January 1994)

Abstract

Even in the absence of potassium periodate, rhodium(III) caused an increase in the chemiluminescence (CL) of luminol both in conventional aqueous basic buffer solution and in a reverse micellar medium of cetyltrimethylammonium chloride in chloroform–cyclohexane (6:5, v/v)–water (buffered with sodium carbonate). The CL emission intensity was observed to decrease significantly when oxygen was excluded from the reaction. The rhodium(III)-catalyzed CL emission from luminol oxidation by oxygen in a reverse micellar medium can be used for analytical purposes. Under the optimized experimental conditions, the present emission was applied to determine rhodium(III) in chloroform using a flow-injection system. A detection limit of 50 ng ml^{-1} Rh(III) and a linear calibration graph was obtained with a dynamic range from $0.40 \text{ } \mu\text{g ml}^{-1}$ to $10 \text{ } \mu\text{g ml}^{-1}$.

Key words: Catalytic methods; Chemiluminescence; Flow injection; Reverse micelles; Rhodium; Luminol; Micelles

1. Introduction

There is a great need for the development of a simple and selective procedure for the determination of platinum group metals using inexpensive instrumentation. Chemiluminescence (CL) provides a valid detection system for routine analysis in several fields of analytical chemistry [1–4]. The simplicity of the procedure and use of cheap instrumentation in addition to high sensitivity are the main advantages associated with CL detection systems. The CL reaction of luminol with potassium periodate in aqueous sodium hydrox-

ide solution at pH 12 has been reported to be catalyzed by transient Rh(V) produced from periodate oxidation of Rh(III) in the basic medium [5]. Furthermore, a similar CL procedure was utilized for the quantification of Rh(III) [6]. Alternatively, the CL reaction in the absence of an oxidizing reagent is simple and more selective. Metal ions such as iron(II) [7], cobalt(II) [8] and gold(III) [9] have been reported to cause CL from luminol in aqueous solution even when no hydrogen peroxide is present. In a preliminary study of luminol CL using Rh(III) as a catalyst, we observed an increase in the emission intensity when the CL reaction was carried out in the absence of periodate.

In CL measurements, an interesting development of analytical significance is the incorpora-

* Corresponding author.

tion of reverse micelles into the detection system with subsequent achievements of multiple benefits [10–18]. Lower detection limits and improved selectivity are reported for reverse micellar mediated CL (RMM-CL) measurements. Owing to the effectiveness of reverse micelles in the CL reactions, it is of particular interest to investigate the catalytic behaviour of different metal ions in the RMM-CL reaction for their quantification at trace levels. In fact, a new CL method for Au(III) based on the oxidation of luminol in reverse micelles with $[\text{AuCl}_4]^-$ in chloroform using a flow-injection (FI) system has been developed [16]. This work was extended to the CL determination of gold in aqueous medium after the analyte was quantitatively transferred from an aqueous acidic solution into chloroform containing tri-*n*-octylphosphine oxide [17]. After studying the interference effect from the presence of different species in aqueous solution, this method was applied to the determination of gold in industrial samples, using both batch extraction [18] and continuous flow extraction through a microporous PTFE membrane [19].

In this paper, the effect of Rh(III) in chloroform on the RMM-CL oxidation of luminol, using a flow-injection method, is described in detail. Preliminary observation revealed that Rh(III) alone is sufficient to give an increased CL emission in reverse micellar as well as in aqueous media. After optimizing the reaction parameters, reproducible calibration graphs and detection limits lower than those for aqueous media were obtained. Since various methods can be used to extract Rh(III) from an aqueous medium [20–22], the present investigation suggests that considerable opportunities exist to develop a new CL procedure for Rh(III) based on the combination of the CL system with on-line liquid–liquid extraction.

2. Experimental

2.1. Reagent

Rhodium(III) was obtained in the form of 99.9% pure rhodium nitrate (Rare Metallic Co., Tokyo). A stock Rh(III) aqueous solution was

prepared in 0.2 M perchloric acid. Analytical grade pure (60%) perchloric acid (Katayama, Osaka) was used for the preparation of acidic solutions. All working solutions of rhodium(III) were prepared by serial dilution of the stock solution using fresh deionized water. To prepare standard Rh(III) solutions in chloroform, a certain volume of the aqueous stock solution of rhodium nitrate was placed in a clean beaker and was evaporated to dryness on an electric hot plate. The solid residue was dissolved in the minimum amount (0.4 ml) of ethanol and was diluted to the required concentration with chloroform (Wako, Osaka). Using the same procedure, a blank solution in chloroform was also prepared.

An aqueous solution of luminol (Aldrich, Milwaukee, WI) was prepared in 0.2 M sodium carbonate (Kanto, Tokyo). The pH of this solution was 12.0. The luminescent reagent was prepared by dispersing a certain volume of the sodium carbonate buffered solution of luminol in a bulk solvent of chloroform–cyclohexane (Wako) 6:5 (v/v) mixture containing 0.010 M cetyltrimethylammonium chloride (CTAC, Tokyo Kasei Kogyo, Tokyo). A water-to-surfactant molar ratio ($R = [\text{H}_2\text{O}]/[\text{CTAC}]$) of 22.2 was used in the present work. All chemicals were used as received.

2.2. Apparatus

The multicomponent instrument used for the determination of flow CL measurements was composed of a Hitachi (Tokyo) Model K-1000 FI analyzer, a Tosoh (Tokyo) Model CCPM computer-controlled pump unit and a Niti-on (Funahashi) Model LF-800 photometer. The CL signals were recorded on a strip-chart recorder. For batch detection of luminescence, a Hitachi Model F-2000 fluorescence spectrophotometer with 1-cm cell was used. For pH measurements, a Horiba (Tokyo) Model M-8L pH meter was used. A YSI (Yellow Springs, OH) Model 58 dissolved oxygen meter was used to measure the content of oxygen in aqueous solutions. Deionized water was freshly collected from an Advantec Toyo (Tokyo) Model GSU-901 water purification apparatus and was used in making all aqueous preparations.

2.3. Procedure

All the analytical conditions were optimized using the FI system reported in our previous studies [13,15–18]. After suction into their respective loops, sample (90 μl) and reagent (100 μl) were simultaneously inserted into the carrier flow streams of chloroform using a rotary injection valve. The carrier flow rate in both streams was 2 ml min^{-1} . CL signals were produced upon mixing sample and reagent solutions in a coiled cell (70 μl) mounted in front of the photomultiplier tube of the CL detector. For the batch CL measurements, 0.5 ml of the luminescent reagent was initially placed in the cell and was mixed with an equal volume of the sample solution injected quickly with a glass syringe [13].

3. Results and discussion

3.1. Rhodium catalyzed chemiluminescence

For luminol chemiluminescence using rhodium(III) as a catalyst in aqueous alkaline solution, it was believed that the presence of periodate is required [5,6]. As reported for gold(III) [9,16], however, CL signals characteristic to luminol alone were observed even in the absence of a co-oxidant like periodate when either a reverse micellar or conventional aqueous solution of the luminescent reagent was placed in the cell. Upon mixing either the former solution with Rh(III) in chloroform (Fig. 1a) or the latter solution with Rh(III) in water (Fig. 1b), intense CL signals were produced at room temperature.

Previous studies of the effect of Rh(III) on the luminol reaction did not mention such an occurrence. In earlier studies on the CL reaction of luminol in the absence of hydrogen peroxide, it has been pointed out that oxygen is required for the CL reaction of luminol with metal ions such as iron(II) [7], cobalt(II) [8], and gold(III) [9], although this has been disputed in the case of iron(II) [23]. In order to verify that oxygen is involved in the luminol CL reaction with Rh(III) in the absence of periodate, experiments were conducted in which oxygen was excluded from

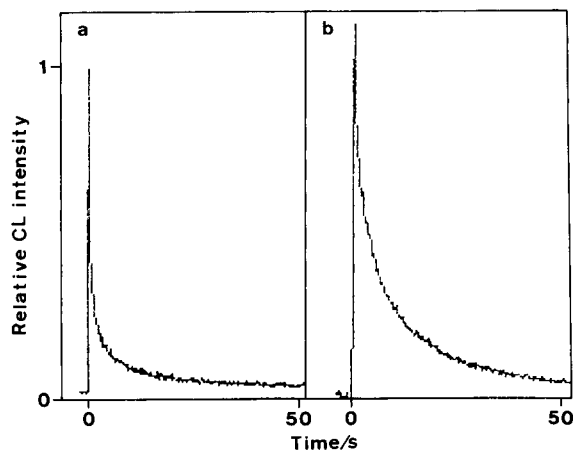


Fig. 1. CL intensity–time profiles observed from the luminol oxidation in CTAC reverse micellar solution (a) and in conventional aqueous solution (b). Standard solutions of 10 $\mu\text{g ml}^{-1}$ rhodium(III) in chloroform and in water were added to the former and latter solutions, respectively.

the reaction. Continuous flow CL measurements were conducted by pumping solutions of Rh(III) and luminol through the flow system and mixing these streams in a coiled glass flow cell. The aqueous solutions run without deaeration (Fig. 2a and c) contained oxygen from the air. At 25°C, the observed content of oxygen in the aqueous solutions at equilibrium with air (air-saturated) was 8.5 mg l^{-1} . When both the conventional aqueous solutions of luminol and Rh(III) were deaerated by bubbling with nitrogen (the oxygen

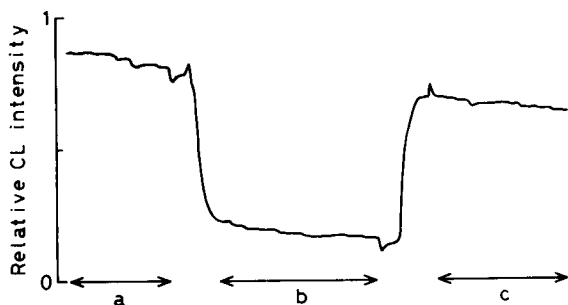


Fig. 2. CL emission intensity obtained with conventional aqueous solutions air-saturated (a), (c) and deaerated (b) using a continuous flow system. Oxygen content: (a) 8.5; (b) 2.0; (c) 8.5 mg ml^{-1} . Luminol, 1 mM; Na_2CO_3 , 0.2 M; Rh(III), 10 $\mu\text{g ml}^{-1}$.

content of these solutions was decreased to 2.0 mg l^{-1} , Fig. 2b) and the CL emission intensity was observed to decrease significantly. A decrease in CL intensity because of the removal of oxygen from the aqueous solutions indicates that oxygen is indeed required for the CL reaction of luminol with Rh(III) ion.

The intensity–time profiles (Fig. 1), in both the conventional aqueous and reverse micellar solutions, were identical, having an intense luminescence for the initial few seconds after mixing followed by a sharp decline. This indicates that uptake of Rh(III) from chloroform into the water pool of the reverse micelle occurs just upon mixing Rh(III) in chloroform with the reverse micellar solution of luminol. After its uptake by the reverse micelle, Rh(III) is apparently capable of catalyzing luminol oxidation in the presence of dissolved oxygen present in the central reverse micellar aqueous pool as observed with the conventional aqueous solution mentioned above. In conventional aqueous as well as in reverse micellar media, the 3-aminophthalate (3-AP) di-anion produced by the Rh(III) catalyzed oxidation of luminol with oxygen is probably the primary emitter. Additionally, when the CL reaction of luminol with Rh(III) ion was run in the presence of the added oxidant, potassium periodate, following the reported procedure [6], there was a negligible increase in the emission intensity in the reverse micellar solution. Additional work will be needed to elucidate the difference between the CL profiles with and without periodate in conventional aqueous and in reverse micellar solutions.

In order to evaluate the behaviour of Rh(III) as a catalyst, CL signals were recorded in conventional aqueous and in reverse micellar media under the same experimental conditions using an FIA system. The calibration graphs shown in Fig. 3 reflect some characteristic features. At higher concentrations ($2.5\text{--}10 \text{ } \mu\text{g ml}^{-1}$) of Rh(III), the graphs are parallel but the signal observed in reverse micellar medium was much higher than that in the aqueous medium. In the latter, below $5 \text{ } \mu\text{g ml}^{-1}$ Rh(III), a suppressive effect of Rh(III) on the CL emission was observed. Similar behaviour has been reported for Au(III) [24], where

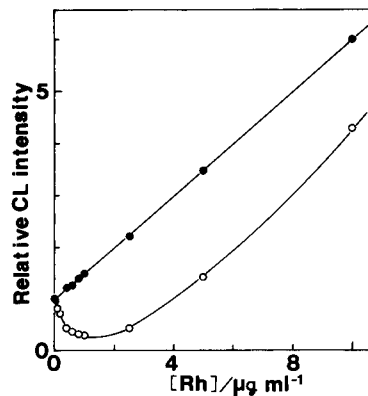


Fig. 3. Dependence of the CL intensity from the luminol reaction on rhodium(III) concentration in reverse micellar medium (●) and in conventional aqueous medium (○).

the intensity of luminol CL decreases to zero owing to hydrolysis and the formation of $[\text{AuCl}_3\text{OH}]^-$. By assuming such an effect of hydrolysis, the present inhibition phenomenon might be due to the formation of a rhodium hydroxide which is produced upon mixing Rh(III) with the basic solution of luminol. As the formation of rhodium hydroxide is increased with an increase in the concentration of Rh(III) in solution, a decrease in the CL intensity is observed (Fig. 3). However, an increase in the CL signals was observed for Rh(III) concentrations above $1.0 \text{ } \mu\text{g ml}^{-1}$. In contrast, in the reverse micellar medium, a linear graph was obtained at all concentrations above 400 ng ml^{-1} Rh(III) (Fig. 3). To explain the linearity, it could be presumed that upon the uptake of Rh(III) by the reverse micelles, a chloro complex of the analyte is produced in the water pool of the reverse micelle rather than the hydroxide as is the case in bulk water. Since a small volume of the water pool is used for accumulation of the chloride counter ion in the CTAC surfactant, the effective chloride counter ion concentration in the water core region of the reverse micelle is much higher than the 0.01 M CTAC stoichiometric concentration. Under the optimum conditions ($R = 22.2$), for example, the effective chloride concentration calculated by taking into account the aqueous core to organic bulk phase volume ratio of 0.004 is 2.5 M . This complex will subsequently participate in the CL reaction with

out any loss due to the formation of a rhodium hydroxide.

3.2. Optimization studies

As the initial investigation demonstrated the usefulness of reverse micelles [13–18], all experimental variables for the reaction of luminol in reverse micelles catalyzed by Rh(III) in chloroform were optimized. Interestingly it was observed that all the reaction parameters, i.e., the effect of the $[H_2O]/[CTAC]$ mole ratio, CTAC concentration, carbonate buffer concentration, luminol concentration in the final total volume, and composition of the bulk organic solvent were almost identical as to those observed for gold(III) [16] (Table 1). The initial studies of the Rh(III) catalyzed CL reaction [5,6] were conducted in strong sodium hydroxide solution. Therefore, a thorough investigation concerning the pH of the luminol buffer solution and the effect of sodium hydroxide was required. As is evident from Fig. 4, considerable changes in the CL intensity were observed when the pH of the luminol solution in 0.2 M sodium carbonate (pH 12) was varied by addition of either hydrochloric acid or sodium hydroxide. CL signals appeared at $pH \geq 9$ and reached a maximum around pH 13.

The 3-aminophthalate (3-AP) di-anion is considered to be the primary emitter in luminol CL reactions. Buffer at high pH will presumably facilitate the formation of these di-anions and result

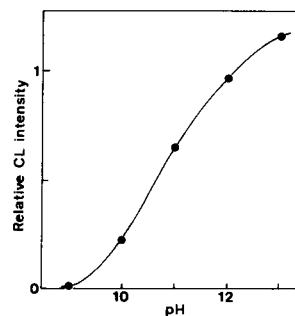


Fig. 4. Variation of CL intensity with the pH of luminol buffer solution in reverse micellar medium.

in enhanced CL signals. However, when sodium hydroxide (5×10^{-3} –1 M) was added to the luminol solution in 0.2 M sodium carbonate, only a slight increase (ca. 50%) in the CL signals was observed. A proportional increase in the blank CL signal and poor reproducibility in the presence of sodium hydroxide were also observed. A plausible explanation for this phenomenon could be the formation of more 3-AP di-anions at the expense of an increase in the total anionic population inside the aqueous pool of reverse micelles. If sodium hydroxide is used, a competition among different anions (e.g., OH^- , CO_3^{2-} and Cl^-) and the 3-AP anion, all present in the same aqueous pool, for the positively charged water–surfactant interface which is the most probable site for the CL reactions [11,12], is highly likely. The water–surfactant interface of the reverse micelle is of great significance in its reactivity [25,26]. Additionally fluorescence quenching at $pH > 12.5$ in reverse micellar medium and the quenching of CL have already been reported [12,27] for hydroxide. Sodium carbonate buffer was preferred over sodium hydroxide because of the stability and reproducibility of the RMM-CL signals in the former, thus the use of sodium hydroxide in the present investigation was not considered further.

3.3. Sensitivity and dynamic range

A study regarding the analytical application of the FI-CL procedure was carried out to establish the utility, dynamic range and reproducibility for the quantification of Rh(III). No increase in the

Table 1
Optimum experimental and instrumental operating conditions for the determination of rhodium(III)

Reagents	
Final luminol concentration	4 μ M
Aqueous buffer concentration	0.2 M Na_2CO_3
$R (= [H_2O]/[CTAC])$	22.2
CTAC concentration	0.01 M
Reverse micellar bulk solvent	Chloroform– cyclohexane (6:5, v/v)
Flow system	
Sample loop size	90 μ l
Reagent loop size	100 μ l
Carrier	Chloroform
Flow rate	2 ml min^{-1}

CL signal was observed for the blank, indicating the absence of any catalysis. The difference in the observed peak heights for the analyte and blank was considered as the analytical signal. Under the optimized experimental parameters, a detection limit of 50 ng ml^{-1} was obtained using the RMM-CL detection system for Rh(III) in chloroform where the detection limit is considered as the concentration of the analyte for which the analytical signal is 3 times higher than the baseline noise. The calibration graph was linear from $0.40 \mu\text{g ml}^{-1}$ to $10 \mu\text{g ml}^{-1}$ Rh(III) in chloroform (Fig. 5). The relative standard deviation ($n = 6$) was 3%. In a similar comparative study, a certain volume of the aqueous Rh(III) standard solution was dispersed directly in the reverse micellar medium ($R = 22.2$) and their CL signals were recorded with a reverse micellar solution of luminol under the same experimental conditions. The calibration graphs were similar in both cases. The RMM-CL signals for the reverse micellar solutions of Rh(III) nevertheless appeared to be slightly higher than those for the sample solutions of Rh(III) in chloroform at the same concentra-

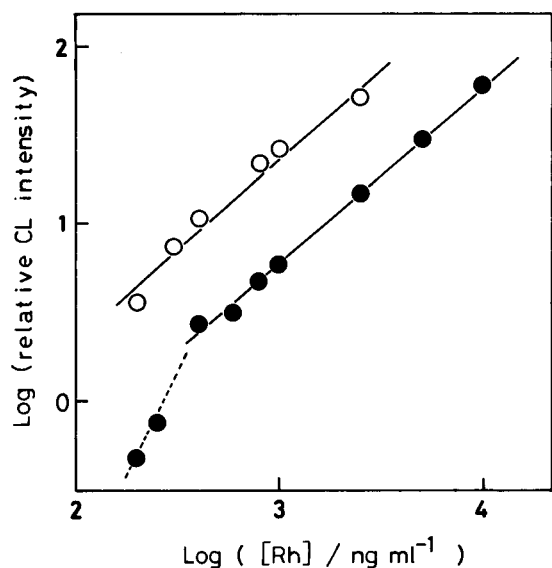


Fig. 5. log-log calibration graphs for the determination of rhodium using the RMM-CL reaction of luminol. Rh(III) sample preparation: (○) Rh(III) aqueous solutions were dispersed in reverse micelles; (●) a concentrated Rh(III) ethanolic solution was diluted with chloroform.

tion of Rh(III) (Fig. 5). The chloroform solution of Rh(III) contains traces of ethanol which most probably damages the reverse micellar structure on mixing with the reverse micellar solution of luminol, thus causing a mild inhibition in the RMM-CL intensity as well as a higher detection limit.

Apart from sensitivity, the present micellar method is no doubt simpler, faster and less expensive than other sophisticated instrumental methods. It is quite likely that this method could be applied to the quantification of Rh(III) in diverse aqueous samples after liquid-liquid extraction. Work is in progress to select a suitable CL-active system for the extraction of Rh(III) and to examine the interference effect from the presence of different species on the rhodium determination.

Acknowledgements

This work was partially supported by a grant-in-aid for scientific research, No. 04453038, from the ministry of Education, Science and Culture of Japan. One of the authors, Imdadullah, also thanks this Ministry for a Scholarship award.

References

- [1] A. Fernandez-Gutierrez and A. Munoz de la Pena, in S.G. Schulman (Ed.), *Molecular Luminescence Spectroscopy. Methods and Applications: Part 1*, Wiley, New York, 1985, pp. 463–546 (and references cited therein).
- [2] A. Townshend, *Analyst*, 115 (1990) 495.
- [3] T. Fujiwara and T. Kumamaru, *Spectrochim. Acta Rev.*, 13 (1990) 399.
- [4] I.M. Warner and L.B. McGown, *Anal. Chem.*, 64 (1992) 343R.
- [5] N.M. Lukovskaya and N.F. Kushchevskaya, *Ukr. Khim. Zh.*, 41 (1975) 643.
- [6] A.T. Pilipenko, N.F. Kushchevskaya, E.P. Parkhomenko and N.F. Falendysh, *Ukr. Khim. Zh.*, 54 (1988) 939.
- [7] W.R. Seitz and D.M. Hercules, *Anal. Chem.*, 44 (1972) 2143.
- [8] L.L. Klopff and T.A. Nieman, *Anal. Chem.*, 55 (1983) 1080.
- [9] N.M. Lukovskaya and T.A. Bogoslovskaya, *Ukr. Khim. Zh.*, 41 (1975) 268.
- [10] J. Georges, *Spectrochim. Acta Rev.*, 13 (1990) 27.

- [11] W.L. Hinze, N. Srinivasan, T.K. Smith, S. Igarashi and H. Hoshino, in I.M. Warner and L.B. McGown (Eds.), *Advances in Multidimensional Luminescence*, Vol. 1, JAI Press, Greenwich, 1991, pp. 149–206 (and references cited therein).
- [12] H. Hoshino and W.L. Hinze, *Anal. Chem.*, 59 (1987) 496.
- [13] T. Fujiwara, N. Tanimoto, J.-J. Huang and T. Kumamaru, *Anal. Chem.*, 61 (1989) 2800.
- [14] T. Fujiwara and T. Kumamaru, in *Proceedings of the International Trace Analysis Symposium '90* held at Sendai and Kiryu, Japan, July, 1990, pp. 187–190.
- [15] T. Fujiwara, N. Tanimoto, K. Nakahara and T. Kumamaru, *Chem. Lett.*, (1991) 1137.
- [16] Imdadullah, T. Fujiwara and T. Kumamaru, *Anal. Chem.*, 63 (1991) 2348.
- [17] Imdadullah, T. Fujiwara and T. Kumamaru, *Anal. Sci.*, 7 (Supp.) (1991) 1399.
- [18] Imdadullah, T. Fujiwara and T. Kumamaru, *Anal. Chem.*, 65 (1993) 421.
- [19] T. Fujiwara, K. Murayama, Imdadullah and T. Kumamaru, *Microchem. J.*, (1994) in press.
- [20] H. Imura, H. Takahashi and N. Suzuki, *Bull. Chem. Soc. Jpn.*, 64 (1991) 882.
- [21] M.T. Kostanski and H. Freiser, *Anal. Chim. Acta*, 242 (1991) 191.
- [22] Y. Baba and T. Fukumoto, *Chem. Lett.*, (1992) 727.
- [23] A.A. Alwarthan and A. Townshend, *Anal. Chim. Acta*, 196 (1987) 135.
- [24] N.M. Lukovskaya and T.A. Bogoslovskaya, *Ukr. Khim. Zh.*, 41 (1975) 529.
- [25] M.P. Pileni (Ed.), *Structure and Reactivity in Reverse Micelles*, Elsevier, Amsterdam, 1989, and references cited therein.
- [26] J. Nishimoto, E. Iwamoto, T. Fujiwara and T. Kumamaru, *J. Chem. Soc., Faraday Trans. 1*, 89 (1993) 535.
- [27] P. Mikuska and Z. Vecera, *Anal. Chem.* 64 (1992) 2187.

Study of the chemiluminescent characteristics of some xanthone dyes

Guo Nan Chen *, Jian Ping Duan, Qing Fu Hu

Department of Chemistry, Fuzhou University, Fuzhou, Fujian 350002, China

(Received 30th September 1993; revised manuscript received 14th December 1993)

Abstract

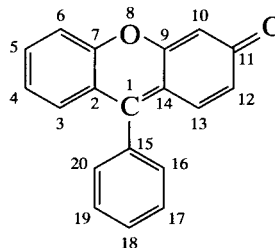
The chemiluminescent characteristics of the oxidation of some xanthone dyes were studied in detail. The chemiluminescence spectra of these dyes and the absorption and fluorescence spectra of some products of the chemiluminescent reactions were investigated; all these dyes were studied by the Hückel molecular orbital method. On the basis of these investigations, an initial explanation for the relationship between the structure of the dye molecules and their chemiluminescent behaviour and a possible mechanism for this chemiluminescent reaction were proposed. The effects of various types of surfactants on the chemiluminescent reaction were also studied. The mechanism of the enhancement of chemiluminescence by surfactants is discussed. The catalysis of some metal ions was also examined, and it was found that trace Co(II) would catalyse the chemiluminescent reaction in the presence of the cationic surfactant cetyltrimethylammonium bromide. The detection limit was 4–10 pg Co ml⁻¹, depending on the dye.

Key words: Chemiluminescence; Cobalt; Dyes; Xanthone dyes

1. Introduction

All xanthone dye molecules have multiple aromatic rings with a rigid plane structure. They are highly fluorescent reagents and all of these kinds of reagents have the basic structure shown. The predominant characteristic of these dye molecules is that there is an oxygen bridge between two benzene rings, the presence of which makes it

much easier to adopt a rigid plane structure [1,2].



These dyes are principally used in analytical chemistry as fluorescent indicators and reagents for spectrophotometric analysis. In the presence

* Corresponding author.

of surfactants, their sensitivity is greatly increased, the molar absorptivity of their complexes generally being $> 1 \times 10^5 \text{ l mol}^{-1} \text{ cm}^{-1}$ [3,4].

It was found that when some xanthone dyes were oxidized with hydrogen peroxide in alkaline solution, chemiluminescence could be observed. In this work, attempts were made to probe the relationship between the structural characteristics of these dye molecules and their chemiluminescent behaviour, and further to elucidate the mechanism of the chemiluminescent reaction. For this purpose some xanthone dyes (dibromalizarin violet, phenylfluorone, *o*-hydroxyphenylfluorone, eosin B, eosin Y, dibromophenylfluorone and fluorescein) were investigated. The effects of various kinds of surfactants on these chemiluminescent reactions and their catalysis by some metal ions were also studied.

2. Experimental

2.1. Apparatus

A Lambda 9 spectrophotometer (Perkin-Elmer), RF-540 spectrofluorimetry (Shimadzu) and HFC-I chemiluminometer (made in the laboratory) were used. A block diagram of the HFC-I is shown in Fig. 1. The detector chamber (A) consists of a reaction cell (I), filter (II), shutter (III), reflecting mirror (IV) and photomultiplier tube (V). The photomultiplier tube used is a GDB-413 (Nanjing Electron Tube Works) with a light detection range of 300–700 nm. The high

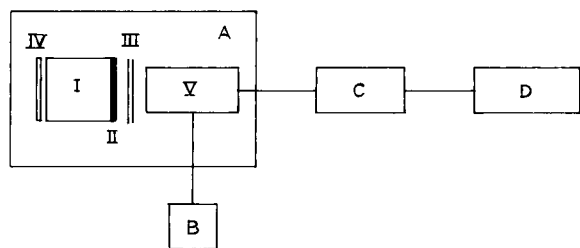


Fig. 1. Block diagram of HFC-I chemiluminometer A = detector chamber (I = reaction cell; II = filter; III = shutter; IV = reflecting mirror; V = photomultiplier tube); B = high-voltage power supply; C = amplifier; D = recorder.

voltage supplied is 900 V from B, C is an amplifier with a low noise level and small baseline shift and D is a recorder.

2.2. Reagents

All reagents were of analytical-reagent grade or better and water doubly distilled in a fused-silica apparatus was used throughout.

The xanthone dyes used were dibromoalizarin violet (Shanghai Chemical), phenylfluorone (Shanghai Chemical), *o*-hydroxyphenylfluorone (Beijing Chemical), eosin B (Guangzhou Chemical), eosin Y (Guangzhou Chemical), dibromophenylfluorone (Shanghai Chemical) and fluorescein (Koch-Light). These dyes were dissolved in absolute ethanol and the solutions were diluted to the required concentration with water.

The surfactants used were cetyltrimethylammonium bromide (CTAMB) (Beijing Chemical), sodium laurylsulphonate (Beijing Chemical) and Triton X-100 (Aldrich).

2.3. Procedures

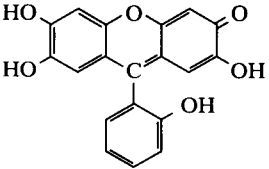
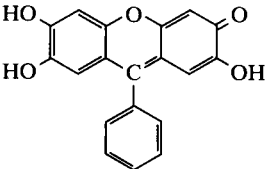
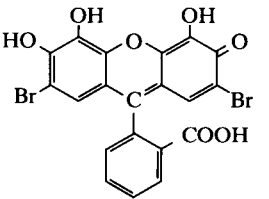
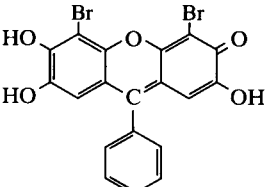
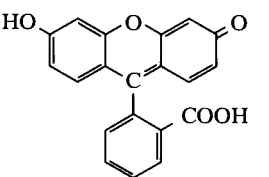
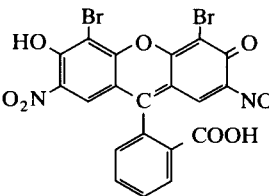
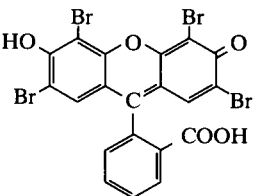
Detection of non-catalysed chemiluminescence

A 0.5-ml volume of xanthone dye solution, 0.1 ml of 1.5 mol l^{-1} NaOH and 0.5 ml of surfactant solution were added in turn by pipette to the reaction cell and mixed. The cell was placed into the detector chamber, the shutter was opened and the zero point of the recorder was adjusted. Then, 0.25 ml of 2.0 mol l^{-1} H_2O_2 solution was injected into the reaction cell and the chemiluminescence signal was recorded.

Detection of catalysed chemiluminescence

A 0.5 ml volume of $3.0 \times 10^{-4} \text{ mol l}^{-1}$ dye solution, 0.1 ml of 2.0 mol l^{-1} H_2O_2 solution and 0.5 ml of $5.0 \times 10^{-3} \text{ mol l}^{-1}$ surfactant solution were added in turn by pipette to the reaction cell and mixed. The cell was placed into the detector chamber, the shutter was opened and the zero point of the recorder was adjusted. Then, 0.25 ml of metal ion (or non-metal ion) solution was injected into the reaction cell and the chemiluminescence signal was recorded.

Table 1
Chemiluminescent behaviour of some xanthone dyes

Xanthone dye	Structure	Optimum concentrations			I_{Cl}
		Xanthone dye ($\times 10^{-4}$ M)	NaOH (M)	H ₂ O ₂ (M)	
<i>o</i> -Hydroxyphenylfluorone		2.5	0.15	0.50	12
Phenylfluorone		2.0	0.10	0.40	17
Dibromoalizarin violet		2.3	0.10	0.37	23
Dibromophenylfluorone		2.2	0.15	0.45	87
Fluorescein		1.8	0.20	0.35	99
Eosin B		1.8	0.25	0.35	840
Eosin Y		2.0	0.20	0.30	1610

I_{Cl} = chemiluminescent intensity, which is represented by peak height (mm). All the results are averages of ten measurements.

Measurement of fluorescence spectra

Measured amounts of dye solution, CTMAB solution and NaOH solution were placed into reaction cell and mixed and the fluorescence spectrum was measured from 400 to 650 nm with excitation at 390 nm. Hydrogen peroxide solution was then added to the cell and the fluorescence spectrum was again measured under the same conditions at regular intervals.

3. Results and discussion

Of the many available xanthone dyes, we selected dibromoalizarin violet, phenylfluorone, *o*-hydroxyphenylfluorone, eosin Y, eosin B, fluorescein and dibromophenylfluorone for investigation. It was found that xanthone dyes gave chemiluminescence when they were oxidized by hydrogen peroxide under alkaline conditions and the chemiluminescent intensity is dependent on the concentrations of dye and hydrogen peroxide. Because there was obvious interaction among these parameters, it was difficult to find the optimum conditions for these systems by traditional methods; the modified simplex method (MSM), however, is readily adaptable to solving such a

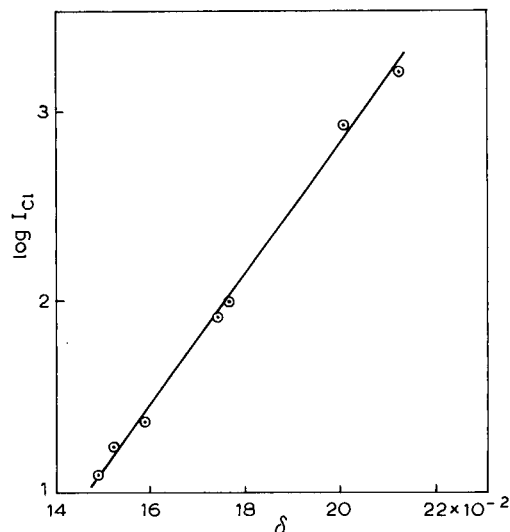


Fig. 2. Relationship between δ and chemiluminescent intensity.

Table 2

Relationship between δ and chemiluminescent intensity

Xanthone dye	δ	I_{Cl}	Log I_{Cl}
<i>o</i> -Hydroxyphenylfluorone	0.1487	12	1.0792
Phenylfluorone	0.1520	17	1.2304
Dibromoalizarin violet	0.1590	23	1.3617
Dibromophenylfluorone	0.1745	87	1.9395
Fluorescein	0.1764	99	1.9956
Eosin B	0.2002	840	2.9243
Eosin Y	0.2194	1610	3.2068

I_{Cl} = chemiluminescent intensity.

problem, and was therefore used for this purpose. The optimum conditions found for these dyes are given in Table 1.

3.1. Relationship between structure of dye molecule and chemiluminescent behaviour

Using the optimum conditions, we investigated the chemiluminescent behaviour of different xanthone dye systems, and found that their chemiluminescent intensities are very different (see Table 1). In order to probe the effects of various substituent groups on the chemiluminescent behaviour, the electron-density distribution in the dyes studied was calculated by the Hückel molecular orbital method. For convenience in discussion, the carbon atoms of the dye molecules are numbered.

The calculation shows that for all the dyestuffs tested the π -electron density at C-1 is lower than that at the other carbon atoms; of the three

Table 3

Linear range, relative standard deviation and detection limit of Co(II)

Xanthone dye	Linear range (ng ml ⁻¹)	R.S.D. (%)	DL (ng ml ⁻¹)
<i>o</i> -Hydroxyphenylfluorone	0.5–400	3.5	10
Phenylfluorone	0.5–400	4.0	10
Dibromoalizarin violet	0.1–100	2.7	5
Dibromophenylfluorone	0.1–100	1.9	5
Fluorescein	0.1–100	5.1	5
Eosin B	0.1–50	3.2	4
Eosin Y	0.1–50	4.5	4

R.S.D. = relative standard deviation [for 0.2 ng ml⁻¹ Co(II); $n = 10$]; DL = detection limit.

atoms connected with C-1, the C-15 atom has the lowest π -electron density. We also found that the chemiluminescent behaviour of the dyes is dependent on the difference in π -electron density between C-1 and C-15 (denoted δ), and the chemiluminescent intensity increases with increasing δ (see Table 2). On plotting the logarithm of relative chemiluminescent intensity against δ , a straight line was obtained (see Fig. 2), with a correlation coefficient of 0.993. Based on the quantum mechanical calculations, several initial conclusions can be drawn, as follows:

The selected dyes could be divided into two kinds, one such as fluorescein with a carboxy group at C-16 and the other kind such as phenylfluorone with no carboxy group at C-16. It is very obvious that the chemiluminescent intensity is increased greatly on introducing a carboxy group at C-16. Because of the electron-withdrawing effect of a carboxy group, not only will the π -electron density at C-1 be lowered, but also the value of δ will be increased and the chemiluminescent intensity, therefore, will be greatly increased.

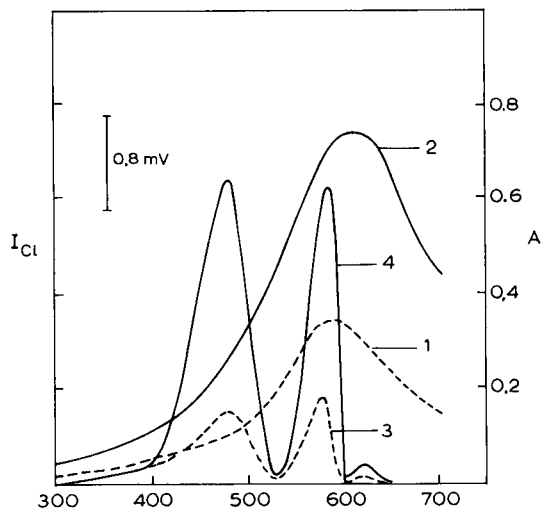


Fig. 3. Chemiluminescence spectra and visible absorption spectra of dibromophenylfluorone. (1) Visible absorption spectrum in the absence of CTMAB; (2) visible absorption spectrum in the presence of CTMAB; (3) chemiluminescence spectrum in the absence of CTMAB; (4) chemiluminescence spectrum in the presence of CTMAB.

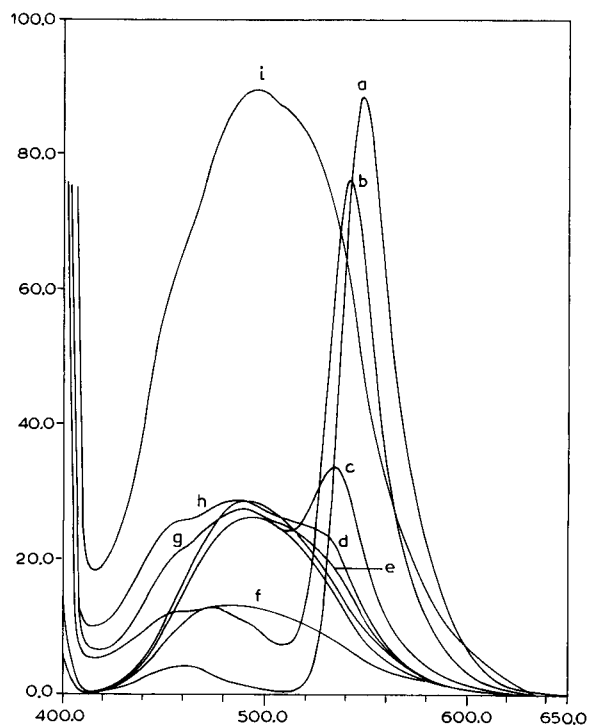


Fig. 4. Fluorescence spectra for the oxidation products of dibromophenylfluorone. (a)–(e) For dibromophenylfluorone [$t = (a) 0, (b) 1, (c) 6, (d) 13$ and $(e) 18$ min]; (f)–(i) for pyrogallol [$t = (f) 0, (g) 1, (h) 3$ and $(i) 8$ min].

From the molecular structures of dibromophenylfluorone, dibromoalizarin violet, eosin Y and eosin B, we know that the chemiluminescent intensity will be increased by introducing a bromine atom at C-4, C-6, C-10 and C-12. This effect is greatest when the bromine atoms are introduced at C-6 and C-10, as shown by comparing the chemiluminescent behaviour of dibromophenylfluorone and dibromoalizarin violet. Introduction of a carboxy group at C-16 in dibromoalizarin violet increases δ , which is favourable for chemiluminescence to occur, whereas there is no carboxy group at C-16 in dibromophenylfluorone. Normally, the chemiluminescent intensity of the former should be greater than that of latter, but when bromine atoms are introduced at C-6 and C-10, their chemiluminescent intensity order is inverted.

Comparison of the chemiluminescent behaviour of eosin Y and eosin B shows that the

introduction of a nitro group at C-4 and C-12 is not as effective as bromine in producing chemiluminescence, which may be due to the stronger electron-withdrawing effect of bromine.

Comparing the chemiluminescent behaviour of phenylfluorone and *o*-hydroxyfluorone, it can be concluded that the π -electron density at C-1 is increased by introducing a hydroxy group at C-16, further decreasing the value of δ , which is not favourable for chemiluminescence.

3.2. Mechanism of chemiluminescence

Chemiluminescence spectra

The chemiluminescence spectra of the selected dyes were measured; and three chemiluminescent peaks, at 475, 580 and 620 nm, can be observed for all of the dyes. Typical chemiluminescent spectra for dibromophenylfluorone are shown in Fig. 3. The first two peaks are very similar to the chemiluminescent peaks from polyphenols, such as pyrogallol, catechol and resorcinol, when they are oxidized by hydrogen peroxide in alkaline solution [5]. This suggests that when these xanthone dyes are oxidized, polyphenols such as pyrogallol and catechol may be produced during the reactions, and that the chemiluminescence occurs on further oxidation of these intermediates.

Absorption spectra

We also investigated the visible absorption spectra of the dyes in alkaline solution, and found that they overlap considerably with the chemiluminescence spectra, and therefore energy transition may occur. Taking dibromophenylfluorone as an example, as shown in Fig. 3, the maximum absorbance is at 582 nm in the absence of CTMAB, but is 532 nm in the presence of CTMAB; both overlap the chemiluminescence spectrum at 580 nm. Therefore, it can be proposed that some dye molecules are oxidized to produce polyphenols, as the luminescence donor part of the oxidation products of polyphenols transfer energy to unoxidized dye molecule, and the latter as the acceptor will provide the energy transfer luminescence, and it will shift in the long wavelength direction, which corresponds to the chemiluminescent peak at 620 nm.

Fluorescence spectra of the products of some dyes

The xanthone dyes and some polyphenols were oxidized by hydrogen peroxide in alkaline solution and the variation of their fluorescence spectra were investigated in detail. It was found that during the oxidation of dyes, the fluorescence spectra gradually became similar to those of polyphenols. Taking dibromophenylfluorone as a typical example (Fig. 4), in alkaline solution it shows two peaks at 460 and 545 nm in the fluorescence spectrum when it is excited at 390 nm (Fig. 4a). After addition of hydrogen peroxide, the peak at 545 nm decreases with time and shifts in the violet direction, while the peak at 460 nm increases with time and shifts in the red direction. When the reaction is complete, the solution only gives a fluorescence peak at 495 nm (Fig. 4e), which is very similar to that of the oxidation

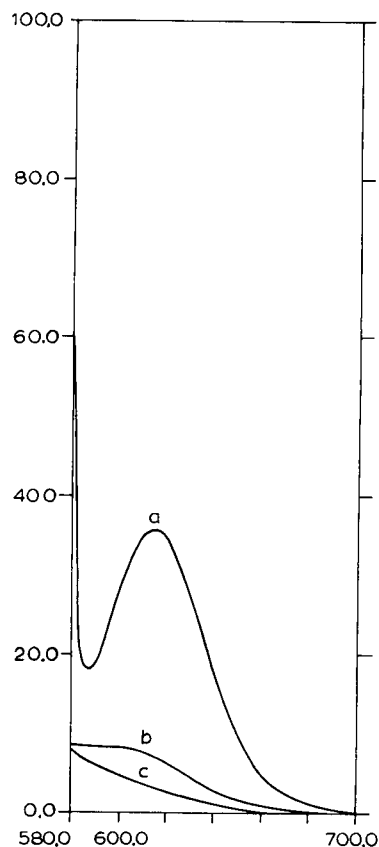


Fig. 5. Fluorescence spectra of dibromophenylfluorone using different excitation wavelengths: (a) 580; (b) 500; (c) 475 nm.

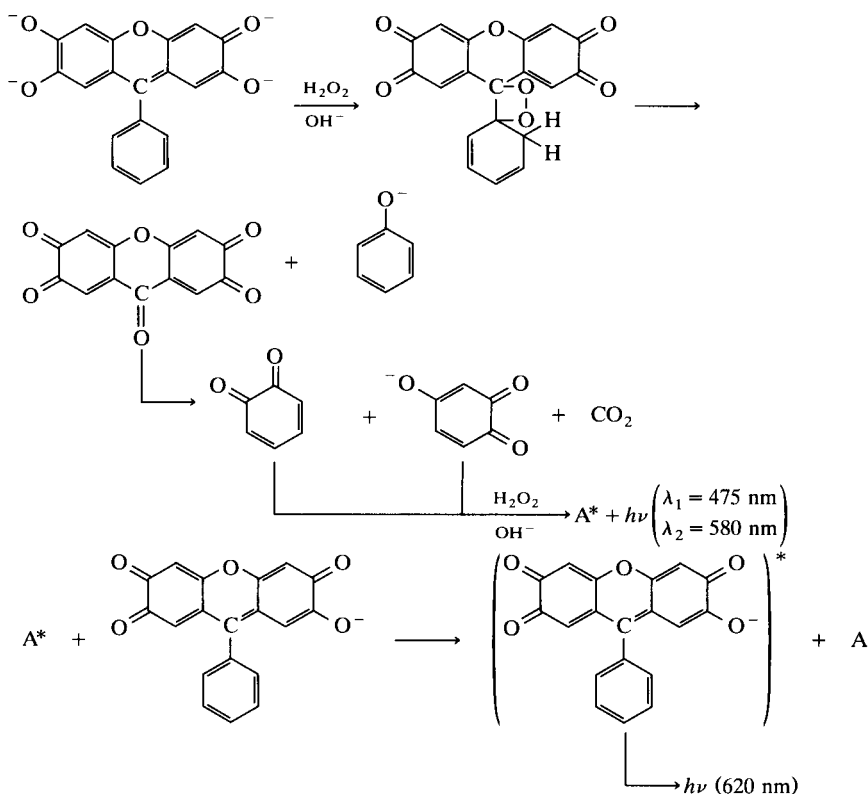
products of pyrogallol (Fig. 4f–i). The other dyes show similar trends. This also suggests that the polyphenols are involved in the reaction mechanism.

Moreover, in order to draw the correct conclusion that the unreacted dye is chemi-excited by the reaction of a portion of the dye with hydrogen peroxide, the fluorescence spectra for dibromophenylfluorone system were recorded using different excitation wavelengths. The results show that the dye gives a fluorescent peak at 620 nm when using 580 nm as excitation wavelength (see Fig. 5a), and it gives only a small peak when using 500 nm (see Fig. 5b) and none at all using 475 nm (see Fig. 5c). This result is in agreement with that from the chemiluminescence spectra and absorption spectra. It can be proposed again that an energy transfer mechanism is involved in the chemiluminescent reaction.

The results of quantum calculations showed that for all the dyestuffs tested the π -electron

density at C-1 is the lowest. It is generally recognized that in alkaline solution hydrogen peroxide produces an $O_2^{\cdot -}$ ion radical. This should attack the C-1 position first, with possible production of a peroxide bridge between C-1 and C-15, followed by formation of the polyphenols. The polyphenols are further oxidized to produce chemiluminescence. The mechanism of the chemiluminescent oxidation of polyphenols has been shown to proceed in several stages to produce low-molecular-weight, water-soluble polymers, and several other as yet unidentified products, and the chemiluminescence is due to emission from singlet oxygen [5]. The mechanism is shown in Scheme 1 for phenylfluorone as an example.

To summarize, two steps could be involved in the chemiluminescent reactions of xanthone dyes. First, the xanthone dyes are oxidized to produce polyphenols in alkaline solution and the polyphenols are further oxidized to produce chemilumi-



Scheme 1.

nescence emitted from singlet oxygen; second, some polyphenols in the excited state, as the luminescence donor, transfer the energy to unoxidized dye molecules and the latter as the acceptor gives the energy transfer luminescence at 620 nm.

3.3. Enhancement of chemiluminescence by surfactants

Recently, there has been increasing interest in investigating the enhancement of chemiluminescence by surfactants and its mechanism. Many chemiluminescence systems have been found to be enhanced by different kinds of surfactants [6,7]. As the enhancement of chemiluminescence by surfactants is very complex, the explanations for the mechanisms in different cases are there-

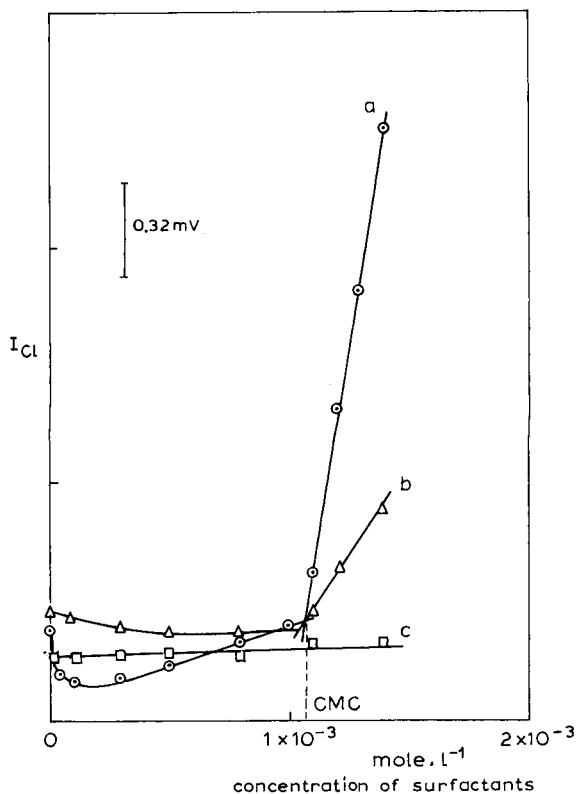


Fig. 6. Enhancement of chemiluminescence by surfactants: (a) CTMAB; (b) Triton X-100; (c) sodium laurylsulphonate.

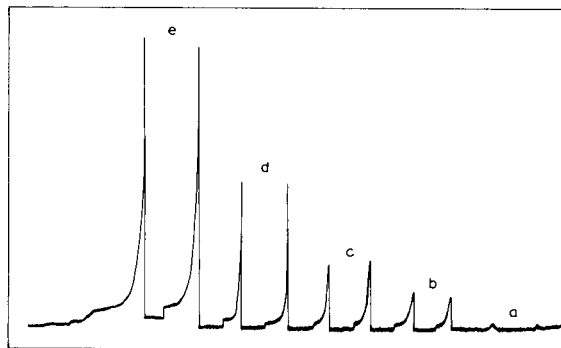


Fig. 7. Typical chemiluminescent signals for the phenylfluorone system. (a) Blank; (b) 0.1; (c) 0.2; (d) 0.4; (e) 0.8 ng ml⁻¹.

fore not the same, but they are always related to the formation of micelles.

We examined the effects of a cationic surfactant (CTMAB), an anionic surfactant (sodium laurylsulphonate) and a non-ionic surfactant (Triton X-100) on the chemiluminescence of xanthone dyes. Fig. 6 shows the effects of these surfactants on the phenylfluorone system. Fig. 6a shows that when the concentration of CTMAB is very low, it actually inhibits the chemiluminescence. This is because CTMAB is present in the form of single molecules when its concentration is very low, which can easily form an ion-association complex with the dye ions. Because of the formation of such a complex, many dye ions in the excited state return to the ground state by a non-radiative internal transfer process, which would lower the chemiluminescent quantum yield.

When the concentration of CTMAB in solution increases gradually, it starts to enhance the chemiluminescent reaction. At this stage the chemiluminescent intensity increases linearly with increasing concentration of CTMAB, but its slope is small. We ascribe this stage to the formation of pre-micelles [8,9]. From Fig. 6a, when the concentration of CTMAB increases continuously and eventually becomes higher than the critical micellar concentration (CMC), the chemiluminescent intensity increases greatly, and is also linearly related to the concentration of CTMAB, but its slope is much larger than previously; a turning point therefore occurs at the CMC. From Fig. 6a,

the CMC can be calculated, and the result is $1.05 \times 10^{-3} \text{ mol l}^{-1}$, whereas the literature value is $0.9 \times 10^{-3} \text{ mol l}^{-1}$ [7]; the slight difference could be ascribed to the different solution conditions.

Fig. 6b shows the effect of Triton X-100 on the chemiluminescence of phenylfluorone. Here the effect of the formation of premicelles with Triton X-100 is not obvious; however, a turning point at the CMC can still be observed. In contrast, the anionic surfactant sodium laurylsulphonate has no effect (Fig. 6c).

3.4. Catalysis of chemiluminescence by metal ions

We examined the catalysis by many metal ions of the chemiluminescence of the dyes studied, and found that $10\,000 \text{ ng ml}^{-1}$ Ca(II), Fe(III), Mg(II) and Zn(II), 1000 ng ml^{-1} Ti(IV), Bi(III), Ge(III), Ag(I), Au(III) and La(III), 200 ng ml^{-1} Al(III), Cr(III), Cu(II), Mo(VI), Pb(II), Cd(II), Nb(V), V(V), Ga(III) and Mn(II) and 20 ng ml^{-1} Ni(II) did not have an obvious catalytic effect on these chemiluminescent systems. Only Co(II) was found to show obvious catalysis; it is very strong especially in the presence of CTMAB, and the chemiluminescent intensity is proportional to the concentration of Co(II). Hence these chemiluminescent systems are suitable for determination of trace Co(II). We therefore tried to find the optimum conditions for the determination of traces of Co(II).

The catalytic chemiluminescent intensity from a xanthone dye is dependent on the concentrations of dye, hydrogen peroxide, CTMAB and sodium hydroxide used. The modified simplex method was used to find the optimum conditions for these catalytic chemiluminescent systems. Under the optimum conditions the linear response range, relative standard deviation and detection limits (defined as three times the concentration corresponding to the standard deviation of the blank signal) for these systems are shown in Table 3. A set of typical chemiluminescent signals for

the phenylfluorone system are shown in Fig. 7. The correlation coefficient ($n = 10$) was 0.9997.

4. Conclusions

The rigid plane structure of xanthone dye molecules is favourable for producing chemiluminescence. Polyphenols are involved in the chemiluminescent reactions of xanthone dyes, and the chemiluminescence is due to emission from singlet oxygen and intermolecular energy transfer. The cationic surfactant CTMAB enhances the chemiluminescent reactions of xanthone dyes. Traces of Co(II) catalyse the chemiluminescent reaction of xanthone dyes, and the catalytic chemiluminescent intensity is proportional to the concentration of Co(II), based on which a sensitive method may be developed for the determination of traces of Co(II).

Acknowledgement

This project was financially supported by the State Education Commission, China.

References

- [1] G.G. Guilbault, *Practical Fluorescence, Theory, Method and Technique*, Dekker, New York, 1973.
- [2] G.Z. Chen, *Fluorescence Analysis*, Science Publishing House, Beijing, 1990.
- [3] S.W. Zhang and Y.R. Shen, *The Basis of Organic Reagents, Fuel and Chemical Industrial Publishing House*, Beijing, 1974.
- [4] S.C. Zhang, *Organic Reagents and Ternary Complexes*, Shanghai Science and Technology Publishing House, Shanghai, 1980.
- [5] D. Slawinska and J. Slawinski, *Anal. Chem.*, 47(1975) 2101.
- [6] E.L. Wehry, *Anal. Chem.*, 58 (1986) 13R.
- [7] F. Zhang and Z.M. Liu, *Fenxi Huaxue*, 17 (1989) 1051.
- [8] G.S. Singhal, E. Rabinowitch, J. Havesi and V. Srinivasan, *Photochem. Photobiol.*, 11 (1979) 531.
- [9] Y. Kusumoto and H. Sato, *Chem. Phys. Lett.*, 68 (1979) 1.

Flow-injection chemiluminescence determination of the hydrazones of aromatic ketones

Taj Elsir Abbas Ahmed, Alan Townshend *

School of Chemistry, University of Hull, Hull HU6 7RX, UK

(Received 3rd December 1993; revised manuscript received 20th January 1994)

Abstract

A flow-injection system for investigating the chemiluminescence of aromatic ketone hydrazones is developed, based on KMnO_4 oxidation with formic acid as a carrier. Rhodamine B has proved to be an efficient sensitizer. The hydrazones studied are benzophenone hydrazone, benzil dihydrazone, acetophenone hydrazone and benzoin hydrazone. The relative standard deviation for ten replicate injections of 1×10^{-5} M benzophenone hydrazone and the detection limit (3σ) are 2% and 3×10^{-6} M (30 pmol, 10- μ l injection), respectively. The interference effect of some metal ions is also investigated. Cu(II), Cd(II), Zn(II), Ca(II), Co(II) and Ni(II) have no effect whilst Mn(II), Mo(VI) and Ce(IV) suppress the signal.

Key words: Chemiluminescence; Flow injection; Hydrazones; Interference effect; Ketones; Sensitizers

1. Introduction

Chemiluminescence (CL) (light emission from a chemically induced electronically excited species) is emerging as a powerful analytical tool with widespread applications in various fields [1,2]. This is attributed to the advantages of CL measurements over its rival techniques spectrofluorimetry, spectrophotometry and spectrophosphorimetry [3]. These advantages include higher sensitivity, wider linear dynamic range and elimination of the light source with its inherent problems of stray radiation. The combination of CL with flow-injection (FI) methods [4] or liquid

chromatography (LC) [5,6] has made the technique even more attractive. These features have led to the detection of a wide range of analytes including organic and inorganic species.

Most of the methods for the determination of carbonyl compounds are based either on spectrophotometry via their 2,4-dinitrophenylhydrazones, or spectrofluorimetry using different fluorophores [6,7]. Few CL methods are known for carbonyl compounds. The most common one involves their conversion to the hydrazone of a fluorophore and detection with peroxyoxalate CL, with a detection limit in the fmol range [6]. CL methods have also been reported for the determination of acetaldehyde via its oxidation in the presence of xanthine oxidase. Hydrogen peroxide is formed which is detected by the luminol- $\text{K}_3[\text{Fe}(\text{CN}_6)]$ CL reaction [8], or by its enhance-

* Corresponding author.

ment of the isopropanol- ClO^- - H_2O_2 CL system [9], down to 4×10^{-7} M and 1.8×10^{-6} M, respectively. Aliphatic aldehydes have also been determined by their inhibition of the H_2O_2 -luminol- $\text{K}_3[\text{Fe}(\text{CN})_6]$ CL system [10]. The lowest concentration measured was 2×10^{-5} M.

This paper describes a flow-injection method for determination of aromatic ketone hydrazones, based on the previously reported hydrazine CL reaction [11], which are readily prepared from the parent ketones. The following aromatic ketones were selected as model reactants: benzophenone (its hydrazone has been the most studied), benzil (to give the corresponding dihydrazone), benzoin (a well known fluorophore) and acetophenone (the simplest aromatic ketone).

2. Experimental

2.1. Reagents

All the chemicals used were analytical grade unless otherwise stated. Doubly distilled, deionized water was used throughout. Hydrazine hydrate (99%), formic acid and rhodamine B were obtained from Merck (Poole, UK). Benzophenone, benzil, benzoin and acetophenone were obtained from Janssen (Newton, UK).

2.2. Apparatus

The measurements were made with the luminescence meter described earlier [11]. The injection valve was a Rheodyne RH-5020 rotary valve obtained from Anachem, (Luton, UK). The manifold tubing was 0.5 mm i.d. PTFE. The peristaltic pump used to deliver the solutions was a Gilson Minipuls 3 (Anachem). The flow-injection manifold used is shown in Fig. 1.

2.3. General procedure

The working hydrazone-rhodamine B solutions were prepared daily from 1×10^{-3} M and 1×10^{-4} M stock solutions, respectively, to give a hydrazone solution in 1×10^{-5} M rhodamine B. The hydrazone solution (10 μl) was injected into

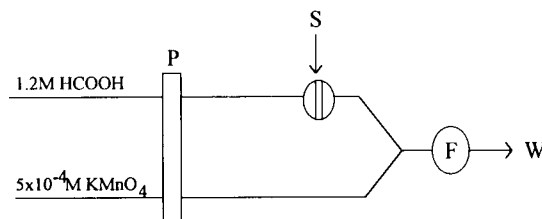


Fig. 1. FIA manifold: P, pump; S, sample; W, waste and F, flow cell.

1.2 M formic acid carrier which merges with 5×10^{-4} M KMnO_4 , both at flow-rates of 1.3 ml min^{-1} , in a T-piece located in front of the coiled glass flow cell.

2.4. Preparation of hydrazones

Few methods are available for the preparation of unsubstituted hydrazones. Those involve either the preparation of the azines [12] or the dimethyl substituted hydrazones [13,14] (as intermediates), which are then reacted with anhydrous hydrazine, or the direct reaction of hydrazine hydrate with the carbonyl compounds in the presence of a dehydrating reagent [15] or alone [16].

The hydrazones were prepared by modifying the procedure reported earlier [15] by using 99% hydrazine hydrate. The general procedure was as follows: the ketone and hydrazine hydrate were refluxed (molar ratio 1:5) for 5 h in a minimum volume of absolute ethanol. The products were recrystallized from aqueous ethanol. Their infrared (IR) spectra and elemental analyses were obtained to verify the nature of the products. The IR spectra showed a band at $1640\text{--}1620 \text{ cm}^{-1}$ ($\text{C}=\text{H}$), two bands at $3500\text{--}3300 \text{ cm}^{-1}$ (NH_2) and the disappearance of the band at $1720\text{--}1680 \text{ cm}^{-1}$ ($\text{C}=\text{O}$). The elemental analysis results confirmed the identity of the hydrazones.

3. Results and discussion

3.1. Reaction conditions and optimization of variables

Benzophenone hydrazone was used throughout to optimize the CL parameters. Because of

Table 1

Effect of the solvent (2 ml) on the emission intensity of 1×10^{-3} M benzophenone hydrazone using 5×10^{-4} M KMnO_4 and 1.2 M HCOOH

Solvent	Emission intensity (mV)	Blank intensity (mV)
DMF	11.6	0.0
THF	12.0	0.0
CH_3CN	8.0	4.0
DMSO	6.5	6.5

the insolubility of the hydrazones in aqueous media and their disproportionation in acidic media [16], different aqueous–organic solvent mixtures were investigated. The organic solvents used were *N,N*'-dimethylformamide (DMF), acetonitrile, dimethyl sulphoxide (DMSO) and tetrahydrofuran (THF). The last two gave a considerable blank signal. With the other two, a higher hydrazone CL signal was obtained with DMF (Table 1) and no blank signal was observed up to a concentration of 2.7 M DMF. Thus the concentrations of DMF used to dissolve the hydrazones were the minimum necessary, and always < 2.7 M.

The CL reaction was first investigated under conditions found to be optimum for hydrazine, i.e. 5×10^{-4} M OCl^- –buffer pH 11.5 or 5×10^{-4} M KMnO_4 – 5×10^{-2} M polyphosphoric acid [11]. However, no signal was observed with the former system up to a hypochlorite concentration of 2 M, nor with the latter system. In addition, no signal was observed with Fenton's reagent [$\text{Fe(II)}/\text{H}_2\text{O}_2$]. Using KMnO_4 as an oxidant and changing the carrier to test the effect of other acids, i.e. H_2SO_4 , HNO_3 , HCl and HCOOH in the range 0.6–1.8 M, all acids gave rise to some CL, but formic acid gave the greatest intensity as shown in Table 2. Therefore, formic acid solution was chosen as a carrier and KMnO_4 as an oxidant for further studies.

The effect of KMnO_4 concentration (6×10^{-4} – 6×10^{-3} M) using a 1×10^{-4} M hydrazone solution and 1 M formic acid carrier was studied. There was only a slight change in the intensity over the range, so 5×10^{-4} M was used in further studies. The effect of formic acid concentration (0.6–1.8 M) using 1×10^{-4} M benzophenone hydrazone is shown in Fig. 2; 1.2 M formic acid

Table 2

Effect of different acid carrier streams on the CL intensity of 1×10^{-3} M benzophenone hydrazone using 5×10^{-4} M KMnO_4

Carrier	Concentration (M)	Emission intensity (mV)
H_2SO_4	2.00	2.8
H_2SO_4	1.00	1.1
H_2SO_4	0.50	1.1
HCl	2.00	1.1
HCl	1.00	1.1
HCl	0.50	1.1
HNO_3	2.00	1.1
HNO_3	1.00	0.0
HCOOH	1.00	11.0

gave the most intense emission, so it was used as a carrier in further studies.

3.2. Effect of sensitizers

Potentially chemiluminescent molecules can transfer their excitation energy to a fluorophore (sensitizer) with the subsequent emission of the energy by the fluorophore (indirect CL), often resulting in an enhancement of the intensity. To be a sensitizer, the fluorophore should possess a high fluorescence efficiency, low oxidation poten-

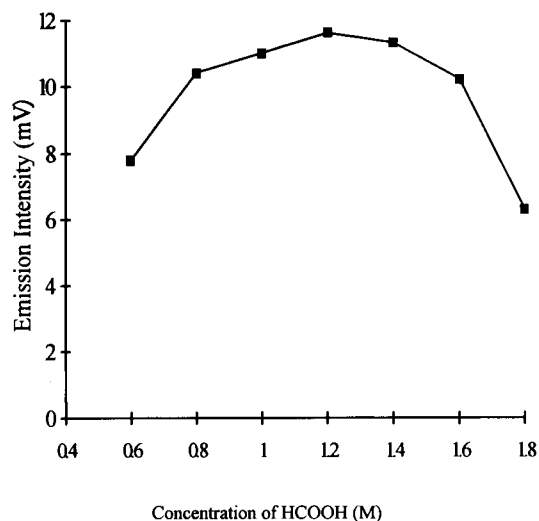


Fig. 2. Effect of HCOOH concentration on the emission intensity of 1×10^{-4} M benzophenone hydrazone using 5×10^{-4} M KMnO_4 .

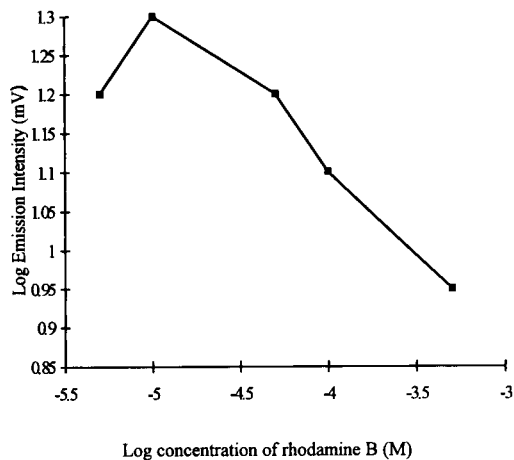


Fig. 3. Effect of rhodamine B concentration as a sensitizer on the CL intensity of 1×10^{-4} M benzophenone hydrazone using 5×10^{-4} M KMnO_4 and 1.2 M HCOOH .

tial and low-energy singlet excited state [17,18]. This phenomenon has been well exploited in determining fluorophores by peroxyoxalate CL [19].

To study their effect as potential sensitizers on the hydrazone CL, riboflavin (1×10^{-4} – 5×10^{-6} M dissolved in the carrier), fluorescein (5×10^{-5} – 1×10^{-6} M) and rhodamine B (5×10^{-4} – 5×10^{-6} M) (both dissolved in 1×10^{-4} M hydrazone solution) were investigated. It was found that both fluorescein and riboflavin suppressed the signal (ca. 50% for the concentration range of fluorescein and ca. 90% for the concentration range of riboflavin). However, rhodamine B enhanced the CL signal. Fig. 3 shows the effect of rhodamine B concentration on the CL signal. As 1×10^{-5} M rhodamine B gave rise to the most intense emission, it was used in all subsequent studies.

3.3. Effect of metal ions

The effect of some metal ions on the CL signal was investigated by adding a third stream for the metal ion solution to the FI manifold to merge with the hydrazone solution immediately after injection or by preparing the metal ion in 1×10^{-4} M hydrazone solutions containing 1×10^{-5} M rhodamine B. Both approaches gave similar results. Cu(II) , Cd(II) , Zn(II) , Ca(II) , Co(II) and

Ni(II) had no effect over the concentration range 0.1 – $25 \mu\text{g ml}^{-1}$, whilst Mn(II) , Mo(VI) and Ce(IV) produced a gradual decrease in signal with increase in concentration. Fig. 4 shows the effect of Mn(II) , Mo(VI) and Ce(IV) ions on the CL emission of 1×10^{-4} M benzophenone hydrazone.

3.4. Analytical performance

The optimum concentrations for the CL reaction were established to be 1.2 M formic acid, 5×10^{-4} M KMnO_4 and 1×10^{-5} M rhodamine B in the hydrazone sample solution. The log–log calibration graphs, prepared from peak height intensities measured under these conditions, for the four aromatic hydrazones are shown in Fig. 5. The detection limits (3σ) were, for a $10\text{-}\mu\text{l}$ injection, 2×10^{-6} M for benzil dihydrazone, 3×10^{-6} M for benzophenone hydrazone and acetophenone hydrazone and 4×10^{-5} M for benzoin hydrazone. The slopes of the least-squares linear log–log plots (Fig. 5) were 0.50 (6), 0.44 (7), 0.42 (7) and 0.56 (4), respectively, for the above compounds (the numbers in parenthesis are the numbers of data points used in the calculation).

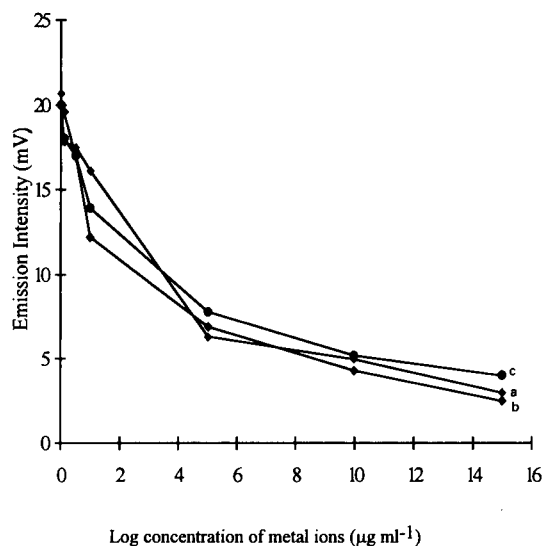


Fig. 4. Effect of (a) Mn(II) , (b) Ce(IV) and (c) Mo(VI) ion concentrations on the emission intensity of 1×10^{-4} M benzophenone hydrazone in 1×10^{-5} M rhodamine B using 1.2 M HCOOH and 5×10^{-4} M KMnO_4 .

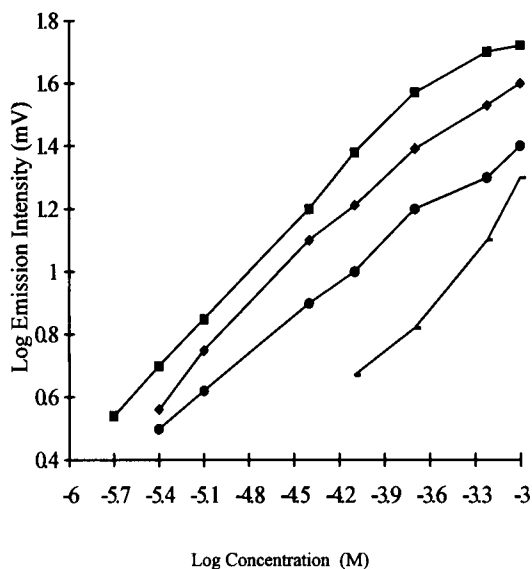


Fig. 5. Calibration for (■) benzil, (◆) benzophenone, (●) acetophenone and (-) benzoin.

The relative standard deviation (R.S.D.) for ten replicate injections of 1×10^{-5} M benzophenone hydrazone and the linear regression coefficient ($n = 7$) for the log-log graph in the range 4×10^{-6} – 6×10^{-4} M were 2.0% and 0.998, respectively.

4. Discussion

The CL of aromatic ketone hydrazones provides a simple, direct method for their determination at trace levels. Conversion of the aromatic ketones to their hydrazones is straight forward. The yield was above 95% for benzophenone, benzil and acetophenone, whereas benzoin gave an oily product which could not be crystallized. The CL intensities decreased in the order benzil, benzophenone, acetophenone and benzoin. Benzil, partly because it has two hydrazone groups, produced the highest sensitivity, whereas the weak intensity observed with the benzoin hydrazone may partly be attributed to the faster oxidation to a weaker emitting fluorophore, similar to benzoin itself [20]. Hydrazine itself was found to give a signal down to 1×10^{-5} M under these conditions. Therefore it must be removed during the

purification of the aromatic hydrazones. Rhodamine B (1×10^{-5} M), in the absence of the hydrazone, gave a blank signal of 2.7 mV. The sensitization of the CL reaction by rhodamine B may be ascribed to its red fluorescence and hence its low excitation energy, in contrast to the other two fluorophores which fluoresce at shorter wavelengths.

Metal ion interference arises only from Mn(II), Mo(VI) and Ce(IV). These are unlikely to be present in samples such as drugs which contain hydrazones. No enhancement by metal ions, which has been observed for hydrazine itself [11], was observed. The suppression of the CL signal by Mo(VI) and Ce(IV) is due to their oxidation of the hydrazone while the reason for the Mn(II) effect is not clear and needs further investigation.

No signal was found for benzophenone hydrazone in DMSO. As DMSO is known to be a weak oxidant [21], it may be that oxidation of the hydrazone by DMSO has occurred so that it is no longer chemiluminescent.

5. Conclusions

The method provides a rapid, reasonably sensitive means of determining hydrazones of aromatic ketones. The method should therefore also be applicable to aromatic ketones themselves, after derivatisation.

Previous methods for unsubstituted hydrazone preparation are tedious and take place under drastic conditions which make their adaptation to analytical work impractical. However, by using highly concentrated hydrazine hydrate it became possible to decrease the reaction time as well as the number of preparation steps. In contrast with aromatic ketones, the synthesis of hydrazones of aromatic aldehydes is rapid and simple, and a study of the CL of these hydrazones will be described in a subsequent paper.

Acknowledgement

T.E.A. Ahmed is grateful to the Government of Sudan (Ministry of the Higher Education and Scientific Research) for financial support.

References

- [1] K. Robards and P.J. Worsfold, *Anal. Chim. Acta*, 266 (1992) 147.
- [2] A.R.J. Andrews, *Anal. Proc.*, 28 (1991) 38.
- [3] A.K. Campbell, *Chemiluminescence, Principles and Application in Biology and Medicine*, Ellis Horwood/VCH, Chichester, 1988.
- [4] A. Townshend, *Analyst*, 115 (1990) 459.
- [5] J.W. Birks (Ed.), *Chemiluminescence and Photochemical Reaction Detection in Chromatography*, VCH, New York, 1989.
- [6] K. Imai, in H. Lingeman and W.J.M. Underberg (Eds.), *Detection-Oriented Derivatization Techniques in Liquid Chromatography*, Marcel Dekker, New York, 1990.
- [7] K. Blau and J.M. Halket (Eds.), *Handbook of Derivatives for Chromatography*, Wiley, Chichester, 2nd edition, 1993.
- [8] K. Sato and S. Tanaka, *Anal. Chim. Acta*, 236 (1990) 459.
- [9] L. Xiaohu, L. Minggang and X. Fang, *Anal. Lett.*, 23 (1990) 1191.
- [10] B. Vogin, F. Baronnet and J.C. Andre, *Anal. Chim. Acta*, 142 (1982) 293.
- [11] A.T. Faizullah and A. Townshend, *Anal. Proc.*, 22 (1985) 15.
- [12] A.C. Day and M.C. Whiting, *Org. Synth.*, 50 (1970) 3.
- [13] G.R. Newkome and D.L. Fishel, *Org. Synth.*, 50 (1970) 102.
- [14] G.R. Newkome and D.L. Fishel, *J. Org. Chem.*, 31 (1966) 677.
- [15] H.H. Szmant and C.J. McGinnis, *J. Am. Chem. Soc.*, 70 (1950) 2891.
- [16] D.H.R. Barton, E.R. O'Brien and J.S. Sternhell, *J. Chem. Soc.*, (1962) 470.
- [17] K.W. Sigvardson, J.M. Kennish and J.W. Birks, *Anal. Chem.*, 56 (1984) 1096.
- [18] K. Honda, K. Miyaguchi and K. Imai, *Anal. Chim. Acta*, 177 (1985) 111.
- [19] K. Honda, K. Miyaguchi and K. Imai, *Anal. Chim. Acta*, 177 (1985) 103.
- [20] I. Kamiya and T. Sugamoto, *Bull. Chem. Soc. Jpn.*, 50 (1977) 2442.
- [21] S. Searles, Jr. and H.R. Hays, *J. Org. Chem.*, 23 (1958) 2029.

Determination of mercury(II), monomethylmercury cation, dimethylmercury and diethylmercury by hydride generation, cryogenic trapping and atomic absorption spectrometric detection

Richard Puk, James H. Weber *

University of New Hampshire, Chemistry Department, Parsons Hall, Durham, NH 03824, USA

(Received 15th November 1993; revised manuscript received 24th January 1994)

Abstract

Mercury(II), monomethylmercury cation (MeHg), dimethylmercury (Me₂Hg) and diethylmercury (Et₂Hg) were simultaneously determined from aqueous samples by hydride generation volatilization, trapping and separation on a chromatographic column, and detection by atomic absorption spectrophotometry in a heated quartz furnace. Simplex optimization showed us the most effective choice of hydride formation and purge conditions. Absolute detection limits are 50 pg for the three organomercury compounds and 110 pg for Hg(II). Calibration curves are linear from 0.05 to 5 ng, and the reproducibility range for 1 ng Hg of the four analytes is 3–7%. Large differences among measured MeHg concentrations in a recent interlaboratory study using different measurement methods confirm that a new, completely independent method for determining mercury compounds in environmental samples is important. The method was applied to estuarine samples of the marsh grass *Spartina alterniflora* and eelgrass (*Zostera marina* L.) and found Hg(II), MeHg (eelgrass only) and Me₂Hg. Our difficulties in determining Me₂Hg suggest that it is more common in the aquatic environment than commonly believed.

Key words: Atomic absorption spectrometry; Hydride generation; Cryogenic trapping; Mercury; Monomethylmercury; Dimethylmercury; Diethylmercury; Environmental analysis

1. Introduction

Many researchers have determined mercury compounds in a variety of environmental samples. Nriagu [1] estimated that anthropogenic mercury emission to the atmosphere in 1983 was 3.6×10^9 g/year of which natural sources contributed 2.5×10^9 g/year, i.e. 41% of the total.

Total mercury concentrations from 0.19 to 2.1 pg/g over 3400 years in Antarctica ice core samples [2] demonstrate the influence of atmospheric deposition over millennia. Recent careful work shows that the concentration of total mercury in sea water is typically less than 0.004 ng/ml and similar values occur in lakes [3]. Not only is inorganic mercury toxic, but it forms extremely toxic methylmercury via environmental methylation processes. In addition researchers have recognized that methylmercury contamination of

* Corresponding author.

food chains leading to humans is a potential health hazard. Major concern has resulted from the large number of pristine lakes in the USA and elsewhere that contain fish with high methylmercury concentrations [3,4]. Marine fish typically contain 4 to 1000 ng/g (dry weight) total mercury of which > 95% is methylmercury [4]. The potential of human health risk from eating fish has driven research for speciation of mercury in environmental samples.

Speciation of inorganic mercury (Hg(II)), monomethylmercury cation (MeHg), and dimethylmercury (Me₂Hg) in environmental samples generally requires steps of extraction and derivatization (not all cases), separation and concentration, and detection [5,6]. Researchers have published hundreds of papers based on many methods, and the following brief summary of methods is necessarily selective. We will, however, summarize major themes.

Many papers use the extraction method of Westöö [7] or modifications of it. The methods typically rely on selective extraction of MeHg from strongly acidic hydrochloric acid or hydrobromic acid solution into a solvent such as benzene, toluene or dichloromethane [8]. Researchers then often determine MeHg by gas chromatography (GC) or atomic absorption spectrometry (AAS). The organic phase extracts MeHgX (X = Cl or Br), but not Hg(II)X₂ (X = Cl or Br), from an aqueous solution [9]; but extraction methods are undesirable because they are extremely tedious, time-consuming, and prone to contamination or loss errors.

Other researchers have avoided the above extraction steps in various ways. For example, Lansens et al. [10] and Decadt et al. [11] used a technique in which iodoacetic acid is the extractant and volatilizing agent for MeHg with resulting formation of MeHgI. They separate MeHgI from headspace components by GC and detect it by spectrophotometric methods.

Bloom [4,12] has developed an ethylation method for determination of Hg(II), MeHg, and Me₂Hg based on a method pioneered by the Weber group [13] for Pb(II) and methyllead compounds. Ethylation converts Hg(II) into diethylmercury (Et₂Hg) and MeHg into methyleth-

ylmercury. After ethylation, the method includes cryogenic trapping, separation, and detection by atomic fluorescence spectrophotometry. The detection limits are sufficiently low for environmental samples. Recently, Fischer et al. [14] applied the method to fish samples using AAS detection.

Two groups have used the hydride derivative of MeHg to determine it. Filippelli et al. [15] derivatized MeHg to volatile methylmercury hydride (MeHgH) by reactions with NaBH₄. After GC separation of headspace gases, they determined MeHgH by Fourier transformed infrared spectrometry (FTIR). MeHgH has never been isolated in the pure state and characterized, but they confirmed it in the head space by comparing its FTIR spectra and mass spectra to the deuterium analogue MeHgD. The 200 ng absolute limit of detection for MeHgH is far too high for environmental determinations. Quevauviller et al. [16] used the method with AAS detection of MeHg and Me₂Hg in sediments, but gave few experimental details.

This paper describes the simultaneous determination of Hg(II), MeHg, Me₂Hg, and Et₂Hg with limits of detection of 50 pg for organomercury compounds and 110 pg for Hg(II). The method is sufficiently rapid that researchers can do approximately five runs per hour. It is an improvement on the two previous publications on the hydride method for two reasons. Previous studies on the hydride generation technique either had a high limit of detection [15] or did not simultaneously measure the three above mercury compounds and give full experimental details [16]. An advantage of our hydride generation method over the ethylation generation method is that the rapid formation of hydrogen gas in the hydride method instantaneously purges the newly formed Hg⁰ and MeHgH as well as unchanged Me₂Hg and Et₂Hg onto the trap. The helium carrier gas in the ethylation method purges more slowly and less effectively. A recent interlaboratory study [17] using several methods including ethylation resulted in large differences in measured MeHg concentrations in mussels and fish and confirmed the need of a new independent method. The hydride generation method developed in this paper is an excellent candidate for a comparison of

the speciation of Hg(II), MeHg, and Me₂Hg in environmental samples with the results of ethylation studies and other published methods.

2. Experimental

2.1. Apparatus

The optimized setup (Fig. 1) includes a hydride generation reaction flask, PTFE transfer lines, a cold trap, and a quartz furnace. The hydride generation flask has a 5 × 4.5 cm round-bottom and a 11 × 2.5 cm neck (100 ml total volume) with an injection port on the side for a septum. It is important to cover the inside tip of the septum with PTFE tape to minimize inorganic mercury blanks. The flask head is heated to prevent H₂O condensation by applying voltage to a 26-gauge Nichrome wire wrapped around it. A Hamilton four-way valve (No. 86731) allows the He carrier gas to bypass the reaction flask. The He flow rate is controlled by a Cole-Palmer flow meter. Hg⁰, MeHgH, Me₂Hg, and Et₂Hg are trapped at -196°C (liquid N₂) on 2.5 g of Chromosorb G AW-DMCS (45/60 mesh) coated with 10% SP-2100 packed in a silanized U-shaped (45 cm × 6 mm id.) Pyrex trap. The 10% Sp-2100 liquid phase gives better separations than the 3%

coating previously used by us [18]. The trap is wrapped with Nichrome wire (26 gauge, 0.088 Ω/cm resistance). Power to the column, transfer lines, and furnace are individually supplied by Variacs.

Flexible PTFE tubing transfer lines (2.5 mm i.d.) are inserted in 3 mm i.d. Tygon tubing. Then Nichrome wire (32 gauge, 0.35 Ω/cm resistance) is coiled around the outer Tygon tubing and insulated by wrapping PTFE tape around it. PTFE-to-PTFE and PTFE-to-Pyrex connections are made with Omnifit PTFE variable-bore connectors.

The 15 cm × 8 mm id quartz furnaces (Fig. 1) are custom-made by Anderson Glassblowing (Fitzwilliam, NH), and treated and annealed by the method of Hatfield [19]. Each is wrapped with a 1 mm wide layer of woven quartz tape (Wale Apparatus Co., No. 17-1790), coiled with a double strand of 26-gauge Nichrome wire then insulated by 2.0 cm wide Waletex high-temperature glass tape wool (Wale, No. 17-1730). The furnace is mounted on a custom-made stainless steel frame placed on the AAS burner head.

The following conditions are optimal in our Perkin Elmer Model 560 atomic absorption spectrometer and derivatization-purge system. The Jarrell-Ash mercury hollow cathode lamp is used at 12 mA in the continuous mode. The AAS operates at 253.7 nm with a 2-nm slit width and a 0.2-s integration repeat mode. The output signal (1-V full deflection) is integrated by a Hewlett-Packard Model 3392A integrator. Integrator parameters are as follows: attenuation, 2–5; threshold, 4; peak width, 0.16; chart speed, 1.0 cm/min; area reject, 0. The helium flow rate is 140 ml/min. The Variacs' outputs to the transfer lines (20 V, ca. 50°C) and furnace (35 V, 825°C) are constant, but output to the column varies (see below). All temperatures are measured with a chromel/alumel thermocouple.

2.2. Reagents, glassware and plasticware

Doubly deionized, distilled water (Corning Mega-pure still), is used in all experiments. All glassware used for preparation storage and dilutions is soaked in 7% HNO₃ (rough bath)

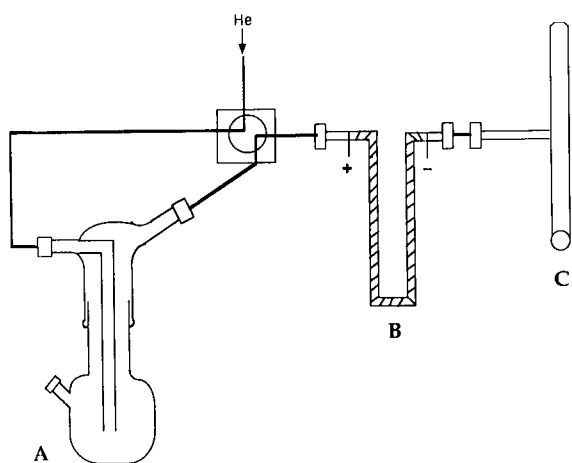


Fig. 1. Hydride generation flask (A), cryogenic trap (B) and quartz furnace (C) for determination of inorganic mercury and organomercury compounds.

overnight and then soaked in a second solution of 7% HNO_3 (final bath) overnight and rinsed with water. Between runs the reaction flask is rinsed successively with a 1% (v/v) HNO_3 –0.002% (w/v) KMnO_4 solution, 1 M HCl and water. Pipetter tips are soaked overnight in 6% aqueous NaBH_4 and then rinsed with 1 M HCl and water to decrease mercury blanks. Aqueous 12% NaBH_4 (m/v) is prepared from 99% sodium tetrahydridoborate (Aldrich) in a beaker. The solution is covered, refrigerated overnight, filtered with a 0.2 μm Nuclepore filter, diluted to a 6% solution in a volumetric flask, and purged with N_2 for 30 min. The overnight standing and purging with N_2 decrease the mercury blank. HCl was isothermally distilled [20]. The HCl is further treated to remove mercury by adding 33 μl of 6% NaBH_4 to 50 ml of ca. 6.3 M HCl and purging it with N_2 for 5 min [21]. All other reagents unless stated otherwise are of analytical grade.

2.3. Standards

Stock solutions of 1000 $\mu\text{g}/\text{ml}$ Hg are made as follows. MeHgCl (Alfa), Me_2Hg (Alfa), and Et_2Hg (Alfa) are dissolved in methanol, and HgCl_2 is dissolved in 0.1 M HCl. All stock solutions are kept at 4°C in the dark in hypo-vials sealed with crimp-on PTFE-lined septa. Working standards (10 $\text{ng}/\mu\text{l}$) and standards (0.1 $\text{ng}/\mu\text{l}$) are made by successive dilution of stock solutions in the stock solution solvents. Working standards remain stable at least seven days and standards are made daily. Standards are injected into the reaction flask using an adjustable 0 to 20 μl Gilson Pipetman.

2.4. Samples

From the Great Bay Estuary (NH) were collected marsh grass (*Spartina alterniflora*) samples from Chapman's Landing and eelgrass (*Zostera marina* L.) samples from Portsmouth Harbor (NH). One gram samples (fresh weight) of *S. alterniflora* or eelgrass are ground to a fine powder in liquid nitrogen using a mortar and pestle and placed in serum vials along with 5 ml of 0.1 M HCl and capped with septa and aluminum

caps. The samples are sonicated 1 h at 40°C and 50/60 Hz in a B-22-4 Branson sonicator and transferred to 30 ml polyallomer centrifuge tubes. The small amount of residual sample is rinsed from vials into centrifuge tubes with 5 ml methanol. The samples are centrifuged for 15 min at 7500 rpm, the extracts are decanted from the solid, and 100 to 500 μl aliquots are used for AAS measurements. Percent recoveries from 5 ml 0.1 M HCl containing 1 g of plant were done by this procedure using 200 ng spikes.

Me_2Hg , which is volatile, was also separated from *S. alterniflora* without use of chemical extractants. A 1 g sample was ground as above and placed in a 50 ml round bottom flask which was attached to a vacuum line. Me_2Hg was volatilized for 1 h by a vacuum of 0.2 mm Hg at room temperature into a U-trap containing glass beads to a height of 5 cm at liquid nitrogen temperature. The sample in the trap was dissolved in 5 ml of methanol and run on the AAS as described below.

2.5. Operating procedures

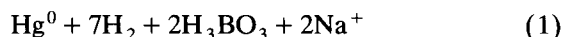
The optimum purge time, HCl concentration and NaBH_4 concentration were determined by simplex optimization. Water (10 ml) and sufficient 0.63 M HCl, using a glass pipet, are introduced into the reaction flask to give a 0.01 M (pH 2) HCl acid solution. Standards (or sample extracts) are then added to the reaction flask. Et_2Hg is used as an internal standard for samples. The reaction flask is capped with the reaction flask head and He is bubbled through the stirred solution for about 30 s to remove O_2 from the flask. Then 0.8 ml of 6% NaBH_4 is injected through the septum below the surface of the solution with a glass syringe at a sufficiently slow rate to prevent excess foaming and the sample is purged 6 min. During this procedure the solution is purged predominantly by the H_2 formed by the reaction between HCl and NaBH_4 . The final pH is 10. The reaction flask is then bypassed by use of the Hamilton four-way valve. At the same time the liquid N_2 is removed from the column, the Variac for the column is turned to 15 V, and the integrator is started. After 2 min, 30 V is applied and

this voltage is maintained for 2 min past the elution of the last compound to ensure removal of water. Retention times with the above conditions are: Hg(II) (1.6 min), MeHgH (2.6 min), Me₂Hg (3.0 min) and Et₂Hg (4.0 min). Temperatures in the trap at times of elution are: 50°C (Hg(II)), 75°C (MeHg), 80°C (Me₂Hg) and 90°C (Et₂Hg). The final temperature 2 min after elution of Et₂Hg is 100°C. Et₂Hg (1 ng) was used as an internal standard in all determinations.

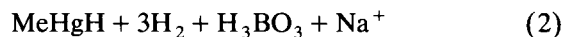
3. Results and discussion

3.1. Formation of Hg⁰ and MeHgH

Mercury(II) reacts with NaBH₄ to produce Hg⁰ (Eq. 1).



Methylmercury cation reacts similarly with NaBH₄ to yield the corresponding methylmercury hydride (Eq. 2).



In contrast to results of Bricker [22], Sarzanini et al. [23] and Rezenda et al. [24], NaBH₄ does not reduce MeHg to Hg⁰ under our reaction conditions. These researchers used air as a carrier gas [22], high HNO₃ concentration and air as a carrier gas [24], or APDC complexes eluting from a liquid chromatography column in acetonitrile and acetic acid [23] in their studies showing reduction of MeHg (and other organomercury compounds) to Hg⁰. In our experiments under a He atmosphere 0.01 M HNO₃ does not decompose any of the three organomercury compounds. However, in the presence of O₂ or O₂ and relatively high HNO₃ concentrations, NaBH₄ very likely forms radicals that cleave the carbon–mercury bond in organomercury compounds and induce their reduction to Hg⁰. It is unclear why the MeHg–APDC complex in a flow of N₂ carrier gas leads to formation of Hg⁰. The observation that under some conditions NaBH₄ reduces MeHg to Hg⁰

demonstrates that researchers must carefully choose reaction conditions for determination of MeHg as MeHgH.

MeHg has never been isolated in pure form, but experiments demonstrate its presence in the gas phase and methanolic solution. MeHgH that forms in the headspace of a closed vial after reaction of an aqueous solution of MeHgCl with NaBH₄ has a half-life of 1.5 h. This half-life is easily long enough for determination of MeHg by our method. In agreement with Filippelli et al. [15] we confirmed the presence of MeHgH vapour by mass spectral analysis. We saw no trace of a cluster near *m/e* 252 for CH₃HgCl. Additional evidence for the formation of MeHgH was a polarographic demonstration of its presence in methanol by Devaud [25].

3.2. Simplex optimization of reaction conditions

Stirring with a PTFE magnetic stirring bar and injection of NaBH₄ beneath the surface of the sample solution is important for maximum reproducibility of MeHgH areas and absence of purged, unreacted MeHgCl. We monitored peak areas for 1 ng amounts of mercury as Hg⁰, MeHgH, Me₂Hg, and Et₂Hg by simplex optimization of purge time and concentrations of HNO₃ and NaBH₄ in 10 ml of water in the hydride generation flask. Because of our emphasis on MeHg relative to Hg(II), we chose conditions that favoured maximum areas for MeHgH. Because neither Me₂Hg nor Et₂Hg form hydrides, their peak areas are relatively insensitive to reaction conditions studied. The highest peak area for MeHgH results from a reaction medium of 0.01 M HCl (pH 2), addition of 0.8 ml of 6% NaBH₄ and a 6 min purge time. The reaction of NaBH₄ with H⁺ at the low pH of 2 results in formation of considerable H₂, which contributes significantly to, or is predominant in, effective purging of Hg⁰, MeHgH, Me₂Hg, and Et₂Hg from solution. This purging effect is a major advantage of hydride derivatization over the ethylation procedure [4,12,14]. We never observed any mercury-containing degradation product of MeHgH.

No appreciable analyte remains in the reaction flask because a second injection of 0.8 ml NaBH₄

after 5 min to the same solution previously containing Hg(II) and MeHg at pH 10 or reacidified to pH 2 yields no appreciable Hg⁰ or MeHgH peaks. This result indicates nearly complete (> 95%) removal of Hg(II) and MeHg from the reaction flask and of Hg⁰ and MeHgH from transfer lines during our standard procedure.

3.3. Optimization of transfer lines and quartz furnace

Heating of transfer lines at different voltages between 10 and 30 V did not affect the peak area of Hg⁰ and organomercury compounds. However, a minimum of 20 V is necessary to remove between-run blanks.

The temperature in the quartz furnace and its configuration contribute to low detection limits for mercury compounds. We tested different configurations of quartz furnaces to optimize peak area and chose a 15 cm × 8 mm i.d. one based on work by Hawley and Ingle [26]. Peak areas are 100% higher with this furnace than one with quartz windows. Temperature vs. peak area curves for Hg(II), MeHg, Me₂Hg, and Et₂Hg analytes (Fig. 2) demonstrate that a temperature of 825°C is sufficient to maximize atomization efficiency and peak areas. At this temperature peak areas for MeHgH, Me₂Hg and Et₂Hg are near their maxima, but that of Hg⁰ is much greater at lower temperatures.

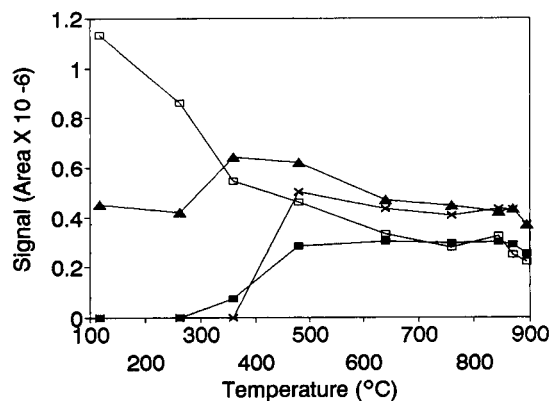


Fig. 2. Peak areas for 1 ng of Hg(II) (□), MeHg (■), Me₂Hg (×) and Et₂Hg (▲) analytes from 118 to 895°C. The areas of Hg(II) were corrected for background.

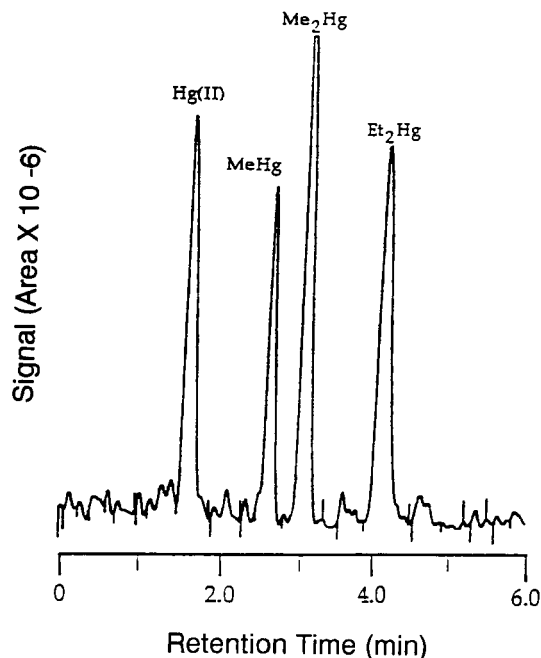


Fig. 3. Chromatogram for 1 ng each of Hg(II), MeHg, Me₂Hg and Et₂Hg analytes.

3.4. Confirmation of analytes and absence of their decomposition

Fig. 3 is a typical chromatogram for simultaneous determination of 1 ng standards of Hg(II), MeHg, Me₂Hg and Et₂Hg. Reproducibility of retention times is less than 5% R.S.D. for all analytes. We confirmed retention times for Hg(II), MeHg and Me₂Hg under conditions listed in the Experimental section in several ways. We used pure Hg⁰ vapour over liquid Hg for Hg(II), and MeHgCl vapour over solid MeHgCl for MeHgCl which rarely appears. We corroborated the retention time of Me₂Hg by its vapour over a solution in methanol and by placing a methanolic solution of it into a dry hydride generation flask and purging it onto the trap. We also authenticated the retention time of MeHgH after forming it in the headspace of a vial [15].

We demonstrated the absence of decomposition of MeHgH, Me₂Hg and Et₂Hg using 5 ng standards. MeHgCl yielded no underivatized MeHgCl or Me₂Hg. Neither Me₂Hg nor Et₂Hg

Table 1

Calibration curve data and detection limits for mercury(II), monomethylmercurycation (MeHg), dimethylmercury (Me₂Hg) and diethylmercury Et₂Hg)

Compound	Linear calibration range (ng) ^a	Slope × 10 ⁻⁵ (area/ng) ^b	detection limit (ng) ^c
Hg(II)	0.05–5	3.15	0.11
MeHg	0.05–5	3.72	0.05
Me ₂ Hg	0.05–5	4.37	0.05
Et ₂ Hg	0.05–5	4.42	0.05

^a R.S.D. for 1 ng samples ranges from 3–7%.

^b Correlation coefficients are generally greater than 0.99.

^c Based on $S/N = 3$.

form the potential monoalkylmercury product MeHg⁺ or EtHg⁺. We know the retention times of MeHgH and Et₂Hg from standards and estimate that of EtHg⁺ to be between 2.6 min (MeHgH) and 4.0 min (Et₂Hg).

3.5. Sensitivity, precision and limits of detection

Table 1 describes calibration parameters and precision for Hg(II) and organomercury compounds. The linear calibration range extends from 0.05 to 5 ng for all analytes. Three or five replicates that typically result in 3–7% R.S.D. for 1 ng standards of Hg(II) and three organomercury compounds demonstrate appropriate repeatability for each analyte. Detection limits ($S/N = 3$) are 110 pg for Hg(II) and 50 pg for organomercury compounds.

3.6. Relative calibration curve slopes

The relative sensitivities of the mercury analytes (Table 1) are: Me₂Hg ≈ Et₂Hg > MeHg > Hg(II). Neither variable mass transport nor efficiency of hydride formation cause different calibration curve slopes because we find no measurable analyte by re-running solutions in the reaction flask. Atomization efficiency in the furnace controls relative sensitivities of the organomercury analytes. This means Me₂Hg and Et₂Hg have higher atomization efficiencies than MeHgH. Hg⁰ requires no atomization in the furnace, but has lower sensitivity than the organomercury compounds because the 825°C furnace temperature is not optimal for Hg⁰ (Fig. 2). We chose to maximize the sensitivity of MeHgH over that of Hg(II) in the simplex optimization because its determination is the main goal of this work.

3.7. Eelgrass and *S. alterniflora* samples

Under the extraction conditions (see Experimental section) percent recoveries for 200 ng spikes in 5 ml of 0.1 M HCl range from 75 to 104% for Hg(II), MeHg and Me₂Hg (Table 2). This result means that neither MeHg nor Me₂Hg demethylate during the extraction procedure. Recoveries from *S. alterniflora* were excellent for MeHg (90%) and Me₂Hg (81%). The disappointing recovery for Hg(II) can undoubtedly be improved by modifying extracting conditions.

Table 2

Percent recoveries of mercury(II), monomethylmercurycation (MeHg) and dimethylmercury (Me₂Hg) and their concentrations in *S. alterniflora* and eelgrass

Compound	%Recovery ^c from 0.1 M HCl (R.S.D. (%))	%Recovery ^c from <i>S. alt.</i> (R.S.D. (%))	Concentration (ng Hg/g) ^{a,b}	
			<i>S. alterniflora</i> (R.S.D. (%))	Eelgrass (R.S.D. (%))
Hg(II)	75 (5)	43 (27)	12.5 (30)	13.7 (48)
MeHg	104 (14)	90 (6)	< 5	7.9 (35)
Me ₂ Hg	98 (12)	81 (7)	9.1 (22)	9.7 (19)

^a Fresh weight.

^b Data from extractions of two separate solid samples and 4–6 AAS runs each extract.

^c Based on 200 ng spike per 5 ml 0.1 M HCl/5 ml methanol (v/v) or per 1 g (fresh weight) plant sample in the same extractant.

Data in Table 2 describe the speciation of mercury in *S. alterniflora* and eelgrass, and Fig. 4 shows the chromatogram for eelgrass. Total mercury concentration of 21.6 ng Hg/g fresh weight in *S. alterniflora* (Table 2), when converted to dry weight basis by a 0.27 dry weight/fresh weight factor [27], is about 80 ng Hg/g. This result is well within the 20 to 190 ng/g range found by Kraus et al. [28] and references quoted therein. The appearance of relatively high concentrations of Me_2Hg in *S. alterniflora* and eelgrass is surprising. Much of the high R.S.D. for mercury concentrations results from difficulty in homogenizing plant samples. Previously Me_2Hg has been found in the aquatic environment only in marine sediments [16] and the Pacific Ocean [29]. For this reason we confirmed the presence of Me_2Hg in *S. alterniflora* by a vacuum technique without added chemicals. The resulting amount of Me_2Hg found approximated that found in HCl/MeOH extracts of *S. alterniflora*.

We cannot overemphasize the difficulty of determining Me_2Hg in environmental samples due to its volatility, potential for demethylation by

strong, concentrated acids and insolubility in aqueous media. We solved the volatility problem by using sealed vials and the demethylation problem by extracting under relatively mild conditions. However the insolubility of Me_2Hg in aqueous media caused us considerable difficulty. Before adding methanol to our aqueous extracts we found Me_2Hg only occasionally but sometimes at large concentrations. The reason for the irreproducibility was that the aqueous extracts were heterogeneous with very insoluble, dense Me_2Hg (ca. 3 g/ml) at the bottom of the vials. The addition of methanol resulted in homogeneous solutions and significantly improved reproducibility.

4. Conclusions

Inconsistent results of an interlaboratory study of MeHg in mussels and fish [17] accentuate the need of a new speciation method for mercury compounds for comparison to current methods. The hydride derivatization procedure developed here for speciation of mercury(II) and organomercury compounds is excellent for that purpose. Our observations of relatively high concentrations of Me_2Hg in *S. alterniflora* and eelgrass, coupled with its volatility and insolubility in aqueous media, suggest that Me_2Hg may be more common in the aquatic environment than commonly thought. This opinion is corroborated by a recent finding of Me_2Hg formation from MeHg and S^{2-} in the presence of sulfate reducing bacteria [30]. Now that we have solved initial problems with the hydride generation method, we will further develop it in the future for speciation of Hg(II) and methylmercury compounds in estuarine plant, shellfish, fish, sediment, and porewater samples.

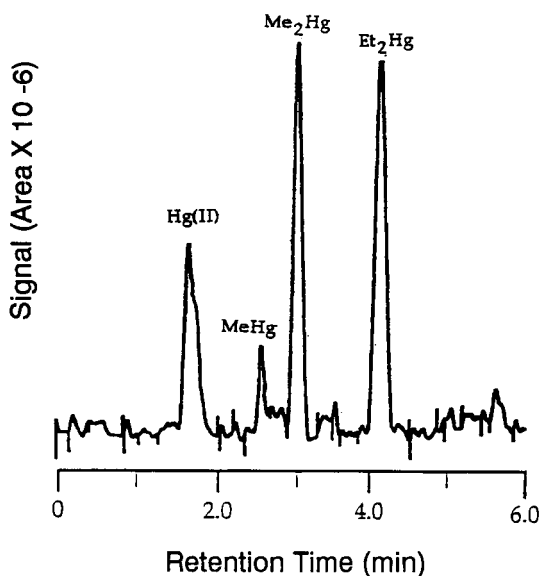


Fig. 4. Chromatogram of Hg(II), MeHg and Me_2Hg from an extract of eelgrass. Et_2Hg is an internal standard.

Acknowledgements

We thank Mike Rooney for considerable help in setting up the AAS apparatus, Anne Falke for *S. alterniflora* samples and Fred Short for eelgrass samples. NSF grant INT-9113676 partially supported this work.

References

- [1] J.O. Nriagu, *Nature*, 338 (1989) 47–49.
- [2] G.M. Vandal, W.F. Fitzgerald, C.F. Boutron and J.-P. Candelone, *Nature*, 362 (1993) 621–623.
- [3] W.F. Fitzgerald and T.W. Clarkson, *Environ. Health Perspect.*, 96 (1991) 159–166.
- [4] N.S. Bloom, *Can. J. Fish. Aquat. Sci.*, 49 (1992) 1010–1017.
- [5] O.F.X. Donard and F.M. Martin, *Trends Anal. Chem.*, 11 (1992) 17–26.
- [6] D.E. Wells, *Mikrochim. Acta*, 109 (1992) 13–21.
- [7] G. Westöö, *Acta Chem. Scand.*, 21 (1967) 1790–1800.
- [8] Y. Thibaud and D. Cossa, *Appl. Organometal. Chem.*, 3 (1989) 257–266.
- [9] G. Cerrati, M. Bernhard and J.H. Weber, *Appl. Organometal. Chem.*, 6 (1992) 587–595.
- [10] P. Lansens, C. Meuleman, C.C. Laiño and W. Baeyens, *Appl. Organometal. Chem.*, 7 (1993) 45–51.
- [11] G. Decadt, W. Baeyens, D. Bradley and L. Goeyens, *Anal. Chem.*, 57 (1985) 2788–2791.
- [12] N. Bloom, *Can. J. Fish. Aquat. Sci.*, 46 (1989) 1131–1140.
- [13] S. Rapsomanikis, O.F.X. Donard and J.H. Weber, *Anal. Chem.*, 58 (1986) 35–38.
- [14] R. Fischer, S. Rapsomanikis and M.O. Andreae, *Anal. Chem.*, 65 (1993) 763–766.
- [15] M. Filippelli, F. Baldi, F.E. Brinckman and G.J. Olson, *Environ. Sci. Technol.*, 26 (1992) 1457–1460.
- [16] P. Quevauviller, O.F.X. Donard, J.C. Wasserman, F.M. Martin and J. Schneider, *Appl. Organometal. Chem.*, 6 (1992) 221–228.
- [17] Ph. Quevauviller, I. Drabaek, H. Muntau and B. Griepink, *Appl. Organomet. Chem.*, 7 (1993) 413–420.
- [18] O.F.X. Donard, S. Rapsomanikis and J.H. Weber, *Anal. Chem.*, 58 (1986) 772–777.
- [19] D.B. Hatfield, *Anal. Chem.*, 59 (1987) 1887–1888.
- [20] C. Veillon and D.C. Reamer, *Anal. Chem.*, 53 (1981) 549–550.
- [21] B. Welz and M. Schubert-Jacobs, *Fresenius' Z. Anal. Chem.*, 331 (1988) 324–329.
- [22] J.L. Bricker, *Anal. Chem.*, 52 (1980) 492–496.
- [23] C. Sarzanini, G. Sacchero, M. Aceto, O. Abollino and E. Mentasti, *J. Chromatogr.*, 626 (1992) 151–157.
- [24] M.R. Rezende, R.C. Campos and A.J. Curtius, *J. Anal. At. Spectrom.*, 8 (1993) 247–251.
- [25] M. Devaud, *J. Organometal. Chem.*, 220 (1981) C27–C29.
- [26] J.E. Hawley and J.D. Ingle Jr., *Anal. Chem.*, 47 (1975) 719–723.
- [27] J.H. Weber, M.R. Billings and A.F. Falke, *Est. Coast. Shelf Sci.*, 33 (1991) 549–557.
- [28] M.L. Kraus, P. Weis and J.H. Crow, *Mar. Environ. Res.*, 20 (1986) 307–316.
- [29] R.P. Mason and W.F. Fitzgerald, *Nature*, 347 (1990) 457–460.
- [30] F. Baldi, M. Pepi and M. Filippelli, *Appl. Environ. Microbiol.*, 59 (1993) 2479–2485.

A screening method for trace mercury analysis using flow injection with urease inhibition and fluorescence detection

D. Narinesingh ^{a,*}, R. Mungal ^a, T.T. Ngo ^b

^a *Department of Chemistry, The University of the West Indies, St. Augustine, Trinidad and Tobago*

^b *Department of Development and Cell Biology, University of California, Irvine, CA 92717, USA*

(Received 22nd January 1993; revised manuscript received 12th January 1994)

Abstract

A flow-injection screening method based on urease inhibition is described for the determination of trace amounts of the heavy metal ions, mercury and silver. The method is based on the inhibitory effect that these ions have on the enzyme urease which catalyzes the conversion of urea to carbon dioxide and ammonia. The liberated ammonia is monitored fluorimetrically using *o*-phthalaldehyde as the fluorophore ($\lambda_{\text{ex}} = 340 \text{ nm}$, $\lambda_{\text{em}} = 455 \text{ nm}$). A detection limit of 2 ppb can be achieved. Comparison of this flow injection method with that of the standard cold vapour atomic absorption technique for mercury determination gave a standard deviation of 0.02 and a coefficient of variation of 2%. Also one-way ANOVA shows no significant difference between these two methods.

Key words: Flow injection; Fluorimetry; Mercury; Silver; Urea

1. Introduction

The determination of traces of pollutants in biological materials, natural waters and air is becoming increasingly important as man becomes more aware of the importance of the environment to their survival. One class of these pollutants which is of major concern is the toxic heavy metals to which the environment is especially vulnerable.

The most widely used techniques for the quantification of these heavy metals are based on atomic absorption spectrometry (AAS) [1], anodic stripping voltammetry (ASV) [2] or resistance

measurements on thin gold films [3], all of which are characterized by high sensitivity and specificity. With specific reference to mercury, the following methodologies have been successfully applied: electrothermal AAS (0.5 ppb) [4], ASV (40 ppb) [5], x-ray fluorescence spectrometry (XRF) (10 ppm) [6], neutron activation analysis (NAA) (10 ppb) [7]; inductively coupled plasma spectrometry (ICP) (10 ppb) [8] and atomic fluorescence spectrometry (10 ppt) [9]. These methods involve, however, considerable instrumentation cost and require skilled and trained personnel. Furthermore, in many cases sample handling prior to analysis involves preconcentration and purification steps which will lengthen the analysis time.

For many purposes, however, a simple and fast

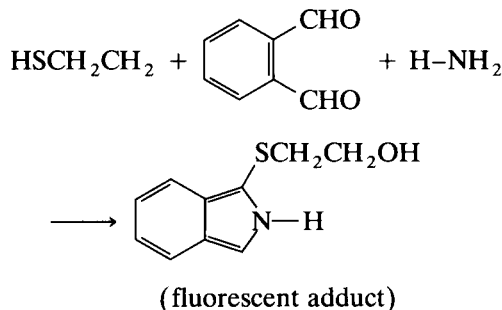
* Corresponding author.

but less specific screening method for the determination of heavy metals in general is desirable. Such a method could be used in fast screening tests of for instance industrial process water or foodstuffs to indicate the existence of heavy metals. In this respect, the use of activity measurements of enzymes appears to have some merits. Detection of enzyme inhibitors can be done in a very sensitive way since the interaction of a single inhibitor molecule with an enzyme can result in a large reduction of the enzyme activity, the enzyme thus acting as an amplifier. Furthermore, the enzymes are often specific for the inhibitor and in many cases the effects of pollutants on enzymatic activity are related to their biological toxicity.

This principle of enzyme activity measurements has already proven useful in a number of applications, such as in the determination of low concentrations of copper and mercury [10], methotrexate [11], and 2,4-dinitrophenol [12]. This principle has also been used for the detection of nerve gases based on the inhibition of the enzyme cholinesterase and has now become a commercial analytical procedure [13].

In the present study, the potential of using urease activity measurements as a basis for the determination of trace amounts of mercury and silver is investigated. The method is based on the inhibitory effect of mercury and silver ions on this enzyme which catalyzes the conversion of urea to carbon dioxide and ammonia. The activity of the enzyme is determined from the rate of the ammonia produced.

The liberated ammonia is monitored fluorimetrically ($\lambda_{\text{ex}} = 340 \text{ nm}$, $\lambda_{\text{em}} = 455 \text{ nm}$) using flow-injection analysis (FIA). The fluorophore used is *o*-phthalaldehyde:



2. Experimental

2.1. Materials

Jack bean urease (E.C. 3.5.1.5, 5020 U/mg protein), was obtained from Sigma (St. Louis, MO), *o*-phthalaldehyde from Merck (Darmstadt), montmorillonite from Aldrich, β -mercaptoethanol from Fluka, while urea, sodium hydroxide, hydrochloric acid, boric acid, ethanol, Tris(hydroxymethyl)aminomethane, silver nitrate, mercury(II) chloride and ammonium chloride were obtained from BDH (Poole).

2.2. *o*-Phthalaldehyde (OPA) reagent

This reagent was prepared by dissolving *o*-phthalaldehyde (0.8 g) and mercaptoethanol (1

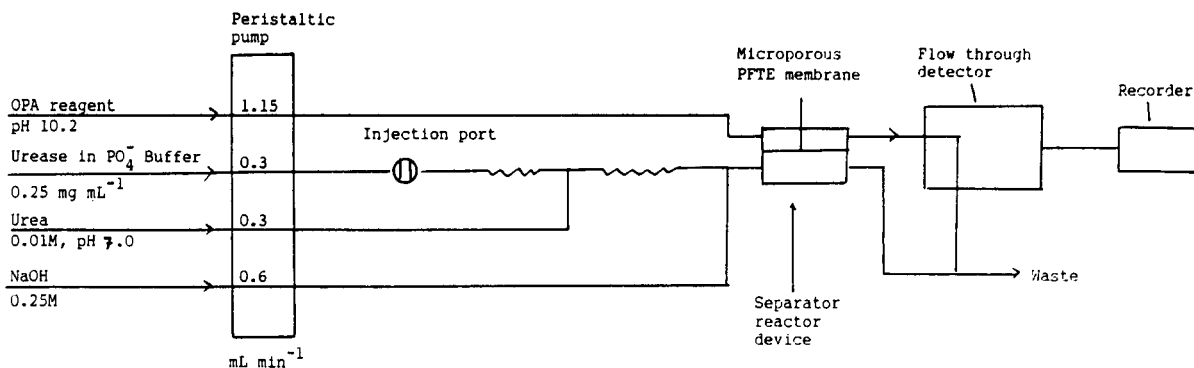


Fig. 1. FIA manifold used in the determination of Hg^{2+} and Ag^+ ions via urease inhibition.

ml) in ethanol (10 ml) and diluting to 1 l with borate buffer (0.44 M, pH 10.2). This solution is stable for up to 2 weeks at 4°C.

2.3. FIA determination of mercury and silver

The arrangements of the FIA module used in this study are shown in Fig. 1 with optimal conditions for operation as indicated. Except for the pump tubing (2 mm i.d.), PTFE tubing (0.5 mm i.d.) was used throughout the system. Reagents were pumped through the FIA manifold via a peristaltic pump (Gilson Minipulse 11). Standards of the inhibitor ions (Hg^{2+} , Ag^+ in the concentration range 10^{-9} to 10^{-6} M) were injected into the urease stream by means of a PTFE rotary injection valve. The function of the sodium hydroxide stream was to ensure complete conversion of any ammonium ions produced as a result of urease action on urea at pH 7.0 to NH_3 .

A separation unit, consisting of a PTFE gas permeable membrane (14 cm diameter), was used to separate the ammonia produced from other components of the system which might otherwise react with the *o*-phthalaldehyde and hence cause interference. The fluorescent adduct formed between ammonia and *o*-phthalaldehyde was monitored at $\lambda_{\text{ex}} = 340$ nm and $\lambda_{\text{em}} = 455$ nm on a Perkin Elmer 650-105 fluorescence spectrometer equipped with a 10- μl flow cell and a strip chart recorder.

2.4. Preparation of soil samples for mercury analysis

Soil samples (montmorillonite clay type) were obtained from a mud volcano (Devil's Woodyard) in Trinidad, West Indies. They were collected using an Eknam Dredge Grab Sampler, drained and immediately stored in polypropylene bags at 0°C. When ready for use samples were homogenized and representative subsamples equivalent to 1.2 g of dry weight were weighed in 100-ml volumetric flasks. The sediment was then rinsed down to the bottom of the flask with not more than 10 ml of distilled deionized water and then 15 ml of conc. H_2SO_4 - HNO_3 (2:1) solution was added slowly in an ice water bath. Upon cooling

HCl (1 M, 2 ml) was added. After expelling the acid fumes from the volumetric flask, samples were placed in a shaking water bath set at 55°C and digested for 2 h. The flasks were then allowed to cool for 30 min. KMnO_4 solution (15 ml, 6%) was added slowly while cooling the flasks in an ice water bath. After 0.5 h potassium persulfate solution (5 ml, 5%) was added with gentle stirring and then allowed to stand overnight. A hydroxylamine sulfate-sodium chloride solution (10 ml, 1:1) was then added, mixed thoroughly until the solution clears and all the precipitated manganese dioxide is dissolved. The solution was then made up to volume. A homogeneous aliquot of the solution was then centrifuged at 10000 *g* for 5 min, and the clear supernatant was used for analysis of mercury as outlined in Fig. 1.

The total concentration of organomercurials present in sediments/soils is usually $\leq 1.5\%$ of the total mercury content. The pretreatment process employed the above results in complete breakdown of organomercurials [14].

2.5. Preparation of mercury and silver standards

These were prepared in the supernatants obtained from a reference montmorillonite clay which was treated in the same manner as the actual soil samples. This was done to compensate for any possible matrix effect. It was found that the differences in fluorescence intensities obtained from standards prepared in this way were insignificant when compared to corresponding standards prepared in distilled, deionized water.

3. Results and discussion

3.1. Optimization of the FIA manifold

In order to determine the optimum operating parameters for the FIA determination of the heavy metals (Hg^{2+} and Ag^+) using the urease inhibition technique a series of preliminary investigations were first conducted in order to determine the influence of urease concentration, sodium hydroxide concentration, sample injection

Table 1

Compromised optimal FIA conditions for mercury and silver determinations at 37°C using the FIA manifold show in Fig. 1

Reagent stream	Flow rate (ml min ⁻¹)	pH	Concentration
OPA	1.15	10.2	0.8 mg ml ⁻¹
Urease	0.30	7.0	250 µg ml ⁻¹
Urea	0.30	7.0	0.01 M
NaOH	0.60	> 10.0	0.25 M

volume and the flow rates of the OPA and NaOH reagent streams on the detection levels of urea.

The effect of urease concentration was studied in order to determine the minimum amount of urease that can be used to give a measurable degree of urea hydrolysis and hence fluorescence detection. It was found that under the operating FIA conditions (Table 1) complete urea hydrolysis occurs at urease concentrations $\geq 250 \mu\text{g/ml}$ and resulted in readily measurable fluorescence intensities (peak heights). It was also observed that when urea solutions of varying concentrations (10^{-3} to 10^{-1} M) were passed through the FIA manifold (Fig. 1) at a flow rate of 0.3 ml min^{-1} , the highest fluorescence intensity was obtained at urea concentrations of 10^{-2} M. Above this concentration there was a rapid drop in fluorescence intensity. This is probably due to product inhibition which is not unique to the urea-urease system [13].

The fluorescence intensity of the OPA-NH₃ adduct was also monitored as a function of the concentration of the NaOH stream. It was found to increase with increasing NaOH concentration up to about 0.1 M and then levels off. Hence a NaOH concentration slightly over 0.1 M was used in all subsequent investigations. This was done to ensure that any NH₄⁺ ions produced as a result of urea hydrolysis are converted into NH₃ and hence maximize the amount of NH₃ under any given set of conditions which will diffuse across the separator membrane to complex with the OPA reagent.

The fluorescence intensity was found to decrease linearly with increasing sample (Hg²⁺ or Ag⁺) volume up to 500 µl injected into the urease stream. Deviation from linearity observed with injection volumes greater than 500 µl may be attributed to increase dispersion of the sample

plug. The best FIA peaks (rapid onset and decay times) were observed with a sample volume of 90 µl. Similar effects of sample volumes on fluorescence intensity were reported by Goyal et al. [15].

Utilizing these optimized conditions, the flow rates of the urease, urea, sodium hydroxide and OPA reagent streams were then varied to obtain compromised optimal flow rates which would lead to maximum fluorescence intensity and sensitivity as well as a reasonable sample throughput rate. As a compromise the best fluorescence intensities were obtained with an OPA-urease-urea-NaOH ratio of 4:1:1:2. It was selected for all further studies since it resulted in sharp FIA peaks, reasonable sample throughputs (40 h^{-1}) and relatively low detection limits (0.1 ppb).

3.2. Calibration graphs

Mercury standards

Utilizing the compromised optimal FIA conditions (Table 1), aliquots of Hg²⁺ standards were injected into the urease stream. Calibration curves are found to be linear up to 22 ppb. Curvature is observed at concentrations outside this range. The following least squares regression equation was found to hold over the linear range: $y = 0.083(\text{Hg}^{2+}, \text{ppb}) + 0.484$, $n = 9$, $r = 0.995$.

As low as 2 ppb, based on variability of the blank (3σ), can be detected at an urease flow rate of 0.3 ml min^{-1} , with a sampling frequency of 40 h^{-1} . Winquist et al. [16] determined trace levels of Hg²⁺ using urease in combination with an ammonia gas sensitive semiconductor detector and found that the enzyme had to be incubated with the inhibitor for at least 3 min to obtain a maximum decrease in the activity. However, in the present study no incubation time was found to be necessary. Winquist et al. [16] also reported a detection limit for Hg²⁺ of at least 0.2 ppm with a sampling frequency of 20 h^{-1} . The present method offers the advantage of much lower detection limits (2 ppb) for screening samples and higher sample throughput when compared to existing enzymatic methods. This detection level is also within the legal levels of Hg permitted in soils and way below the probable background levels found (10 ppb).

Silver standards

Utilizing the same compromised optimum conditions (Table 1), aliquots of Ag^+ standards were injected into the urease stream. Calibration curves were found to be linear over the concentration range 0.1 to 1.0 ppb. However at Ag^+ concentrations higher than 1.0 ppb, curvature was observed. It was also found that fluorescence intensity decreased with increased Ag^+ concentrations as expected since Ag^+ is a known inhibitor to urease activity [13]. The following least squares regression equation was found to hold over the linear range: $y = 7.89(\text{Ag}^+, \text{ppb}) + 0.195$, $n = 9$, $r = 0.999$.

The detection limit is (as expected) flow rate dependent and is found to be 0.1 ppb (based on the variability of the blank, 3σ) at a carrier stream flow rate of 0.3 ml min^{-1} . At such a flow rate a manual sampling frequency rate of 40 h^{-1} can be achieved. This compares extremely favourably to the flame atomic absorption method for Ag^+ where detection limits of 0.2 ppm are usually obtained with a sampling frequency of $60 \text{ analyses h}^{-1}$ [17].

3.3. Analysis of Hg^{2+} in soil samples

In these analyses soil extracts and mercury standards were injected into the urease stream of the FIA manifold (Fig. 1) and the fluorescence intensities monitored. Soil “blanks” were analysed for any “free” ammonia present by injecting samples into the FIA manifold except that in this case the urease stream was replaced by a phosphate buffer stream (pH 7.0). The difference in fluorescence intensities between the sample and the “blank” was taken as that due to heavy metal inhibition.

A comparison of the FIA method developed in the present study with the cold vapour technique [17] used routinely at the Institute of Marine Affairs (IMA, Trinidad and Tobago) for Hg^{2+} analysis was performed on five samples. The results are reproduced in Table 2. The following least squares regression was found to hold: $\text{IMA} = 0.998\text{FIA} - 0.001$, $n = 5$, $r = 0.999$.

Comparison of the two methods for Hg^{2+} determination gave a standard deviation of 0.02 and

Table 2

Analysis of mercury in soil samples by atomic absorption spectrometry (cold vapour technique) and by the fluorescence (FIA) method

Sample number	Fluorescence FIA method (Hg^{2+} , $\mu\text{g g}^{-1}$)	Atomic absorption method (Hg^{2+} , $\mu\text{g g}^{-1}$)
1	0.065	0.064
2	0.066	0.064
3	0.058	0.056
4	0.067	0.065
5	0.023	0.022

a coefficient of variation of 2%. One-way analysis of variance (ANOVA) gave no significant differences between the above-mentioned methods [the calculated F value was found to be 4.444; the theoretical value is 5.05 ($p = 0.05$)]. Therefore, these methods can be considered to be comparable and give quite similar estimates for the Hg^{2+} content in the samples.

4. Conclusions

The FIA–urease inhibition method described herein offers a simple, fast, cost effective and reliable alternative for screening samples for their $\text{Hg}^{2+}/\text{Ag}^+$ content. Detection limits are 0.1 ppb for Ag^+ and 2 ppb for Hg^{2+} . However, the method cannot separately quantify Hg^{2+} and Ag^+ in a sample since both ions are inhibitors of urease. The small test samples ($90 \mu\text{l}$) could make this method very useful in analyses of samples from small areas such as on the surface of amalgam fillings in teeth.

References

- [1] D. Welz and M. Melcher, *Anal. Chem.*, 57 (1985) 427.
- [2] D. Chakrabort, F. Adams, W. Van Mol and K. Irgolic, *Anal. Chim. Acta*, 196 (1987) 23.
- [3] F. Scholz, L. Nietschke and G. Henrion, *Anal. Chim. Acta.*, 199 (1987) 167.
- [4] B.Y. Xu, T.-M. Xu, M.-N. Shen and Y.-Z. Fang, *Talanta*, 32 (1985) 1016.
- [5] K. Liu, Q. Wu and H. Lin, *Analyst*, 115 (1990) 835.

- [6] D.E. Leyden, W. Wegscheider, W.B. Bodnar, E.D. Sexton and W.K. Nonidez, in J. Albaiges (Ed.), *Comparison of Methods of Trace Element Enrichment for XRF Determination in Analytical Techniques in Environmental Chemistry*, Pergamon, Oxford, 1980, pp. 469–476.
- [7] J.C. Yu, J.M. Lo and C.M. Wai, *Anal. Chim. Acta*, 154 (1983) 307.
- [8] M. Thompson and B.J. Coles, *Analyst*, 109 (1984) 529.
- [9] A. D'ulivo, R. Fuoco and P. Papoff, *Talanta*, 32 (1985) 103.
- [10] B. Mattisson, *FEBS Lett.*, 85 (1978) 2, 203.
- [11] P. Seegopaul and G.A. Rechnitz, *Anal. Chem.*, 56 (1984) 852.
- [12] B. Mattiason, *Nature*, 268 (1977) 519.
- [13] J.B. Sumner, *The Enzymes*, Vol. 1, Academic Press, New York, 1951, pp. 873–891.
- [14] M.L. Schafer, U.R. James, J.T. Peeler, C.H. Hamilton and J.E.A. Campbell, *J. Agric. Food Chem.*, 23 (1975) 1079.
- [15] S.S. Goyal, D.W. Rains and R.C. Huffaker, *Anal. Chem.*, 60 (1988) 175.
- [16] F. Winquist, I. Lundstrom and B. Danielsson, *Anal. Lett.*, 21 (1988) 1801.
- [17] *Analytical Methods Manual*, Naquadat No. 80050, Water Quality Branch, Ottawa, 1978.



ELSEVIER

Analytica Chimica Acta 292 (1994) 191–199

**ANALYTICA
CHIMICA
ACTA**

Dispersion behaviour of chromogenic reagents in a microwave field in a flow system. Application to the spectrophotometric flow-injection determination of palladium and rhodium

Yanjun Xu, Xingguo Chen, Zhide Hu *

Department of Chemistry, Lanzhou University, Lanzhou 730000, China

(Received 18th January, 1993; revised manuscript received 30th June 1993)

Abstract

Microwave heating associated with flow-injection (FI) analysis was used to expand the field of application of FI analysis. A laboratory-made microwave-irradiation flow-injection analyser and a chromogenic reagent, 4-(5-chloro-2-pyridylazo)-1,3-diaminobenzene (5-Cl-PADAB), were used to establish an FI spectrophotometric method for the sequential determination of Pd and Rh. The relationship between the dispersion coefficient D of various chromogenic reagents and the microwave irradiation time, t_m , was established as $D = a + bt_m/(t_m + c)$, where a , b and c are constants. The relationship between D and the molecular weight M of the solvent (methanol, ethanol, propan-1-ol, propan-2-ol, butan-1-ol and pentan-1-ol) was found to be $D = a' + b'M$, where a' and b' are constants. The effect of microwave irradiation on the coordination reactions between 5-Cl-PADAB and Pd, Rh, Ru, Os, Ir and Pt was studied.

Key words: Flow injection; UV-visible spectrophotometry; Dispersion; Microwave irradiation; Palladium; Rhodium

1. Introduction

Microwave irradiation has been increasingly applied in chemistry in recent years, mainly for the rapid decomposition of samples in analytical chemistry and the acceleration of reactions in organic chemistry. Heseck and Wilson [1] used the microwave technique for sample preparation in analytical chemistry and the first report in which microwave energy was used as the heat source in acid digestion of samples appeared in 1975 [2]. Most of the early work on the use of microwave

energy as a heat source in acid digestion related to biological samples [3,4]. Because an open vessel was used in the digestion of samples, it unavoidably led to mechanical or volatile loss of the analyte. Also, the highest digestion temperature was limited by the boiling point of the acids used. In an attempt to avoid these problems, some researchers used closed digestion vessels made of polytetrafluoroethylene (PTFE) or polycarbonate to obtain elevated temperature and pressure [5–11]. In flow-injection analysis (FIA), Burguera and co-workers [12–14] used a microwave oven in a flow system to digest solid samples. In 1986, Gedye et al. [15] first used microwave irradiation in organic synthesis.

* Corresponding author.

In research on the determination of noble metals, we found that the reaction between noble metals and organic chromogenic ligands was often slow, and required heating for an appreciable time. In FIA, the analyte stays in the reaction coil for a very short time, so only fast reactions can normally be used, although some slow reactions can be accommodated by use of stopped flow. This meant that the sample throughput rate decreased significantly. The use of microwave irradiation, however, might accelerate such reactions.

This paper describes the effect of microwave irradiation on the rate of reactions between 5-Cl-PADAB (see Table 1) and Pd, Rh, Os, Ru, Ir and Pt ions in a flow-injection analyser. As a result, a spectrophotometric method for the sequential determination of Pd and Rh was established. In addition, the effect of microwave irradiation on the dispersion coefficient D of 5-Cl-PADAB [16], 5-Br-PADAP [17,18], DBC-arsenazo [19] and chlorophosphonazo-mN [20] in

solvents such as water, methanol, ethanol, propan-1-ol, propan-2-ol, butan-1-ol and pentan-1-ol, was studied and quantitative relationships between D , the microwave irradiation time, t_m , and molecular weight, M , of the solvent were studied.

2. Experimental

2.1. Apparatus

A microwave oven (Model ER-761MD, Qingdao Refrigerator Factory) was used, the frequency being 2450 MHz. The power levels can be adjusted in steps from setting 1 to 10, equivalent to 70–700 W. The range of microwave heating time is from 0 to 100 min. All functions of the microwave oven are controlled by an integral microprocessor.

All experiments were performed on a flow-injection analyser (Hitachi Model K-1000) equipped with a peristaltic pump, a sixteen-way injection valve, a two-channel plunger pump and an electric oven. The carrier stream was driven by the two-channel plunger pump. The sample and reagent streams were driven by a peristaltic pump. A UV-visible spectrophotometric detector (Hitachi Model L-4200) was used for flow-injection and batch measurements, the flow-through cell having a 5-mm optical path length and an 11.3- μ l volume.

A spectrophotometer (Beckman Model DU-7) was used to measure the maximum absorbance wavelengths of the 5-Cl-PADAB–noble metal ion complexes and all chromogenic reagents.

To obtain Eq. 2 (see later), the software used for non-linear curve fitting was written in Microsoft MBASIC. The algorithm used was the damped least-squares method.

The reaction coil (10 m \times 0.5 mm i.d.) was wound into a ring 10 cm in diameter and placed on the centre of a glass turn-table in the cavity of the microwave oven. The two ends of the reaction coil passed through the air vents of the oven and were connected to the flow-injection analyser. The reaction coil length in the cavity of the microwave oven was 7 m. The flow diagram of the experimental device is shown in Fig. 1.

Table 1
Chromogenic reagents

Reagent ^a	Concentrations ^b (mol l ⁻¹)	Sources ^c
5-Cl-PADAB	1.61×10^{-3}	1
	8.05×10^{-5}	
5-Br-PADAP	8.59×10^{-4}	1
	3.44×10^{-5}	
DBC-arsenazo	1.20×10^{-3}	2
	6.00×10^{-5}	
Chlorophosphonazo-mN	1.40×10^{-3}	3
	7.00×10^{-5}	

^a 5-Cl-PADAB = 4-(5-chloro-2-pyridylazo)-1,3-diaminobenzene; 5-Br-PADAP = 2-(5-bromo-2-pyridylazo)-5-diethylaminophenol; DBC-arsenazo = 2-(2-arsenophenylazo)-7-(2,6-dibromo-4-chlorophenylazo)-1,8-dihydroxynaphthalene-3,6-disulphonic acid; chlorophosphonazo-mN = 2-(4-chloro-2-phosphonophenylazo)-7-(3-nitrophenylazo)-1,8-dihydroxynaphthalene-3,6-disulphonic acid.

^b When the effect of microwave irradiation on dispersion coefficients in different solvents was studied, more concentrated ethanolic solutions of the chromogenic reagents were diluted to a certain concentration with the corresponding solvent. In order to ascertain the effect of microwave irradiation on the reactions between 5-Cl-PADAB and noble metal ions and to determine Pd and Rh, 1.61×10^{-3} mol l⁻¹ 5-Cl-PADAB solution in ethanol was used in the experiments.

^c 1 = Beijing Chemical Works; 2 = Department of Chemistry, Wuhan University; 3 = East China Normal University Chemical Works.

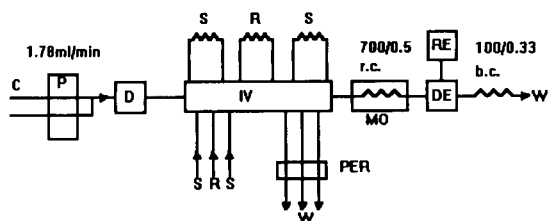


Fig. 1. Flow diagram of experimental device. C = carrier stream; P = two-channel plunger pump; D = damper; IV = sixteen-way injection valve; S = sample; R = reagent; PER = peristaltic pump; MO = microwave oven; r.c. = reaction coil; DE = detector; RE = recorder; b.c. = back-pressure coil; W = waste. Experimental conditions for measuring dispersion coefficient *D*: flow-rate, 1.78 ml min⁻¹; microwave power, 533 W; reagent volume, 520 μl. Experimental conditions for studying the reactions between 5-Cl-PADAB and noble metal ions: flow-rate, 1.78 ml min⁻¹; microwave power, 533 W; sample volume, 392.4 μl; reagent volume, 127.5 μl.

2.2. Reagents

The concentrations and sources of the reagents studied are given in Table 1, and their structures are shown in Fig. 2.

Pd(II) and Pt(IV) stock standard solutions (1.00 mg ml⁻¹) were prepared by dissolving 0.1000 g of palladium and platinum metal in aqua regia, adding 0.2 g of NaCl to the solutions and evaporating the solutions on a boiling water-bath nearly to dryness. The solutions were diluted to 100 ml with 10 ml of concentrated HCl and water successively. Working standard solutions were prepared by diluting the stock standard solutions with water to appropriate concentrations.

Ru(III), Rh(III), Os(IV) and Ir(IV) stock standard solutions (0.100 mg ml⁻¹) were prepared by dissolving the appropriate amounts of (NH₄)₂RuCl₅ · H₂O, (NH₄)₂RhCl₅ · H₂O, (NH₄)₂OsCl₆ and (NH₄)₂IrCl₆ in 10 ml of concentrated HCl and water and diluting the solutions to 100 ml with water. Working standard solutions were prepared by diluting the stock standard solutions with water to appropriate concentrations.

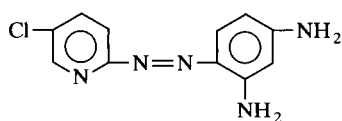
2.3. Procedure

The microwave oven was connected to the flow-injection analyser as shown in Fig. 1. While

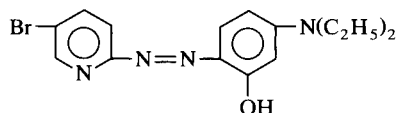
the carrier stream was pumped into the flow system, the sample and reagent were pumped into the injection valve. A sample was not injected into the flow system until a steady baseline had been obtained. When a sample plug reached the reaction coil in the cavity of microwave oven, the microwave oven was immediately switched on. When the sample plug passed the flow-through cell of the detector, the absorbance was measured at the maximum absorption wavelength.

The procedure for the sequential determination of Pd and Rh is as follows. First the absorbance of Pd is measured, with no microwave heating. Then total absorbance of Pd and Rh is measured after microwave heating. The absorbance of Rh is obtained by subtracting the absorbance of Pd from the total absorbance. The system is calibrated with standard solutions of Pd and Rh (see later).

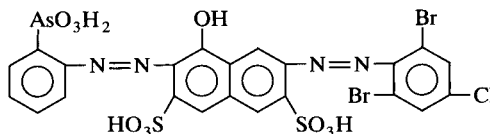
When the relation between dispersion coefficient *D* and microwave time *t_m* or molecular weight *M* of the solvents was studied, the solvent



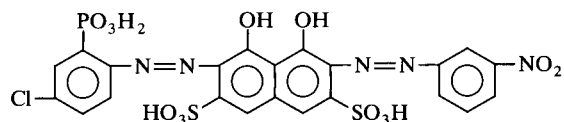
5-Cl-PADAB



5-Br-PADAP



DBC-arsenazo



Chlorophosphonazo-mN

Fig. 2. Structures of the reagents studied.

to be studied was used as the carrier stream and only the chromogenic reagent solution was injected into the flow system. Under these conditions, there was only physical dispersion and no chemical reaction occurred.

When the effect of microwave irradiation on the chemical reactions was studied, a buffer solution was used as the carrier stream and the chromogenic reagent and noble metal ions were injected into the flow system.

The maximum absorbance wavelengths of 5-Cl-PADAB–noble metal ion complexes were determined in a 1-cm cell. A 5.0-ml volume of pH 4.0 HOAc–NaOAc buffer solution, 2.0 ml of 8.05×10^{-4} mol l⁻¹ 5-Cl-PADAB solution in ethanol and 2.0 ml of 10.0 μ g ml⁻¹ noble metal ion solutions were added to a 25-ml test-tube and the mixed solution was heated on a boiling water-bath for 1 h and subsequently diluted with water to 25 ml. The absorption spectra of the solution obtained was measured.

3. Results and discussion

3.1. Evaluation of the available power in the microwave cavity

The following equation was used to calculate the maximum output power of the oven [10]:

$$W_a = (Kc\Delta Tm)/t \quad (1)$$

where W_a is the apparent power absorbed by the sample (W), K is the conversion factor from thermochemical calories to watts (4.184 J cal⁻¹), c is the heat capacity (cal g⁻¹ K⁻¹), $\Delta T = T_f - T_i$ is the difference between the final and initial temperatures (K), m is the mass of sample (g) and t is time (s). At full power, it takes 95 s for the temperature of 200 g of distilled water in a 500-ml beaker to increase from 19.5 to 80°C. The available power in the microwave cavity is 533 W. Because the microwave energy in the microwave cavity of the oven is not uniformly distributed, the location of the reaction coil must be same during experiments, which will ensure reproducible results.

3.2. Effect of microwave irradiation on dispersion coefficient D

We studied the effect of microwave irradiation on the dispersion coefficients of 5-Cl-PADAB, 5-Br-PADAP, DBC-arsenazo and chlorophosphonazo-mN in water, methanol, ethanol, propan-1-ol, propan-2-ol, butan-1-ol and pentan-1-ol, and obtained the relationship between dispersion coefficient D and microwave time t_m for the chromogenic reagents as follows:

$$D = a + \frac{bt_m}{t_m + c} \quad (2)$$

where a , b and c are constants whose values vary with particular reagents and solvents. Eq. 2 was obtained by measuring the absorbance of original and dispersed solutions of 5-Cl-PADAB, 5-Br-PADAP, DBC-arsenazo and chlorophosphonazo-mN at 460, 445, 535 and 545 nm in the different solvents and computer simulation. Constants a , b and c in Eq. 2 for different chromogenic reagent–solvent systems are given in Table 2.

Microwave irradiation affects the dispersion coefficient of every chromogenic reagent in different solvents, decreasing it to some extent. After the solvents have absorbed microwave radiation, microwave energy is converted into thermal energy with macroscopic dielectric loss heating effects associated with the solvents. Both water and alcohols have high dielectric loss tangents and are effective in converting microwave energy into thermal energy [21]. These efficient heating effects rapidly lead to elevated temperatures of the solvents and the radial mass transfer of the solute is thereby enhanced. The enhanced radial mass transfer leads to a decrease in solute dispersion or of the dispersion coefficient. It should be emphasized that these considerations are merely speculative. The dispersion coefficient of every chromogenic reagent decreased slightly when the same reaction coil as that in the microwave oven was heated to 150°C in an electric heating oven. Based on the above findings, it appears that there is also a non-temperature effect between microwave irradiation and the solvent molecules. There is no effect of microwave irradiation on the

Table 2
Constants a , b and c in Eq. 2 for different chromogenic reagent–solvent systems

Solvent	Con-stant	5-Cl-PADAB	5-Br-PADAP	DBC-arsenazo	Chloro-phos-phono-azo-mN
Water ^a	a	–	–	1.53	1.51
	b	–	–	–0.22	–0.24
	c			8.71	14.34
Methanol	a	1.33	1.34	1.57	1.58
	b	–0.13	–0.15	–0.38	–0.62
	c	8.19	15.87	40.80	87.08
Ethanol	a	1.74	1.73	2.06	1.98
	b	–0.46	–0.34	–0.49	–0.55
	c	27.46	12.81	13.34	17.54
Propan-1-ol	a	2.34	2.31	2.89	2.89
	b	–0.98	–1.59	–1.54	–4.75
	c	45.12	86.38	52.02	191.79
Propan-2-ol	a	2.45	2.28	2.65	3.25
	b	–2.05	–1.43	–2.57	–2.83
	c	103.33	77.65	111.31	98.80
Butan-1-ol	a	2.58	2.60	2.97	3.73
	b	–0.72	–1.15	–2.77	–4.08
	c	30.30	62.92	165.48	137.92
Pentan-1-ol	a	3.03	3.06	3.54	4.55
	b	–0.60	–1.72	–0.94	–1.86
	c	25.68	98.11	63.49	38.32

^a Because 5-Cl-PADAB and 5-Br-PADAP are not soluble in water, the values of a , b and c could not be measured.

dispersion coefficient of 5-Br-PADAP in benzene, acetone or carbon tetrachloride. It is assumed that the phenomenon can be attributed to little or no microwave energy absorption by benzene, acetone and carbon tetrachloride. The effects of microwave irradiation on the dispersion coefficients of 5-Cl-PADAB, DBC-arsenazo and chlorophosphonazo-mN in benzene, acetone and carbon tetrachloride were not examined.

Constant a in Eq. 2 is equivalent to the dispersion coefficient D without microwave irradiation. The constant b reflects the extent to which D is influenced by microwave irradiation.

3.3. Relationship between dispersion coefficient D and molecular weight M of solvents

The relationship between the dispersion coefficients of 5-Cl-PADAB, 5-Br-PADAP, DBC-

arsenazo and chlorophosphonazo-mN and the molecular weights of methanol, ethanol, propan-1-ol, propan-2-ol, butan-1-ol and pentan-1-ol was studied. On the basis of a series of experimental results, it was found that there was a good linear relationship between D and M :

$$D = a' + b'M \quad (3)$$

where a' and b' were constants whose values varied with particular chromogenic reagents and microwave irradiation time. Constants a' and b' and the correlation coefficients in Eq. 3 for different chromogenic reagents and microwave times are given in Table 3.

An increase in solvent molecular weight leads to a decrease in molecular diffusion coefficient of the chromogenic reagents or a decrease in radial mass transfer. Hence the dispersion coefficient increases with increasing solvent molecular weight. On the other hand, the viscosities of the solvents increase with increasing solvent molecular weight, which leads to an increase in the thickness of the boundary layer near the wall of the flow tube and hence an increase in axial dispersion. Thus the dispersion coefficient increases with increasing solvent molecular weight.

Table 3
Constants a' and b' and correlation coefficients, r ($n = 6$), in Eq. 3 for different chromogenic reagents and microwave times

t_m (s)	Con-stant	5-Cl-PADAP	5-Br-PADAP	DBC-arsenazo	Chloro-phos-phono-azo-mN
0	a'	0.42	0.39	0.55	–0.28
	b'	0.0300	0.0302	0.0342	0.0540
	r	0.9824	0.9946	0.9781	0.9878
10	a'	0.39	0.30	0.38	–0.33
	b'	0.0288	0.0298	0.0346	0.0523
	r	0.9805	0.9947	0.9840	0.9842
20	a'	0.34	0.31	0.27	–0.0882
	b'	0.0274	0.0279	0.0342	0.0438
	r	0.9907	0.9958	0.9910	0.9800
30	a'	0.37	0.40	0.34	–0.16
	b'	0.0260	0.0247	0.0312	0.0431
	r	0.9940	0.9969	0.9836	0.9812

Eq. 3 is not obeyed by the dispersion coefficients of DBC-arsenazo and chlorophosphonazo-mN in water. If the molecular weight M in Eq. 3 is replaced with the carbon number N of the solvent, a linear relationship between D and N still holds: $D = a'' + b''N$.

3.4. Effect of microwave irradiation on the coordination reactions between noble metal ions and 5-Cl-PADAB

Coordination reaction between Pd(II) and 5-Cl-PADAB [22,23]

In pH 4.0 HOAc–NaOAc buffer solution and at 568.5 nm; the effect of microwave irradiation on the coordination reaction between 5-Cl-PADAB and Pd(II) was studied using a laboratory-made microwave flow-injection analyser. Before the experiments were done, it was expected that microwave effect would accelerate the coordination reaction and enhance the complex absorbance. However, the results indicated no effect of microwave irradiation on the coordination reaction between 5-Cl-PADAB and Pd(II). It seems that the reaction between 5-Cl-PADAB and Pd(II) is rapid enough to reach an equilibrium at room temperature within a very short time.

Coordination reaction between Rh(III) and 5-Cl-PADAB [24]

In pH 4.0 HOAc–NaOAc buffer solution and at 555 nm, the effect of microwave irradiation on the coordination reaction between 5-Cl-PADAB and Rh(III) was studied using a laboratory-made microwave flow-injection analyser. The results indicated that after the sample plug had passed through a 7-m reaction coil heated to 150°C by an electric oven or at room temperature, no reaction took place between 5-Cl-PADAB and Rh(III). When the reaction coil was heated at 533 W microwave power for 30 s, the sample plug containing $10.0 \mu\text{g ml}^{-1}$ Rh(III) produced an absorbance of 0.57.

Coordination reaction between Ru(III) and 5-Cl-PADAB

In pH 5.0 HOAc–NaOAc buffer solution and at 562.5 nm, the effect of microwave irradiation

on the coordination reaction between 5-Cl-PADAB and Ru(III) was studied, using a laboratory-made microwave flow-injection analyser. The results indicated that after the sample plug had passed through a 7-m reaction coil heated to 90°C by an electric oven or at room temperature, no reaction took place between 5-Cl-PADAB and Ru(III). When the reaction coil was heated at 533 W microwave power for 30 s, the sample plug containing $10 \mu\text{g ml}^{-1}$ Ru(III) produced an absorbance of 0.31.

Coordination reaction between Os(IV) and 5-Cl-PADAB

In pH 5.0 HOAc–NaOAc buffer solution and at 516 nm, the effect of microwave irradiation on the coordination reaction between 5-Cl-PADAB and Os(IV) was studied, using a laboratory-made microwave flow-injection analyser. The results indicated that after the sample plug had passed through a 7-m reaction coil heated to 90°C by an electric oven or at room temperature, no reaction took place between 5-Cl-PADAB and Os(IV). When the reaction coil was heated at 533 W microwave power for 30 s, a sample diluted with ethanol and containing $20.0 \mu\text{g ml}^{-1}$ Os produced an absorbance of 0.35. Both microwave heating and the presence of ethanol were necessary. Based on the above finding, it seems that after Os(IV) has been reduced to Os(III) by ethanol under microwave heating, the reaction between Os(III) and 5-Cl-PADAB proceeds rapidly. It should be emphasized that the above suggestion is only speculative.

Coordination reaction between Ir(IV) and 5-Cl-PADAB [25]

In pH 5.0 HOAc–NaOAc buffer solution and at 535 nm, the effect of microwave on coordination reaction between 5-Cl-PADAB and Ir(IV) was studied, using a laboratory-made microwave flow-injection analyser. The results indicated that after the sample plug had passed through a 7-m reaction coil heated to 90°C by an electric oven or at room temperature, no reaction took place between 5-Cl-PADAB and Ir(IV). To accelerate the rate of reaction between 5-Cl-PADAB and Ir,

Ir(IV) was reduced to Ir(III) with 2.5% ascorbic acid before injecting the sample. When the reaction coil was heated at 533 W microwave power for 30 s, the reduced sample containing $20.0 \mu\text{g ml}^{-1}$ Ir produced an absorbance of 0.24. Both microwave heating and ascorbic acid reduction were necessary.

Coordination reaction between Pt(IV) and 5-Cl-PADAB

In pH 4.0 HOAc–NaOAc buffer solution and at 575 nm, the effect of microwave on coordination reaction between 5-Cl-PADAB and Pt(IV) was studied, using a laboratory-made microwave flow-injection analyser. The results indicated that after the sample plug had passed through a 7-m reaction coil heated to 90°C by an electric oven or at room temperature, no reaction took place between 5-Cl-PADAB and Pt(IV). To accelerate the reaction between 5-Cl-PADAB and Pt, Pt(IV) was reduced to Pt(II) with 2.5% ascorbic acid before injecting the sample. When the reaction coil was heated at 533 W microwave power for 30 s, the reduced sample containing $20.0 \mu\text{g ml}^{-1}$ Pt produced an absorbance of 0.08. Both microwave heating and ascorbic acid reduction were necessary.

Summary

According to the above findings, Pt(IV) is chemically inert and Pd(II) the most chemically active of the six noble metals studied. It is difficult for Pt to react with 5-Cl-PADAB even if microwave heating and ascorbic acid reduction are applied.

An attempt was made to explain the difference in the chemical activities between Pd(II) and Pt(IV) on the basis of their ion potentials z/r where z is ionic charge and r is ionic radius. The z/r values for Pt(IV), Pt(II) and Pd(II) are 5.7, 2.4 and 2.3, respectively [26]. Because the values of Pt(II) and Pd(II) are approximately the same, both Pt(II) and Pd(II) react with 5-Cl-PADAB. As there is a great difference in the reaction rates between 5-Cl-PADAB and Pt(II) and Pd(II), it is possible to a certain extent to estimate the chemical activities of ions from the ion potentials z/r .

3.5. Conditions for determining Rh and Pd with 5-Cl-PADAB

According to literature [22], the reaction rate between 5-Cl-PADAB and Rh is very slow. It is impossible for a slow reaction to be used in flow-injection analysis. However, microwave irradiation accelerates the reaction between 5-Cl-PADAB and Rh so that a flow-injection spectrophotometric method for the determination of Rh can be established. The maximum absorbance wavelength of the 5-Cl-PADAB–Rh complex is 555 nm. The optimum experimental conditions are as follows: pH 4.0 HOAc–NaOAc buffer solution, flow-rate 1.78 ml min^{-1} , $1.61 \times 10^{-3} \text{ mol l}^{-1}$ 5-Cl-PADAB solution in ethanol, microwave time 30 s, microwave power 533 W, sampling volume $392.4 \mu\text{l}$, reagent volume $127.5 \mu\text{l}$ and sampling frequency 25 h^{-1} . Beer's law is obeyed in the range $2.0\text{--}10.0 \mu\text{g Rh ml}^{-1}$. The calibration equation for peak absorbance measurements is $A = (-2.50 \times 10^{-2}) + [5.80 \times 10^{-2} c (\mu\text{g ml}^{-1})]$ under the optimum conditions. The correlation coefficient is 0.9934 ($n = 6$) with a detection limit of $0.05 \mu\text{g Rh ml}^{-1}$.

There is no effect of microwave irradiation on the reaction between 5-Cl-PADAB and Pd(II), but the reaction between 5-Cl-PADAB and Rh(III) is accelerated by microwave irradiation. The difference in the chemical properties of Pd(II) and Rh(III) was taken advantage of to establish a microwave flow-injection spectrophotometric method for sequential determination of Pd and Rh. The experimental conditions for determination of Pd are the same as those for Rh. Beer's law is obeyed in the range $2.0\text{--}10.0 \mu\text{g Pd ml}^{-1}$. The calibration equation for peak absorbance measurements is $A = (3.90 \times 10^{-2}) + [-2.99 \times 10^{-2} c (\mu\text{g ml}^{-1})]$. The correlation coefficient is 0.9999 ($n = 6$) a detection limit of $1.0 \mu\text{g Pd ml}^{-1}$.

3.6. Accuracy and precision

The precision was evaluated by measuring the absorbance of Pd and Rh for artificial sample 4 (see Table 5) five times under the experimental conditions described above. The Pd and Rh con-

Table 4
Effect of other ions (4.0 $\mu\text{g Rh ml}^{-1}$)

Other ion	Concentration of other ion ($\mu\text{g ml}^{-1}$)	Recovery of Rh (%)
Pt(IV)	40.0	106
Os(IV)	20.0	97
Ru(III)	4.0	106
Ir(IV)	10.0	103
Ir(III)	10.0	103
Au(III)	40.0	97
Cu(II)	5.0	97
Ni(II)	47.0	94
Fe(III)	40.0	103

centrations in the sample solution were determined from the respective calibration equations. The Pd and Rh concentrations in artificial sample 4 and standard deviations were 6.9 ± 0.12 and $3.2 \pm 0.11 \mu\text{g l}^{-1}$, respectively.

To check the accuracy of the method, the recoveries of Pd and Rh were determined in artificial sample 4 by adding known amounts of Pd and Rh. The recoveries were 103% and 98% on adding $3.0 \mu\text{g Pd l}^{-1}$ and $5.0 \mu\text{g Rh l}^{-1}$, respectively.

3.7. Effect of other ions on Rh–5-Cl-PADAB system

It can be seen from Table 4 that Pd(II) and Co(II) interfere in the determination of Rh. Ag^+

and Cl^- in solution produce an AgCl precipitate and the absorbance of the solution will increase owing to the presence of this precipitate.

3.8. Sequential determination of Pd and Rh in artificial samples

The results for the determination of the concentrations of Pd and Rh in artificial samples are given in Table 5.

4. Conclusion

It is convenient to use an in-line microwave oven in a flow system to study the effect of microwave irradiation on dispersion coefficients and chemical reactions. With microwave irradiation, the dispersion coefficient of chromogenic reagents decreases and some chemical reactions are significantly accelerated. According to the experimental results, two situations were observed: either the reactions could be accelerated by microwave irradiation, or there was no effect of microwave irradiation on the reactions. This difference in chemical reactions under microwave heating can be used to establish a microwave irradiation flow-injection spectrophotometric method for the sequential determination of Pd and Rh.

Acknowledgement

This project was supported by the National Natural Science Foundation of China.

References

- [1] J.A. Heseck and R.C. Wilson, *Anal. Chem.*, 46 (1974) 1160.
- [2] A. Abu-Samra, J.S. Morris and S.R. Koirtiyohann, *Anal. Chem.*, 47 (1975) 1475.
- [3] P. Barrett, L.J. Davidowski, Jr., K.W. Penaro and T.R. Copeland, *Anal. Chem.*, 50 (1978) 1021.
- [4] R. Blust, A. van der Linden and W. Declair, *At. Spectrosc.*, 6 (1985) 163.

Table 5
Determination of Pd and Rh in samples

Sample No.	Concentration present ($\mu\text{g ml}^{-1}$)	Concentration found ($\mu\text{g ml}^{-1}$)	Relative error (%)
1	Pd 4.1	4.2	2.4
	Rh 4.0	4.2	5.0
2	Pd 5.1	5.1	0.0
	Rh 7.0	6.7	-4.3
3	Pd 5.1	4.9	-3.9
	Rh 5.0	4.7	-6.0
4	Pd 7.2	6.9	-4.2
	Rh 3.0	3.2	6.7
	Ru 1.0		
	Ir 1.0		
	Pt 5.0		
	Os 4.0		

- [5] P.J. Lamothe, T.L. Fries and J.J. Consul, *Anal. Chem.*, 58 (1986) 1881.
- [6] L.A. Fernando, W.D. Heavner and C.C. Gabrielli, *Anal. Chem.*, 58 (1986) 511.
- [7] L.B. Fischer, *Anal. Chem.*, 58 (1986) 261.
- [8] F. Smith and B. Cousins, *Anal. Chim. Acta*, 177 (1985) 243.
- [9] C.S.E. Papp and L.B. Fischer, *Analyst*, 112 (1987) 337.
- [10] H.M. Kingston and L.B. Jassie, *Anal. Chem.*, 58 (1986) 2534.
- [11] S. Nakashima, R.E. Sturgeon, S.N. Willie and S.S. Berman, *Analyst*, 113 (1988) 159.
- [12] M. Burguera, J.L. Burguera and O.M. Alarcon, *Anal. Chim. Acta*, 179 (1986) 351.
- [13] M. Burguera, J.L. Burguera and O.M. Alarcon, *Anal. Chim. Acta*, 214 (1988) 421.
- [14] V. Carbonell, M. de la Guardia, A. Salvador, J.L. Burguera and M. Burguera, *Anal. Chim. Acta*, 238 (1990) 417.
- [15] R. Gedye, F. Smith, K. Westaway, H. Ali, L. Baldisera, L. Laberge and J. Rousell, *Tetrahedron Lett.*, 27 (1986) 279.
- [16] S. Shibata, M. Furukawa, Y. Ishiguro and S. Sasaki, *Anal. Chim. Acta*, 55 (1971) 231.
- [17] S.I. Gusev and L.M. Shehurova, *Zh. Anal. Khim.*, 21 (1966) 1042.
- [18] X.Z. Yang, *Dizhi Shiyanshi*, 4, No. 1 (1988) 22.
- [19] H. Li, R.X. Cai, X.M. Yu, Y.E. Zeng and L.T. Zhu, *Fenxi Huaxue*, 13 (1985) 651.
- [20] B.C. Wu, Y.X. Qu and H.Y. Liu, *Lihua Jianyan (Huaxue Fence)*, 16 (1980) 1.
- [21] D.R. Baghurst, D.M.P. Mingos and M.J. Watson, *J. Organomet. Chem.*, 368 (1989) C43.
- [22] X.G. Chen, M.C. Liu and Z.D. Hu, *Fenxi Huaxue*, 17 (1989) 248.
- [23] S. Shibata, Y. Ishiguro and R. Nakashima, *Anal. Chim. Acta*, 64 (1973) 305.
- [24] Y.Z. Gong and H.L. Zhou, *Fenxi Shiyanshi*, 4, No. 2 (1985) 16.
- [25] H.L. Zhou, Y.Z. Gong and X.Y. Ye, *J. Lanzhou Univ., Nat. Sci. Ed.*, 20 (1984) 231.
- [26] J.A. Dean, *Lange's Handbook of Chemistry*, McGraw-Hill, New York, 13th edn., 1972, pp. 3-124.

Flow-injection determination of kanamycin by inhibition of the lucigenin–H₂O₂–Co²⁺ system

Abdulrahman A. Alwarthan *, Saad A. Al-Tamrah, Akel A. Akel

Chemistry Department, College of Science, King Saud University, P.O. Box 2455, Riyadh-11451, Saudi Arabia

(Received 1st June 1993; revised manuscript received 25th October 1993)

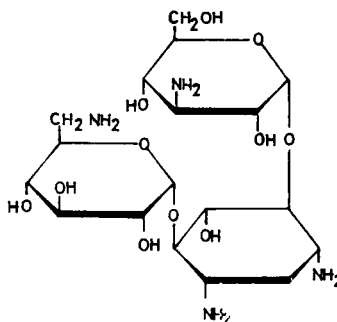
Abstract

The application of lucigenin chemiluminescence for the determination of trace concentrations of kanamycin is described. The method is based on the inhibiting effect that kanamycin has on the reaction of lucigenin and hydrogen peroxide in a basic solution. The effect of the concentrations of the reagents was studied and the reaction conditions are discussed. The proposed method allows the determination of kanamycin in the range of 1×10^{-13} to 1×10^{-5} M with a relative standard deviation of ca. 1.91%. The method is relatively free from the interference of common excipients accompanying the drug in pharmaceutical samples. The results obtained for the assay of commercial preparations compared well with those obtained by another known method and showed good accuracy and precision.

Key words: Flow injection; Chemiluminescence; Kanamycin; Lucigenin system; Pharmaceutical preparations

1. Introduction

Kanamycin [I, 6-O-(3-amino-3-deoxy- α -D-glucopyranosyl)-4-O-(6-amino-6-deoxy- α -D-glucopyranosyl)-2-deoxy-D-streptamine] is a polybasic aminoglycoside antibiotic which possesses clinically useful activity against a variety of pathogenic bacteria [1]. It has a bactericidal effect and a broad spectrum of activity against a range of Gram-negative and Gram-positive organisms [2].



Chemiluminescence (CL) is the emission of radiation, usually in the visible or near-infrared region, as a result of a chemical reaction. Chemi-

* Corresponding author.

luminescent reactions can occur very rapidly (≤ 1 s) or can be long lasting (≥ 1 days) and the light intensity produced is dependent on the CL quantum yield. Analytical interest in CL has increased considerably over the last decade [3].

Probably the most thoroughly investigated application of CL is for metal analyses. Luminol–hydrogen peroxide, lucigenin–hydrogen peroxide and lophine (2,4,5-triphenylimidazole)–hydrogen peroxide are three very popular systems used for trace metal detection and quantitation [4–10].

Very few reactions leading to CL are known for organic analytes, except those which have been found by Townshend and co-workers [11–13] and others [14–16]. The organic compounds can be determined via their influence on the CL of some systems. The most sensitive analyses are possible with compounds containing a metal such as haem compounds (containing iron metal) and vitamin B₁₂ [containing cobalt(III)] [17,18]. Other organic compounds such as EDTA, 8-hydroxyquinoline and amino acids have been determined by their inhibition of CL from metal-enhanced systems [19–21].

A variety of techniques have been utilized to detect kanamycin (KM) in clinical as well as in pure and pharmaceutical samples. The most commonly used and official method for determining KM potency is the microbiological [22,23] assay procedure. Because of many disadvantages associated with the microbiological assays which include specific variables (media, test organism and conditions of incubation), reproducibility, and day-to-day variation [24,25], other methods for determining KM concentrations have been developed. In particular, UV–visible spectrophotometry [26–28] and liquid chromatography [29,30]. Other procedures for determining KM, e.g., fluorimetry [31,32], radioenzymatic methods [33] and mass spectrometry [34] have also been reported.

In recent years flow injection (FI) has been used with CL (FI–CL) as a simple means for detection of some organic analytes [35–37]. In this paper a new FI method is described for the determination of KM based on its remarkable suppression of the CL of lucigenin systems.

If KM is made to be the rate-limiting reagent, then the amount of emission suppressed is pro-

portional to the concentration of KM, and can be used to quantify KM by measuring the decrease in the CL.

2. Experimental

2.1. Reagents

Kanamycin monosulphate stock solution (1×10^{-2} M). Prepared by dissolving 0.4845 g of kanamycin monosulphate (Sigma) in 100 ml of distilled water. Working standard solutions were prepared by appropriate dilution of the stock solution. A 1×10^{-2} M stock solution of lucigenin (Aldrich) was prepared by dissolving 0.5105 g of the chemical in 100 ml of distilled water. Cobalt(II) nitrate hexahydrate (AnalaR, BDH) stock solution (1×10^{-2} M) was prepared by dissolving 0.2910 g in 100 ml of distilled water. Hydrogen peroxide solution was prepared daily by diluting a measured amount of 30% (m/v) H₂O₂ (Merck) with distilled water. Potassium hydroxide (AnalaR) stock solution (1×10^{-2} M) was used.

2.2. Instrumentation

All chemiluminescent measurements were made with the instrumentation described previously [35,36].

2.3. Flow system for the determination of KM

A schematic diagram of the flow manifold is shown in Fig. 1. A 4-channel peristaltic pump (Gilson Minipuls 3MP4) was used to deliver the lucigenin solution through R₁ which acts as a carrier stream for the cobalt(II) solution which is injected via a solenoid activated rotary valve (Rheodyne 5020). This stream was merged 10 cm downstream with a stream of hydrogen peroxide (R₂) at a PTFE T-piece and merged again 6 cm downstream with a stream of potassium hydroxide (R₃) at a second PTFE T-piece. At 5 cm further downstream, all the three solutions merge at a third PTFE T-piece with a stream of KM monosulphate (R₄). All four streams were

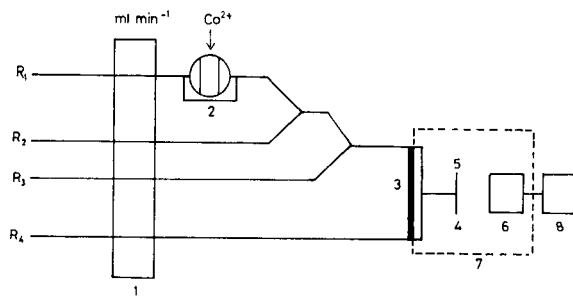


Fig. 1. Schematic diagram of the flow-injection system used for the determination of KM monosulphate and some of its pharmaceutical preparations: (1) peristaltic pump; (2) sample injection; (3) Perspex T-piece; (4) waste; (5) coiled flow cell; (6) PMT; (7) housing; (8) recorder; (R_1 , R_2 , R_3 , R_4) flow streams.

pumped at the same flow rate via the Gilson pump (3.5 ml min^{-1} in each channel). PTFE tubing (0.8 mm i.d.) was used throughout the remainder of the manifold. The four merged zones travelled 2.5 cm (the smallest practical distance) before passing into the flow cell. The output from PMT was fed to a strip-chart recorder (Yokogawa Model 3021) and the peak heights were measured manually. All results are the mean of five injections of Co(II) solution into five different KM solutions (KM solutions having the same concentrations), unless otherwise stated.

2.4. Optimization of the flow system

A series of experiments was conducted in order to optimize the analytical conditions for the CL determination of KM by using the lucigenin- H_2O_2 - Co^{2+} reaction in alkaline medium. The variables studied were the lucigenin, hydrogen peroxide, potassium hydroxide and cobalt(II) solution concentrations, flow rate and the buffers used as a solvent for lucigenin and hydrogen peroxide.

The influence of the lucigenin concentration on the analytical signal was investigated. Lucigenin solutions of different concentrations were prepared (1×10^{-2} – 1×10^{-6} M). The maximum CL intensity was obtained with a 1×10^{-3} M lucigenin solution. Fig. 2 shows the variation of the CL emission intensity expressed as peak

height with the concentration of lucigenin solution. In order to ensure maximum sensitivity, a lucigenin concentration of 1×10^{-3} M was chosen.

The effect of hydrogen peroxide on the CL reaction was investigated. By appropriate dilution of the stock solution of hydrogen peroxide a series of solutions was prepared (1×10^{-1} – 1×10^{-4} M). Fig. 3 shows the variation of the CL intensity expressed as peak height with the hydrogen peroxide concentration; 1×10^{-2} M H_2O_2 was found to be suitable. Higher concentrations (up to 0.01 M) gave higher emission, but the signal was noisy and irreproducible.

Since the conventional CL reaction of lucigenin with hydrogen peroxide catalyzed by various metal ions, three metals (Cr^{3+} , Co^{2+} and Fe^{2+}) were tested for their effect on the lucigenin- H_2O_2 system in the presence of KM. The results obtained are shown in Table 1. Since cobalt(II) was the only metal ion that catalysed the lucigenin CL reaction, as reported by Montano and Ingle Jr. [9], optimization of KM deter-

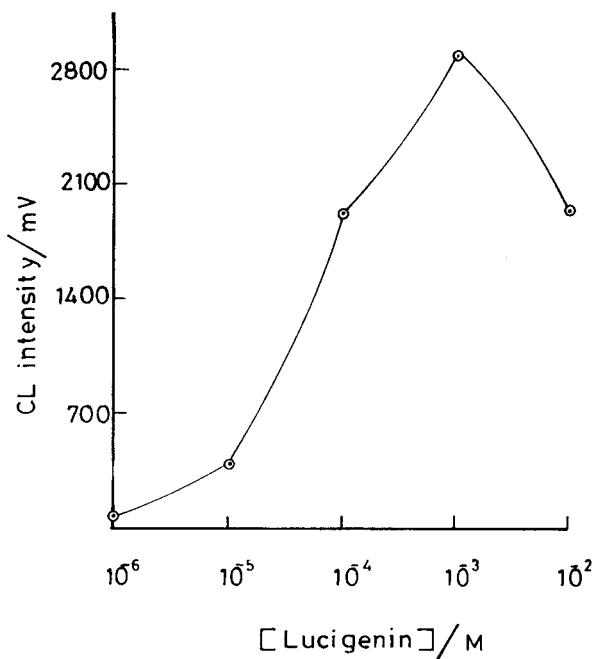


Fig. 2. Effect of lucigenin concentration on the net CL intensity for 1×10^{-5} M KM, 1×10^{-2} M H_2O_2 , 0.1 M KOH and 1×10^{-4} M cobalt(II) solution.

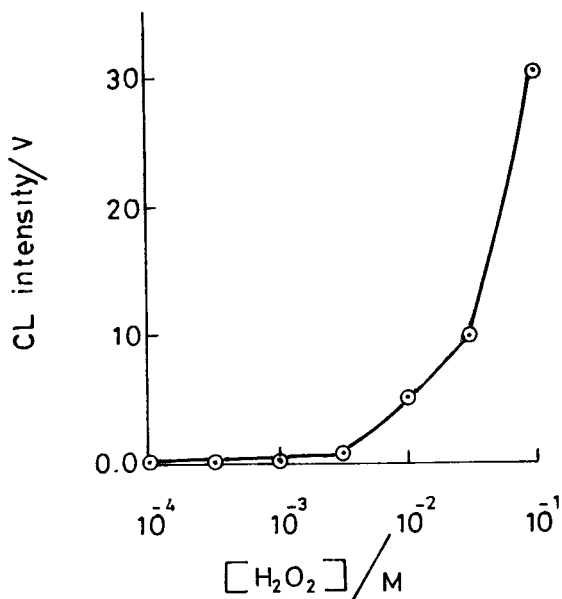


Fig. 3. Effect of H₂O₂ concentration on the net CL intensity for 1 × 10⁻⁵ M KM, 1 × 10⁻³ M lucigenin and 1 × 10⁻⁴ M cobalt(II) solution.

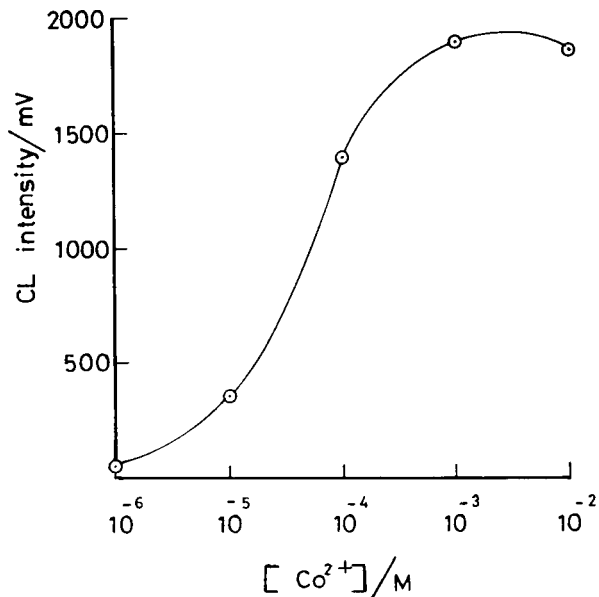


Fig. 4. Effect of cobalt(II) concentration on the net CL intensity for 1 × 10⁻⁵ M KM, 1 × 10⁻² M H₂O₂ and 1 × 10⁻³ M lucigenin.

mination was based on this catalyst. Hence the effect of its concentration was optimized. Different concentrations of cobalt(II) solution were prepared (1 × 10⁻²–1 × 10⁻⁶ M) and their effects on the net CL intensity were investigated. Fig. 4 shows that 1 × 10⁻³ M cobalt(II) solution gave the greatest intensity and was chosen for further study in order to achieve the maximum possible sensitivity. The result of the hydroxide ion optimization study is shown in Fig. 5. The maximum response was obtained at 0.1 M KOH, therefore, this level was chosen for all further work.

In the chemiluminescent reactions the effect of the flow-rate is essential because its variation

has a great influence on the CL intensity. Using the above optimized experimental parameters for maximum CL intensity, the effect of total flow-rate was studied. Flow rates of 5.8, 8.6, 11.4, 14.0, 16.90 and 19.6 ml min⁻¹ were employed. The results (Table 2) show that the CL intensity continues to increase with increasing total flow rate. A flow-rate of 14 ml min⁻¹ was selected for further studies, because at higher flow rates no significant increase in the CL intensity was shown.

3. Results and discussion

3.1. Choice of manifold and FI technique

The determination of KM is based on the inhibition of the lucigenin system so that the peaks resulting from the indicator reaction will be decreased in proportion to the inhibitor concentration.

In a preliminary study, several manifold arrangements were tested using similar conditions. In a system where the Co(II) solution was in-

Table 1

Effect of various metal ions (all 1 × 10⁻⁵ M) as catalysts for the lucigenin–hydrogen peroxide reaction in the presence of KM (1 × 10⁻⁵ M)

Metal ion	Salt	Observation
Cr ³⁺	Nitrate	No signal obtained
Co ²⁺	Nitrate	Strong enhancement
Fe ²⁺	Sulphate	No signal obtained

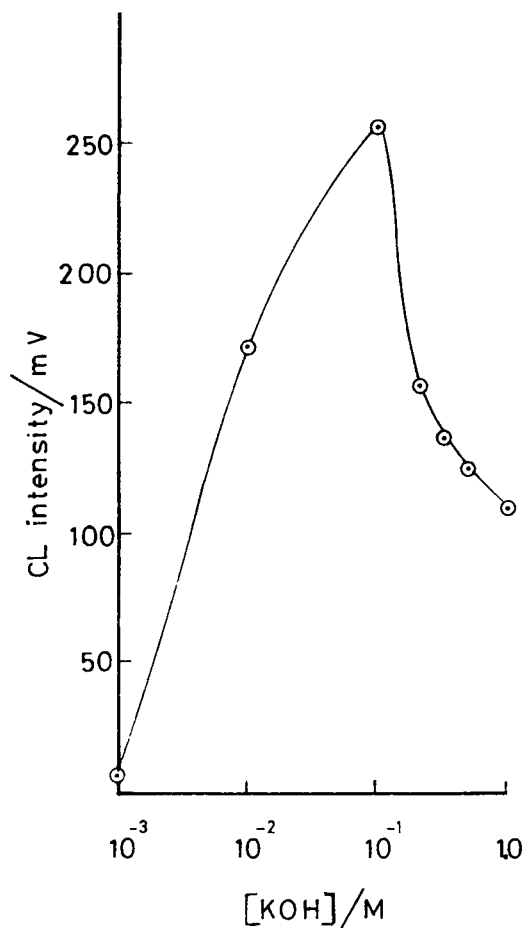


Fig. 5. Effect of potassium hydroxide on the net CL intensity for 1×10^{-5} M KM, 1×10^{-3} M lucigenin, 1×10^{-3} M cobalt(II).

Table 2

Effect of flow-rate on the emission intensity from 1×10^{-5} M KM, 1×10^{-2} M H_2O_2 , 1×10^{-3} M lucigenin and 1×10^{-3} M cobalt(II) solution

Flow-rate (ml min ⁻¹)	Emission intensity (mV)
5.8	110
8.6	158
11.4	184
14.0	206
16.9	240
19.6	245

jected into a lucigenin carrier and mixed with a continuously flowing hydroxide solution stream, then with the hydrogen peroxide stream, and then with the KM stream, the intensity obtained was not strong (ca. 140 mV). In a similar system in which the lucigenin carrier was mixed with hydrogen peroxide stream instead of the hydroxide solution, the CL intensity obtained was slightly greater (ca. 188 mV). In a third arrangement, where Co(II) solution was pumped through R_4 (instead of KM solution), so that a steady light emission would be obtained, if KM solution was injected into the carrier stream, then an inhibiting signal directly proportional to the concentration would be recorded. However, this version did not show chemiluminescence, and therefore no signal was obtained.

Improved results were obtained if the Co(II) solution was injected into the lucigenin stream which mixes with hydrogen peroxide before it mixes with potassium hydroxide. the KM solution should be pumped through R_4 , meeting the other solutions in front of the detector.

Other oxidants

Since CL arises most frequently from oxidation reactions involving large free energy changes, several oxidizing systems were examined to see if they offered any advantages over hydrogen peroxide. A 1×10^{-3} M solution of potassium periodate, hydrogen peroxide, sodium hypochlorite solution, sodium thiosulphate, potassium bromate and ammonium peroxodisulfate, were prepared and pumped through R_2 . No signals were observed from any of these oxidants except hydrogen peroxide, which was selected for further study.

Effect of buffers

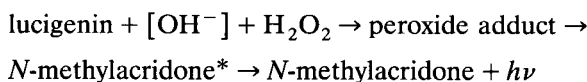
Since most of the CL systems occur under alkaline conditions, various buffer solutions (0.1 M sodium carbonate, 0.1 M sodium phosphate and 0.1 M ammonium citrate) were prepared and used as solvents for the lucigenin and hydrogen peroxide. The pH of each buffer solution was adjusted to 10.5. Phosphate and ammonium citrate buffers did not give any emission, while carbonate buffer gave only a weak emission. Best

results were obtained when lucigenin and hydrogen peroxide were prepared in water.

3.2. Inhibition mechanism

The cobalt(II) ion is a catalyst for the lucigenin–H₂O₂ system. KM alone does not function as a catalyst because in an alkaline solution of lucigenin–H₂O₂–KM without cobalt(II), no chemiluminescence is observed.

The CL reaction mechanism can be briefly expressed by the following reactions [38]:



In solution, there are two forms of oxygen which may play an important role in the reaction with lucigenin. One is singlet oxygen and the other is the superoxide anion (O_2^-). However, previous work [39] has shown that singlet oxygen is not stable in alkaline solution. Therefore it is concluded that the superoxide anion is probably the only species involved in the oxidation of lucigenin to *N*-methylacridone.

The lifetime of the superoxide anion is only several milliseconds [40], even in alkaline solution. Addition of KM monosulphate to the lucigenin–H₂O₂–Co²⁺ system shortens the duration of CL. In the concentration range studied, the inhibition is increased as the drug sample concentration is increased. This probably indicates that KM can combine with the superoxide anion to form a peroxide adduct which speeds up the decomposition of the superoxide. The luminescent species is *N*-methylacridone with or without KM. This means that the KM peroxide adduct can react with lucigenin to exchange superoxide anions. Clearly a much more extensive investigation of these reactions is needed.

3.3. Calibration data

Under the conditions established an analytical calibration curve was obtained. The linear dynamic range, slope and the correlation coefficient of the corresponding log–log working curve, detection limit and specific reaction conditions are

Table 3

Summary of data for the analytical working curve [$\log(\text{CL signal})$ vs. $\log(\text{concentration})$] and detection limit for KM

Linear dynamic range (M)	1×10^{-13} – 1×10^{-5}
Linear regression equation	$\log I(\text{mV}) = 3.125 - 0.038 \log C(10^{-7} \text{ M})$
Correlation coefficient ($n = 5$)	0.994
Detection limit (M)	1×10^{-13}
Precision (R.S.D., %) ($n = 10$) at $6 \times 10^{-7} \text{ M}$	1.91

summarized in Table 3. The relative standard deviation is 1.91% for ten determinations of $6 \times 10^{-7} \text{ M}$ KM. A non-logarithmic graph for a narrower concentration range [$(2-10) \times 10^{-7} \text{ M}$] has a regression equation of emission intensity (I) on KM concentration (C) of $I = 3378 - 0.986C(10^{-7})$ ($r = -1.000$, $n = 5$).

3.4. Effect of some organic compounds of clinical significance

The reaction of lucigenin in basic solution with some clinically important organic compounds have been investigated previously [41–44]. Therefore, we have also examined the CL reaction of lucigenin with various organic compounds that are related to kanamycin, such as aminoglycosides (neomycin, streptomycin), amino sugars (glucosamine), reducing sugars (fructose, glucose, galactose) and amino acids (glycine, alanine, tryptophan). All these compounds were effective in producing CL from alkaline solutions of luci-

Table 4

Recovery of $1 \times 10^{-6} \text{ M}$ KM from solutions containing 10 and 1000-fold concentration of various excipients

Excipient	Recovery (%)	
	$1 \times 10^{-5} \text{ M}$	$1 \times 10^{-3} \text{ M}$
Glucose	95.3	82.6
Fructose	97.4	87.6
Polyethylene glycol (Carbowax)	98.5	93.0
Magnesium stearate	104.5	106
Cellulose acetate hydroxyphthalate (CAHP)	95.6	93.2
Starch	99.4	95.4

Table 5
Determination of KM in commercial formulations with CL and Rizk and Younis (R and Y) methods

Formulation	Amount of KM (mg) found ^a			Recovery (%)	
	Claimed	CL	R and Y	CL	R and Y
KM injection (250 mg) (Misr Co., Egypt)					
Sample 1	250	255	251	102	100.4
Sample 2	250	249	253	99.6	101.2
Sample 3	250	250	248	100	99.2

^a Average of five determinations per sample.

genin. These results suggested the possibility of using the lucigenin reaction to develop CL methods of analysis for such compounds.

Since the reaction does not differentiate between kanamycin and other compounds related to, the analysis would be most direct if the analytes were separated from each other. Thus, a major strength of this CL reaction could lie in its application for detection in liquid chromatography.

3.5. Effect of interference

In order to assess the potential analytical applications of the described CL procedure, the effect of some common excipients used in pharmaceutical preparations was studied by analyzing synthetic sample solutions containing 1×10^{-6} M KM and two different concentrations of each excipient (i.e., 1×10^{-3} and 1×10^{-5} M). Any undissolved material was filtered before measurement. The recoveries obtained are given in Table 4. Slight interferences were observed from the excipient tested. Fortunately, this effect is minimized by using dilute sample solutions. Therefore, the method can be applied directly to solutions prepared from the drug formulations without further treatment.

The proposed CL method was tested by analyzing commercial formulations of KM. It was considered of interest to compare the figures of merit for this proposed procedure with those for a spectrophotometric assay for KM [45], which involves formation a charge-transfer complex be-

tween chloranil and KM in borate buffer at pH 9.0. Statistical analysis of the results obtained reveals that there is no significant difference between them (see Table 5).

4. Conclusion

The proposed method for the determination of KM by CL–FIA demonstrates that CL has many potential applications in the area of pharmaceutical analysis. The method is superior to other conventional methods in that it is very fast, simple, sensitive and does not require the removal of excipients prior to analysis. Also, the manipulation and intervention of the operator is minimal.

References

- [1] P.A. Bunn, *Med. Clin. N. Amer.*, 54 (1970) 1245.
- [2] J.E.F. Reynolds and A.B. Prasad, *Martindale, The Extra Pharmacopeia*, 28th edn., The Pharmaceutical Press, London, 1982, p. 1175.
- [3] A. Townshend, *Analyst*, 115 (1990) 495.
- [4] W.R. Seitz and D.M. Hercules, in M.J. Cormier, D.M. Hercules and J. Lee (Eds.), *Chemiluminescence and Bioluminescence*, Plenum Press, New York, 1973, p. 427.
- [5] L.I. Dubovenko and N.V. Beloshitskii, *J. Anal. Chem. USSR*, 29 (1974) 85.
- [6] A.K. Babko, L.I. Dubovenko and A.V. Terletskaya, *Sov. Prog. Chem.*, 32 (1966) 1326.
- [7] L.I. Dubovenko and A.P. Tovmasyan, *J. Anal. Chem. USSR*, 25 (1970) 812.
- [8] L.I. Dubovenko and A.P. Tovmasyan, *Sov. Prog. Chem.*, 39 (1973) 68.
- [9] L.A. Montano and J.D. Ingle, Jr., *Anal. Chem.*, 51 (1979) 919.
- [10] A. MacDonald, K.W. Chan and T.A. Nieman, *Anal. Chem.*, 51 (1979) 2077.
- [11] R.W. Abbott, A. Townshend and R. Gill, *Analyst*, 111 (1986) 635.
- [12] A.A. Alwarthan and A. Townshend, *Anal. Chim. Acta*, 185 (1986) 329.
- [13] S.A. Al-Tamrah and A. Townshend, *Anal. Chim. Acta*, 202 (1987) 247.
- [14] D.F. Marino and J.D. Ingle, Jr., *Anal. Chim. Acta*, 124 (1981) 23.
- [15] J.R. Bowyer and S.R. Spurlin, *Anal. Chim. Acta*, 192 (1987) 289.
- [16] H. Imai, H. Yoshida, T. Masujima and T. Owa, *Bunseki Kagaku*, 33 (1984) 54.

- [17] U. Isaccson and G. Wettermark, *Anal. Chim. Acta*, 68 (1974) 339.
- [18] T.L. Sheehan and D.M. Hercules, *Anal. Chem.*, 49 (1977) 446.
- [19] A.K. Babko, L.I. Dubovenko and L.S. Mikhailova, *Zh. Anal. Khim.*, 21 (1966) 548.
- [20] A.K. Babko and N.M. Lukovskaya, *Ukr. Khim. Zh.*, 35 (1969) 1060.
- [21] S. Pantel and H. Weisz, *Anal. Chim. Acta*, 74 (1975) 275.
- [22] *British Pharmacopeia*, HM Stat. Office, London, 1980.
- [23] *United States Pharmacopeia XX-National Formulary XV*, U.S. Pharmacopoeial Convention, 1980.
- [24] S.K. Maitra, T.T. Yoshikawa, L.B. Guze and M.C. Schotz, *Clin. Chem.*, 25 (1979) 1361.
- [25] D.M. Benjamin, J.J. McCormack and D.W. Gump, *Anal. Chem.*, 45 (1973) 1531.
- [26] J.A. Ryan, *J. Pharm. Sci.*, 73 (1984) 1301.
- [27] M. Rizk, *Anal. Lett.*, 17 (1984) 1803.
- [28] N.A. Zakhari, *Anal. Lett.*, 23 (1990) 1843.
- [29] J.R. Lawrence and R.W. Frei, in *Chemical Derivatization in Liquid Chromatography*, Elsevier, Amsterdam, 1976, p. 1.
- [30] T.T. Yoshikawa, S.K. Maitra, M.C. Schotz and L.B. Guze, in G.L. Hawk (Ed.), *Biological/Biomedical Applications of Liquid Chromatography*, Marcel Dekker, New York, 1978, p. 603.
- [31] R.C. Evangelista and E.E.S. Schapoval, *Rev. Cienc. Farm.*, 5 (1983) 35; *Anal. Abstr.*, 47 (1985) 6 E 38.
- [32] N.M. Alykov, *Zh. Anal. Khim.*, 36 (1981) 1387; *Anal. Abstr.*, 42 (1982) 3 D 52.
- [33] R.K. Holmes and J.P. Sanford, *J. Infect. Dis.*, 129 (1974) 519.
- [34] B.V. Rozynov, Yu.V. Zhdanovich, A.D. Kuzovkov, R.N. Elizabeth and A.S. Tikhonova, *Antibiotiki*, 25 (1980) 652.
- [35] A.A. Alwarthan, *Analyst*, 118 (1993) 639.
- [36] A.A. Alwarthan, S.A. Al-Tamrah and A.A. Akel, *Anal. Chim. Acta*, 282 (1993) 169.
- [37] A.A. Alwarthan and A. Townshend, *Anal. Chim. Acta*, 205 (1988) 261.
- [38] R. Maskiewicz, D. Sogah and T.C. Bruice, *J. Am. Chem. Soc.*, 101 (1979) 5348.
- [39] R.W. Ware and M.P. Richter, *J. Chem. Phys.*, 48 (1968) 1595.
- [40] F. Ross and A.B. Ross (Eds.), *Natl. Stand. Ref. Data Series, Natl. Bur. Stand.*, (1977) 59.
- [41] R.L. Veazey and T.A. Nieman, *Anal. Chem.*, 51 (1979) 2092.
- [42] R.L. Veazey and T.A. Nieman, *J. Chromatogr.*, 200 (1980) 153.
- [43] L.L. Klopff and T.A. Nieman, *Anal. Chem.*, 57 (1985) 46.
- [44] M. Maeda and A. Tsuji, *J. Chromatogr.*, 352 (1986) 213.
- [45] M. Rizk and F. Younis, *Anal. Lett.*, 17 (1984) 1803.

Recovery of polonium from microwave bomb digestions

P.H. Towler, J.D. Smith *

Marine Chemistry Laboratory, School of Chemistry, The University of Melbourne, Parkville, Victoria 3052, Australia

(Received 8th September 1993)

Abstract

The use of microwave digestion of plant and animal tissue in preparation for measurement of the volatile element polonium was evaluated. Digestion in concentrated nitric acid in a closed vessel at up to 1380 kPa took up to 2 h. The nitric acid was removed by evaporation in an open beaker and the Po transferred to hydrochloric acid. This transfer is necessary as Po is determined by alpha-spectrometry after plating onto silver from HCl solution. In real samples the amount of Po present is small. Recovery of Po after standard additions of 4.6×10^{-15} g (0.1 Bq) of ^{208}Po through the microwave digestion and acid transfer was complete within 95% confidence limit.

Key words: Biological samples; Microwave digestion; Polonium

1. Introduction

Determination of the activity of α -emitting radionuclides in biological samples usually requires dissolution of the tissue with complete destruction of organic matter. Digestion in an open vessel or under reflux using a mixture of nitric and perchloric acids is commonly used. Acid digestion in closed vessels using microwave heating is becoming widely used [1,2]. These digestions use pressure vessels constructed from or lined with polytetrafluoroethene (PTFE)-type materials and the acid is heated using a microwave oven. The use of these “microwave bombs” for digestions has advantages over open vessel techniques, especially decreased digestion times, the ability to use small volumes of reagents

and complete digestion without the use of perchloric acid. There is lower risk of contamination, but with the application of temperatures well above the normal boiling point of the acids there is the potential for loss of volatile elements. Our laboratory has been involved in the determination of ^{210}Po in biological samples for some years [3] and we report here our recent investigation into the use of microwave bombs in sample preparation.

Our primary concern was the volatility of polonium at temperatures higher than 150°C [4]. After the digestion is complete the vessels are opened and the gaseous products of the digestion are lost. It is possible that polonium could also be lost at this stage. The problem of possible losses is acute for polonium because of its volatility and the small masses present. The standard addition of 0.1 Bq of ^{208}Po (half-life 2.9 years) corresponds to 4.6×10^{-15} g. The same activity of the shorter

* Corresponding author.

lived ^{210}Po (half-life 138.8 days) corresponds to 6×10^{-16} g. The recovery of polonium was determined by measuring the recovery of standard additions of ^{208}Po tracer to animal (liver) and plant (leaf) tissues. Samples were digested in concentrated nitric acid in a microwave bomb. The polonium was transferred to a hydrochloric acid solution, plated onto silver discs and the activity of the polonium measured by alpha-spectrometry. Complete recovery of ^{208}Po through the digestion was achieved and we are now routinely using this technique.

2. Experimental

2.1. Reagents

The standard ^{208}Po solution of 2.31 ± 0.11 kBq/ml (June 25, 1989) in 1 M HCl was supplied by the UK Atomic Energy Authority, Harwell. This was diluted by weight to give a working solution of about 0.22 Bq/g (July 30, 1992). Acids used were analytical grade.

2.2. Tissues examined

The animal tissue used was liver of a Saw Shark (*Pristiophorus cirratus*) from Port Phillip Bay, Australia, homogenised wet and stored frozen. The plant tissue used was NBS standard reference material 1571 (Orchard Leaves). For each experiment 0.50 g of tissue was used.

2.3. Apparatus

Digestions were carried out in CEM (Indian Trail, NC) low pressure microwave digestion bombs. These are double vessels with Dupont Perfluoroalcohol (PFA) liners and rupture discs rated to 1380 kPa. An unmodified Sharp R6750E domestic microwave oven with turntable and 650 W maximum power at 2450 MHz was used on its lowest setting. Polonium was plated onto silver discs (17 mm diameter, 0.3 mm thickness) cut from fine grade (> 99.9%) silver polished to bright finish. During plating each disc was held in a PTFE block fitted with a magnetic stirrer bar

and rotated using a stirrer hotplate. Polonium was measured by alpha-spectrometry using a Canberra (Meriden, CT) Quad alpha-spectrometer with passively implanted planar silicon (PIPS) detectors connected to a PC based Canberra S100 multichannel analyser.

2.4. Sample digestion

Replicate samples of animal and plant tissues (0.50 ± 0.01 g) were weighed into microwave digestion vessels. Standard additions of ^{208}Po tracer (0.50 ml containing ca. 0.12 Bq) were made, checking the additions by weight. 5 ml of concentrated nitric acid was added to each sample. The vessels were fitted with new rupture discs and securely screwed closed. The digestions were carried out in the microwave oven in sets of four. Previous experimentation had shown that digestion took up to 2 h with the oven set on its minimum power, depending on the type of sample. When the next higher power was used the rupture disc burst and this indicates that we were operating near the pressure limit of 1380 kPa. The vessels were heated for 60 min then removed from the oven, allowed to cool, then heated for a further 60 min at the same power setting. The vessels were allowed to cool to room temperature and weighed before opening. In all experiments, weight loss during the digestion was less than 50 mg, indication that there was no leakage during digestion. The digests were transferred to 50-ml beakers and placed on a hotplate under an infrared lamp to remove the nitric acid. Care was taken not to allow the solution to go to complete dryness because of the volatility of polonium at temperatures greater than 150°C. 2 M hydrochloric acid was added and the polonium plated onto spinning silver discs by autodeposition at 75°C for 90 min using the method of Hamilton and Smith [5].

Alpha-spectra were recorded for 200000 s and the activity of the ^{208}Po compared with the activity obtained by plating 0.20 ml of the standard ^{208}Po solution directly from 2 M hydrochloric acid under the same conditions. The method adopted for the plating of polonium on to a silver disc requires a solution free of organic material,

particularly charred material, if it is to approach 100% recovery. Digestion times of up to 1 h were sufficient for the plant tissue, but did not digest all the organic material in the liver sample. When organic material remained in the digested liver sample, charring occurred during the evaporation of the nitric acid before uptake in HCl. This gave variable recoveries of ^{208}Po in the range 78–102%. Digestion for 2 h destroyed all the organic material and no charring occurred when evaporating off the nitric acid.

3. Results and discussion

The activity of standard additions of ^{208}Po after microwave digestion, transfer from nitric to hydrochloric and plating on to silver discs was compared to the ^{208}Po plated directly onto silver from hydrochloric acid. Results of standard additions of ^{208}Po to plant and animal tissues show that there is no significant loss of the polonium tracer in the microwave digestion or the subsequent evaporation stages of the procedure, Table 1. Calculations were carried out using the integrated counts in the ^{208}Po peak of the α -spectrum. In all experiments 1000 to 5000 counts were recorded in the ^{208}Po peak. This number of counts is characteristic in low-activity α -spectrometry of environmental samples and gives a coefficient of variation of 3.3–1.4% from counting statistics alone. The measured activity of ^{208}Po was adjusted to take into account the small variations in the mass of tracer solution added. The measured activities for the animal and plant tissues were compared to the activities from plating alone using the Student's t -test. For seven degrees of freedom and $P = 0.05$ the tabulated value of t is 2.36. The experimental values of t were 1.63 and 0.75 for the liver and leaf samples, respectively. Hence, recovery of ^{208}Po through the microwave bomb digestion procedure, plating and counting is indistinguishable from the recovery during plating and counting within a confidence limit of 95%.

It can be seen in Table 1 that the measured standard deviations are similar to those predicted from counting statistics alone. This indicates the

Table 1
Results for measurement of ^{208}Po

No.	Measured activity (1) (counts/ks/g soln.)	Counting error (2) (counts/ks/g soln.)
(A) Tracer only		
1	44.4	1.05
2	38.6	0.98
3	43.1	1.03
4	39.0	0.99
5	39.6	0.99
6	40.9	1.01
Mean	40.9	1.01
s	2.4	
R.S.D. (%)	5.7	
(B) Liver		
7	43.6	0.65
8	43.4	0.65
9	42.6	0.65
Mean	43.2	0.65
s	0.5	
R.S.D. (%)	1.3	
(C) Leaves		
10	42.7	0.65
11	42.8	0.65
12	40.5	0.65
Mean	42.0	0.65
s	1.3	
R.S.D. (%)	3.0	

(1) Measured activity is counts/ks ^{208}Po per g of tracer solution added. The activities are corrected for radioactive decay to the date of digestions. (2) Counting error is based on one standard deviation of the total counts and is in units of counts/ks ^{208}Po per g of tracer solution added. (A) Tracer only is for ^{208}Po tracer plated directly onto silver disc then counted. (B) Liver and (C) leaves are for ^{208}Po yield tracer added to animal (B) or plant (C) tissues then digested in nitric acid in a PFA bomb heated with microwaves, transferred to hydrochloric acid, then plated on to silver disc then counted. s = Standard deviation; R.S.D. = relative standard deviation.

good reproducibility of the procedure. Bomb digestions of nitric acid with no addition of ^{208}Po , run before and after digestions with added ^{208}Po gave ^{208}Po counts < 1% the standard additions showing that the bomb liners had no memory effect for Po.

The measured activity concentration of ^{210}Po in the NBS Orchard Leaves was 14 mBq/g ($\sigma_{n-1} = 3$ mBq/g). This represents ^{210}Po supported by ^{210}Pb . The shark liver, which had been stored

frozen for 12 months, contained $< 1 \text{ Bq kg}^{-1}$ ^{210}Po .

4. Conclusion

Digestion of plant and animal tissue in nitric acid in a closed PFA bomb heated by microwaves did not result in loss of the potentially labile element polonium. There was no loss of polonium in its subsequent transfer from nitric to hydrochloric acid solution in preparation of plating as a thin source. Microwave bomb digestion is a rapid and clean method for preparation of plant and animal tissues for low level ^{210}Po determination.

Acknowledgements

JDS thanks the ARC (Australia) for a grant permitting purchase of the equipment used. PHT thanks the Commonwealth Government (Australia) for support through an APRA.

References

- [1] M. Bettinelli, U. Baroni and N. Pastorelli, *Anal. Chim. Acta*, 225 (1989) 159.
- [2] R. Uhrberg, *Anal. Chem.*, 54 (1982) 1906.
- [3] J.D. Smith and T.F. Hamilton, *Anal. Chim. Acta*, 160 (1984) 69.
- [4] A. Martin and R.L. Blanchard, *Analyst*, 94 (1969) 441.
- [5] T.F. Hamilton and J.D. Smith, *Appl. Radiat. Isot.*, 37 (1986) 628.

Book Reviews

Dictionary of Analytical Reagents, A. Townshend, D.T. Burns, G.G. Guilbault, R. Lobinski, Z. Marczenko, E.J. Newman and H. Onishi (Eds.), Chapman and Hall, London, 1993 (ISBN 0-412-35150-1). 1370 + xxix pp., Price £625.00.

This book perhaps represents one of the last of its kind in Analytical Chemistry, namely a massive single volume compendium with a wealth of data on a given topic, compiled from original sources and secondary reviews as an information resource, but with no intention of recommending procedures or evaluating methods. As a sheer source of information it succeeds admirably. In a style reminiscent of such volumes as the *Handbook of Chemistry and Physics*, it assembles and cross-references under various categories a very wide range of reported analytical chemical reagents. It is certainly the only such source so devised and the concept is thus most valuable.

The major part of the volume which comprises 964 pages, consists of an alphabetical listing of reagents arranged usually according to IUPAC nomenclature but with accepted 'trivial' names in some cases. It is simple to find a particular compound. Each reagent is also given an alphabetical reference number based upon the first letter of its chemical name, thus A-00001 – acenaphthenequinone. Each entry shows chemical formula and/or structure, physical and chemical properties, hazard information, a summary of usage and a number of essential literature references. The reader is thus able to obtain a complete basis for further investigation and use of the reagent. Literature references are current through 1992.

There follows a 'Name' index comprising 95 pages, a useful feature again being an indication

of 'hazard' information in each case. A 90 page 'Molecular Formula' index provides another useful feature, as does the following Chemical Abstracts registry number index. Of great value to the user is then the index for the 'Type of Compound' for which the reagent is applied. This is divided into two parts, that according to the element to be determined, and that for the compound class and functional group to be measured. There is finally a 'Use' index which lists the application for which the reagent is employed, e.g., 'indicator', spectrophotometric reagent', etc. The monumental work involved in assembling these indexes has been undertaken with meticulous care and the end result is impressive indeed. This is an eminently 'practical' volume which is accessible to novice and expert alike. To assist the reader there is a clearly written 18 page introduction which discusses general reagent classes and chemical goals.

The authors and editors have succeeded in bringing a daunting task to an accessible outcome. The book is most attractive, clearly presented and unique in concept and implementation. This is not a book for individual purchase but should be in all analytical chemical library collections, both academic and industrial. In today's world of 'instrumental' emphasis this volume should serve to re-emphasize the importance of the 'chemistry' in analytical chemistry.

Peter C. Uden

Allen J. Bard (Ed.), *Electroanalytical Chemistry: a Series of Advances*, Vol. 17, New York, Dekker, 1993 (ISBN 0-8247-8409). xii + 393 pp. Price US \$165.00. Vol. 18, 1993 (ISBN 0-8247-9092-8). xii + 400 pp. Price US \$165.00.

These volumes are part of a continuing series describing advances in the general field of electroanalytical chemistry. Volume 17 contains substantive sections covering: applications of the quartz crystal microbalance to electrochemistry; optical second harmonic generation as an in situ probe of electrochemical interfaces; new developments in electrochemical mass spectroscopy and carbon electrodes – structural effects on electron transfer kinetics. Volume 18 contains chapters on: electrochemistry in micelles, microemulsions and related microheterogeneous fluids; the mechanism of charge transport in polymer modified electrodes and scanning electrochemical microscopy.

The 82-page chapter in Volume 17 on applications of the quartz crystal microbalance by Daniel Buttry (Wyoming) contains references up to and including 1989 and provides a useful introduction to experimental methods, monolayer systems, some multilayer systems and polymer films, including redox polymers and conducting polymers. It is clear that as the subject matures and theoretical treatments for impedance analysis evolve the technique will become a very powerful tool in the electrochemist's armoury. The chapter on optical second harmonic generation by Geraldine Richmond (Oregon) provides a summary of the current state of the field as applied to electrochemical systems. There is a detailed examination of the influence of molecular and ionic absorption and of the application to single crystal electrodes. Altogether the chapter includes some 173 references. The shortest chapter (40 pages) is on new developments in electrochemical mass spectroscopy and is contributed by Barbara Bittins-Cattaneo, Eduardo Cattaneo, Peter Königshoven and Wolf Vielstich (Bonn). This section starts with a historical overview before going on to describe the experimental approaches which may be taken to exploit the technique. Limitations are discussed and a series of applications is reported. The applications include studies of ethanol and carbon monoxide as adsorbates, gas evolution, oxidation of propylene carbonate, electroreduction of CO₂ and oxygen evolution on metal electrodes. The chapter concludes with a brief mention of the newer techniques of electrochemical

thermospray mass spectroscopy (ETMS) and electrochemical thermal desorption mass spectroscopy (ECTDMS).

The final substantive chapter of Volume 18 is an examination of structural effects on electron transfer kinetics at carbon electrodes by Richard McCreery (Ohio). The chapter examines the structure of bulk carbon and carbon electrode surfaces and then goes on to discuss methods of preparation and the resulting electrode performance and characteristics.

The first chapter of Volume 18 by James Rusling (Connecticut) on electrochemistry in micelles, microemulsions and lamellar and vesicle dispersions treats each topic methodically. It shows how reaction pathway and kinetics can be controlled by surface aggregates and how electrochemical probes can be used to develop models of and measure diffusion.

György Inzelt (Budapest) has contributed a chapter on the mechanism of charge transport in polymer modified electrodes. This excellent chapter brings together about 300 references and interprets many of the papers in a critical and useful manner.

The final chapter by the group of Allan Bard, Fu-Ren Fan and Michael Mirkin at Texas (Austin) introduces and reviews the subject of scanning electrochemical microscopy (SECM). The chapter provides an excellent and comprehensive grounding in the area. It covers the practical approaches to SECM in detail and indicates the type of information that can be obtained. The theory is carefully covered and easy to follow.

Overall, these volumes are excellent reference books which extend an authoritative series in a timely manner. For a researcher entering a new field covered in the series they are a worthwhile personal purchase; otherwise they will serve as good library reference books.

Jonathan Slater

L.M.C. Buydens and P.J. Schoenmakers (Eds.), *Intelligent Software for Chemical Analysis, Data Handling in Science and Technology*, Vol. 13, Elsevier, Amsterdam, 1993 (ISBN 0-444-89207-9). xviii + 347 pp. Price US \$200.00/Dfl.350.00.

This book gives an excellent overview over the various techniques to implement intelligent laboratory functions on computers in the context of an analytical laboratory. The methods described include knowledge-based expert systems, neural networks, genetic algorithms, and the ID3 algorithm for inductive classification. It describes how these methods work and gives hints as to possible applications in analytical chemistry. Furthermore, data and information necessary to develop and test such systems are given. The authors are all experts in their respective field, so the descriptions given are complete and precise. Much work has gone into the presentation, so the text is as easy to read and as easy to understand as is possible in a field with such a high degree of complexity. The authors also obviously have much practical experience with the type of systems described, so the texts are of direct practical relevance.

This book should be studied by all chemists who intend to build and/or regularly use intelligent laboratory systems. Managers, laboratory supervisors and people responsible for quality control will also benefit from reading this book, thereby acquiring the knowledge necessary to understand the potentialities and limitations of such systems.

J.T. Clerc

N. Purdie and H.G. Brittain (Eds.), *Analytical Applications of Circular Dichroism*, Elsevier, Amsterdam, 1994 (ISBN 0-444-89508-6). x + 348 pp. Price Dfl.355.00.

Circular dichroism (CD) is a technique which provides unique information about dissymmetric molecules. The properties of such compounds are now realised to be of great significance in fields such as natural product chemistry, molecular biology and in pharmaceuticals in the post-thalidomide-tragedy world.

This multi-authored book deals with the unique aspects of circular dichroism and how these are applied in various fields. Topics include a basic introduction into chiroptical phenomena, CD in-

strumentation including that for the IR region, followed by a series of detailed application reviews (solution confirmation of biological molecules, absolute configuration, protein structures, study of molecules in electronically excited states, determination of steroids, induced CD via association of achiral with chiral molecules, applications in the forensic, pharmaceutical, clinical and food sciences and as a chromatographic detector).

This text should provide a stimulus to further CD studies as it provides a convenient entry point to this fascinating, problem driven, field of modern analytical chemistry.

Duncan Thorburn Burns

Eberhard Breitmaier (translated by Julia Wade), *Structural Elucidation by NMR in Organic Chemistry, A Practical Guide*, Wiley, New York, 1993 (ISBN 0-471-93745-2). 265 + xii pp. Price £39.95/US \$63.95. (A paperback edition is also available.)

In two chapters and 69 pages this book surveys the essentials of nuclear magnetic resonance (NMR) spectroscopy as applied to the structural elucidation of organic compounds. The author assumes that readers will have some prior knowledge of NMR and indeed this is necessary. Chapter 1 outlines the principles of NMR together with an explanation of the common terms, parameters and techniques whilst Chapter 2 proceeds to the details of the strategies and approaches that can be adopted for determining structural details of organic compounds. All students would benefit from reading this text if only for the way the book places the various approaches into context. Page 69 includes a flow diagram of a systematic approach to structural elucidation which could usefully be adopted by anyone needing to solve such problems. It is all too common to find a random approach used to solve structural problems from NMR spectra.

And then to the problems... 50 of them, graded in difficulty and drawn from different areas of organic chemistry including natural

products, heterocyclic, alicyclic and aromatic. Problems are grouped into several classes requiring different approaches including ^1H and ^{13}C , one- and two-dimensional spectra and combinations of each. Solutions to problems are then given in some detail serving both as an additional learning experience and as a relief when the problem concerned appears to defy resolution!

This book can be recommended to all those who need to use NMR in organic chemistry with the major benefits accruing from its use as a workbook rather than simply as a text for reading.

John D. Green

T.R. Yu and G.L. Ji, *Electrochemical Methods in Soil and Water Research*, Pergamon, Oxford, 1993 (ISBN 0-08-041887-2). xvi + 462 pp. Price £65.00/US \$105.00.

This extensive treatise is primarily concerned with the principles of potentiometric methods of analysis, the fabrication of indicator electrodes such as glass, solid state membrane, liquid state membrane and gas sensor electrodes and their incorporation in electrochemical measuring devices for the determination of chemical species of significance in soil and water research e.g., H_3O^+ , Na^+ , K^+ , Ca^{2+} , Ba^{2+} , Pb^{2+} , F^- , Cl^- , S^{2-} , CN^- , NO_3^- , NH_3 , H_2S and CO_2 . It has been written by the staff of the Institute of Soil Science of the Chinese Academy of Sciences which has had particular experience in this area of research for the past three decades. T.R. Yu and G.L. Ji, who have contributed to several of the chapters, have been responsible for the editing of the manuscript, resulting in well organised and comprehensive contents. Overall, the text reads well following its translation and updating from the original Chinese version, published in 1980. The text is illustrated by many mathematical derivations, tables and figures, together with analytical methodologies for particular determinations in soils and waters. Only one chapter is, however, devoted to voltammetric methods of analysis which, in the light of the number of recent publications on the

applications of voltammetry and stripping voltammetry to the determination of inorganic and organic molecules of environmental significance, would seem to be inadequate. In conclusion, the text is particularly useful for those unfamiliar with the principles and applications of these electrochemical techniques for the determination of inorganic entities and is a valuable reference work for those involved in research in soil, water, environmental, earth and biological sciences.

W.F. Smyth

L. Newman (Ed.), *Measurement Challenges in Atmospheric Chemistry*, American Chemical Society, Washington, DC, 1993 (ISBN 0-8412-2470-6). xiii + 407 pp. Price US \$94.95.

The global impact of issues such as ozone depletion and greenhouse warming have provided a catalyst for research into fundamental aspects of atmospheric chemistry. This has in turn required increasingly sophisticated analytical techniques (including sampling devices and in situ measurement) capable of providing "quality" data to support theoretical studies and the acquisition of global databases.

This monograph is Volume 232 in the ACS *Advances in Chemistry* series and provides state-of-the-art descriptions of thirteen selected topics relating to the measurement of atmospheric constituents. In general the contents are well presented and extensively referenced and there is a good collective index.

There are two contributions dealing with sampling (of labile atmospheric pollutants and sampling from aircraft) and three chapters discussing specific aspects of aerosols (chemical dynamics, composition and strong acid content). In terms of generic techniques there are comprehensive chapters on automated diffusion-based devices for collecting and analysing atmospheric trace gases and on the in situ measurement of stratospheric reactive trace gases and a brief contribution on chemical sensors used for eddy correlation flux measurements.

Four chapters discuss analytical approaches to

the determination of atmospheric nitrogen species, non-methane organic compounds, peroxy radicals and the hydroxy radicals. The challenges presented by such species include their transient and reactive nature, temporal and spatial variation and low concentrations, all of which suggest that in situ methods are becoming increasingly important if not essential. The final chapter provides an interesting account of the requirements for the measurement of personal exposure to air pollution.

Overall this is a very good compilation of well written articles discussing the challenges that atmospheric monitoring presents to the analytical community.

P.J. Worsfold

Richard G. Brereton (Ed.), *Multivariate Pattern Recognition in Chemometrics illustrated by Case Studies*, Elsevier, Amsterdam, 1992, xi + 325 pp., plus 2 software supplements. Price hard-cover (ISBN 0-444-89783-6): US \$176.50/Dfl.305.00; paperback (ISBN 0-444-8974-4): US \$85.50/Dfl 150.00.

This book is a collection of eight chapters, and two software appendices (with demo-versions of software included) by different authors. The book was difficult to review. On the one hand it contains some very educational chapters on the geometry of multivariate data and analysis, and three good chapters on PCA, cluster analysis and

SIMCA classification. On the other hand, the chapter on “hard modelling” is substandard with lots of factual errors. There is also a lot of redundancy and overlap between the four introductory chapters on multidimensional geometry and matrix algebra. There is little coherence between the chapters in the book, and an almost total absence of interesting examples and applications. Data transformation, scaling, normalization and other preprocessing, all of which can have dramatic effects on the results of the data analysis, are largely neglected.

The most serious flaw with the book is the almost complete lack of chemistry. The book promises in the title to be “illustrated by cases stories”, but only one such illustration is given (in the SIMCA chapter by Kvalheim). The other illustrations are superficial and mainly non-chemical; in vivo pharmacology of neuroleptics, simulated NMR spectra of mixtures, morphological data of insects (aphids), and amino acid composition of elastins. This is misleading labeling and sad to see; after all chemometrics is supposed to be the interface between chemistry and statistics.

Hence, this book is just an incomplete introduction to multivariate classification with some bright spots. It can neither be recommended as “one of reference and training for the professional chemometrician”, nor as an introduction to the beginner. And the price is much too high for its content.

Svante Wold

PUBLICATION SCHEDULE FOR 1994

	S'93	O'93	N'93	D'93	J	F	M	A	M	J	J	A
Analytica Chimica Acta	281/1 281/2 281/3	282/1 282/2 282/3	283/1 283/2	283/3 284/1 284/2	284/3 285/1-2 285/3	286/1 286/2 286/3	287/1-2 287/3 288/1-2	288/3 289/1 289/2	289/3 290/1-2 290/3	291/1-2 291/3 292/1-2	292/3 293/1 293/2-3	294/1 294/2 294/3
Vibrational Spectroscopy		6/1			6/2		6/3		7/1		7/2	

INFORMATION FOR AUTHORS

Detailed "Instructions to Authors" for *Analytica Chimica Acta* was published in Volume 289, No. 3, pp. 381-384. Free reprints of the "Instructions to Authors" of *Analytica Chimica Acta* and *Vibrational Spectroscopy* are available from the Editors or from: Elsevier Science B.V., P.O. Box 330, 1000 AH Amsterdam, The Netherlands. Telefax: (+31-20) 5862459.

Manuscripts. The language of the journal is English. English linguistic improvement is provided as part of the normal editorial processing. Authors should submit three copies of the manuscript in clear double-spaced typing on one side of the paper only. *Vibrational Spectroscopy* also accepts papers in English only.

Rapid publication letters. Letters are short papers that describe innovative research. Criteria for letters are novelty, quality, significance, urgency and brevity. Submission data: max. of 2 printed pages (incl. Figs., Tables, Abstr., Refs.); short abstract (e.g., 3 lines); no proofs will be sent to the authors; submission on floppy disc; no revision will be possible.

Abstract. All papers and reviews begin with an Abstract (50-250 words) which should comprise a factual account of the contents of the paper, with emphasis on new information.

Figures. Figures should be prepared in black waterproof drawing ink on drawing or tracing paper of the same size as that on which the manuscript is typed. One original (or sharp glossy print) and two photostat (or other) copies are required. Attention should be given to line thickness, lettering (which should be kept to a minimum) and spacing on axes of graphs, to ensure suitability for reduction in size on printing. Axes of a graph should be clearly labelled, along the axes, outside the graph itself. All figures should be numbered with Arabic numerals, and require descriptive legends which should be typed on a separate sheet of paper. Simple straight-line graphs are not acceptable, because they can readily be described in the text by means of an equation or a sentence. Claims of linearity should be supported by regression data that include slope, intercept, standard deviations of the slope and intercept, standard error and the number of data points; correlation coefficients are optional.

Photographs should be glossy prints and be as rich in contrast as possible; colour photographs cannot be accepted. Line diagrams are generally preferred to photographs of equipment. Computer outputs for reproduction as figures must be good quality on blank paper, and should preferably be submitted as glossy prints.

Nomenclature, abbreviations and symbols. In general, the recommendations of IUPAC should be followed, and attention should be given to the recommendations of the Analytical Chemistry Division in the journal *Pure and Applied Chemistry* (see also *IUPAC Compendium of Analytical Nomenclature, Definitive Rules, 1987*).

References. The references should be collected at the end of the paper, numbered in the order of their appearance in the text (not alphabetically) and typed on a separate sheet.

Reprints. Fifty reprints will be supplied free of charge. Additional reprints (minimum 100) can be ordered. An order form containing price quotations will be sent to the authors together with the proofs of their article.

Papers dealing with vibrational spectroscopy should be sent to: Dr J.G. Grasselli, 150 Greentree Road, Chagrin Falls, OH 44022, U.S.A. Telefax: (+1-216) 2473360 (Americas, Canada, Australia and New Zealand) or Dr J.H. van der Maas, Department of Analytical Molecular Spectrometry, Faculty of Chemistry, University of Utrecht, P.O. Box 80083, 3508 TB Utrecht, The Netherlands. Telefax: (+31-30) 518219 (all other countries).

No part of this publication may be reproduced, stored in a retrieval system or transmitted in any form or by any means, electronic, mechanical, photocopying, recording or otherwise, without the prior written permission of the publisher, Elsevier Science B.V., Copyright and Permissions Dept., P.O. Box 521, 1000 AM Amsterdam, The Netherlands.

Upon acceptance of an article by the journal, the author(s) will be asked to transfer copyright of the article to the publisher. The transfer will ensure the widest possible dissemination of information.

Special regulations for readers in the U.S.A.—This journal has been registered with the Copyright Clearance Center, Inc. Consent is given for copying of articles for personal or internal use, or for the personal use of specific clients. This consent is given on the condition that the copier pays through the Center the per-copy fee for copying beyond that permitted by Sections 107 or 108 of the U.S. Copyright Law. The per-copy fee is stated in the code-line at the bottom of the first page of each article. The appropriate fee, together with a copy of the first page of the article, should be forwarded to the Copyright Clearance Center, Inc., 27 Congress Street, Salem, MA 01970, U.S.A. If no code-line appears, broad consent to copy has not been given and permission to copy must be obtained directly from the author. The fee indicated on the first page of an article in this issue will apply retroactively to all articles published in the journal, regardless of the year of publication. This consent does not extend to other kinds of copying, such as for general distribution, resale, advertising and promotion purposes, or for creating new collective works. Special written permission must be obtained from the publisher for such copying.

No responsibility is assumed by the publisher for any injury and/or damage to persons or property as a matter of products liability, negligence or otherwise, or from any use or operation of any methods, products, instructions or ideas contained in the material herein.

Although all advertising material is expected to conform to ethical (medical) standards, inclusion in this publication does not constitute a guarantee or endorsement of the quality or value of such product or of the claims made of it by its manufacturer.

Ⓢ The paper used in this publication meets the requirements of ANSI/NISO 239.48-1992 (Permanence of Paper).

Flow-Through (Bio)Chemical Sensors

By **M. Valcárcel** and **M.D. Luque de Castro**, Department of Analytical Chemistry,
University of Córdoba, 14004 Córdoba, Spain

Techniques and Instrumentation in Analytical Chemistry Volume 16

Flow-through sensors are more suitable than classical probe-type sensors for addressing real (non-academic) problems. The external shape and operation of flow-through (bio)chemical sensors are of great practical significance as they facilitate sample transport and conditioning, as well as calibration and sensor preparation, maintenance and regeneration, all of which result in enhanced analytical features and a wider scope of application.

This is a systematic presentation of flow-through chemical and biochemical sensors based on the permanent or transient immobilization of any of the ingredients of a (bio)chemical reaction (i.e. the analyte, reagent, catalyst or product) where detection is integrated with the analytical reaction, a separation process (dialysis, gas diffusion, sorption, etc.) or both.

The book deals critically with most types of flow-through sensors, discussing their possibilities and shortcomings to provide a realistic view of the state-of-the-art in the field. The large numbers of figures, the wealth of literature references and the extensive subject index complement the text.

Contents: 1. **Sensors in Analytical Chemistry.** Analytical chemistry at the turn of the XXI

century. Analytical information. What is a sensor? Sensors and the analytical process. Types of sensors. General features of (bio)chemical sensors. (Bio)chemical sensors and analytical properties. Commercial availability. Trends in sensor development.

2. Fundamentals of Continuous-Flow (Bio)Chemical Sensors. Definition. Classification. The active microzone. Flow-through cells. Continuous configurations. Regeneration modes. Transient signals. Measurement modes. The role of kinetics. Requirements for proper sensor performance.

3. Flow-Through Sensors Based on Integrated Reaction and Detection. Introduction. Flow-through sensors based on an immobilized catalyst. Flow-through immunosensors. Flow-through sensors based on an immobilized reagent. Flow-through sensors based on an *in situ* produced reagent.

4. Flow-Through Sensors Based on Integrated Separation and Detection. Introduction. Integrated gas diffusion and detection. Integrated liquid-liquid separation and detection. Integrated retention and detection. Flow-through sensors for multi-determinations based on integrated retention and detection. Ion-selective electrodes (ISEs) and ion-sensitive field-effect transistors (ISFETs).

5. Flow-Through Sensors Based on Integrated Reaction, Separation and Detection. Introduction. Integration of gas-diffusion, reaction and detection. Integration of dialysis, reaction and detection. Integration of sorption, reaction and detection.

Index.

© 1994 332 pages Hardbound
Price: Dfl. 355.00 (US\$ 202.75)
ISBN 0-444-89866-2

ORDER INFORMATION
ELSEVIER SCIENCE B.V.

P.O. Box 330
1000 AH Amsterdam
The Netherlands
Fax: (+31-20) 5862 845

For USA and Canada

P.O. Box 945
Madison Square Station
New York, NY 10159-0945
Fax: (212) 633 3680

US\$ prices are valid only for the USA & Canada and are subject to exchange rate fluctuations; in all other countries the Dutch guilder price (Dfl.) is definitive. Customers in the European Union should add the appropriate VAT rate applicable in their country to the price(s). Books are sent postfree if prepaid.



**ELSEVIER
SCIENCE**



0003-2670(19940630)292:1/2;1-7